UNIVERSITY
of
GLASGOW

SOME ASPECTS OF THE MECHANICAL BEHAVIOUR OF MIXTURES OF KAOLIN AND COARSE SAND

Garimella Vijaya Kumar

A thesis submitted for the degree of
Doctor of Philosophy at the University of Glasgow

Department of Civil Engineering - February 1996

ProQuest LLC.
789 East Eisenhower Parkway
P.O. Box 1346
Ann Arbor, MI 48106 – 1346

To Santosh

SUMMARY

The work presented in this thesis describes an investigation into the mechanical behaviour of kaolin and coarse sand mixtures with a major component of experimental work. The objective of the research is to investigate the extent to which the mechanical response is controlled by the clay phase. After the initial introductory chapter, subsequent chapters present studies made of different aspects of mechanical behaviour.

Chapter 1 gives the introduction to the research and presents a basis for the study as well as the aim of the research. The methodology used in accomplishing the aims is presented.

Chapter 2 looks at the influence of the coarse fraction on the index properties of clay soils. This study involves laboratory testing using a fall cone to determine the liquid limit of clay-sand mixtures. The extent to which the index properties of the mixtures are controlled by the clay phase alone is considered.

Chapter 3 presents one dimensional consolidation characteristics of clay/sand mixtures with an aim to discover a threshold clay content at which the interaction between sand particles becomes dominant during consolidation. The consolidation was carried out in a hydraulic oedometer or in a consolidation tube using incremental loading.

Chapter 4 is concerned with permeability characteristics of clay/sand mixtures in order to develop a generalised approach to predict changes in permeability with the aim again to discover the extent to which the response is controlled by the clay phase. This study involves laboratory testing of various mixtures using computer controlled flow through a hydraulic oedometer. Permeability tests were performed by applying constant flow rates - providing, in addition, data which could be used to check the validity of Darcy's law.

Chapter 5 deals with the general stress:strain response of clay/sand mixtures from drained and undrained shear tests performed at different overconsolidation ratios in a conventional triaxial apparatus with an aim to present a description of the response of the mixtures within the general framework of critical state soil mechanics.

Chapter 6 is concerned with simple finite element analyses of the effects of coarse fraction on shear behaviour of normally consolidated mixtures. These results are compared with experimental and theoretical predictions.

In Chapter 7 it is concluded that for clay contents above about 30-40% the mechanical behaviour of the mixture is controlled by the clay phase alone and that no interaction of the sand particles occurs. The sand particles do, however, act as volume fillers and volumetric deformations in consolidation and drained shear tests must be corrected to allow for the actual volume of clay matrix that is present.

Numerical and theoretical analyses have not proved successful in matching the patterns of response that are clearly shown from the experimental study.

ACKNOWLEDGEMENTS

This dissertation would have been impossible if it was not for various individuals and institutions who by extending their fullest co-operation and assistance, have made it possible.

My supervisor, Prof. David Muir Wood has always been the first person to encourage and inspire me throughout my research work and I take this opportunity to express my sincere respect and gratitude for all his valuable guidance and advice.

I would also like to thank Dr. A. Chan, Dr. P. Smart, Dr. T.G. Davies, and Dr. W.M. Stewart for their valuable advice and help.

Invaluable assistance was provided by the technical support staff of the Soil Mechanics group, particularly W. Henderson and Tim Montgomery, who devoted such care and attention to the fabrication of consolidation tubes and computer set up of the testing apparatus. And I would also like to thank Kenneth McColl, Eileen Davies and Barbara Grant, for their kind co-operation and patience to put up with the most mundane matters.

I should also like to extend my thanks to Stuart McSporran who allowed me to use his computer at 76 Oakfield Avenue during last six months.

This study was made possible by an award of a Commonwealth scholarship from The Association of Commonwealth Universities, London and a study leave granted me by Andhra University, Visakhapatnam, India and I am grateful to both bodies and to the staff of the British Council who administered the scholarship. Some support from the Registrar's Office, University of Glasgow is also gratefully acknowledged.

I would also like to thank my friends and colleagues, especially, Dr.AbuBakar Hamidon, Dan Lee, Lim, Dr. M.I. Alsayed, Dr. S. Bu, Santosh Kumar and Vincent Peloutier. It was their presence which made the time that I spent at Glasgow such an enjoyable and educational period of my life.

I would like to express my gratitude to my parents who have always been a constant source of support and encouragement in the course of my career. Finally, I thank my wife for her sacrifices and encouragement.

G.V. Kumar

TABLE OF CONTENTS

LIST OF SYMBOLS

This list contains definitions of symbols and also an indication of the section in the thesis where they are first used.

A	cross-sectional area of sample	(4.0)
A	activity	(2.3.2)
A	pore pressure parameter	(5.3.1.3)
A_c	reference value of clay specific volume at σ'_v = 1kPa in v_c:lnσ'_v plane	(5.4.1.2)
A^*_c	reference value of clay specific volume at σ'_v = 1kPa in lnv_c:lnσ'_v plane	(3.3.2)
a, b	hyperbolic experimental constants	(6.2.1)
A, B	constants	(4.1.1)
A, B′	constants	(4.1.1)
A*, B*	reference values of specific volume at σ'_v = 1kPa in lnv:lnσ'_v plane	(3.2)
b_m	matrix factor	(6.2)
B	pore pressure parameter	(3.1.1.2)
c_k	permeability change index	(4.1.1)
c_s	pore shape factor	(4.1.1)
c_u	undrained shear strength	(2.0)
c_v	coefficient of consolidation	(3.2)
C	clay content	(1.1)
d	diameter of sand particles	(1.1)
d	penetration of fall-cone	(2.0)
D	drained	(5.1.2.3)
e	void ratio	(1.1)
e_c	clay void ratio	(1.1)
e_g	granular void ratio	(1.1)
e_L	void ratio at liquid limit	(4.1.1)
e_o	initial void ratio	(4.1.1)
ESP	effective stress path	(5.3.1.4)
f	granular volume fraction	(6.0)
F	axial force in triaxial apparatus	(5.2)
FE	finite element	(6.3)
G	shear modulus	(5.3.1.6)

G_c	composite shear modulus	(6.2)
G_i	shear modulus of inclusion	(6.2)
G_m	shear modulus of matrix	(6.2)
G_s	specific gravity of soil particles	(1.1)
h	half height of triaxial sample	(5.1.2.2)
h	differential hear across the sample	(4.3.2.2)
2H	height of sample	(3.2)
$\overline{H}$	head ratio	(4.3.2.2)
i	hydraulic gradient	(4.0)
I_L	liquidity index	(3.3.2)
I_p	plasticity index	(2.0)
k	permeability	(3.2)
K	constant	(4.1.1)
k_o	initial permeability	(4.1.1)
k_α	cone factor	(2.0)
K_0	earth pressure coefficient at rest	(3.2)
l	length of triaxial sample	(5.2)
l_{cm}	equivalent length of clay matrix	(5.2)
L	length of sample	(4.3.2.2)
L	apparent flow length	(4.1.1)
L_e	effective flow length	(4.1.1)
m_c	mass of clay solids	(1.1)
m_g	mass of granular solids	(1.1)
m_v	coefficient of volume compressibility	(3.2)
m_w	mass of water filling voids	(1.1)
M	slope of critical state	(5.4.1)
M100	mixture with 100% clay content	(1.3.2)
M90	mixture with 90% clay content	(1.3.2)
M80	mixture with 80% clay content	(1.3.2)
M70	mixture with 70% clay content	(1.3.2)
M60	mixture with 60% clay content	(1.3.2)
M50	mixture with 50% clay content	(1.3.2)
M40	mixture with 40% clay content	(1.3.2)
M30	mixture with 30% clay content	(1.3.2)
M20	mixture with 20% clay content	(1.3.2)
M10	mixture with 10% clay content	(1.3.2)
N	location of isotropic normal compression line in v_c:lnp' plane	(5.4.1.3)

OCR	overconsolidation ratio	(5.1.2.3)
p'	mean effective stress	(5.2)
p'_c	maximum preconsolidation pressure	(5.1.2.3)
p'_e	mean effective stress on a normal compression line	(5.4.1.3)
p'_{cs}	equivalent critical state pressure for a state s	(5.4.1.3)
p'_s	mean effective stress at a state s	(5.4.1.3)
p'_o	mean effective stress at the start of shearing	(5.3.1.6)
q	deviator stress	(5.2)
Q'	flow rate	(4.0)
Q	volume of flow	(4.3.1)
R	ramp	(4.2)
s	centre to centre spacing between sand particles	(1.1)
s_s	surface area per unit volume	(4.1.1)
S	slope of the plot: induced pressure difference vs flow rate	(4.4.1)
t	time	(3.2)
t_{90}	time for 90% consolidation	(3.2)
t_{100}	time for 100% consolidation	(5.1.2.2)
t_f	time required to failure	(5.1.2.2)
T	tortuosity factor	(4.1.1)
T_v	time factor for 90% consolidation	(3.2)
TH	theoretical	(6.3)
u	pore pressure	(3.2)
U	undrained	(5.1.2.3)
$\bar{U}$	average degree of consolidation	(3.2)
v	specific volume	(1.1)
v_c	clay specific volume	(1.1)
$v_{c\lambda}$	intercept on critical compression line in v_c:lnp' plane	(5.4.1.3)
v_g	granular specific volume	(1.1)
v_s	reference value of clay specific volume	(5.4.1.3)
V	volume of sample	(1.1)
V_c	volume of clay solids	(1.1)
V_g	volume of granular solids	(1.1)
V_w	volume of water filling voids	(1.1)
w	water content	(1.1)
w_c	clay water content	(1.1)
w_{cL}	liquid limit of clay fraction	(2.3.1)
w_L	liquid limit	(2.3.1)

w_p	plastic limit	(2.3.2)
W	weight of fall cone	(2.0)
X, Y	experimentally determined constants depending on the type of the mixture	(4.4.2)
z	vertical distance from the top of the specimen	(3.2)
γ	unit weight of permeating fluid	(4.1.1)
γ_w	unit weight of water	(3.2)
Γ	location of critical state line in v_c: ln p' plane	(5.4.1.2)
δ	indicates increment value	(3.2)
ε_a	axial strain	(5.2)
ε_r	radial strain	(5.2)
ε_{ac}	clay axial strain	(5.2)
ε_p	volumetric strain	(5.2)
ε_{pc}	clay volumetric strain	(5.2)
ε_q	shear strain	(5.2)
ε_{qm}	shear strain of matrix	(6.2)
ε_{qc}	composite shear strain	(6.2)
η	stress ratio	(5.2)
κ	slope of unloading-reloading line in v:ln σ'_v plane	(3.2)
κ^*	slope of unloading-reloading line in lnv:ln σ'_v plane	(3.2)
κ_c^*	slope of unloading-reloading line in $\ln v_c$:ln σ'_v plane	(3.3.2)
λ	slope of normal compression line in v:ln σ'_v plane	(2.0)
λ_c	slope of critical state line in v_c:lnp' plane	(5.4.1.2)
λ^*	slope of normal compression line in lnv:ln σ'_v plane	(3.2)
λ_c^*	slope of normal compression line in $\ln v_c$:ln σ'_v plane	(3.3.2)
μ	viscosity of the permeating fluid	(4.1.1)
ν	Poisson's ratio	(6.1.1)
ν_m	Poisson's ratio of matrix	(6.2)
β_m	matrix factor	(6.2)
σ_v	vertical stress	(3.1.1.2)
σ'_v	vertical effective stress	(1.2)
σ_a	axial stress	(6.3.1)
σ_r	radial stress	(6.3.1)
σ'_a	axial effective stress	(5.2)
σ'_r	radial effective stress	(5.2)
σ'_c	composite effective stress	(6.2)
σ'_m	effective stress of matrix	(6.2)

Δu	pore pressure response to an increment of vertical stress	(3.1.1.2)
Δp	induced steady state pressure difference between drainage boundaries	(4.3.1)
ϕ'	Mohr-Coulomb friction angle	(5.4.1)
ϕ'_{cs}	critical state angle of shearing resistance	(1.2)

LIST OF TABLES

LIST OF FIGURES

CHAPTER 1

INTRODUCTION

All man made structures, except those which float or fly, are supported by natural soils and many civil engineering structures, such as water retaining banks, roads and air field pavements are constructed from soil. Geotechnical engineers are concerned with safe and economical transfer of the structural loads to soil and for the purpose of analysis they require to know the mechanical behaviour of soil when it is compressed or sheared or when water flows through it.

Investigations into the mechanical behaviour of soils have generally concentrated on pure clays or sands. But, frequently, natural soils - particularly glacial tills, alluvial soils, boulder clays and residual soils - and man made fills contain a great range of particle sizes from colloid to coarse sand or gravel. It appears that the clay particles in such soil may form packets surrounding or bridging between larger particles (e.g. Collins and McGown 1974). The mechanical response of such soils can be expected to reflect a mixture of the responses of the coarse granular structure and of the fine clay bridges.

The determination of the mechanical behaviour of such soils intermediate between clays and coarse fractions would be simplified if the engineering characteristics of the individual components of the soils could be used to predict or estimate the overall characteristics as a function of the percentage of the components. The difficulty inherent in using the engineering characteristics of the individual soil components to estimate the behaviour of the soil mass is that the soil components do not act independently of each other but interact with each other to influence the behaviour of the mixture. The overall response can seldom be assessed from the properties of its components as a simple linear function of the relative amounts of the components. Thus, the generalised principle of mixture theory may not be valid. It is a well known fact that the presence of clay components in small quantities can exert a great influence on the mechanical behaviour of soils. It is of interest to study the transitions of mechanical response that occur as the proportions of coarse and fine material are varied.

1.1 PROCEDURE FOR INTERPRETATION

For a soil which is made up of quite distinct particle sizes conventional definitions of volumetric packing may no longer be appropriate. It is convenient to visualise soil components as three materials: water (filling the voids), clay

solids and granular solids as shown in Fig. 1.1. It will be convenient to assume that the specific gravity of clay and granular solids is the same. The clay content C is given exactly by

$$C = \frac{m_c}{m_c + m_g} \tag{1.1}$$

and is then given approximately by

$$C \approx \frac{V_c}{V_c + V_g} \tag{1.2}$$

Void ratio e can be defined conventionally as

$$e = \frac{V_w}{V_c + V_g} \tag{1.3}$$

but it is useful to define a clay void ratio e_c for the clay paste, assuming that the coarse sand plays no part:

$$e_c = \frac{V_w}{V_c} = \frac{e}{C} \tag{1.4}$$

and a clay specific volume

$$v_c = \frac{V_w + V_c}{V_c} = \frac{e + C}{C} \tag{1.5}$$

Equally, a granular void ratio e_g can be defined, assuming that the voids in the coarse sand are filled with a mixture of clay and water:

$$e_g = \frac{V_w + V_c}{V_g} = \frac{e + C}{1 - C} \tag{1.6}$$

and a granular specific volume

$$v_g = \frac{V_w + V_c + V_g}{V_g} = \frac{1 + e}{1 - C} \tag{1.7}$$

$$v_g = \frac{v}{1-C} = 1 + \frac{Cv_c}{1-C} \qquad (1.7a)$$

Water content, w is defined as

$$w = \frac{m_w}{m_c + m_g} = \frac{e}{G_s} \qquad (1.8)$$

but a clay water content w_c can be defined as

$$w_c = \frac{m_w}{m_c} = \frac{w}{C} \qquad (1.9)$$

for the clay paste alone without regard for the presence of the coarse particles.

The granular specific volume v_g directly reflects changes in packing of the coarse particles due to compression of the mixture and squeezing of water out of the clay paste. It is useful to consider an ideal soil consisting of equally sized spherical sand particles in symmetrical arrays, within a clay-water matrix. Graton and Fraser (1935) have presented mathematical calculations of porosity conditions in regular arrays of spheres. The loosest packing of the spheres is cubic (Fig.1.2a) and the densest is hexagonal close packed (Fig.1.2b) which, when spheres are in contact, give v_g values of 1.91 and 1.35 respectively. If the sand particles of diameter d are separated, then the relationship between v_g and the centre to centre spacing s, is given by the following equations and is shown in Fig. 1.3.

$$v_g = \frac{6}{\pi}\left(\frac{s}{d}\right)^3 \qquad \text{for cubical packing} \qquad (1.10)$$

$$v_g = \frac{3\sqrt{2}}{\pi}\left(\frac{s}{d}\right)^3 \qquad \text{for hexagonal packing} \qquad (1.11)$$

This spacing s or the value of granular void ratio should indicate the probability of a failure surface forming in a soil without interference from the sand particles present in it. Lupini et al. (1981) have shown that the granular specific volume v_g is the most satisfactory parameter to account for the predictions of residual strength of cohesive soils.

1.2 PREVIOUS STUDIES

Early studies on liquid limit characteristics of various mixtures of clays with medium to fine sand were reported by various authors e.g. Seed et al. (1964), Rao (1974) and Tan et al. (1994). They found that the variation of liquid limit with clay fraction is linear. The summary of published studies of liquid limit characteristics of various mixtures will be discussed further in Section 2.1.

Nakase and Kamei (1983); Kamei and Nakase (1989) investigated undrained shear behaviour of natural marine clay with plasticity index I_p 30 and three kinds of artificial natural soils with plasticity index I_p 20, 15 and 10 made by mixing natural marine soil with different amounts of Toyoura sand. The corresponding grading curves of their studies are presented in Fig.1.4. Some of the observed effective stress paths of normally consolidated mixtures are shown in Fig.1.5. They concluded that the critical state friction angle ϕ'_{cs}, in triaxial compression is constant irrespective of plasticity index. Nakase et al. (1988) have also shown that the critical state friction angle ϕ'_{cs}, during triaxial compression tests hardly changed from 39° to 40° for a large number of Japanese marine clays over a range of plasticity index from 10 to 50.

Fukue et al. (1986) investigated consolidation properties of compacted sand-clay mixtures used as reclamation materials. The mixtures used in their study were prepared from bentonite with fine to medium Toyoura sand. The authors investigated the effects of sand on consolidation properties of mixtures with clay content 72, 26, 20.3 and 35.4% by examining the relationships between granular void ratio e_g and vertical effective stress. The maximum vertical effective stress applied in their study is around 2.75 MPa. In their study, the clay content represents particles of size smaller than 2 μm and bentonite contains 72% of clay content. The authors have shown that the compressibility of the mixtures decreases greatly if e_g reaches a threshold granular void ratio as shown in Fig.1.6. The threshold is evaluated from the intersection of tangents of curves (e_g-ln σ'_v) as shown in Fig.1.6. The authors concluded that if the mixture has e_g less than e_g (threshold), the soil can be classified as sandy and can be used as reclamation material.

Graham et al. (1989) investigated stress-strain-time behaviour of compacted sand-bentonite mixture, a 'buffer' material intended for containing nuclear-fuel wastes. The buffer material consists of 50:50 mixture by weight of medium fine sand and natural bentonite. They investigated shear behaviour in short-duration and long-duration tests and assumed that the buffer reached equilibrium when the volume change rate is less than 0.1% per day. In short-duration tests consolidation pressure was applied in one increment for 18 days. In long-duration tests confining pressures were applied in 5 increments each kept

for 5 days. In some cases they applied the final increment of pressure for up to 60 days in order to obtain a volume change rate less than 0.1% per day. The authors have shown that the buffer material in shear behaves like strain softening clay in short duration tests and strain hardening clay in long duration tests. The scanning electron micrographs of microstructure of buffer at the end of shearing have shown that the sand particles are separated from each other by matrix of clay particles and they concluded that the behaviour of the buffer is controlled by the density of clay. This hypothesis is also supported by one dimensional compression test results shown in Fig.1.7. The results of Fig.1.7a were from compression tests on different sand-bentonite mixtures containing 25 to 100% bentonite. Fig.1.7b represents the data in Fig.1.7a in terms of clay specific volume, v_c. With the help of Fig.1.7b and from the shear behaviour of buffer, the authors provided a critical state model to describe stress-strain-time behaviour of buffer material.

Georgiannou et al. (1990) investigated the undrained behaviour of clayey sands formed by sedimenting medium fine Ham river sand into suspensions of kaolin in water with different clay contents between 6 and 30%. Some of the grading curves of their investigations were presented in Fig.1.4 Some of the results of their study i.e. the effects of increasing of clay content on the undrained behaviour of normally consolidated sand-clay mixtures are summarised in Fig.1.8. The effective stress paths in Fig.1.8 are almost identical and differ only at the point of phase transformation, where dilatant behaviour is initiated. The points of phase transformation correspond to increasingly lower shear stress value and higher axial strain as the clay content increases from 6 to 10%. There is a reversal in this trend for clay contents in excess of 20%. At a clay content of 30% dilation was suppressed and they concluded that 30% clay content forms a limiting value at which the dilatant behaviour of the granular phase ceases to influence the mechanical behaviour of clay-sand mixtures during shear.

Georgiannou et al. (1991) compared the undrained shear behaviour of the model clayey sands (Fig.1.8) with reconstituted natural clayey sand from the site of the Gullfaks C oil production platform in the North Sea and concluded that the pattern of its behaviour in compression is almost similar to that of the artificial clayey sand.

Kimura et al. (1994) investigated shear behaviour of Kawasaki marine clay with plasticity index 30 and the mixtures with plasticity index from 2-30. The mixtures are manufactured by adding sand to marine clay. The soils with plasticity index 30, 20, and 10 are similar to the ones used by Nakase et al. (1983, 1988). The grading curves of the mixtures with plasticity index 2 and 5

are shown in Fig.1.4. The observed stress:strain behaviour of soils with plasticity index 10 and 2 are presented in Fig.1.9. From Fig.1.9 the authors concluded that the drained strength of mixture with plasticity index 2 is lower than the mixture with plasticity index 10. The corresponding critical state friction angle ϕ'_{cs} are 35.26° and 37°. They explained this unusual behaviour by considering that the mixture with plasticity index 2 is extremely loose. Georgiannou et al. (1990) have investigated shear behaviour of sands with small quantities of kaolin (Fig.1.8) but not observed decrease in ϕ'_{cs} with decrease in clay content. Furthermore reconstituted North sea natural clayey sand (Georgiannou et al. 1991) have not shown decrease in ϕ'_{cs} with decrease in clay content.

Tan et al. (1994) reported the shear strength of very soft clay-sand mixtures. The mixtures used in their study were manufactured from Singapore marine clay, montmorillonite, and montmorillonite+kaolinite with medium sand in proportion from 20 to 60% by weight at 20% intervals. Shear strengths between 2 and 500 Pa were measured by a plate penetration method. They observed marked increase in shear strength of the clay slurries when the granular void ratio was less than 5.

Compacted sand-bentonite mixtures are one of the lowest-cost technologies available for constructing an impermeable liner for waste water ponds etc. Permeability characteristics of sand-bentonite mixtures for this purpose are dealt with by Chapuis et al. (1990); Kenney et al. (1992); and Daniel (1993) described in detail the underlying principles for design and construction of clay liners. The permeability tests on compacted sand-clay liners will usually be performed to determine, for the selection of soil mix, the degree of imperviousness provided by the clay. Their purpose is to minimise the cost of the mix and to achieve hydraulic conductivity of the compacted soil liner less than or equal to 1×10^{-7} cm/s.

1.2.1 Summary of previous attempts and the need for an investigation

The above review reveals that there is experimental evidence that the liquid limit obeys a linear law for soils and when it comes to shear behaviour the existing data base is not sufficient to interpret in a generalised framework. For example, in an attempt to find out the boundary of response between the shear behaviour expected of cohesive soils and cohesionless soils, Nakase et al. (1983, 1988); Kimura et al. (1994) used plasticity index for classification. This type of classification is useful for fine-grained soils, but cannot be extended to coarse-grained soils, because of the limit of determination of liquid limit. Furthermore critical state friction angle ϕ'_{cs} weakly dependent on plasticity index of soil and is

more strongly dependent on the mineralogy of soils, pore water chemistry, organic content etc. The general trend from UK clays (Vaughan et al. 1979) suggests that the variation of ϕ'_{cs} on average is around 25% for plasticity index variation from 10 to 45%.

Georgiannou et al. (1990, 1991) were concerned with undrained shear behaviour of sands with small quantities of clay. Graham et al. (1989) concentrated on compacted shear behaviour of a single sand-bentonite mixture made with a swelling type of clay. But their consolidation results in Fig.1.7b are very interesting and show that the consolidation behaviour of the mixture is controlled by bentonite even at sand content 75% which is conflicting with the findings of Fukue et al. (1986). Fukue et al. (1986) have shown that for clay contents less than 50%, the final stages of compression are influenced by the frictional resistance between sand particles. But from Fig.1.7b it is clear that Graham et al. (1989) applied much higher stresses than Fukue et al. (1986) and have not noticed the effects of frictional resistance of sand particles at higher stresses. There is no experimental evidence available at this juncture on consolidation characteristics of non-swelling mixtures to compare with consolidation results of bentonite-sand mixtures.

From the above review it is clear that our understanding of the mechanical behaviour of clay-sand mixtures is incomplete and to interpret its behaviour in a generalised framework, a systematic study of various geotechnical properties of mixtures over wide range of clay content is essential. The information on behaviour of such soils is needed because of three practical considerations: 1) The prospect that the engineering behaviour of soils can be predicted with more confidence and greater accuracy when the extent of clay phase is identified and correlations between compositional variables and engineering characteristics are established. 2) It may be economically feasible to reduce the quantity of soft clayey sediments that must be displaced by granular materials obtained off-site. 3) It may eventually become possible to provide a theoretical basis for numerical modelling

1.3. METHODOLOGY AND PROCEDURE

1.3.1 Selection of materials

The investigation of the contribution of the coarse fraction in the mechanical behaviour of soils may be approached in two ways. In the first, natural soils can be used. This method has the advantage that measured properties are those of the soils in nature. However, though soils are naturally

variable at any one site, the variation of the proportion of coarse material may be small and insufficient to give an overall picture of the contribution of the coarse fraction to the behaviour of the soil. In addition, natural soils contain several different minerals or other constituents, such as organic matter, so that the influence of any one constituent may be difficult to isolate. A number of researchers have however, used reconstituted natural soils for their studies: e.g. Nakase et al. (1983, 1988) for undrained behaviour of cohesive soil and Georgiannou et al. (1991) for undrained behaviour of natural clayey sands.

The second approach is to use synthetic soils. Soils of known composition can be prepared by blending commercially available clay minerals of relatively high purity with commercial sands. Although this approach is much easier, it has the disadvantage that it may not be possible to extrapolate features of mechanical response to natural soils. However, it is believed the results will be of sufficient value to illuminate, at least qualitatively, aspects of the behaviour of natural soils. Some of the synthetic clay-sand mixtures that have been used include compacted sand-bentonite buffer materials for containing hazardous wastes (Graham et al. 1989); the undrained behaviour of very loose clayey sands (Georgiannou et al. 1990); permeability characteristics of compacted bentonite-sand mixtures as soil liners (Kenney et al. 1992) and properties of some kaolin based model clays (Rossato et al. 1992).

Kaolin based artificial soils have been particularly popular because of commercial availability, relatively high permeability (Al Tabbaa and Wood 1987) and the existence of a large data base of tests on kaolin soils which can be used to develop models to explain and describe soil behaviour. (e.g. Parry and Nadarajah 1974; Amerasinghe and Parry 1975; Al Tabbaa and Wood 1989).

Kaolin was chosen to be the clay constituent for the present programme of tests. The kaolin was obtained in powder form from English China Clays, Lovering and Pochin Ltd., St Austell, Cornwall. Details of the kaolin are summarised in Table 1.1.

The Coarse sand used for the mixtures was sieved from a Scotsand obtained from Isle of Arran, Scotland to give a narrow grading curve as shown in Fig.1.10, passing through 3.35 mm sieve and retained on 2 mm sieve. The index properties of this Scotsand are presented in Table 1.2. The particles are mainly sub rounded as shown in Fig. 1.11. According to Gribble (1995), the sand consists of broken granite grains (80%), quartz (10%) and other minerals like red feldspar and jasper (10%).

1.3.2 Preparation of mixtures

Little is known about the interactions between sand grains and clay matrix in a saturated clay-sand mixture under stress. In this study only homogeneous macro texture is considered in which coarse sand particles are dispersed uniformly throughout the clay matrix.

The clay-sand mixtures were prepared on the basis of a specified proportion by weight of kaolin with sand. The kaolin was first mixed thoroughly under vacuum with a quantity of distilled water equal to approximately 120% of the dry weight of kaolin in the mixture. The chosen proportion of sand was added to the clay and both were mixed together for an hour. Then the mixture was kept in an airtight container for one week for saturation. These artificially prepared mixtures will be described as M100, M90, M80, M70, M60, M50 etc. respectively referring to their clay contents, 100% 90%, 80%, 70%, 60% , 50% etc. Typical particle size distributions for the mixtures are shown in Fig.1.10. In describing the grading of cohesive soils the term clay fraction will be used for the percentage by weight of particles smaller than 2 μm mean particle diameter as determined by sedimentation. The term clay content will be used in this study for the proportion of kaolin present in the clay-sand mixture irrespective of the particle size.

1.4 AIMS OF THE RESEARCH

The general aims of the research described in this thesis are

- to investigate experimentally the mechanical behaviour of clay-sand mixtures by adding coarse sand to kaolin in proportions of 0-70% to discover the extent to which response is controlled by the clay phase by considering
  - a) Index properties
  - b) Consolidation characteristics
  - c) Permeability characteristics
  - d) Undrained and drained shear behaviour

- to compare experimentally measured shear stress:strain response with patterns of response obtained using finite element predictions and existing theoretical methods.

- to establish a general framework to describe the mechanical behaviour of soils with different proportions of coarse material.

Table 1.1 Physical properties of kaolin

Description	Values
Specific gravity	2.62
Liquid limit (%)	80
Plastic Limit (%)	39
Plasticity index (%)	41
Clay fraction (%)	95

Table 1.2 Physical properties of sand

Description	Values
Specific gravity	2.65
Maximum void ratio	0.99
Minimum void ratio	0.58
Water absorption (%) (Roberts, 1995)	0.52
Internal friction angle from shear box at void ratio = 0.83	30°
Mineralogy (Gribble, 1995)	broken granite (80%), quartz (5-10%), few % of basic igneous and jasper

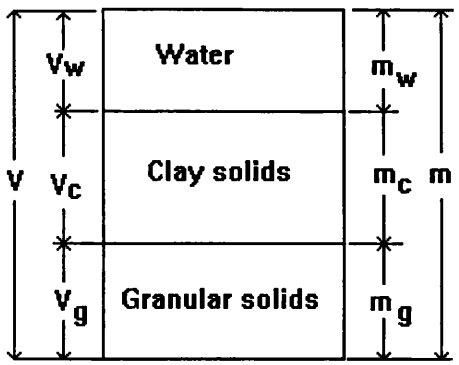

Fig.1.1 Three material model

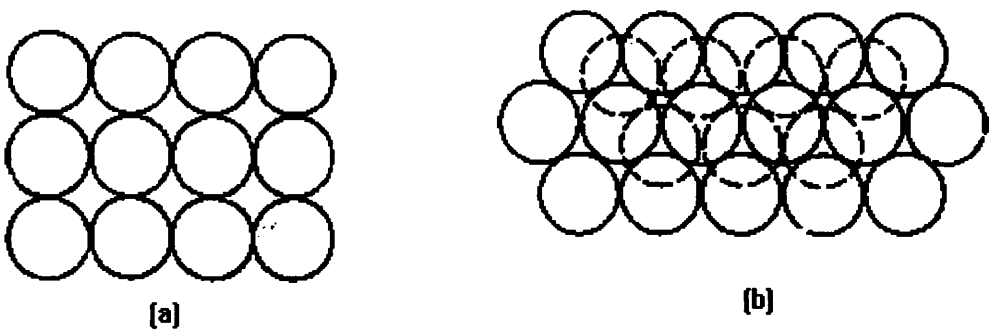

Fig.1.2 State of packing of equal spheres: (a) square, (b) hexagonal. Spheres of higher layers are shown in dashed lines. Plan view.

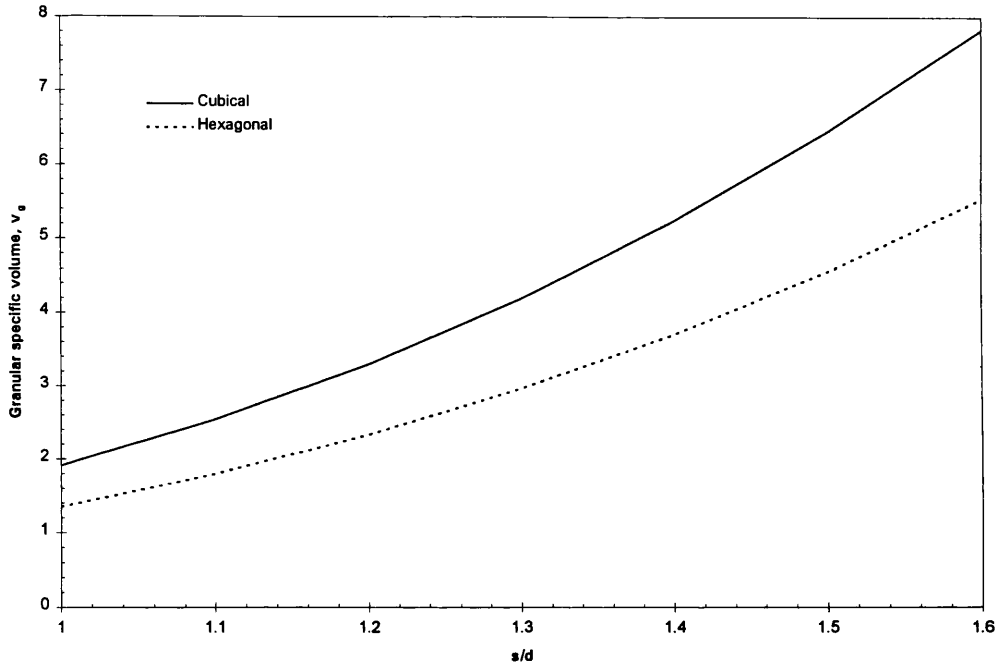

Fig.1.3 Uniform spherical particles separation as a function of granular specific volume

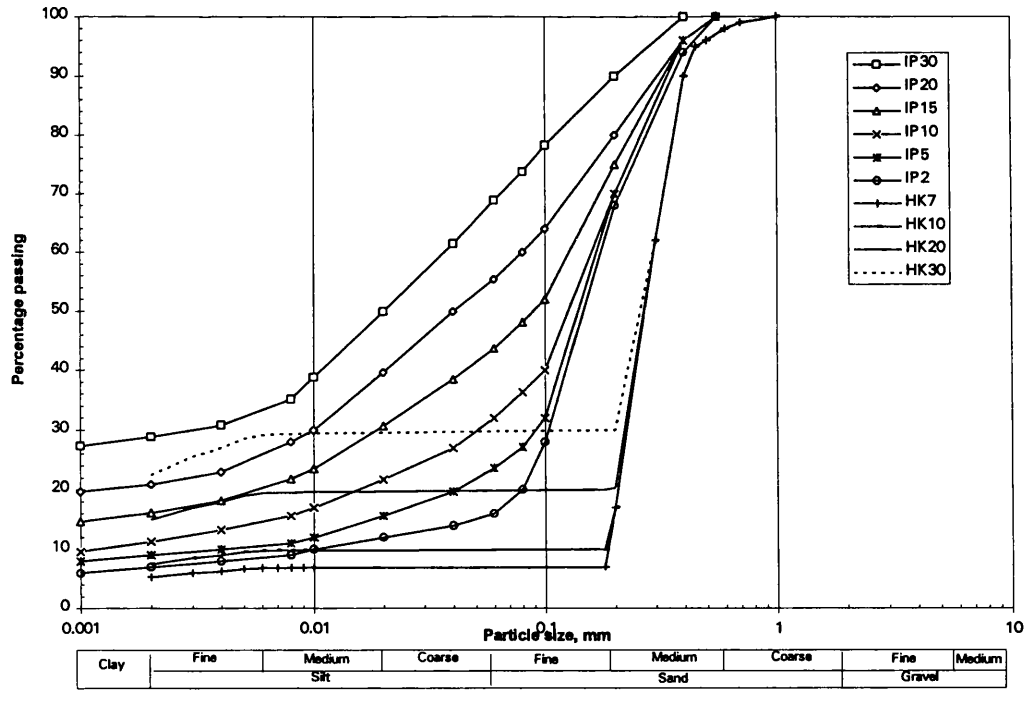

Fig.1.4 Grading curves for the mixtures used by various investigators:
IP30-IP10 - data from Nakase and Kamei (1983);
IP5-IP2 - data from Kimura et al.(1994);
HK7-HK30 - data from Georgiannou et al. (1990)

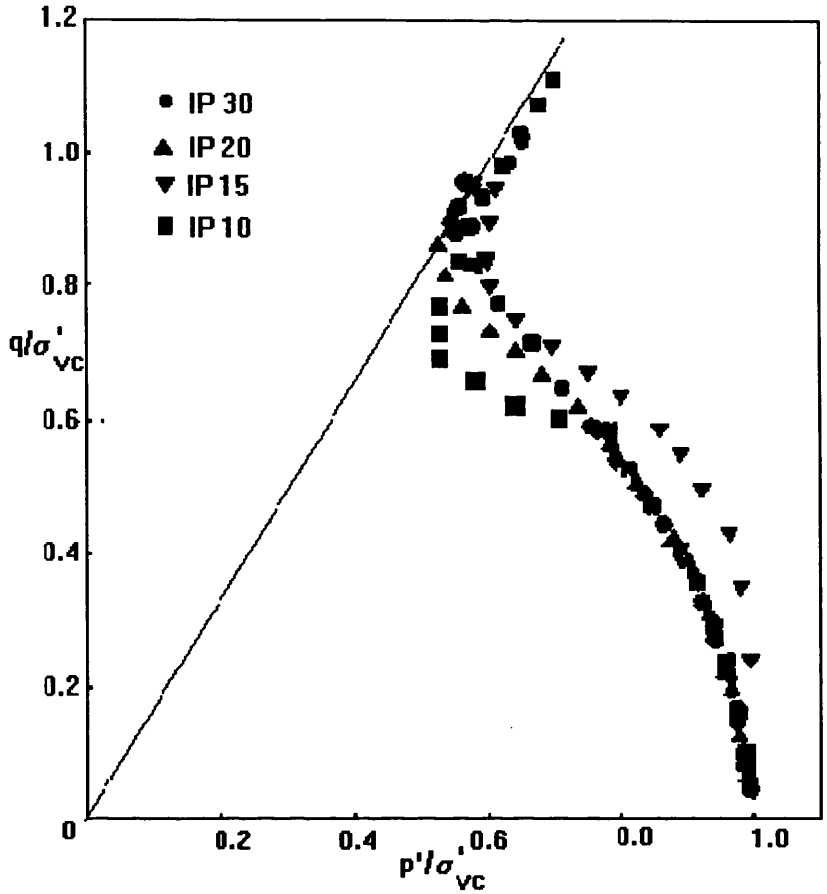

Fig.1.5 Typical effective stress paths (Nakase and Kamei, 1983)

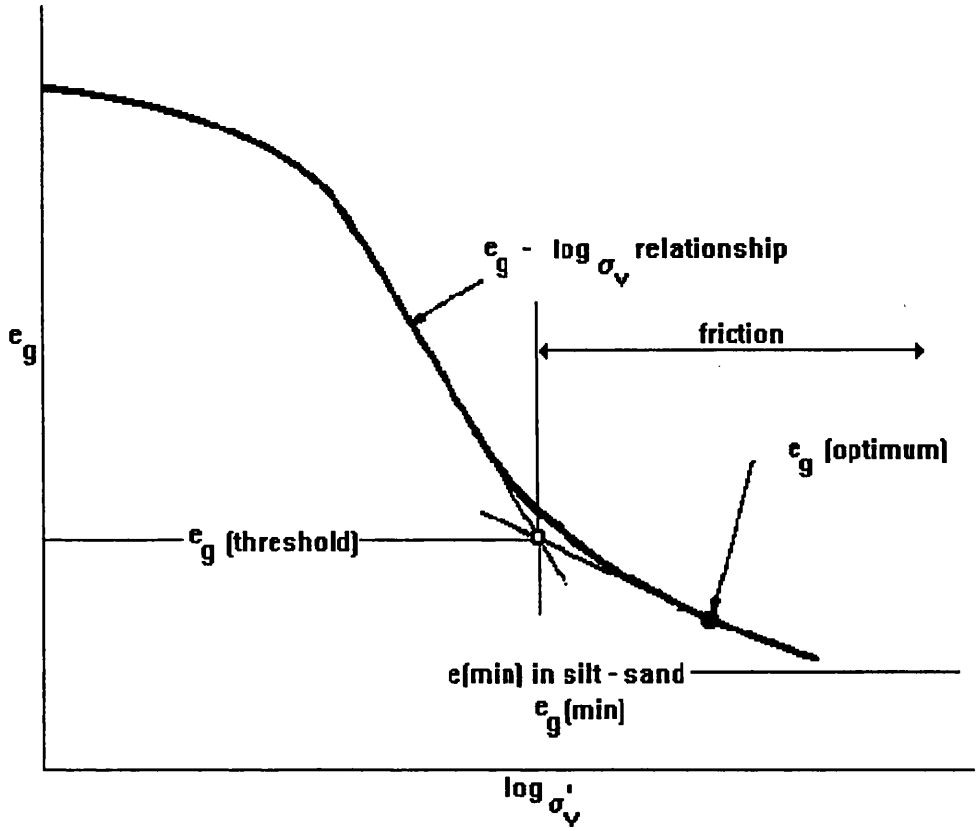

Fig.1.6 Definition of threshold granular void ratio (Fukue et al. 1986)

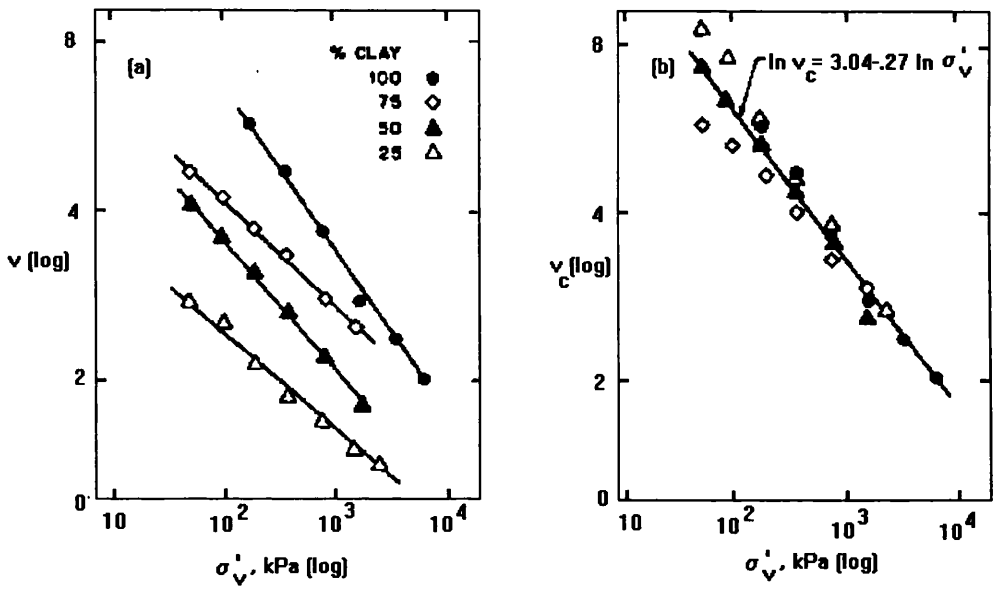

Fig.1.7 (a) Specific volume and (b) clay specific volume versus vertical stress in 1D - Compression (Graham et al. 1989)

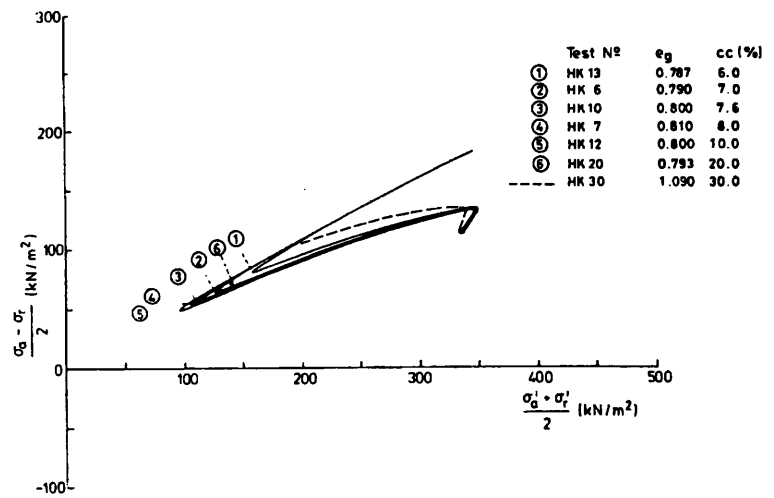

Fig.1.8 Effective stress paths for undrained compression of clayey sands normally consolidated (Georgiannou et al. 1990)

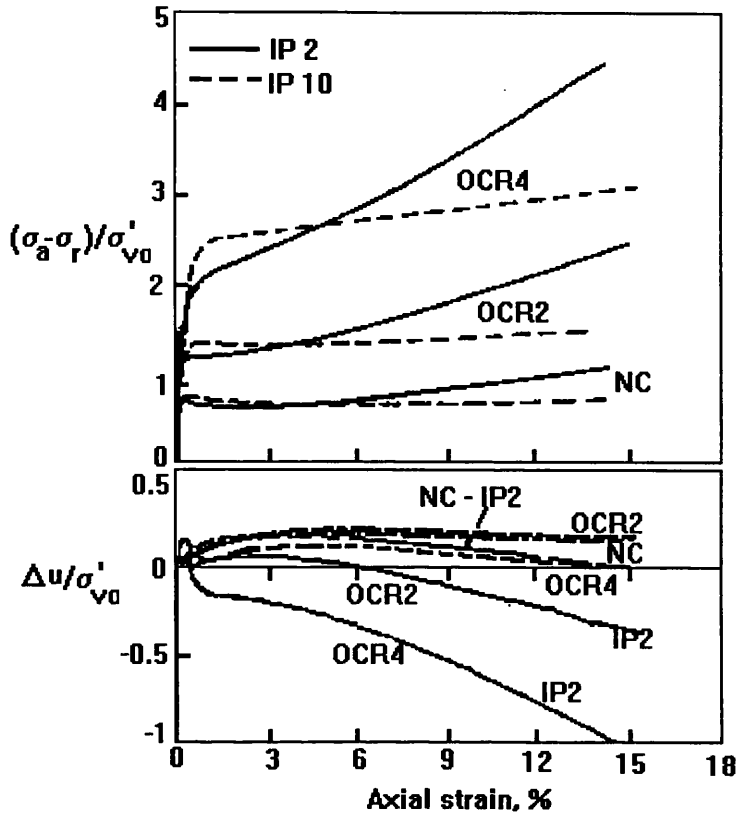

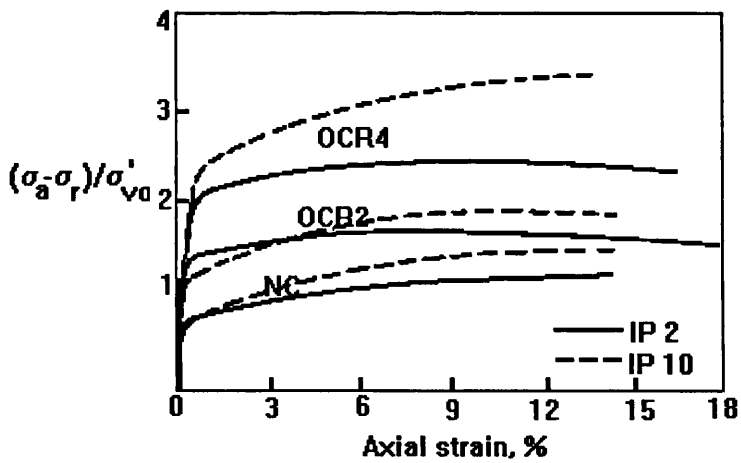

Fig.1.9 Results of K_0 consolidated triaxial compression tests: (a) undrained (b) drained (Kimura et al. 1994)

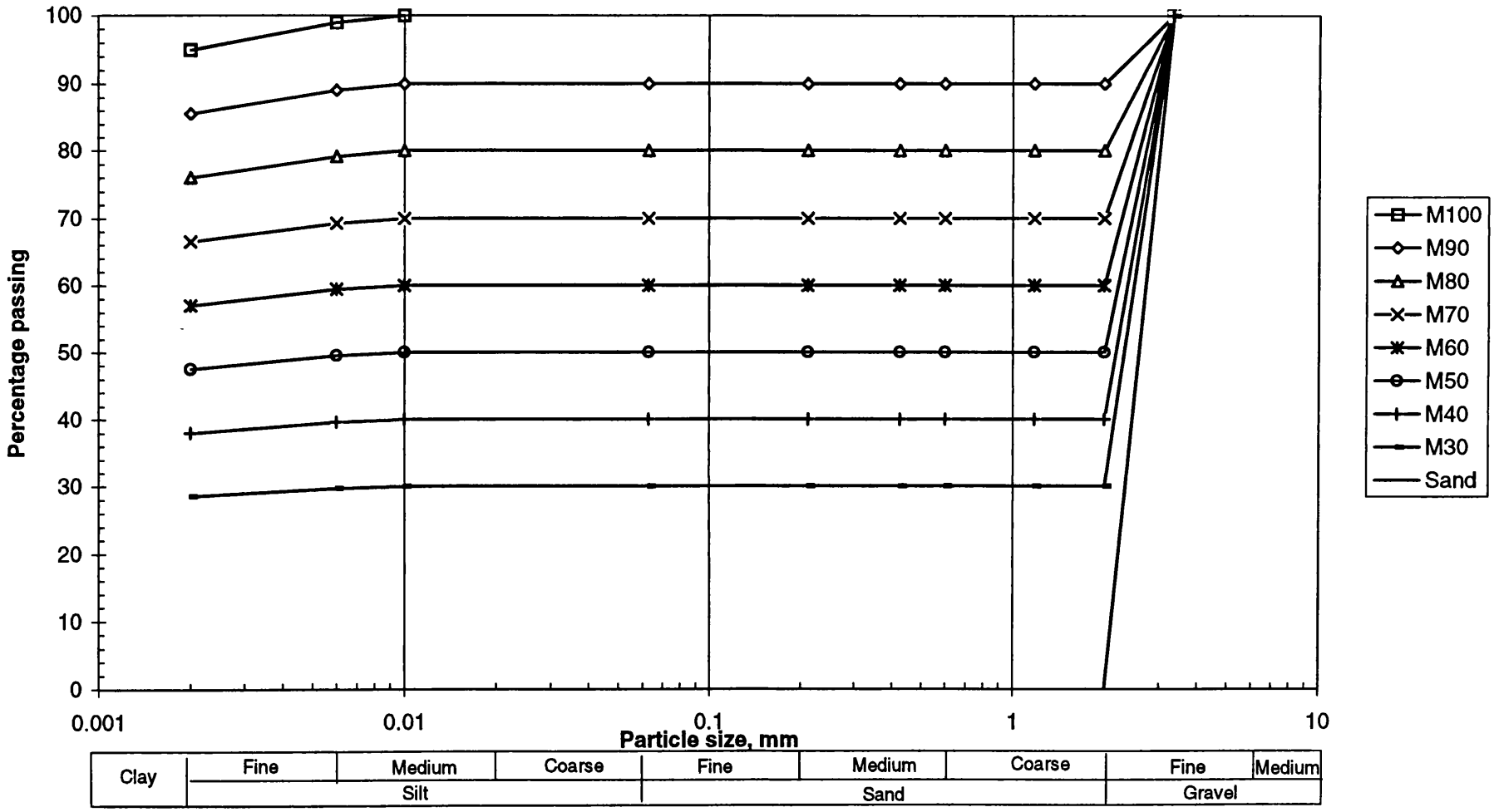

Fig.1.10 Grain-size distribution curves of different mixtures

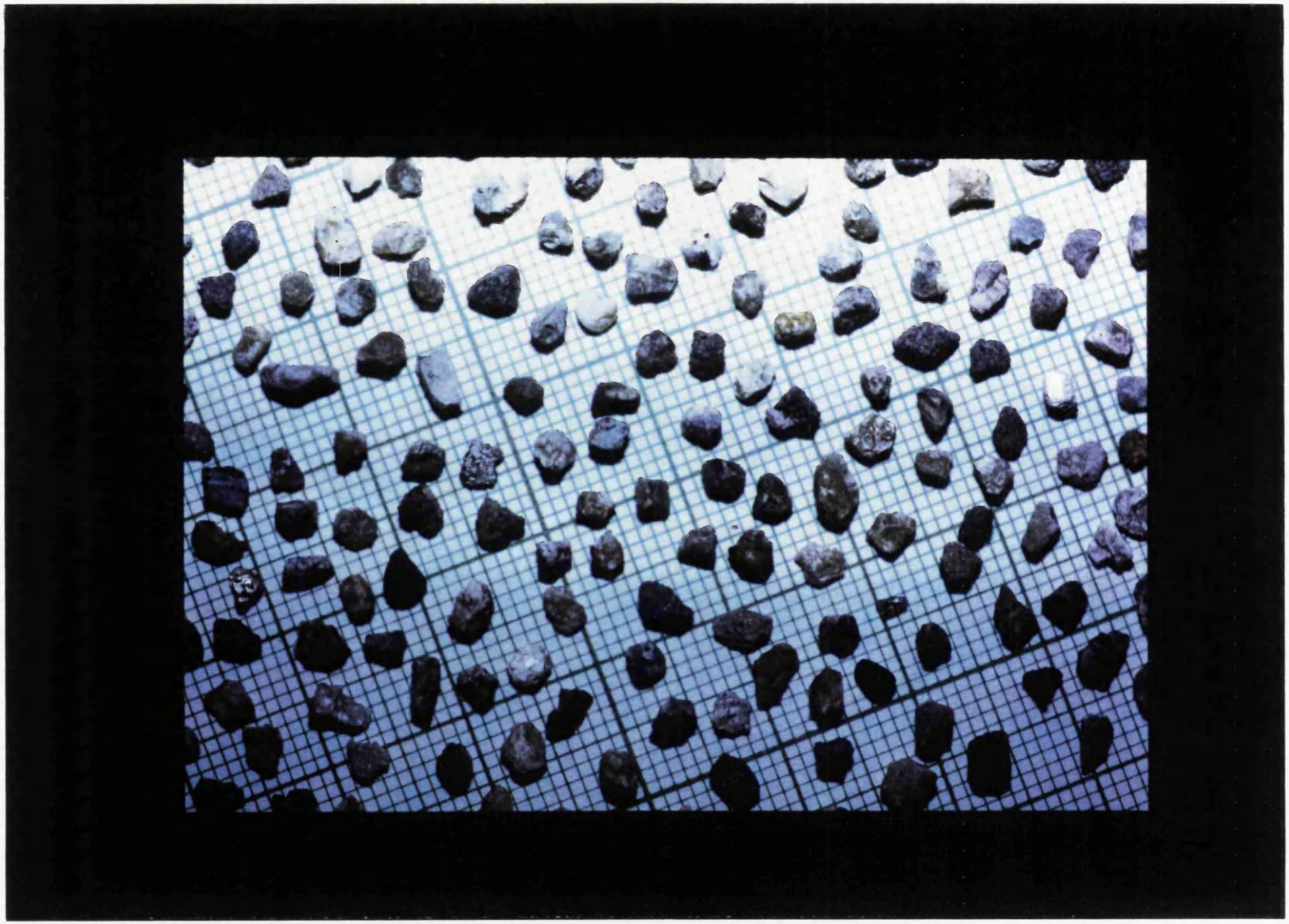

Fig.1.11 Micro photo graph of scotsand grains

CHAPTER 2

INDEX TESTS

The so called Atterberg limits developed following the work of Atterberg (1911) have been widely used in soil mechanics since their potential value was first indicated by Terzaghi in 1926. Terzaghi (1926) wrote of this subject " -- the results of the simplified soil tests (Atterberg limits) depend precisely on the same physical factors which determine the resistance and the permeability of soils only in a far more complex manner --". Recognising its important Casagrande (1932) developed a standard device for determination of liquid limit which is widely used throughout the world as a standard test for classifying soils. Norman (1958) and Casagrande (1958) have recognised the shortcomings of Casagrande apparatus, particularly with regard to reliability, repeatability and consistency. Casagrande (1958) suggested that the liquid limit test as defined by Atterberg is a dynamic shear test and cannot provide a uniform basis for comparing fine-grained soils which differ in their reaction to a shaking test and a simple direct shear test or an indirect shear test, e.g. a static penetration test, would eliminate many of the difficulties of the liquid limit device.

The Geotechnical Commission of the Swedish State Railways between 1914 and 1922 experimented with cone penetrometers as a means of determining the undrained shear strength of soils and a detailed study of the relationships between cone penetration and soil strength is reported by Hansbo (1957). Sherwood and Ryley (1970) have shown that a fall cone test gives a more consistent estimate of the liquid limit than the Casagrande device with greater repeatability and less operator susceptibility.

Wroth and Wood (1978) have gone further and derived the following expression linking undrained shear strength c_u with the weight of the cone W and depth of cone penetration d (Fig.2.1) on the basis of dimensional analysis

$$\frac{c_u d^2}{W} = k_\alpha \qquad (2.1)$$

where k_α is a cone factor which depends on the angle of the cone.

Introducing ideas of critical state soil mechanics (see section 5.4.1), and using Eq.2.1, the authors have shown that a plot of water content w against d for a constant cone weight gives a line

$$w - \frac{2\lambda}{G_s} \ln d = \text{constant} \qquad (2.2)$$

which will be a straight line on a semi-logarithmic plot (Fig.2.2) with gradient $\frac{2\lambda}{G_s}$, where λ is slope of normal compression line in $v:\ln\sigma'_v$ plane (see section 3.2); G_S is the specific gravity of soils particles.

Muir Wood (1990) has discussed in detailed the analysis of the fall cone test in terms of critical state strength and has shown the ways in which the fall cone test can be used to deduce information concerning the compressibility, plasticity, and water content - strength relationships for soils. In the analysis Muir Wood assumes a standard undrained shear strength of soil at liquid limit approximately equal to 2 kPa (Norman 1958; Wroth and Wood 1978) and strength at plastic limit is 100 times the strength at the liquid limit, based on experimental evidence from Skempton and Northey (1953); and strength data collected by Mitchell (1976). Muir Wood has shown the link between plasticity index I_p and compressibility λ:

$$I_p = \frac{\lambda \ln 100}{G_s} \qquad (2.3)$$

The method proposed by Muir Wood (1990) allows the determination of both liquid and plastic limits from fall cone tests. Since the liquid limit gives a rough indication of the undrained shear strength of a soil, the extent to which the liquid limit of the clay/sand mixtures is controlled by the clay phase, which is the main subject of this chapter, is part of a wider consideration of the influence of the sand phase on the undrained strength of the mixtures.

In the standard method of liquid limit determination (BS 1377:1991), the soil fraction passing through the 425 μm sieve is used. This limiting particle size has been chosen based on the assumption that particles coarser than this size will not contribute to the plasticity of the soil. Further, the cutting of a groove in the Casagrande percussion liquid limit device is not possible in soils containing coarse particles. Natural soils often also contain particles coarser than 425 μm, and the liquid limit of such soils, as conventionally determined, gives only an incomplete indication of their mechanical characteristics. In this study, the effectiveness of the fall cone method in determining the liquid limit of soils which contain particles of 2 mm size (coarser than 425 μm) will be investigated . There is nothing intrinsic to the fall cone test which should prevent its use with soils containing coarse particles.

2.1 PREVIOUS STUDIES

Seed et al. (1964) have indicated that the presence of sand particles smaller than 425 μm will reduce the liquid limit in linear proportion to the sand content of the soils (such as kaolinite, illite, montmorillonite and their mixtures) provided that the clay content is greater than 10% for inorganic clays and 20% for organic clays.

In 1966, Dumbleton and West investigated the influence of coarse fraction on liquid limit of kaolinite and montmorillnite soils. Various coarse fractions considered were: spheres (glass), angular glass, angular quartz and flaky particles. They found that the linear mixture law is valid only with glass spheres. They concluded that small particles of coarse materials produced greater effect on the liquid limit than the larger particles due to their higher specific surface area.

Rao (1978) investigated liquid limit characteristics of illite, bentonite mixtures with fine to medium sand and concluded that the linear law proposed by Seed et al. (1964) holds good up to sand content 70% in the mixture.

Sivapullaiah and Sridharan (1985) studied a wide range of bentonite mixtures with sand fraction smaller than 425 μm and came to the conclusion that liquid limit of mixtures of soils is not governed by the linear law.

Nagaraj et al. (1987) investigated the effectiveness of cone penetration method to determine the liquid limit of black cotton and red earth soils containing particles coarser than 425 μm by selecting 1) smooth spherical glass of uniform size of 0.5 mm and 2) crushed angular quartzite particles passing through 2 mm sieve and retained on 0.6 mm sieve. They concluded that the surface frictional characteristics of coarse particles have no influence on the liquid limit of soils which is in contradiction to the observations of Dumbleton and West (1966).

Tan et al. (1994) investigated the influence of medium sand on the liquid limit of marine clay, montmorillonite and montmorllonite+kaolinite soils and proposed a different linear law by considering clay and silt fraction. The authors concluded that the linear law is valid up to sand content 60% in the mixture. But Seed et al. (1964) wrote about the silt fraction: " -- it may be questioned whether the use of the proportion of particles finer than 0.002 mm provides a valid basis for determining the proportion of clay present in the soils, but for a given type of clay any error resulting from the use of this arbitrary boundary would simply change the slope of the relationship but not the form ".

The above review reveals that there is experimental evidence that the liquid limit obeys a linear law for soils consisting of clay mixed with fine to medium sand and the main objective of this chapter is to investigate the extent to which a similar relationship applied also to mixtures of clay and coarse sand.

2.2 TEST PROCEDURE

Clay-sand mixtures were prepared with the weights of kaolin and sand according to the chosen proportion. All components were in the air dry condition when mixed together (BS1377 : 1991). After adding sufficient quantity of water, the mixture was cured for 24 hours to allow water to permeate through the soil mass.

The liquid limit values of the mixtures were determined by the standard procedure specified in BS 1377 (1991) using a fall cone penetrometer with a cone of mass 80 g with tip angle of 30° and penetrating 20 mm. The experiments were conducted in the normal range of penetration of 15 to 25 mm in order to generate the flow curves. Several experiments were repeated in order to check the reproducibility of the results.

2.3 TEST RESULTS AND DISCUSSION

2.3.1 Liquid limit

The flow curves in terms of moisture content of the mixture and the penetration (mm) are shown in Fig. 2.3. The moisture content corresponding to cone penetration of 20 mm is defined as the liquid limit w_L of soil, and it is calculated from Fig. 2.3. These values are shown in Fig. 2.4 as a function of clay content.

If the coarse fraction played no part in determining the liquid limit of clay-sand mixtures except by occupying some bulk of the mixture, so that the liquid limit of the mixture was reached when just enough water was present to bring the clay fraction to its liquid limit, then the relation between liquid limit and clay content would be a straight line passing through both the origin and the value for 100 % clay. This linear relation is shown in Fig. 2.4 as a solid line. From this plot it is clear that the linear law holds down to a clay content of 40% in the mixture. However, after that, for clay contents of 30% and below in the mixtures, the data suggest that deviations will become significantly large.

If the clay water content w_{cL} (Eq. 1.9) is calculated for the measured liquid limit of each mixture, then it is found that this is more or less independent of clay content until the clay content falls below about 40% (Fig. 2.5). This

implies that the presence of the coarse sand is not affecting the penetration resistance of the clay at the low strength that it has for water contents around the liquid limit (where the undrained strength of the clay is of the order of 2 kPa (Muir Wood, 1990)) until 70% of the volume of solid material is made up of hard sand particles. Tan et al. (1994) have also reached similar conclusion for the mixtures of clay with medium sand. However, Seed et al. (1964) and Rao (1978) found that the linear law holds up to sand content 70% for the mixtures with fine to medium sand. The authors used Casagrande device for determination of liquid limit. The results in Fig.2.4 & 2.5 and the findings of Tan et al. (1994) confirms that the linear law holds up to sand content 60% for soils with medium to coarse sand.

For the mixture with clay content C = 40%, and with the clay water content equal to the liquid limit of the pure clay, the implied granular specific volume is around 3.1 and the corresponding particle spacing in a close packed hexagonal array of spherical particles from Fig.1.3 is 1.3d. The volume of soil displaced by 20 mm penetration of a 30° cone is 600 mm^3 and with granular specific volume 3.1 and typical particle diameter 2 mm it can be deduced that roughly 50 sand particles are displaced together with the clay paste as the cone penetrates. It is perhaps surprising that even at this density of packing the presence of the sand particles appears to have no mechanical effect on the penetration of the cone.

2.3.1.1 Estimation of compressibility λ from fall cone test data

The predicted values of compressibility λ of mixtures are presented in Fig.2.6 against clay content. The values of λ are deduced from the fall-cone test data in Fig.2.3 and working from the gradient of the lines (Eq.2.2) and by taking $G_S = 2.65$.

2.3.2 Plastic limit

It is not possible to follow the standard procedure for the plastic limit test and to roll out a 3 mm thread of the clay/coarse sand mixture. However, the effective plastic limit of the mixture can be determined by assuming that the mixture has a certain activity A (Skempton, 1953) independent of clay content

$$A = \frac{I_p}{C} \tag{2.4}$$

where I_p is plasticity index. The estimated plastic limits w_p of the mixtures are shown in Fig. 2.7 and the implied plotting on the plasticity chart I_p : w_L is shown in Fig. 2.8.

The plastic limits of the mixtures can alternatively be estimated from fall cone test data by Eq.2.3 with λ values in Fig.2.6. The estimated plastic limits from fall cone tests are compared in Fig.2.9 with the values in Fig.2.7 obtained from assumed activity of clay. Fig.2.9 also shows the best fitting line obtained by linear regression analysis. The agreement between the estimated plastic limit values obtained from fall cone test data and from activity of clay is quite satisfactory in Fig.2.9 and confirms that the fall cone test data can be used for the determination of plastic limit as discussed by Muir Wood (1990).

2.4 CONCLUSION

The results of the fall cone liquid limit tests indicate that for a large range of clay contents (40-100%) this soil property is controlled only by the water content of the clay phase and that the presence of the sand particles has no mechanical effect.

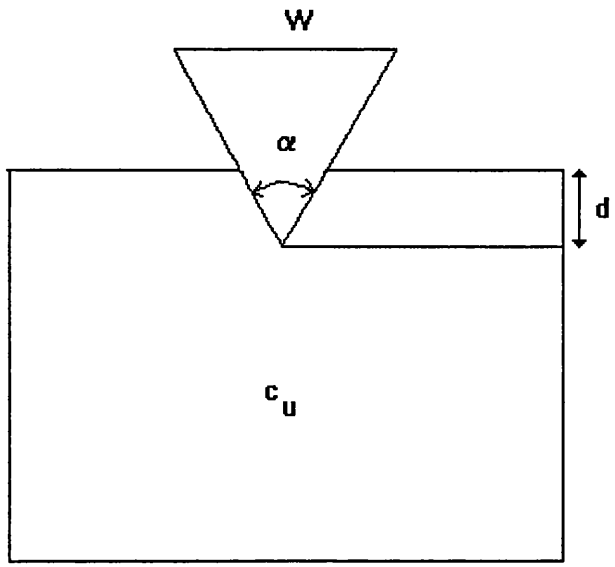

Fig.2.1 Diagram of fall cone test

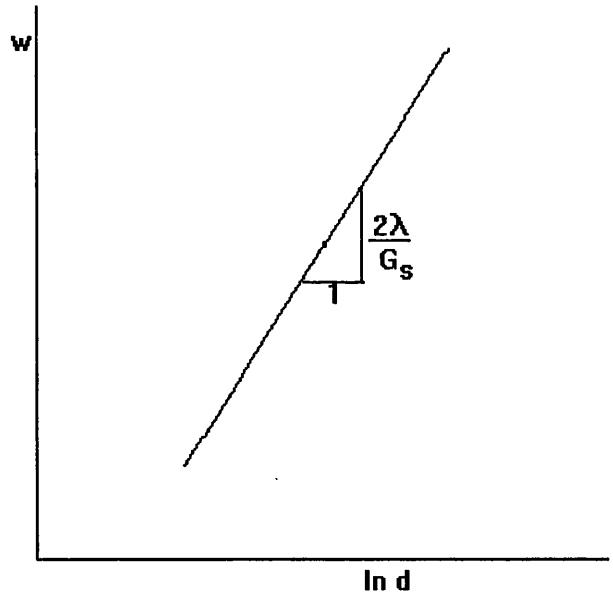

Fig.2.2 Diagram of fall cone result

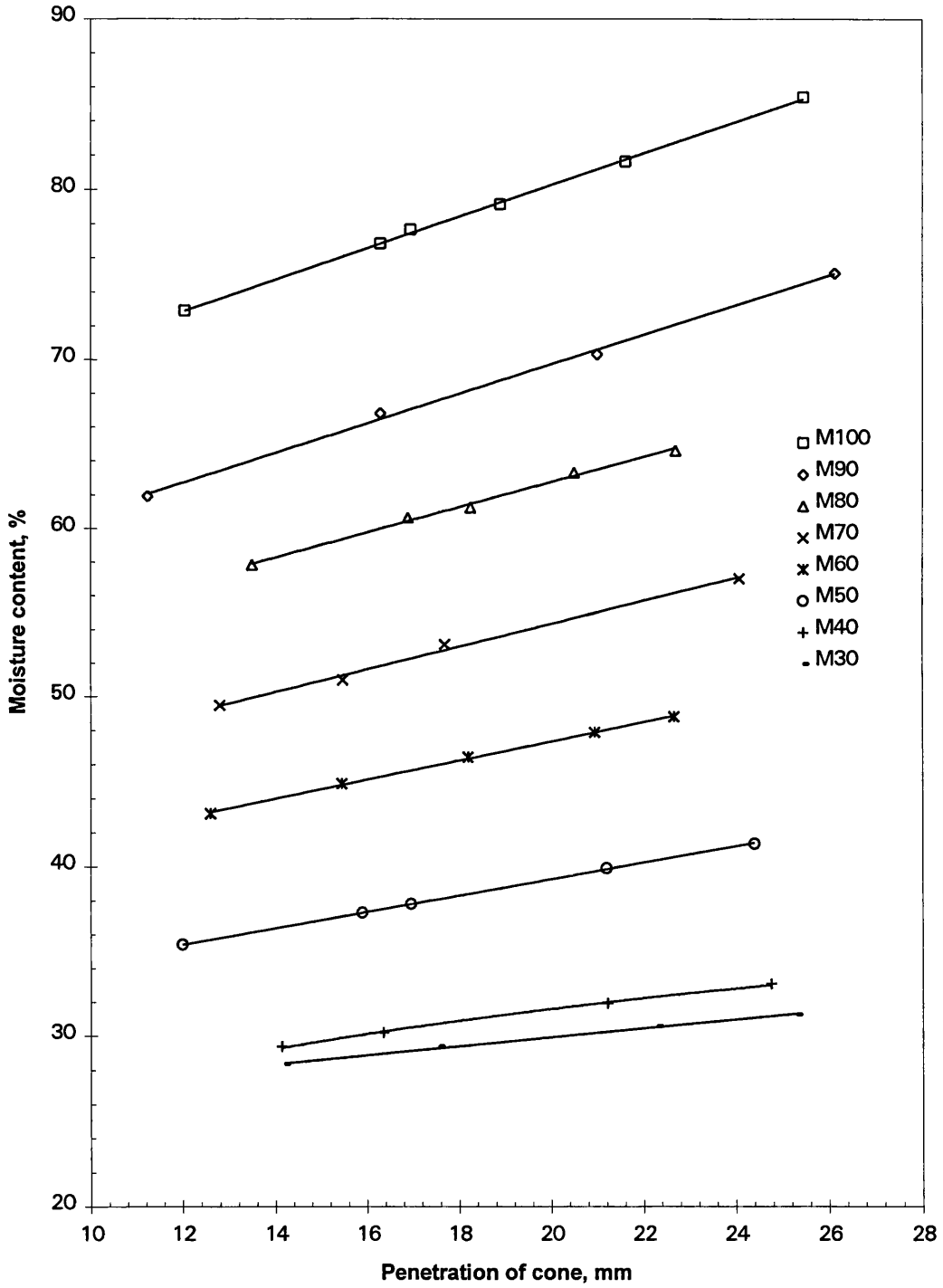

Fig.2.3 Flow curves

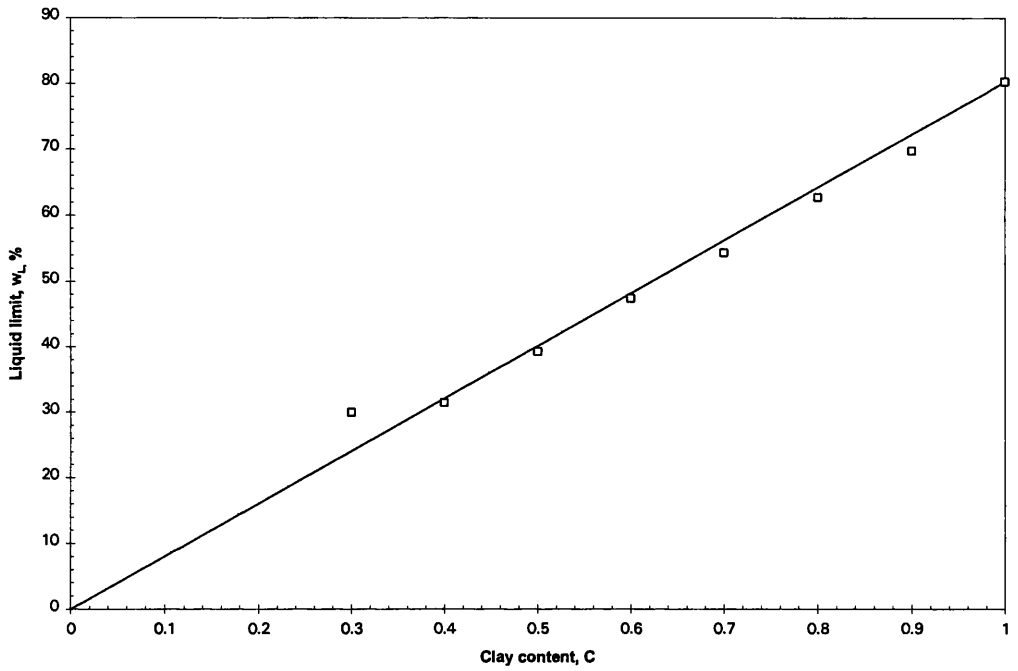

Fig.2.4 Variation of liquid limit with clay content

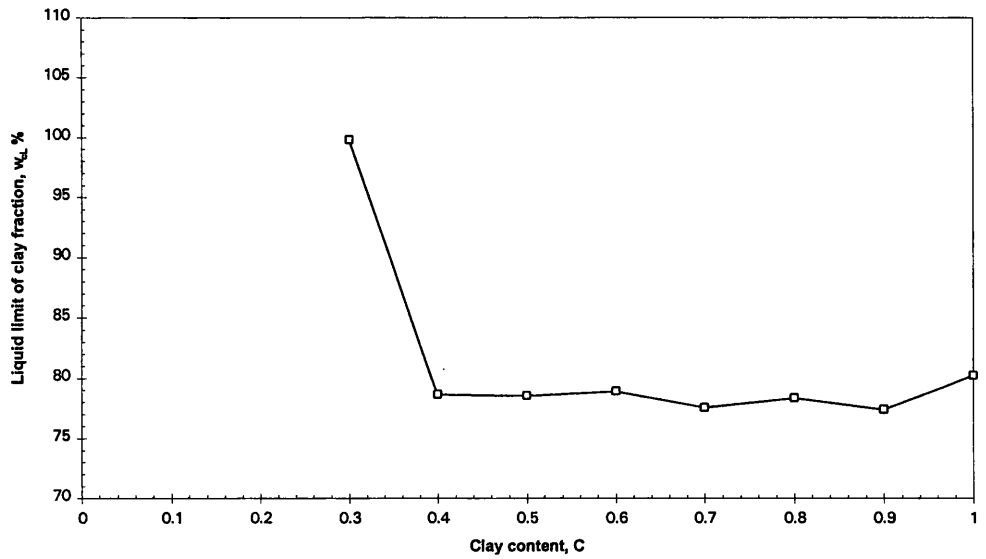

Fig.2.5 Liquid limit of clay fraction and clay content

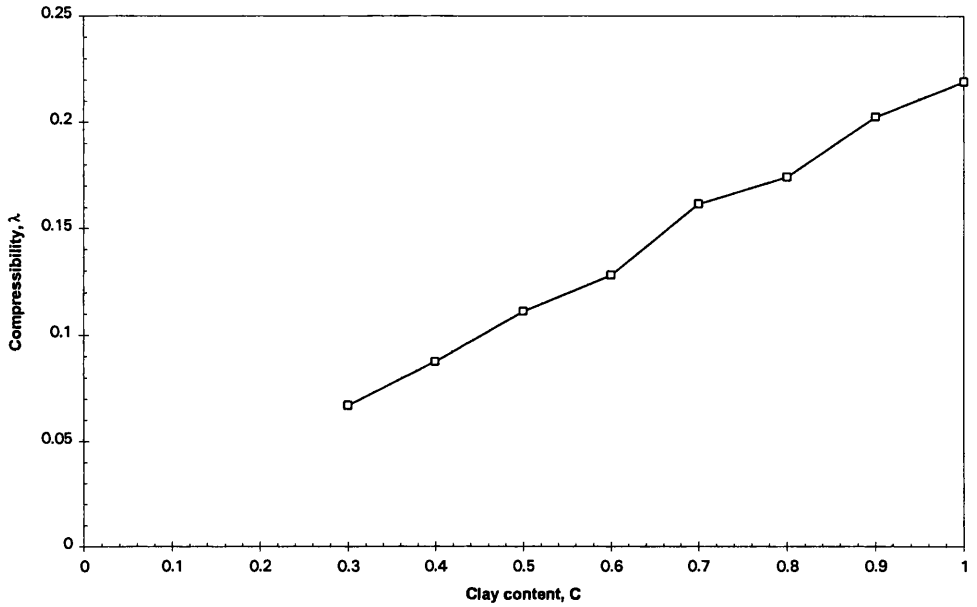

Fig.2.6 Estimated λ against clay content

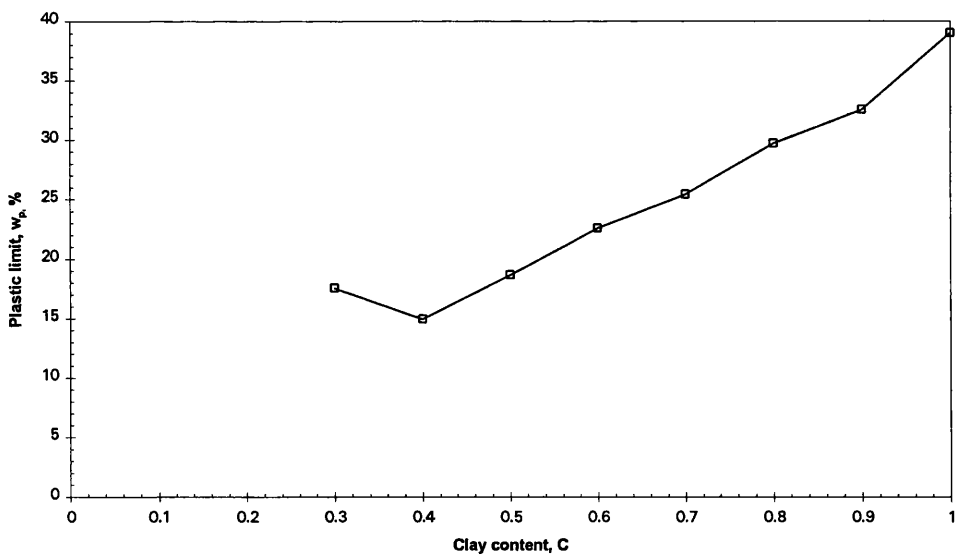

Fig.2.7 Estimated plastic limit-clay content for mixtures

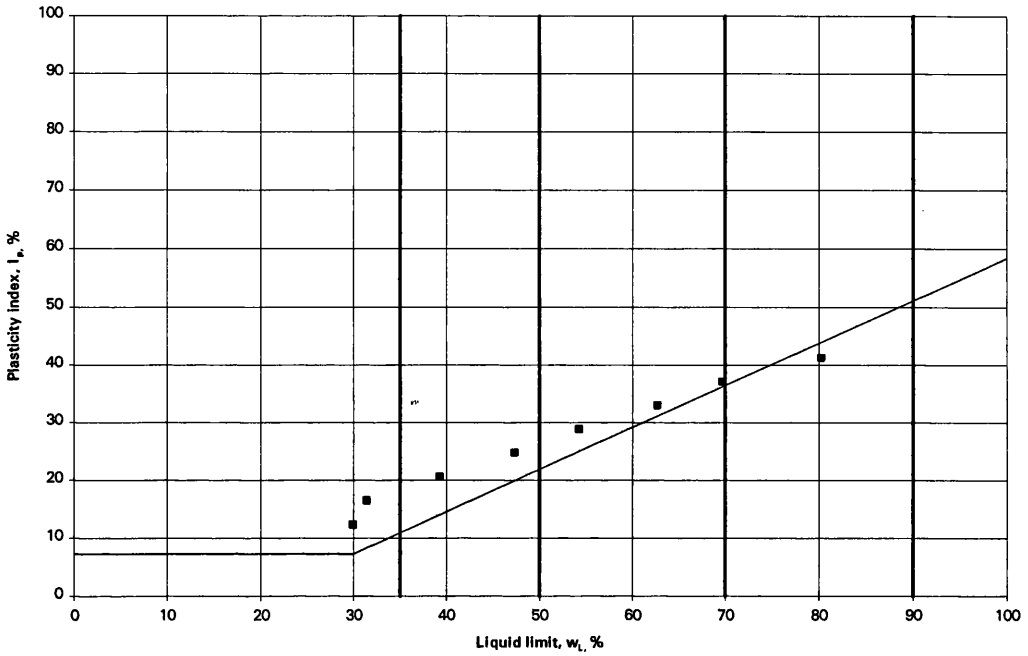

Fig.2.8 Estimated plasticity index and liquid limit for mixtures

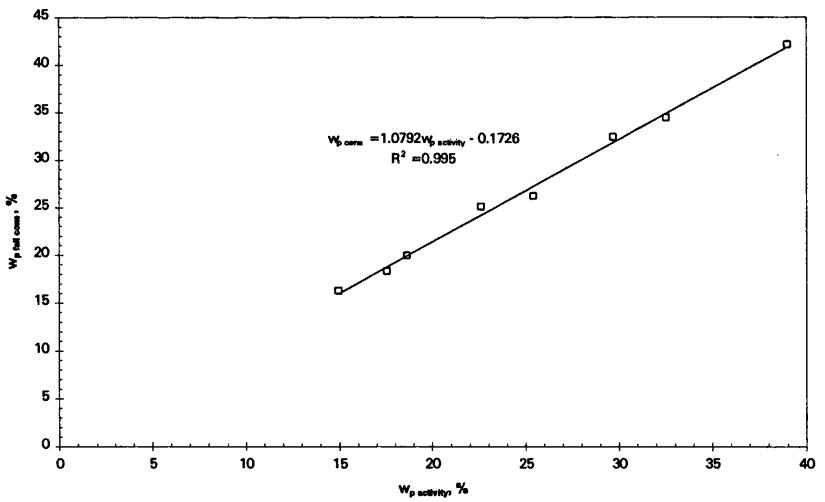

Fig.2.9 Relationship between plastic limit (fall cone) versus plastic limit from activity

CHAPTER 3

CONSOLIDATION CHARACTERISTICS

Compressibility of soil refers to the property of decrease in volume by the reduction of the pore space as the soil grains come into closer packing. This reduction can be brought about in several ways, for instance by consolidation with slow gradual expulsion of pore water which is so important in settlement problems. Since about 1930, engineering practice for predicting the magnitude and rate of settlements of soil foundations has been based on Terzaghi 's theory of one dimensional consolidation. The information for application of this theory is generally obtained from parameters measured in oedometer tests. This chapter examines the one dimensional compression properties of clay/sand mixtures with the objective of discovering the extent to which the presence of the coarse sand influences the compressibility of the mixtures.

In this chapter, section 3.1 explains the apparatus and experimental procedures followed to perform one-dimensional compression tests, section 3.2 outlines the solution to conventional interpretation of one-dimensional consolidation and formulates the basis for presentation and discussion of experimental results in section 3.3.

3.1 APPARATUS AND EXPERIMENTAL PROCEDURES

This section describes the apparatus used in the experimental investigation, the preparation of clay-sand samples, and the procedure followed in performing the tests. One dimensional consolidation tests were performed in a hydraulic oedometer up to a vertical effective stresses of 480 kPa and in a consolidation tube, with dead weight loading, in order to apply higher stresses ranging up to nearly 1600 kPa. All the tests were performed in a climatically controlled laboratory with the temperature held constant at 20° C.

3.1.1 One-dimensional compression in hydraulic oedometer

Consolidation testing has been carried out using a hydraulic oedometer - Rowe cell (Rowe and Barden 1966). The general layout of the system is shown in Fig.3.1. The oedometer has three plumbing connections (Fig.3.1): water pressure (controlled from a central air pressure system through a bladder air-water interface) provides the jack pressure which drives the consolidation process; drainage is controlled by GDS digital pressure controllers (manufactured

by GDS Ltd.) which measure both the pressure and the flow of water on the drainage lines connected to top and bottom drainage points which are connected to GDS1 and GDS2 respectively, the two GDS pressure controllers.

A Rowe cell with internal diameter 76.2 mm as shown in Fig.3.2 was used. Drainage is vertical between porous plastic discs covering the full cross section of the sample, formed from a sheet of 1.6 mm Vyon cut to fit neatly inside the consolidation ring. The jack pressure is applied to a shaped membrane. The jack pressure can be controlled by a bleed valve to a maximum of about 700 kPa.

The digital pressure controllers can provide pressures in the range of 0-2000 kPa and pressures are reported to the controlling computer with a resolution of 0.2 kPa. The volume change capacity is 200 cm^3 and volume changes can be recorded with a resolution of 0.5 mm^3. A detailed description of the GDS pressure controllers is given by Menzies (1988). These devices were controlled by a simple computer program which can be used to impose constant back pressure during consolidation stage and constant flow rate during permeability stage and to monitor current values of pressure and volume.

The digital pressure controllers and computers were kept switched on at all times in order to maintain thermal equilibrium and constant performance.

3.1.1.1 Sample set up in oedometer

Clay-sand slurry samples were set up in the oedometer as shown in Fig.3.3. The drainage lines through the base and cover of the oedometer were de-aired before each test by flushing de-aired water and then their ends were closed. The porous metal disc and porous plastic sheet were de-aired by boiling them for an hour before use. Before setting up, the inner wall of the cell was greased with silicon grease to help reduce the side wall friction. The setting up procedure is as follows:

a) Oedometer cell was placed on the circular perspex plate as shown in Fig 3.3a. A spacer was then slid into the oedometer cell. A saturated perforated brass disc and a wet porous plastic sheet were placed over the spacer.

b) The clay-sand slurry was then spooned into the oedometer in small amounts and tapped to ensure that no air bubbles were trapped. When the cell was completely filled up, the surface of the sample was levelled using spatula. To allow for small projected area of the base and porous sheet (i.e. 3 mm), a preformed thin perspex piece was used to level the slurry surface as in the Fig.3.3b

c) A saturated porous sheet was placed on the top and the surface was topped up with de-aired water. Meanwhile, the ring bottom was greased and the base was then placed over the cell as shown in Fig.3.3c. During this operation care was taken not to drop the O-ring seal from its groove.
d) The inverted oedometer (with base and perspex plate held firmly) was then turned quickly to its upright position and the spacer was slowly pulled out (Fig.3.3d).

A layer of water was placed in the top of the oedometer and the top of the oedometer with the shaped jack membrane was attached carefully, avoiding the trapping of any air between the membrane and the soil with its drainage boundaries. The completed sample set up is shown in Fig.3.2.

Once the sample was completely set up in the oedometer but before it was connected it to the permeability measurement system, a final measure to de-air the apparatus and fully saturate the sample was achieved by applying a vacuum. The whole oedometer set up was submerged in water in a desiccator and the drainage ports to the bottom and top and the connection the jack chamber were submerged and opened. A vacuum was slowly applied through the top of the desiccator cover for an hour. This technique ensures that the sample is not subjected to undue stress while the air is removed. Valves to all the ports were closed under water and the oedometer was then connected to the consolidation measurement system as shown in Fig.3.1.

3.1.1.2 Experimental procedure

Once the sample was set up as shown in Fig.3.1, the volumes displayed by GDS1 and GDS2 were recorded and the reading of the dial gauge, showing the change in height of the sample, was recorded. Before the consolidation stage, to check that 100% saturation had been reached, the two controllers were set to constant volume mode in order to maintain an undrained condition in the sample. The jack pressure, which is equal to the vertical total stress (σ_V), was raised in steps of 10 kPa every 5 minutes until it reached 60 kPa. If the sample is fully saturated and there is no leakage in the system, the pore pressure increase will be equal to the jack pressure increment after a short time. The value of the pore pressure parameter B is calculated as the ratio $\Delta u/\Delta\sigma_V$ where Δu is the pore pressure response to an increment of total vertical stress $\Delta\sigma_V$. This assumes that the increment of horizontal total stress is also $\Delta\sigma_V$. Saturation is generally accepted as being complete when the B value reaches about 0.96 (Black and Lee 1973). In routine tests a degree of saturation of 99% was achieved. After the saturation stage, the sample was ready for the consolidation stage.

In the consolidation test, equal strain loading to maintain a uniform sample thickness was applied with double drainage. To start the test, the back pressure in the sample was finally brought to 50 kPa by setting the GDS digital controllers to maintain a target pressure of 50 kPa. With this procedure, the initial consolidation pressure was brought to a vertical effective stress of 10 kPa. The dial gauge reading was noted and the data logging was switched on at a 0.3 minute interval. After 15 minutes, the data were logged at 15 min interval to avoid excessive data at too close intervals being obtained. The data consisted of pressure and volume quantities corresponding to various elapsed times. Simultaneously dial gauge readings were noted manually for the first 30 minutes, immediately after starting the test.

Typical tests consisted of alternating consolidation and permeability stages. Consolidation under a given load increment was allowed to occur over a period of 24 hours. Permeability testing was then performed over the next few hours and is discussed separately in Chapter 4. The standard loading history is shown in Fig.3.4.

After completion of the test with the final unloading stage, the pressure was reduced to the initial seating pressure. When equilibrium had been achieved, the final settlement and volume change readings were recorded. The cell top was unbolted and final height of the sample was recorded for the final sample volume. The sample was removed intact from the cell and four representative portions were used for final moisture content measurement. After moisture content determination, wet sieving was performed for the determination of percentage of sand present in the sample. The maximum difference observed in the final water content and sand content down and across the sample was found to be 0.2-0.35%. Void ratios and specific volumes at various stages during the tests were back calculated from the final water content together with the volume changes measured with the GDS pressure controllers for comparison with the changes in height monitored using a dial gauge.

3.1.2 One-dimensional compression in consolidation tube

One dimensional compression tests with pressures ranging from 0-1592 kPa, were conducted on clay/sand samples using a consolidation tube shown in Fig.3.5. This consists of a piece of thick walled aluminium cylinder of internal diameter 38 mm, wall thickness of 12 mm and 235 mm height. This cylinder was precision machined to fit exactly around the bottom pedestal and top cap of a triaxial cell base for a 38 mm specimen. Pairs of o-ring seals were used in the grooves around the bottom pedestal and top cap to avoid any leakage.

A large quantity of silicon grease was smeared round the consolidation tube to minimise side friction. One Vyon porous disc (1.6 mm thick) was placed on the bottom pedestal and kept submerged in water. The clay/sand mixture was then spooned in carefully to a height of 60 mm in the consolidation tube. Then at the top of the tube, a vacuum of 20 kPa was applied for an hour so as to remove any trapped air bubbles. The above process was repeated for the next two layers. Enough slurry was put in the tube to fill it up to 180-190 mm. After completing placement of the slurry, the top of the specimen was levelled and a Vyon disc was placed on the top of the slurry and the top platen with the top drainage connection was lowered into the consolidation tube and placed on the top of the slurry. The triaxial cell for 38 mm specimen was fitted to the base pedestal and a loading piston was lowered into the consolidation tube and placed on the top platen. The triaxial cell acts as stabiliser to maintain the alignment of the loading piston. The vertical load was then applied using dead weights on a hanger which balanced on the piston as shown in Fig.3.6. The piston was able to slide into the consolidation tube as the sample consolidated.

In the consolidation tube the clay/sand samples were consolidated one-dimensionally to a vertical effective stress of 1592 kPa. This was achieved by applying a total vertical load 406 lb including the weight of the hanger in increments of 2.5, 5, 10, 20, 40 , 80, 160, 323, 406 lb. Time intervals of about 24 hours were left between each load increment to allow complete consolidation.

At the end of consolidation, the bottom and top drainage valves were closed and the triaxial cell and top cap were carefully removed and the specimen was extruded with hand operated hydraulic jack for water content determination. The quality of the specimen, in terms of variation of sand content and water content along its height from the top, was checked by measuring the sand and water contents along its height as shown in Fig.3.7 and Fig.3.8. The maximum variation of sand content observed was 0.7-0.8%, whereas the variation of water content was 0.5-0.8%.

3.2 ONE DIMENSIONAL THEORY OF CONSOLIDATION

Consolidation tests are routinely performed in geotechnical engineering and rates of consolidation will be evaluated based on Terzaghi's theory of one dimensional consolidation.

Terzaghi's theory is based on the following assumptions:

1) The soil is homogeneous.

2) The soil is fully saturated.

3) The soil grains and the pore water are incompressible.

4) The flow is one-dimensional and occurs according to Darcy's law.

5)The soil's compressibility and permeability are constant during the consolidation process.

6) There is a linear relationship between effective stress and strain.

7) The strains in soil are small and one dimensional.

8) The soil presents no creep or secondary deformation.

The differential equation of one dimensional consolidation (Terzaghi 1943) developed in terms of excess pore water pressure u, depth z and time t is :

$$c_v \frac{\partial^2 u}{\partial z^2} = \frac{\partial u}{\partial t} \tag{3.1}$$

where c_V is coefficient of consolidation

$$c_v = \frac{k}{m_v \gamma_w} \tag{3.2}$$

m_V is coefficient of volume compressibility, k is coefficient of permeability and γ_w is unit weight of water.

The boundary conditions of the problem of the conventional one dimensional consolidation of a sample of height 2H are:

1) There is complete drainage at the bottom of the sample, $z = 0$; $u = 0$.

2) There is complete drainage at the top of the sample, where $z = 2H$; $u = 0$.

3) The initial hydrostatic excess pressure is equal to the increment of vertical total stress; $t = 0$; $u = u_i$.

The solution to Equation(3.1) for the above three boundary conditions is

$$\overline{U} = 1 - \frac{8}{\pi^2} \sum_{n=0}^{n=\infty} \frac{1}{(2n+1)^2} \exp\left[\frac{-(2n+1)^2 \pi^2 T_v}{4}\right] \tag{3.3}$$

$\overline{U}$ is average degree of consolidation and is the ratio of the settlement at time t to the final settlement.

In Eq.3.3, $T_v = \frac{c_v t}{H^2}$ (3.4)

and is a dimensionless time factor, a function of coefficient of consolidation c_V, time t and drainage path H.

In conventional consolidation analysis two graphical methods are routinely used for evaluating c_V: the square root of time method (Taylor 1948) and the logarithm of time fitting method (e.g. Taylor 1948).

In this study, Taylor's square root of time method was used. A theoretical curve (Fig.3.9) on the square root of time plot is a straight line up to about 60% consolidation. In the square root of time graphical construction the experimental time for 90% primary consolidation, t_{90}, is deduced by drawing a line from the origin at a slope of 1.15 times the initial linear slope. The point where this line cuts the graph represents t_{90}. The coefficient of vertical consolidation c_V, can then be calculated from

$$c_v = \frac{T_v H^2}{t_{90}} \tag{3.5}$$

At 90% consolidation $T_V = 0.848$ and hence

$$c_v = \frac{0.848\ H^2}{t_{90}} \tag{3.6}$$

The solution to Eq.3.1 outlined above will be helpful in Chapter 4 to understand steps involved in the evaluation of the permeability from consolidation data and from transient phase flow pump tests.

In critical state soil mechanics data of one dimensional compression are usually plotted in terms of specific volume and natural logarithm of vertical effective stress (Muir Wood, 1990) and the coefficient of volume compressibility (m_V) can be defined in terms of specific volume as

$$m_v = \frac{-\delta v}{v \delta \sigma'_v} \tag{3.7}$$

where δv is an increment of specific volume caused by a change of vertical effective stress $\delta \sigma'_v$ and v is the specific volume at the start of the loading increment.

The data from one dimensional compression on clays may usually be idealised by the straight lines shown in Fig.3.10. The slope of the lines for normal consolidation and swelling (λ, κ) from one dimensional compression tests are close to the slopes obtained from isotropic compression tests (Muir Wood 1990) although some differences arise in principle during unloading due to the variation of K_O in the oedometer during unloading so that the ratio of vertical

stress and mean stress is not constant. Butterfield (1979) noted that the normal compression and the swelling lines may be more accurately described by straight lines in lnv- $\ln\sigma'_v$ space rather than v- $\ln\sigma'_v$ space over a wider range of effective stress. In this study the relationship between v and σ'_v is plotted in lnv - ln σ'_v space, such that the equation of the normal compression phase is

$$\ln v = \ln A^* - \lambda^* \ln\sigma'_v \tag{3.8}$$

and the equation of the swelling phase is

$$\ln v = \ln B^* - \kappa^* \ln\sigma'_v \tag{3.9}$$

where A* and B* are reference values of specific volume for vertical effective stress σ'_v= 1 kPa. Note that the values of λ^*, and κ^* obtained from Eq.3.8 and 3.9 will be different from those obtained from v : $\ln\sigma'_v$.

3.3 RESULTS AND DISCUSSION

3.3.1 Consolidation test data

One-dimensional compression data for the clay/sand mixtures obtained from Rowe cell are shown in Fig.3.11 as a series of relationships between specific volume and vertical effective stress in lnv - $\ln\sigma'_v$ space. One-dimensional compression tests were also performed in consolidation tube in order to apply higher stresses and the observed relationships between specific volume and vertical effective stress are shown in Fig.3.12. The variations of specific volumes during normal compression in Fig.3.11 & 3.12 are shown in Fig.3.13 against vertical effective stress. The shapes of the curves obtained from Rowe cell and consolidation tube are similar within the range of experimental scatter, but complete matching of individual specific volume or individual curves is a rare event for the given ranges of stresses. Differences in specific volume were observed in the initial stages of loading and are probably due to effect of slight difference in placement water content and the sample being thicker in the early stages. During the final stages of consolidation good correlation is obtained between the two sets of test data.

3.3.2 Influence of clay phase on one-dimensional compression

The relationships in Fig.3.11 & 3.12 do not show the extent to which the clay controls the compressibility behaviour of clay-sand mixtures. The

relationships in Fig.3.11 are replotted in terms of clay specific volume v_c and vertical effective stress in Fig.3.14. The specific volume of the clay phase v_c can easily be calculated using Eq.1.5. It is found that for clay contents down to about 40%, the relationships are more or less unique within the range of experimental scatter and it is only for lower clay contents - sand contents above 60% - that the sand particles interact sufficiently to affect the one-dimensional compression relationship. A similar phenomenon can be seen in Fig.3.15 for the compression data obtained from consolidation tube (Fig.3.12).

One can argue (e.g. Fukue et al. 1986, see Fig.1.6) that for different mixtures, the final stages of consolidation are affected by the frictional resistance between sand particles. It would be expected that the effect of the coarse particles would become progressively more significant as the water is squeezed out of the clay, as the clay void ratio decreases with increasing vertical effective stress. The extent to which the clay controls the behaviour can be viewed by plotting the relationships between clay void ratio and clay content at different stages of consolidation. The values of clay void ratio e_c from Rowe cell for each vertical stress σ'_v are plotted in Fig.3.16 as a function of clay content C: there is a slight tendency for e_c to rise as C falls at the vertical stress of σ'_v = 480 kPa but this tendency is almost negligible for C≥40%. One-dimensional compression tests taken to much higher stresses using dead loading on a consolidation tube confirm that even at vertical stress σ'_v= 1592 kPa the effect of the presence of granular particles is negligible for clay contents above 40% as shown in Fig.3.17. It is clear from Fig.3.17 that the clay controls the consolidation behaviour of clay-sand mixtures even at high stresses which conflicts with the findings of Fukue et al. (1986) on sand-bentonite mixtures. But Graham et al. (1989) have applied much higher stresses than Fukue et al. (1986) and shown that bentonite controls the consolidation behaviour of bentonite-sand mixtures down to a bentonite content 25% (Fig.1.7b). It appears from Fig.3.14-3.17 that the kaolin controls the consolidation characteristics of kaolin-sand mixtures down to a clay content 40%.

An alternative way of showing the above behaviour is to plot the volume change relationships using liquidity index as suggested by Muir Wood (1990) and shown in Fig 3.18a & b. The data of water contents w in Fig.3.18a&b have been plotted in terms of liquidity index I_L which scales water contents of mixtures between their liquid and plastic limits (w_L, w_p):

$$I_L = \frac{w - w_P}{w_L - w_P} \tag{3.10}$$

The values of liquid limits and plastic limits in Fig.2.4 & 2.7 are used in the calculation of I_L in Fig.3.18a &b. The various e-logσ'_v relations down to a clay content 40% in the mixture converge in a narrow band. The position of the curve for M70 is different from the others showing that the dominant influence of the clay phase ceases at a sand content 70% in the clay-sand mixture but the spread is greater than when the data are plotted in terms of clay specific volume.

It is of interest to approximate the curves (M100 to M40) in Fig.3.14 & 3.15 into average normal and swell lines. All the curves are concave up and there appears to be a change in the slopes of normal compression line at about 160 kPa. A similar phenomena was observed by Hamidon (1994) for a wide range of kaolin soils and occurred at 180 kPa. Difference in the clay void ratio seems to become small as the vertical effective stress increases. Thus at low effective stresses, say σ'_v= 10 kPa in Rowe cell, the value of v_c ranges from 2.47-2.81 and this range decreases to from 1.33 to 1.28 at the higher stress level of 480 kPa. More or less similar trends can be seen Fig.3.15 in which the compression data were obtained from consolidation tube.

The slopes of the normal compression lines (λ_c*) in high stress ranges (σ'_v> 160 kPa) in Fig.3.14 & 3.15 are plotted against clay content as shown in Fig.3.19. The slope of swell lines (κ_c*) in Fig.3.14 are also shown in Fig.3.19. The λ_c* values from Rowe cell and consolidation tube are almost identical. The slopes of the normal compression lines for different mixtures are almost constant to a clay content 40% in the mixture. At the clay content 30% in the mixtures, the slope of the normal compression line is decreased drastically. This indicates that intergranular friction is dominating at sand content 70% causing the mixture to have a higher clay void ratio.

The slope of the swelling lines in Fig.3.19 is almost constant down to a clay content 40% indicating that the intergranular interaction is low which allows particles to slide over each other easily and promotes more swelling when compared to clay:sand mixtures with sand contents 80% and 90%.

The resulting average consolidation lines for the mixtures M100 to M40 in Fig.3.14&3.15 are shown in Fig.3.20. The normal compression line is seen to be bilinear with the kink occurring at σ'_v= 160 kPa. Then the one-dimensional normal compression of clay phase can be represented by Eq.3.8 of the form:

$$\ln v_c = \ln A_c^* - \lambda_c^* \ln \sigma'_v \qquad (3.11)$$

and in high stress ranges, the reference clay specific volume A_c^* is 4.08 and the slope of line $\lambda_c^* = 0.094$. The swelling line can be represented by Eq.3.9. But according to Muir Wood (1990), swelling line for one-dimensional unloading and reloading is not unique but depends on the maximum previous stress. In Eq.3.9, neither v or B* is a soil constant, but κ_c^* is a soil constant and the mean value of the gradient in Fig.3.20 is 0.019.

3.3.3 Compressibility as change of granular specific volume

Granular specific volume v_g is primarily an indicator of the potential for interaction of the coarse sand particles. The relationships between v_g and vertical effective stress σ'_v are plotted in Fig.3.21. The relationships between v_g and clay content at different stages of consolidation are plotted in Fig.3.22. In Fig.3.21 & 3.22 v_g values from consolidation tube are deduced from Fig.3.12 with Eq.1.7. It is apparent (Fig.3.22) that v_g (that is to say packing of coarse sand particles) at given vertical stress falls off extremely rapidly with clay content. Fig.3.14 & 3.15 show that all the values of v_c from tests with clay contents of 40% or higher lie more or less on a unique normal compression line, and inspection of Fig.3.21 & 3.22 therefore suggests a critical value of v_g (at which sand interaction becomes important) of less than 2.4. Conversely, the values of v_c from tests with a clay content of 30% do not fall on the unique line (Fig.3.14 & 3.15) and by inspection of Fig.3.21 & 3.22 this suggests a critical value of v_g of greater than 2.5. This suggests that the threshold value of v_g at which sand interaction occurs may not be entirely unique (it seems to depend slightly on clay content), but it is typically around 2.4 to 2.5. A link can then be established between clay content and the vertical effective stress required to reach a specified granular specific volume, v_g with Eq.3.11 and Eq.1.7a:

$$\sigma'_v = \left[\left(\frac{1-C}{C}\right)\left(\frac{v_g - 1}{A_c^*}\right)\right]^{-\frac{1}{\lambda_c^*}} \qquad (3.12)$$

It is clear on the basis of this simple approach that the threshold v_g of 2.4-2.5 will never be crossed at stresses of common engineering concern for clay contents of 50% and above (Fig.3.21 & 3.22).

Seed et al. (1964) assumed that the value of v_g at which the clay component fills up the void of a sand skeleton was 1.8. This value is considerably smaller than the v_g of 2.4-2.5 obtained in this study. But a v_g of 1.8 in sand is not a very loose state.

Fukue et al. (1986) concluded for bentonite-sand mixtures that for clay contents less than 50%, the final stage of one-dimensional compression is due to frictional resistance between sand particles. They found a threshold v_g around 2.25-2.48 which varies slightly with clay content in the mixture.

3.3.4 Comparison of compressibility λ from fall cone

A comparison between experimental and predicted values of λ from fall cone (Fig.2.6) is given in Fig.3.23 for different clay-sand mixtures. The experimental λ values of different mixtures are reduced from the slope of normal compression lines in v-lnσ'_v space for the data in Fig.3.12. In the calculations of λ values, vertical effective stresses greater than 160 kPa are used since normal compression lines are approximately linear in higher stress ranges in v-lnσ'_v space. It can seen in Fig.3.23 that the agreement between the experimental and predicted values of λ is quite satisfactory with a good coefficient of correlation, $R^2 = 0.99$.

3.4 CONCLUSION

One dimensional compression response of mixtures of clay and coarse sand is not affected by the presence of the coarse sand for sand contents up to 60% even for consolidation pressure up to nearly 1600 kPa.

Compressibilities of the clay/sand mixtures in oedometer tests correlate well with compressibilities deduced from fall cone tests used to determine liquid limits.

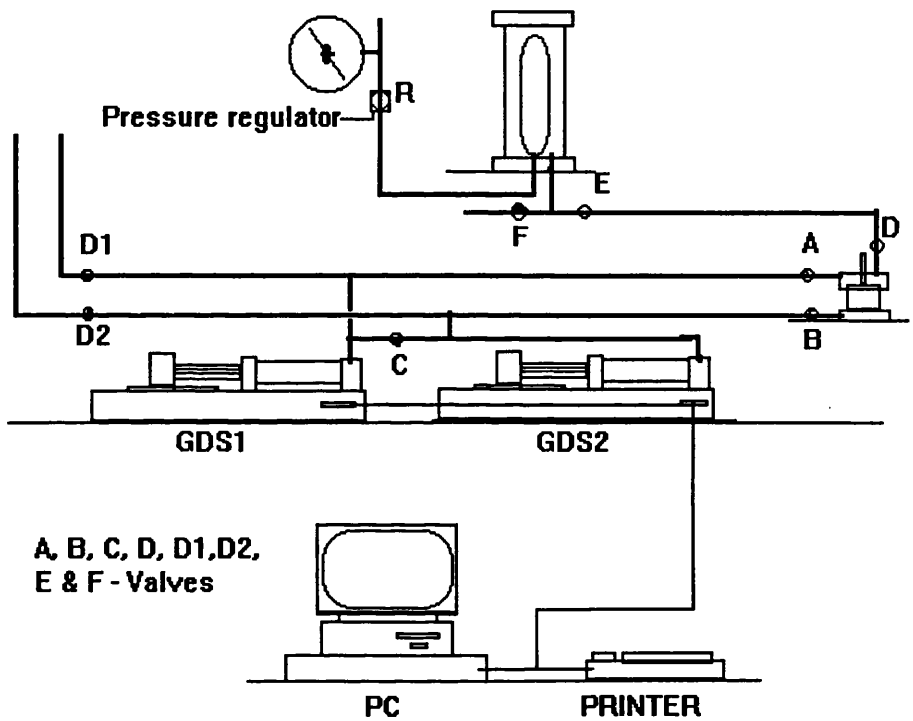

Fig. 3.1 Lay out of computer controlled consolidation test (Hamidon 1994)

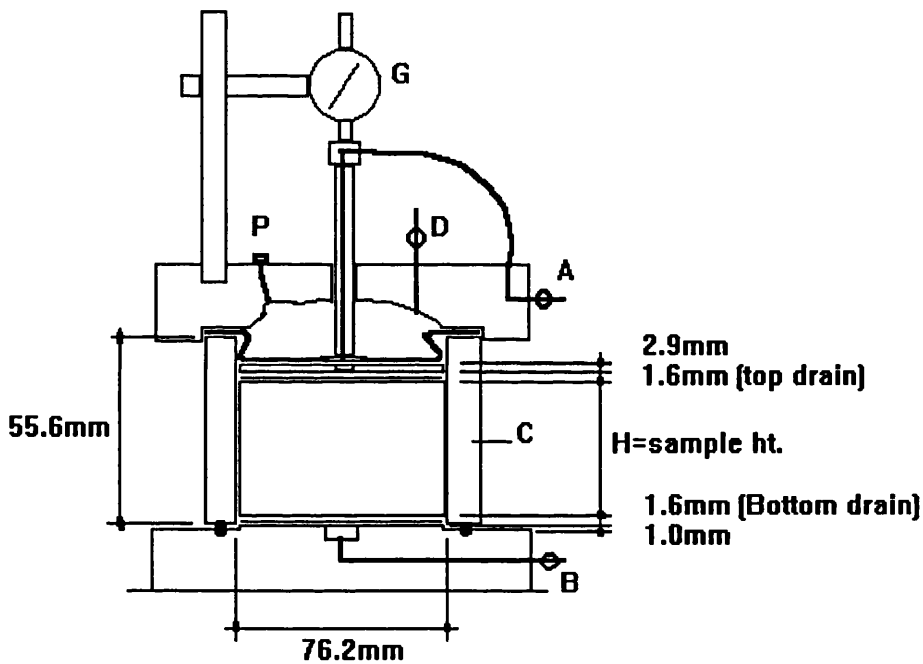

Fig. 3.2 Rowe cell (Hamidon 1994)

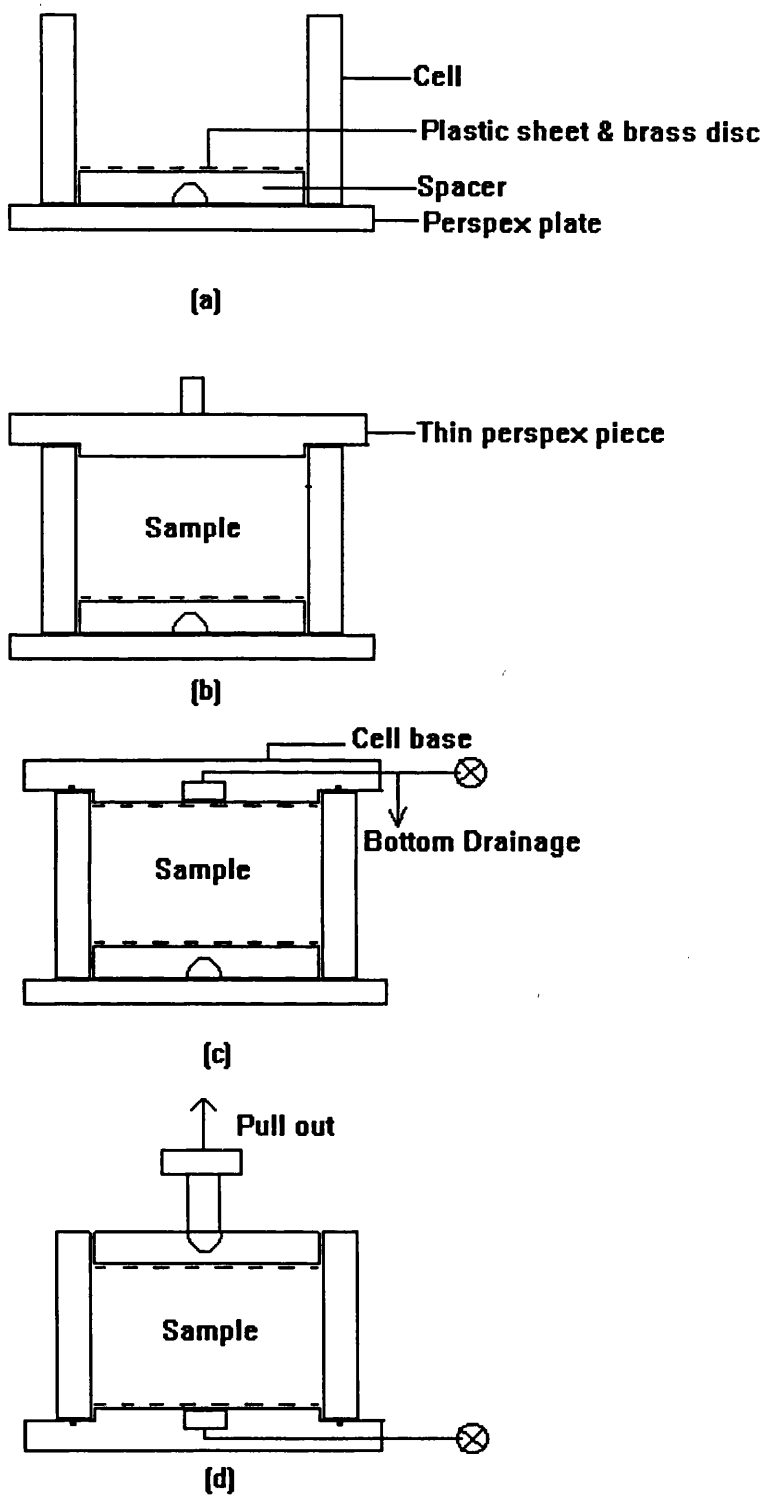

Fig. 3.3 Setting up of sample in oedometer

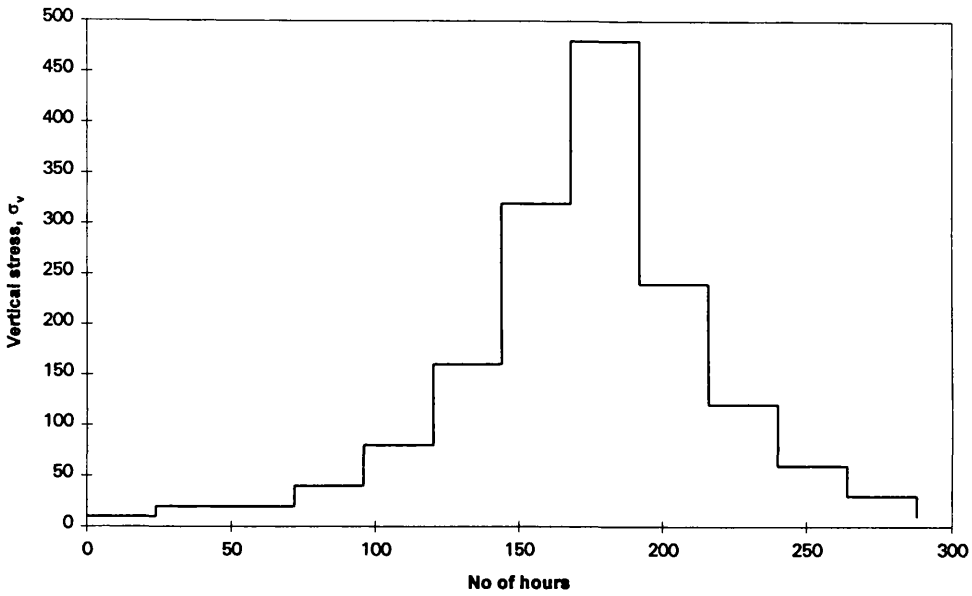

Fig.3.4 Loading history

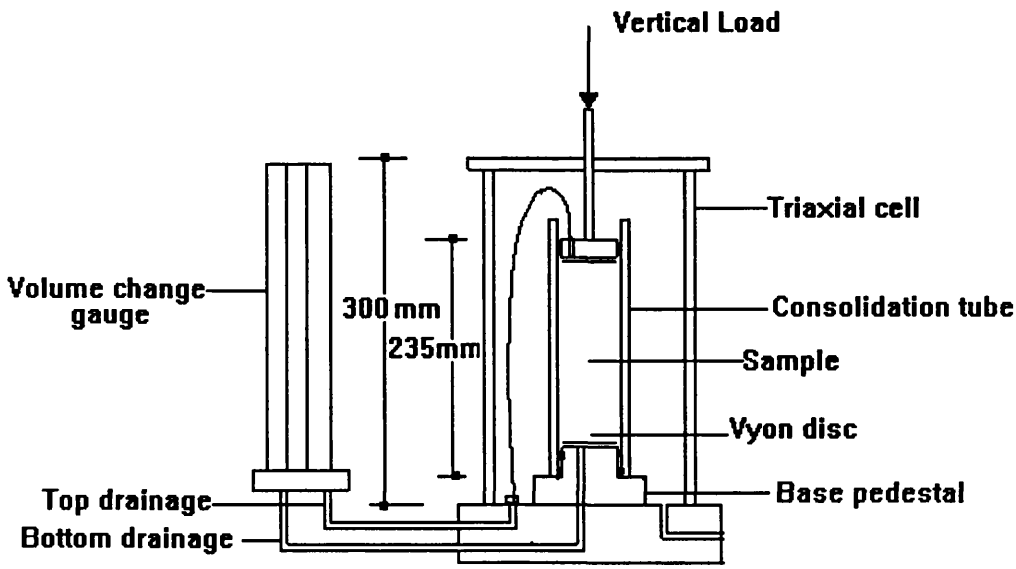

Fig. 3.5 Consolidation Tube in use

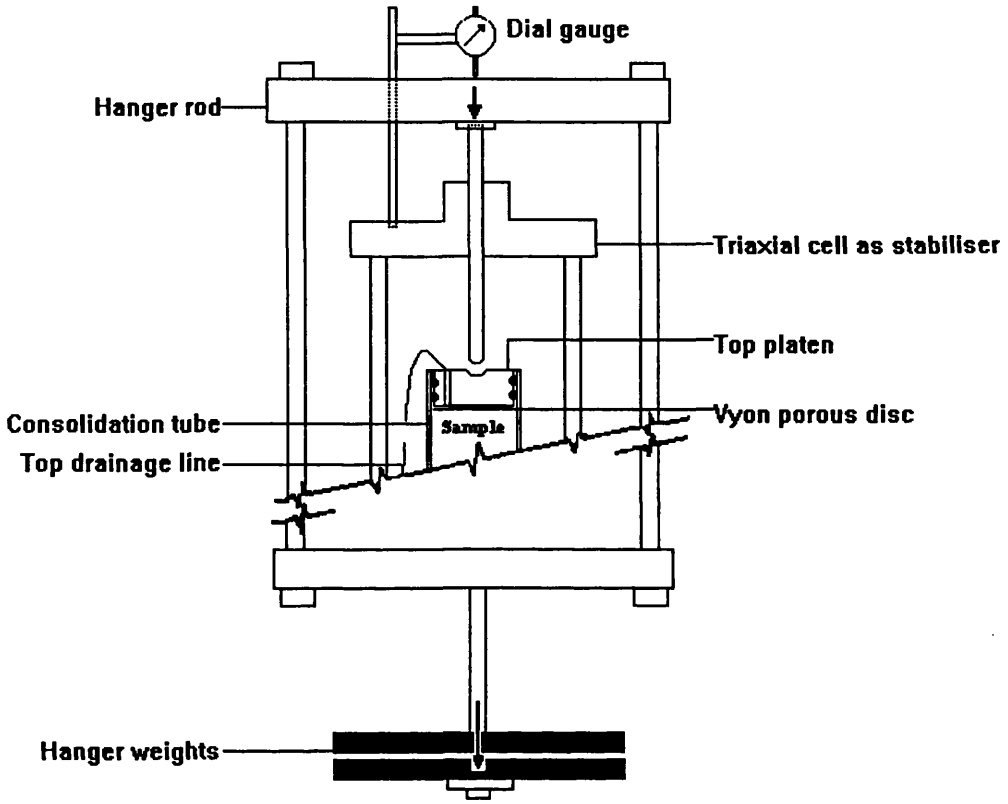

Fig.3.6 Dead weight loading

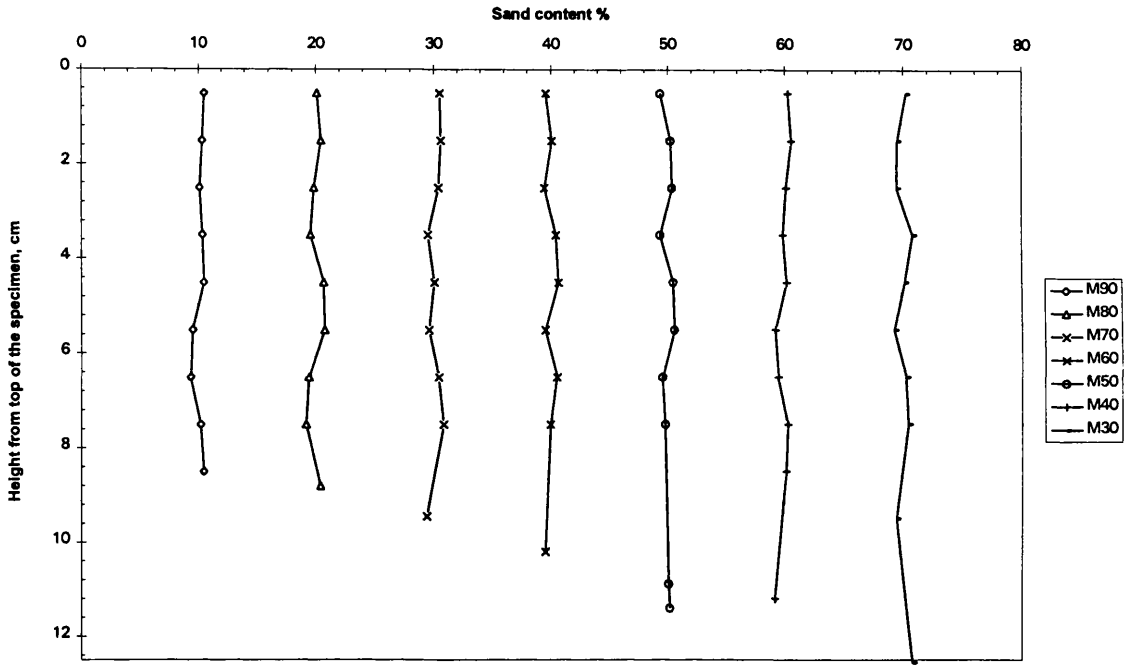

Fig.3.7 Variation of sand content

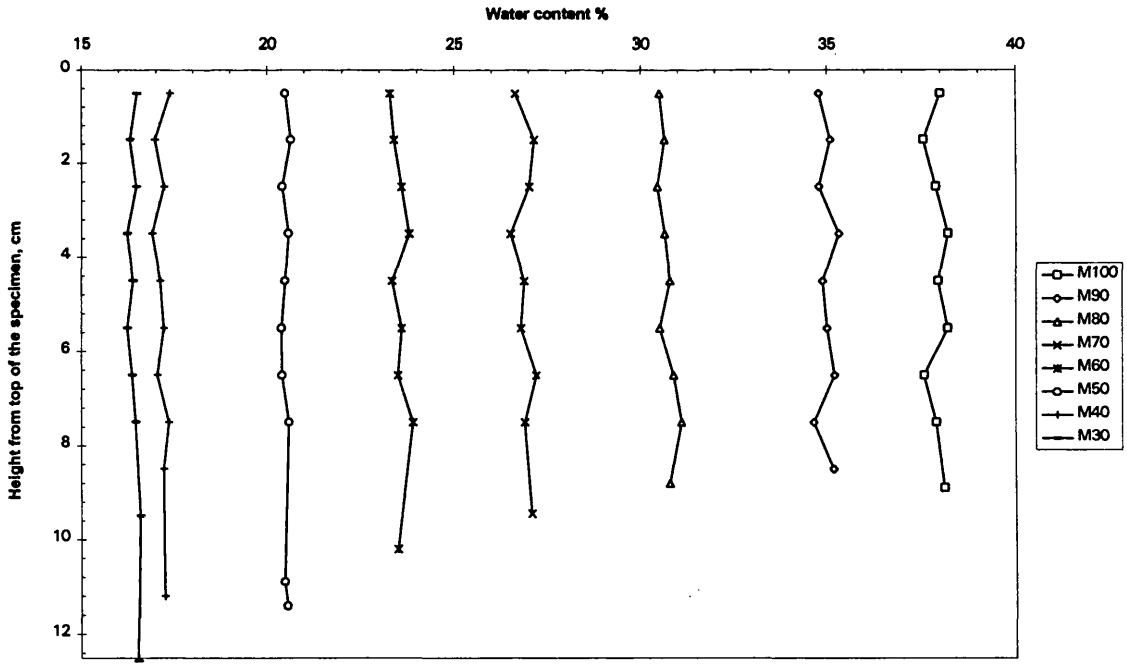

Fig.3.8 Variation of water content

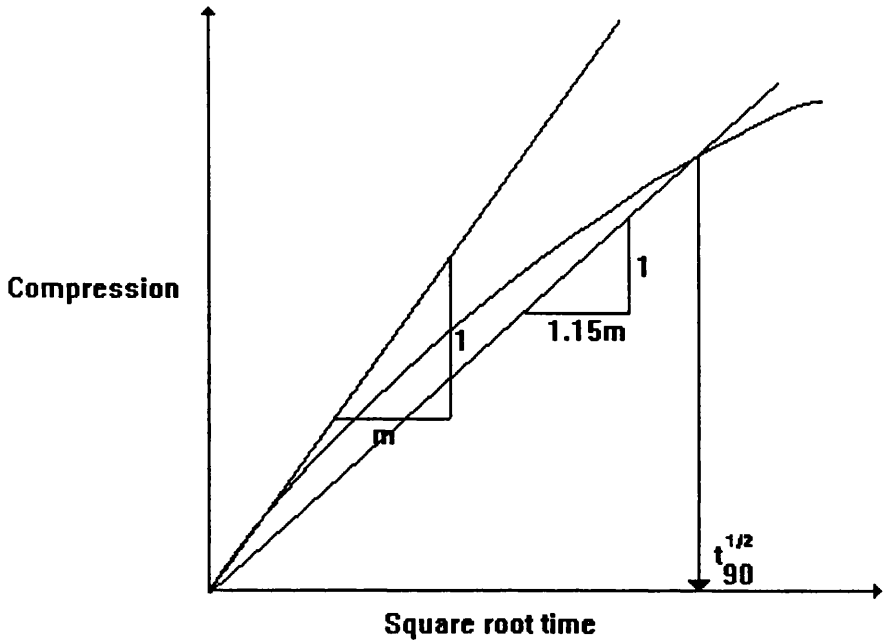

Fig.3.9 Estimation of 90% consolidation - square root fitting method

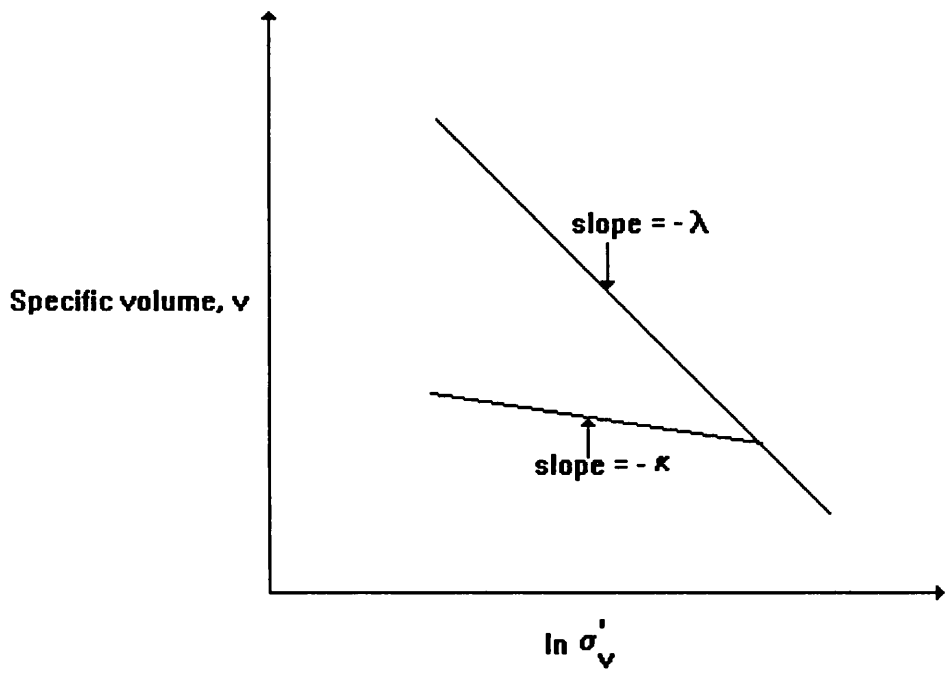

Fig.3.10 Idealised one-dimensional compression of clays

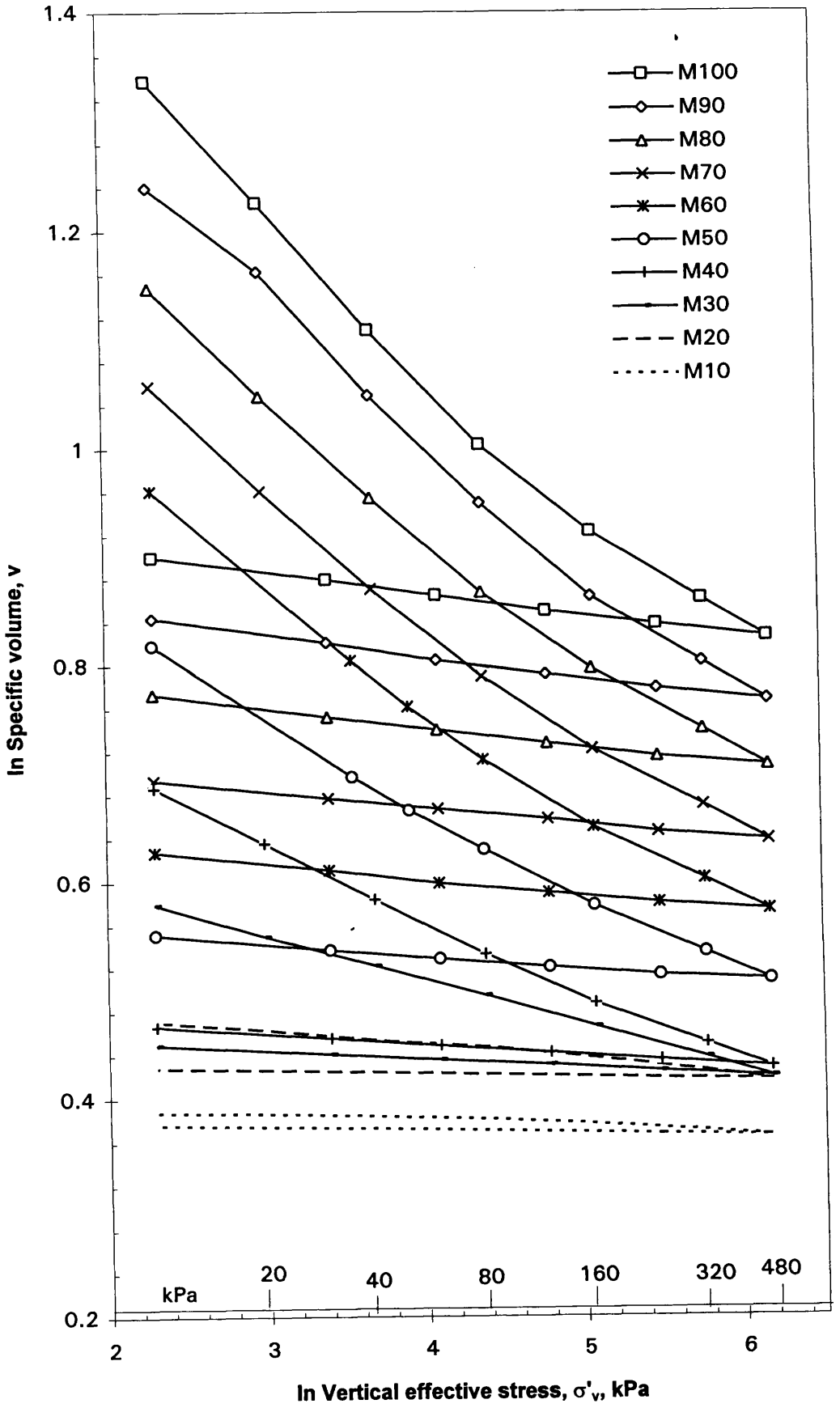

Fig.3.11 One-dimensional compression results from Rowe cell

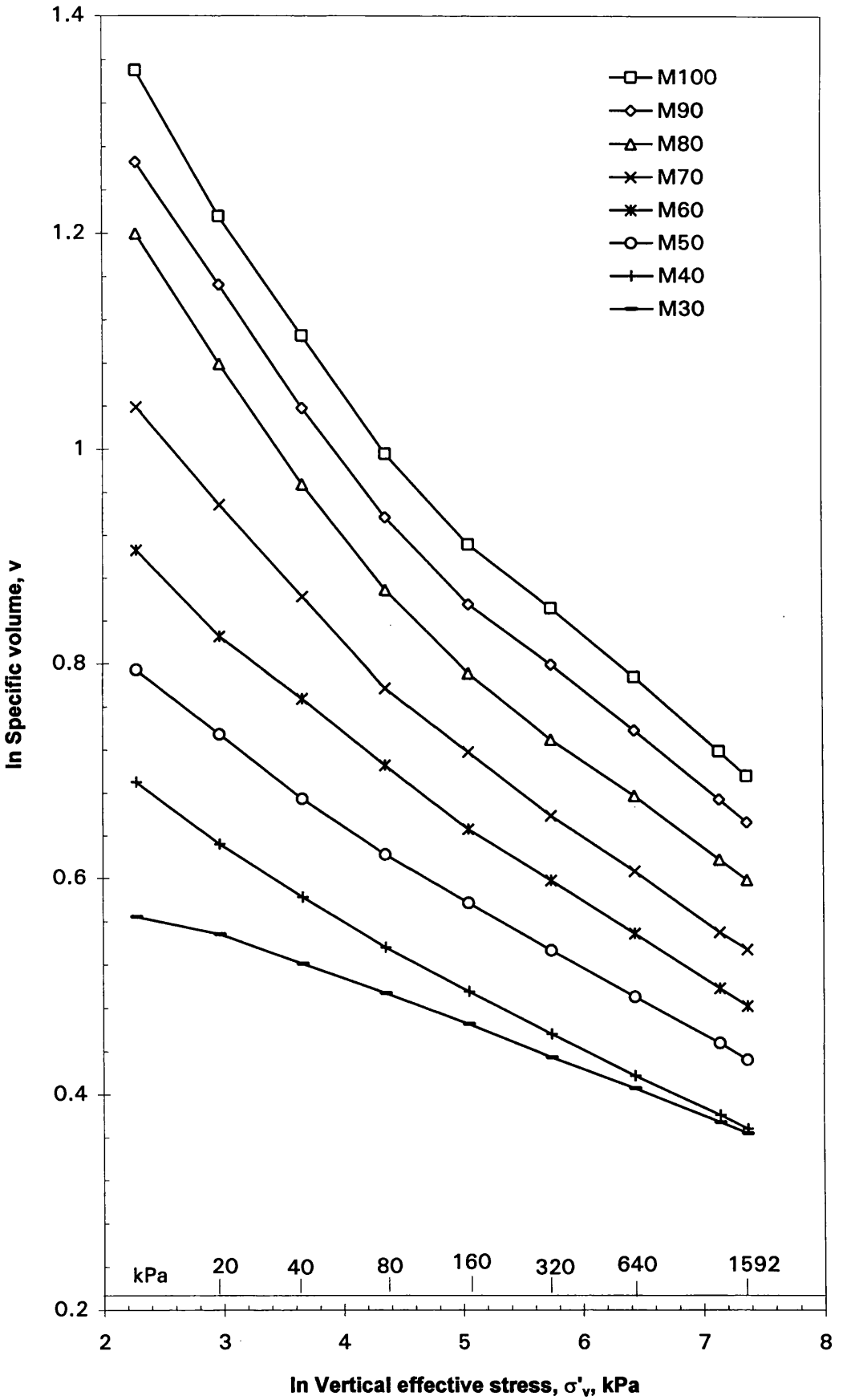

Fig.3.12 1D - compression of mixtures - data from consolidation tube

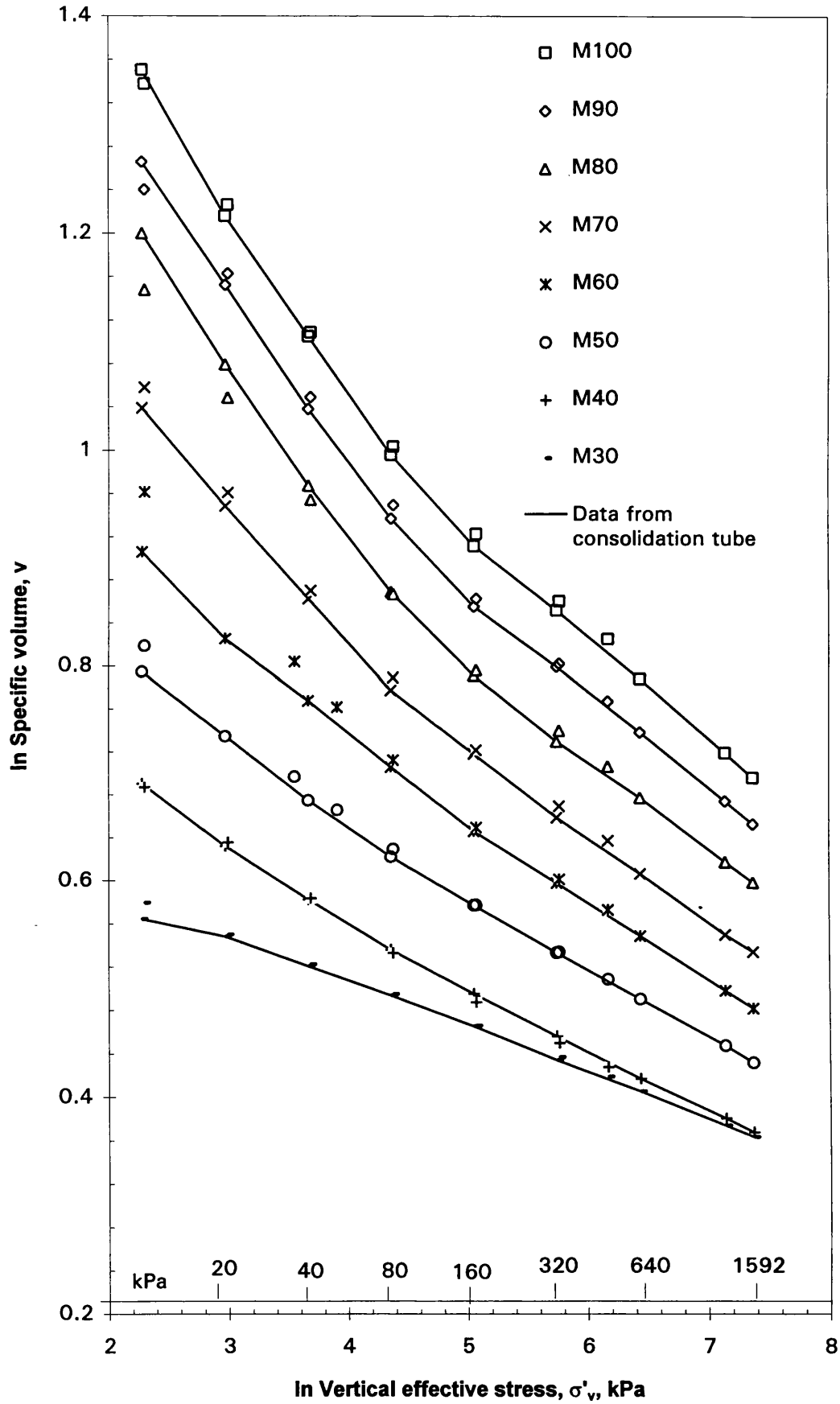

Fig.3.13 Specific volume changes, Rowe cell, consolidation tube tests

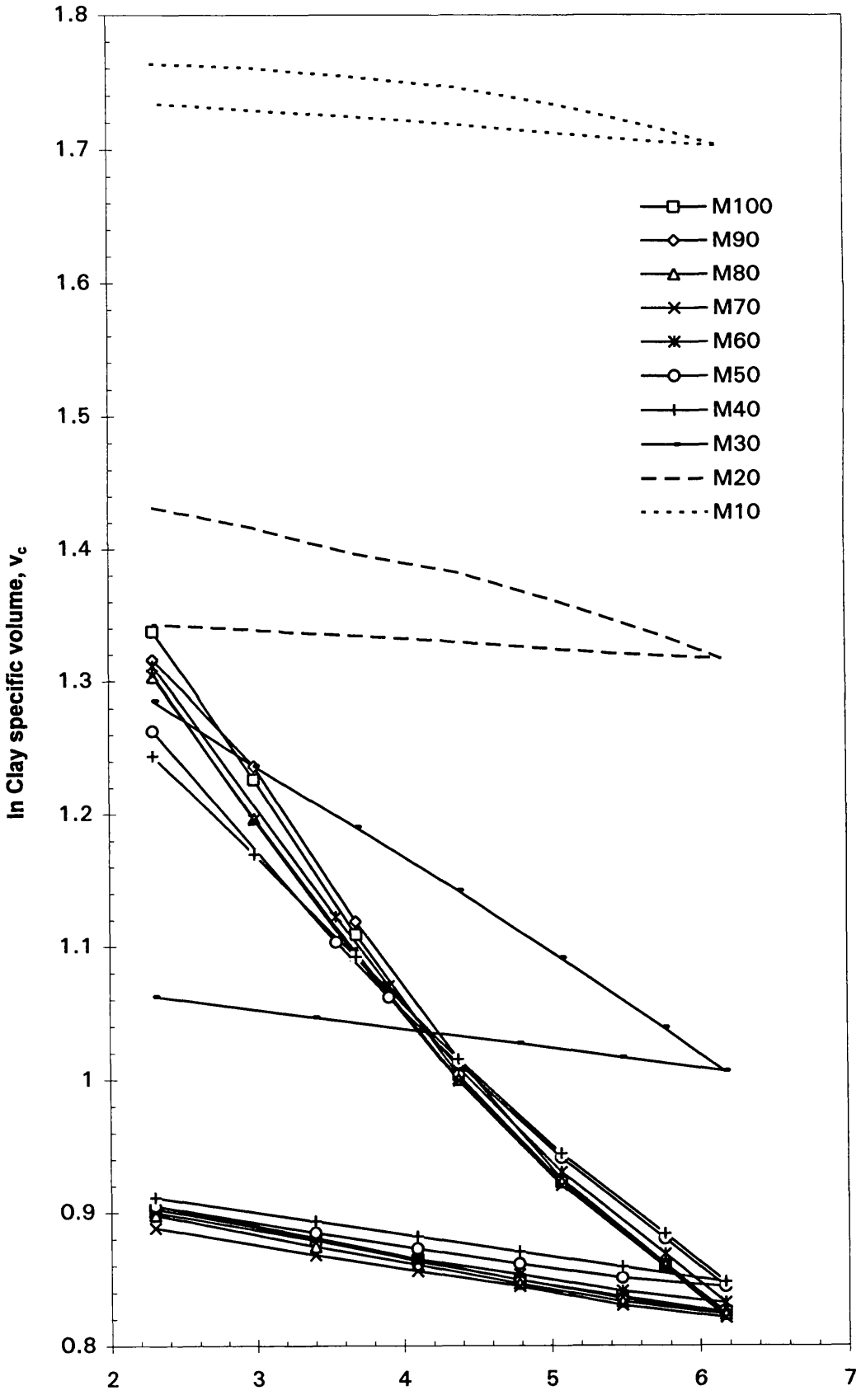

Fig.3.14 One-dimensional compression of mixtures in Rowe cell - clay specific volume

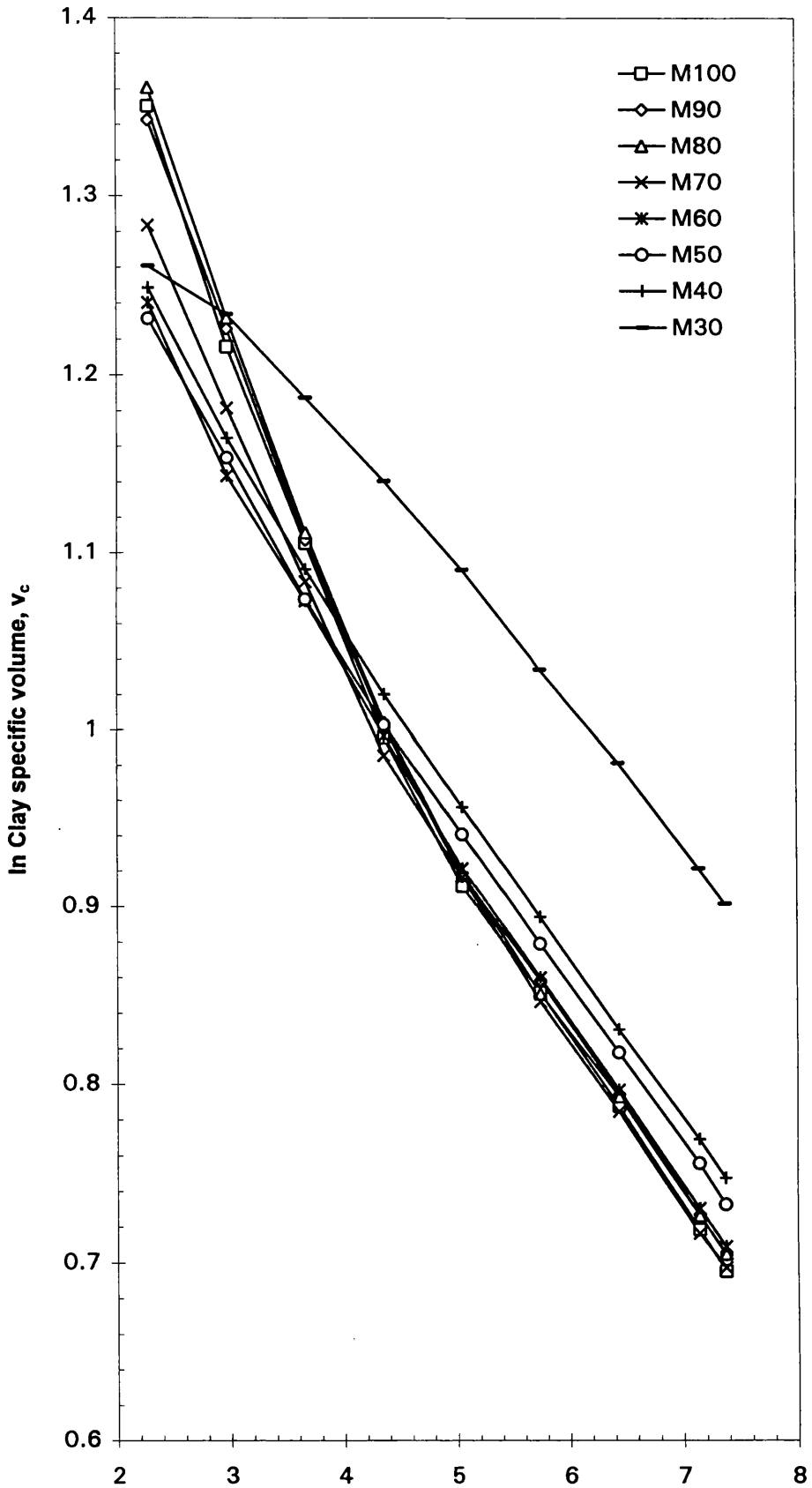

Fig.3.15 1-D compression of mixtures - clay specific volume - data from consolidation tube

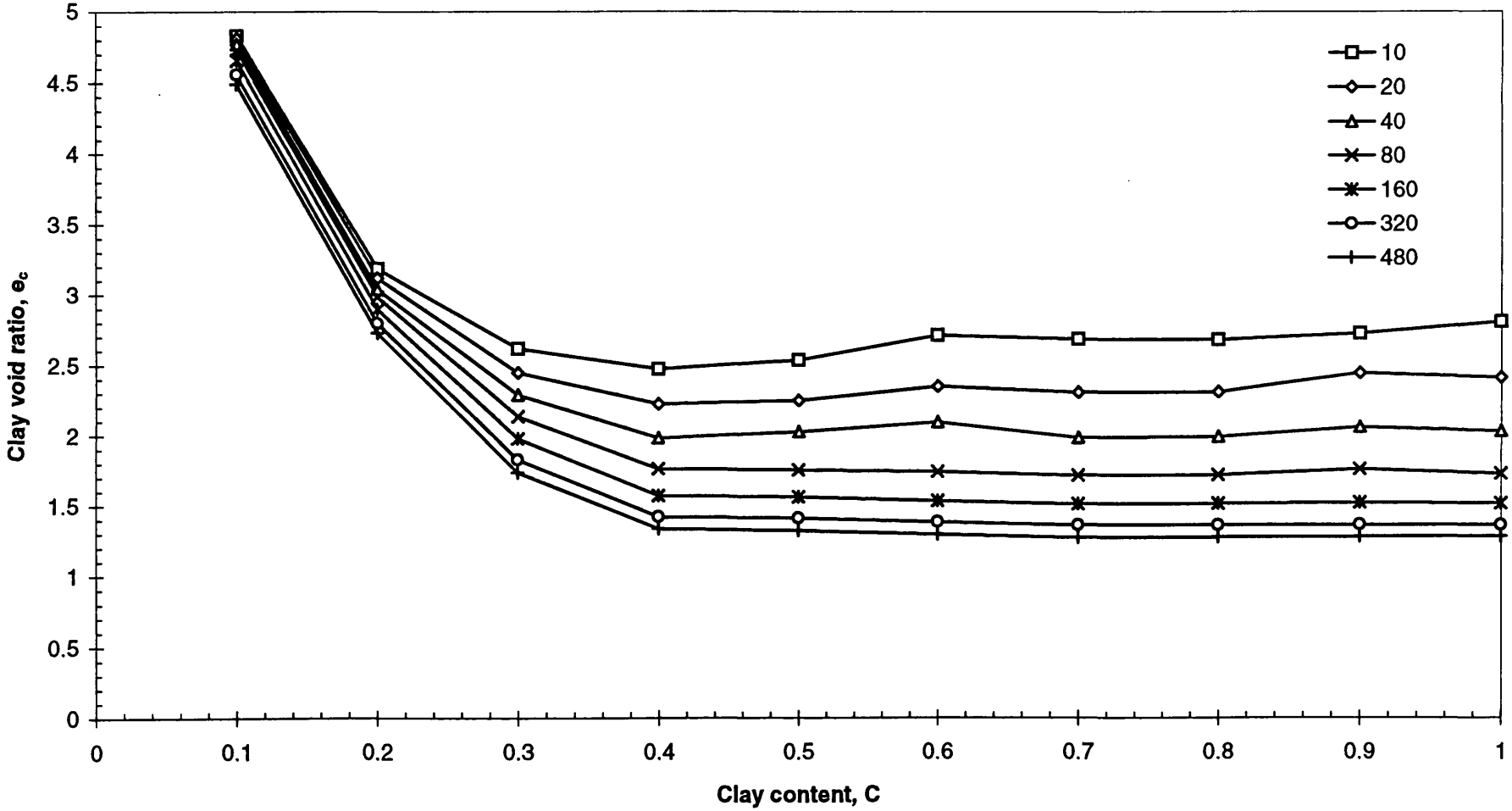

Fig.3.16 Variation of clay void ratio with clay content (Data from Rowe cell)

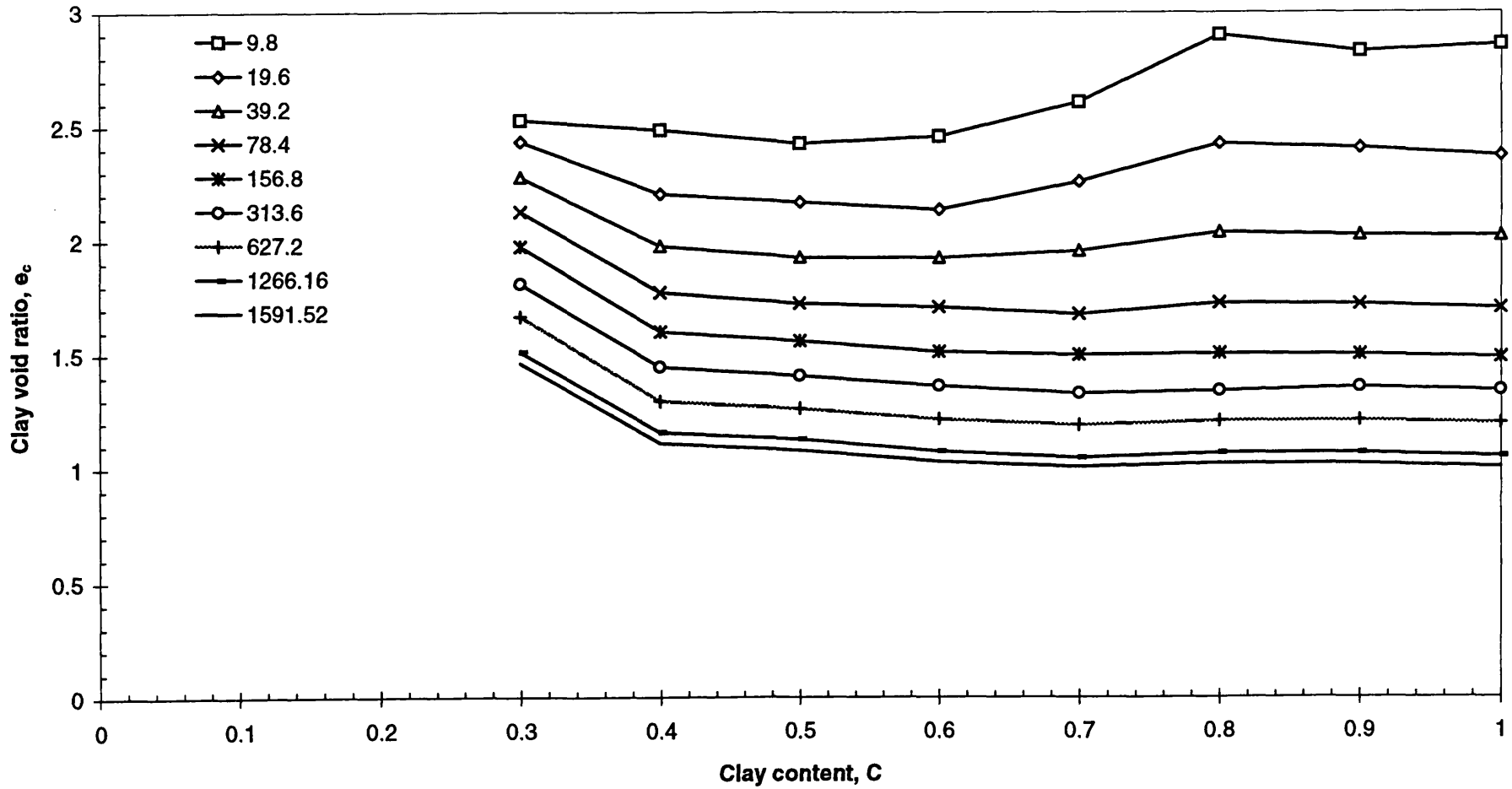

Fig.3.17 Variation of clay void ratio with clay content (Data from consolidation tube)

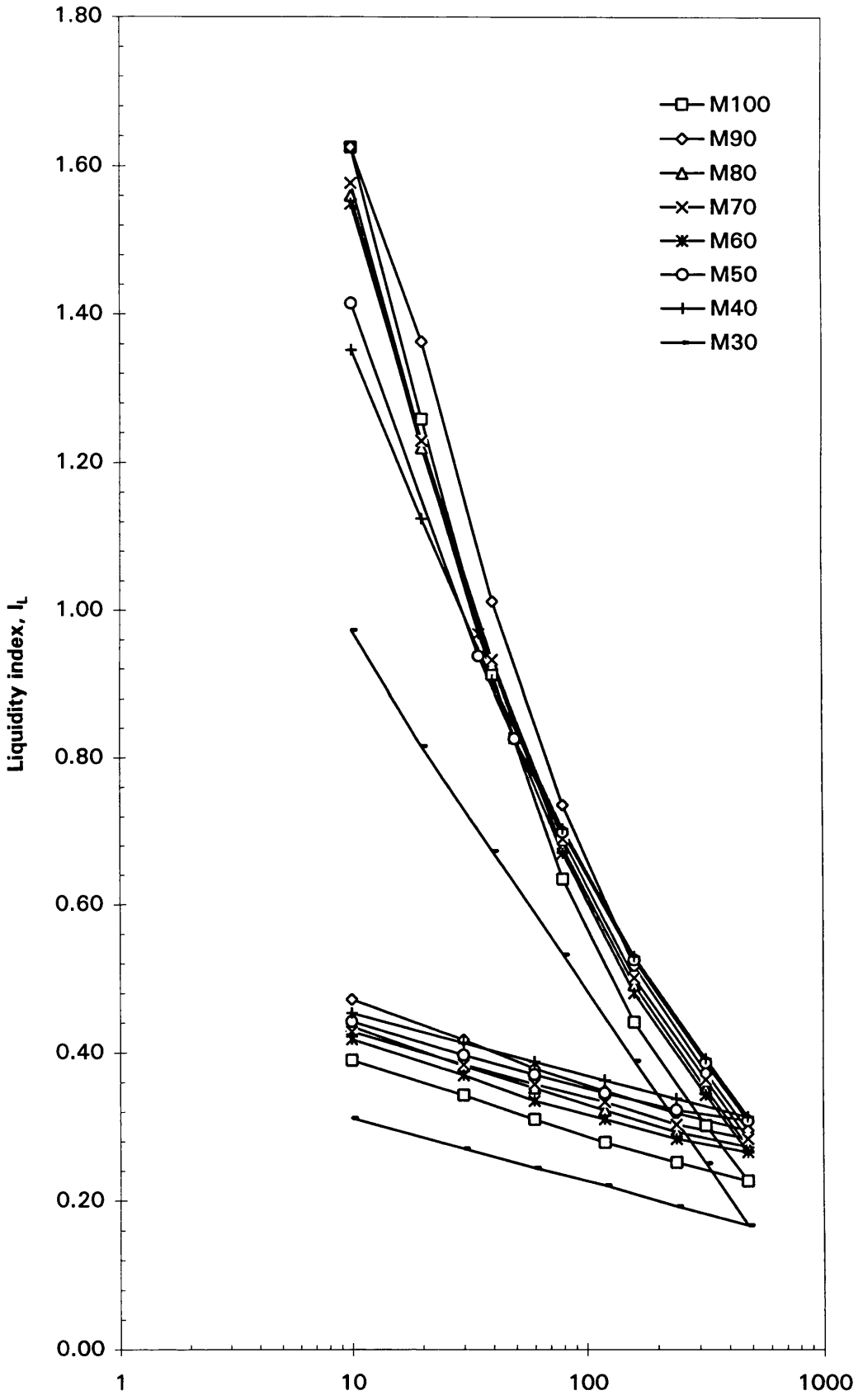

Fig.3.18a Data of water contents normalised to liquidity index
(Data from Rowe cell)

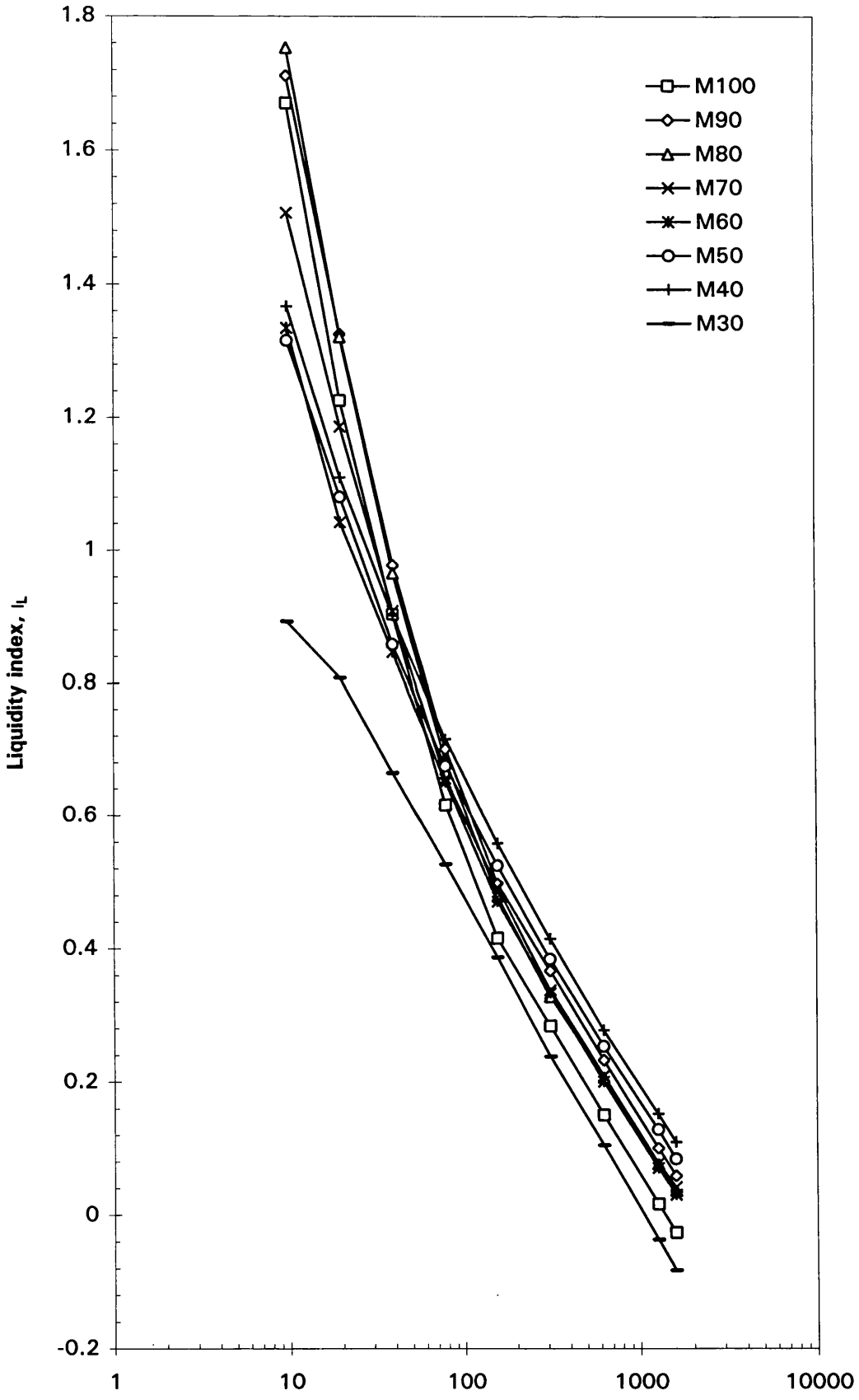

Fig.3.18b Data of water contents normalised to liquidity index
(Data from consolidation tube)

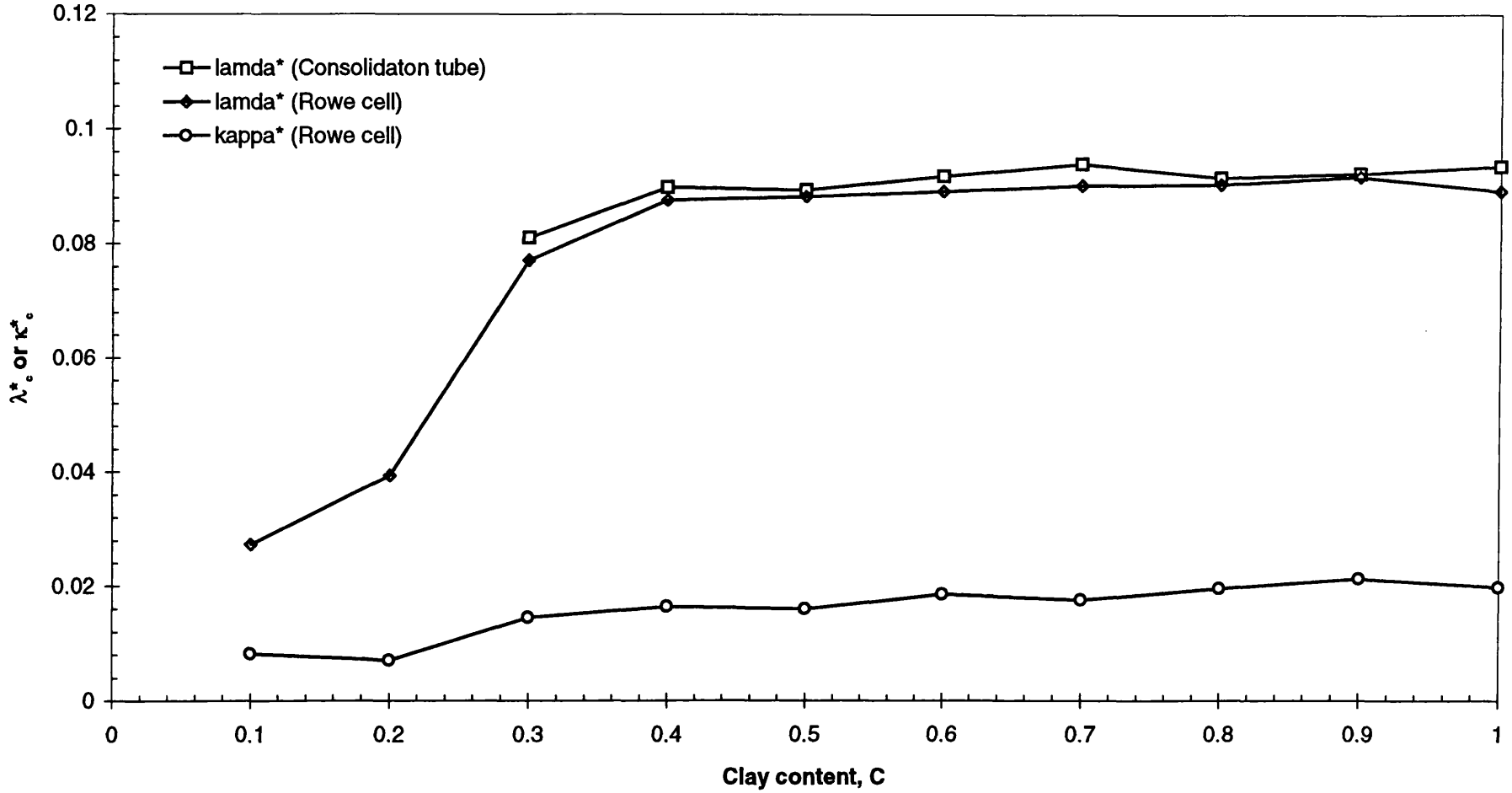

Fig.3.19 Variation of lambda* and kappa* with clay content

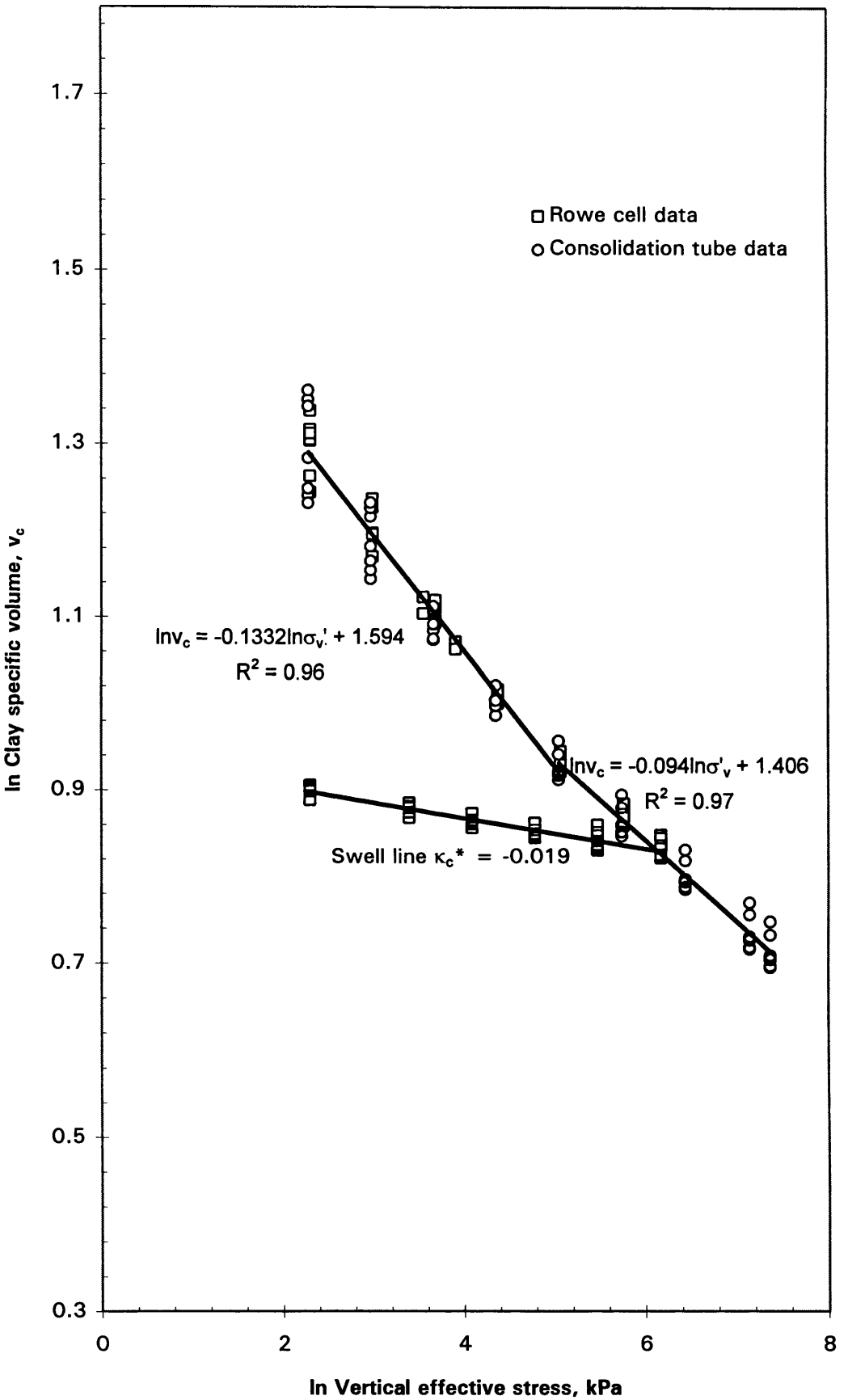

Fig.3.20 1-D compression of mixtures with C = 100 to 40%:
Average data from results in Fig.3.14 3.15

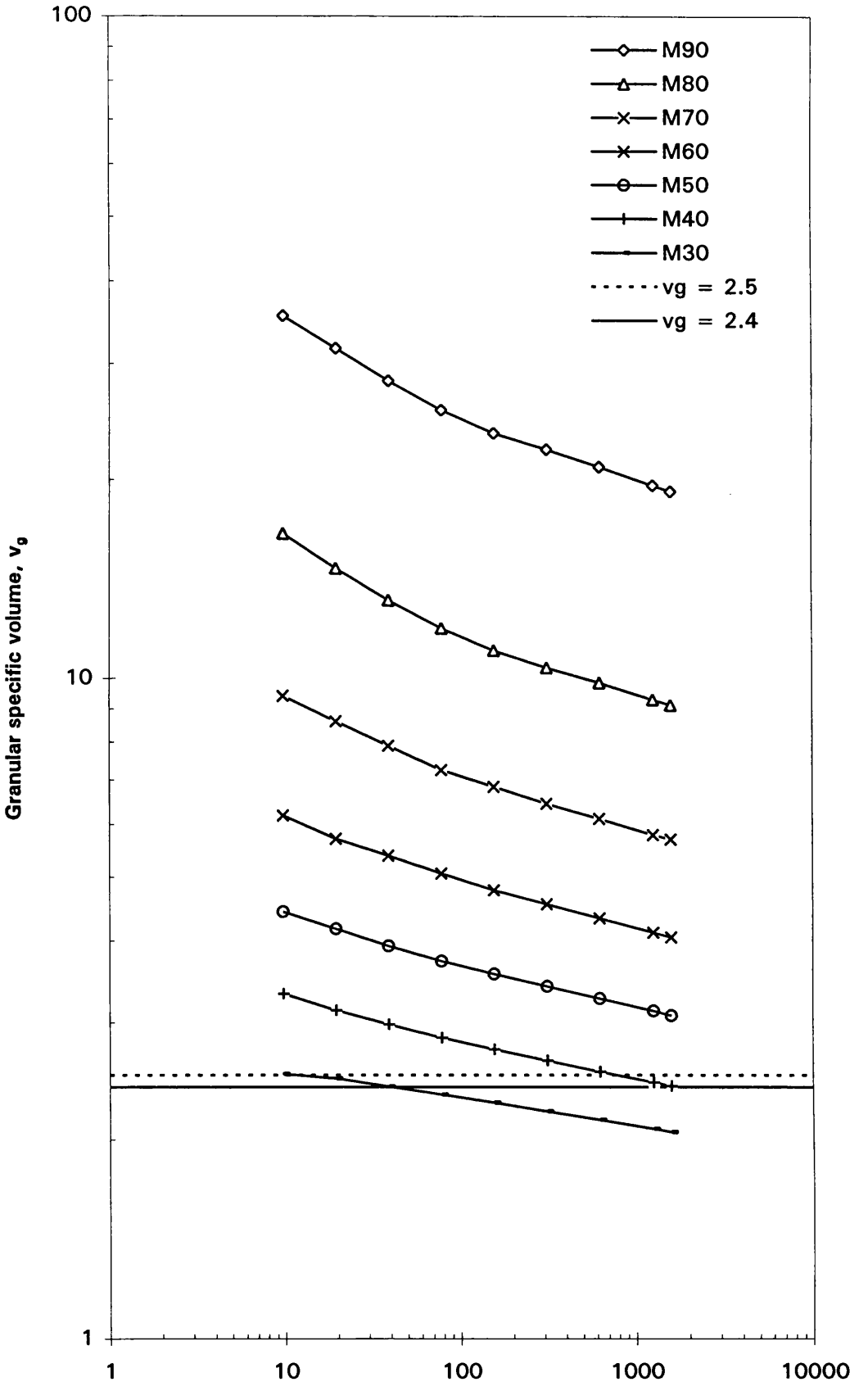

Fig.3.21 Granular specific volume - vertical effective stress relations
(Data from consolidation tube)

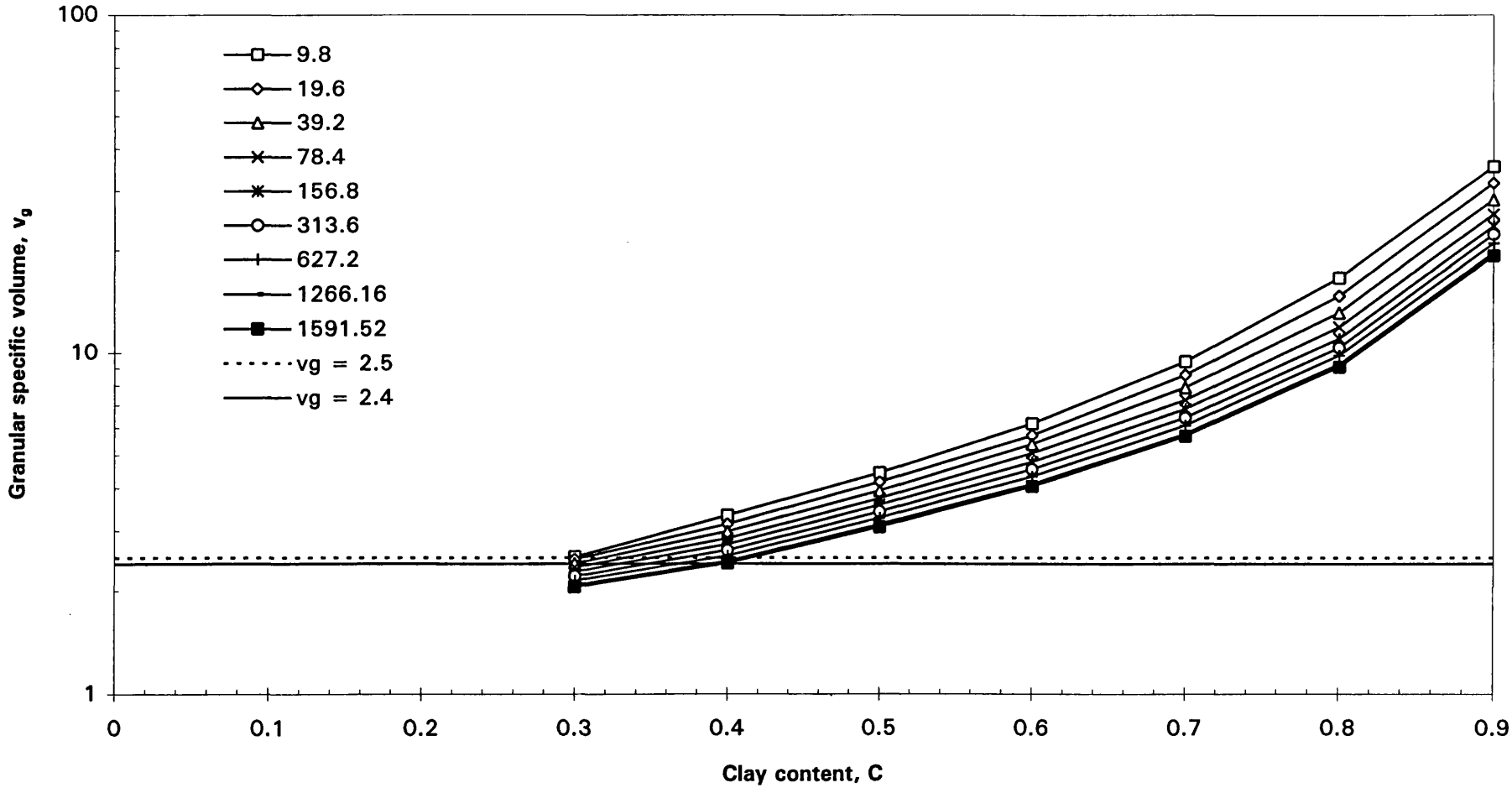

Fig.3.22 Variation of granular specific volume vg with clay content (Data from consolidation tube)

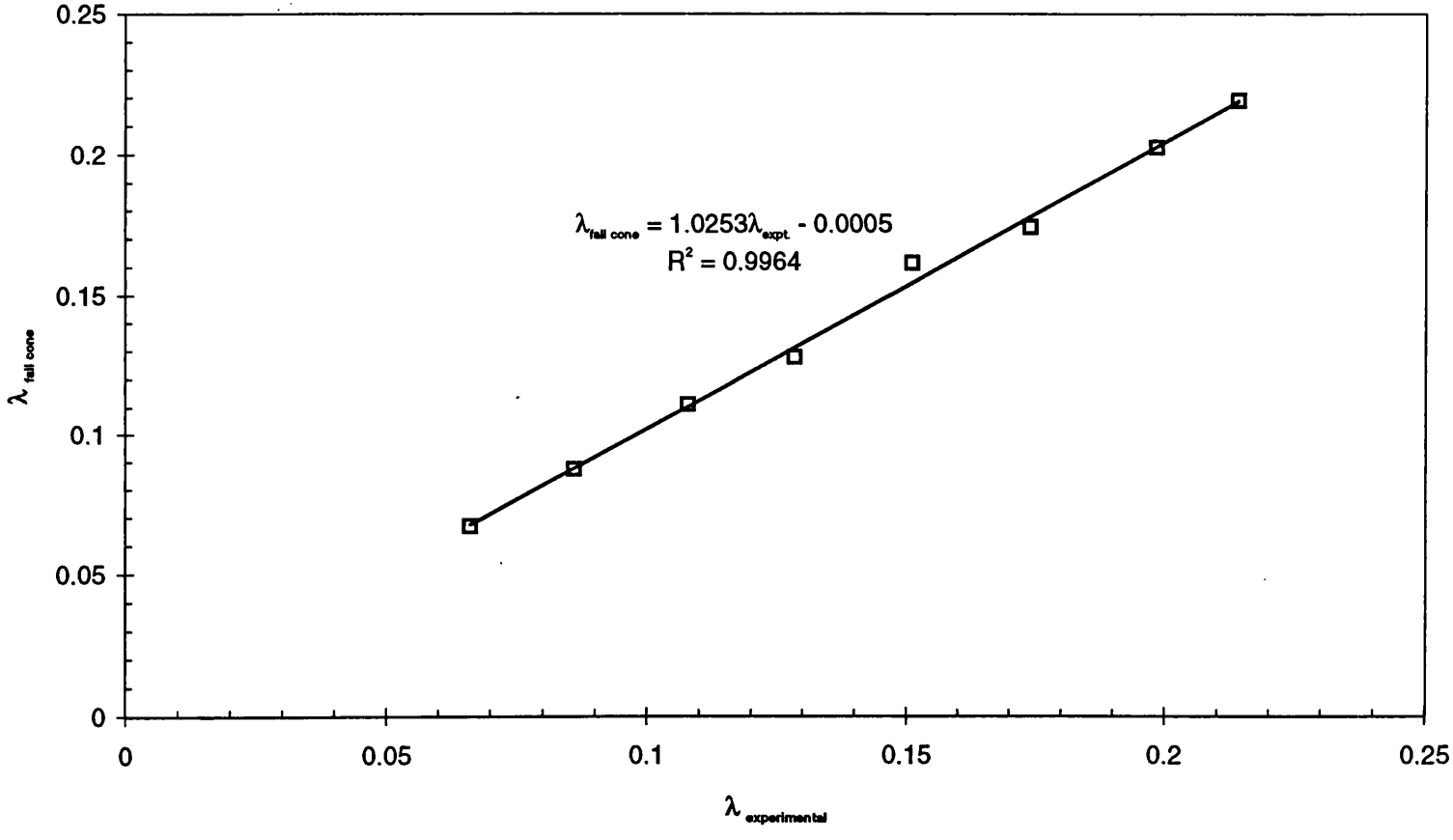

Fig.3.23 Comparison of compressibility from fall cone and experiment

CHAPTER 4

PERMEABILITY CHARACTERISTICS

The fundamental equation which governs the streamlined flow of water through soils is Darcy 's law (Darcy 1856):

$$Q' = A.k.i \qquad (4.1)$$

in which Q' is the volume of water flowing through an area A of the soil in unit time under the influence of a hydraulic gradient, i. The constant of proportionality, k, is called the permeability of the soil. The measurement of permeability of soil has been a problem of growing importance in geotechnical engineering in the past few years. The permeability is a key element in modelling seepage, and consolidation, in influencing stability analysis and in the prediction of accurate fluid movement through soils associated with the disposal of hazardous waste in search of acceptable solutions to environmental problems.

In consideration of the importance and widespread use of permeability, there have been numerous studies in the past dealing with (1) fundamental aspects of permeability of soils such as the validity of Darcy 's law (e.g. Hansbo 1960; Olsen 1966; Mitchell 1976; Law and Lee 1981) (2) the fundamental factors controlling the coefficient of permeability (Mesri and Olson 1971) (3) the measurement of the value itself. The majority of the past investigations on the measurement of permeability were concerned with granular soils (Loudon 1952; Amer and Award 1974, Kenney et al. 1984) or fine grained soils (Tavenas et al. 1983-b; Al Tabbaa and Wood 1987; Hamidon 1994 and others). In spite of the above studies, the important aspect of the extent to which permeability characteristics are controlled by the clay phase in soils with coarse fraction at different stress levels is not established. Establishing this link is the main aim of this chapter.

The contents of this chapter are as follows: section 4.1 is concerned with the background to permeability characteristics, section 4.2 describes the procedures followed to measure permeability, and section 4.3 deals with well known equations required for interpretation of experimental data. The results of the experimental data are presented and discussed in section 4.4.

4.1 PERMEABILITY CHARACTERISTICS

4.1.1 Permeability - void ratio relationships

In general, permeability of coarse grained soils will be related to the void size and the distribution of particle sizes. The relevant relationship was developed by Kozeny (1927) and Carman (1956) and is written in the form:

$$k = \frac{1}{c_s T^2 s_s^2} \frac{\gamma}{\mu} \frac{e^3}{(1+e)} \tag{4.2}$$

Where k = permeability, c_S = pore shape factor, e = void ratio, γ = unit weight of permeating fluid, and μ = viscosity of the permeating fluid. S_S = surface area per unit volume of particles, T = tortuosity factor defined as,

$$T = \left(\frac{L}{L_e}\right)^2 \tag{4.2a}$$

where L is the apparent flow length and L_e is the effective flow length. Eq (4.2) is based on the assumption that particles are approximately equidimensional, uniform and larger than 1 μm and that the flow is laminar.

Taylor (1948) showed that Eq (4.2) was valid only for sands and could not be applied to clay and suggested an empirical linear relationship between the logarithm of k and the void ratio, e for clays:

$$\log k = A + Be \tag{4.3}$$

Samarasinghe et al. (1982) have suggested a modified version of Eq (4.2),

$$k = K\frac{e^n}{(1+e)} \tag{4.4}$$

would be generally applicable to normally consolidated clays, with the power n typically in the order of 4-5, while K is a reference permeability indicating the soil characteristics. A plot of k verses $\frac{e^n}{1+e}$ results in a straight line passing through the origin.

Mesri and Olson (1971) observed that the linear relationship between logk and e (Eq.4.3) is not valid for a very wide range of void ratios and suggested instead a linear relationship in a double logarithmic plot :

$$\log k = A \log e + B \tag{4.5}$$

Later Eq(4.5) was confirmed by Al Tabbaa and Wood (1987) for matching experimental observations of permeability of kaolin. and this form of relationship will be used in the present study.

Tavenas et al. (1983-b) suggested that for many natural clays the permeability depends on the values of the initial permeability and void ratio k_o, e_o respectively and according to a relation:

$$\log k = \log k_o - \frac{e_o - e}{c_k} \tag{4.6}$$

in which c_k is permeability change index. This Eq.4.6 is just another form of Eq.4.3 with

$$A = \log k_o - \frac{e_o}{c_k} \tag{4.6a}$$

$$B = \frac{1}{c_k} \tag{4.6b}$$

Tavenas et al. (1983-b) showed that for many natural clays $c_k = 0.5e_o$.

Nagaraj et al. (1994) suggested a generalised permeability relationship for fine grained soils based on void ratio at liquid limit water content as follows

$$\log k = A + B' \left(\frac{e}{e_L}\right) \tag{4.7}$$

Eq.4.7 is again another form of Eq.4.3 with:

$$B = \frac{B'}{e_L} \tag{4.7a}$$

Most of the empirical relationships Eq (4.2-4.7) are useful for fine grained soils and imply that for a given soil, the permeability falls with decrease in void ratio. The generalised approach suggested by Nagaraj et al. (1994) is based on normalisation with void ratio at the liquid limit which may be a serious limitation for soils containing a large coarse fraction although as shown in Chapter 2 the fall cone can in principle be used to deduce a sort of liquid limit qualitatively even for soils containing coarse particles. These different

approaches to prediction of permeability for clay:sand mixtures will be explored here.

4.1.2 Effect of overconsolidation on permeability

Natural soils usually exist in an apparent overconsolidated state as a result of several mechanisms such as glaciation, fluctuations in water table, changes in soil structure due to secondary compression, change of strain rate on loading, etc. The effect of overconsolidation on the permeability is not clearly established, some authors suggesting dependence on overconsolidation (Samarasinghe et al. 1982) whereas Al Tabbaa and Wood (1987) and Hamidon (1994) concluded that the permeability is dependent on void ratio and not separately dependent on overconsolidation ratio. It is of interest to study the effect of overconsolidation on permeability of different clay/sand mixtures.

4.1.3 Permeability measurements

Accurate measurement of permeability is of paramount importance especially for fine grained soils. The constant head and the falling head tests are widely used in every geotechnical laboratory because of their simplicity and commercial viability. The constant head method is used for testing soils with relatively high permeability such as sands, while the falling head method is used for soils with relatively low permeability (Head 1982).

Difficulties with constant head and falling head methods have been discussed by Olsen 1966; Remy 1973; Hardcastle and Mitchell 1974; Olsen et al. 1985; Al Tabbaa and Wood 1987; and others. In both methods flow rates have been measured by using conventional volume change equipment such as capillary tubes. Accurate measurements of flow can be achieved only if the tests run for long periods of time or if high gradients of pore pressure are imposed. Both of these requirements are undesirable for the following reasons: Long term testing with low gradients is impractical and unreliable. The control of low gradients is limited by experimental errors arising from contaminant effects on capillary menisci involved in flow rate measurements and also by the expansion and contraction of equipment components due to temperature variations. In addition, there is an increased chance of bacterial growth in the sample which may cause fabric and permeability changes (e.g. Mitchell 1976).

The effects of high gradient will give rise to plugging or unplugging of voids (e.g. Mitchell 1976) and produce a large variation of effective stress within the sample, causing the sample to become less homogeneous and affect the measured permeability. In addition, the pressure gradients in situ are generally

quite low, hence high gradient testing may cause a significant discrepancy between laboratory obtained permeability values and the values relevant in the field.

Approaches for minimising and avoiding the difficulties with conventional methods have been developed in research studies: The falling head method was improved with applications of differential pressure transducers (Remy 1973). The difficulty with the falling head test is the continuous change of hydraulic gradient during the test. In order to minimise the problem with changing gradients several constant head systems for measuring permeability for fine grained soils have been developed (Hardcastle and Mitchell, 1974; Tavenas et al. 1983-a; Dunn and Mitchell 1984). The other problems described were not avoided in these apparatus.

Olsen (1966) proposed the flow pump technique for measuring permeability of fine grained soils. In this method constant flow is forced through the sample by a pump and the pressure difference induced thereby is measured with pressure transducers. The advantage of this test is that it avoids measurement of varying flow rate and permeability measurements can be conducted more rapidly at low gradients. This test is most widely used because of its advantages (Pane et al 1983; Olsen et al. 1985; Aiban and Znidarcic 1989; Little et al. 1992; Hamidon 1994).

4.2 EXPERIMENTAL PROCEDURE

Permeability tests were performed after the end of every consolidation stage (Fig.3.4) in a hydraulic oedometer, using flow rate control (Fig.3.1) because of the advantages mentioned in section 4.1.3

In each test a constant flow rate was applied through the specimen and the corresponding induced pressure difference that developed was monitored with time. The act of imposing a flow rate through the sample will tend to produce swelling at the inflow end and further consolidation at the outflow boundary. In all the tests suitable flow rates were imposed such as to develop an induced pressure difference of not greater than 10-15% of applied vertical effective stress in order to minimise void ratio changes across the sample. The change in sample height due to seepage induced consolidation or swelling was recorded for several tests. The maximum reductions in sample height and average void ratio were both less than 0.3%. If the flow direction shown in Fig.4.1 was from the bottom to the top drain, the flow is called upward flow and downward flow is from top to bottom drain. Permeability tests using different flow rates during upward and downward flow were performed to check the general validity of Darcy's Law.

The test was started by setting GDS1 and GDS2 into withdrawal and infusion mode respectively. This was done by setting positive and negative ramps on GDS1 and GDS2 respectively. A ramp, R of 1 s represents a constant flow rate of 0.5 mm^3/s (one volume step per second) . The pressure difference between the top and bottom drains was monitored at 1.0 minute intervals until a steady value was obtained. Then the pressures in the GDS1 and GDS2 were again set back to the initial back pressure of 50 kPa. Then the sample was ready for the next flow rate test.

A typical permeability test consisted of 6 sets of data from three different flow rates introduced in upward and downward flow directions. Once the flow rate tests were completed at a given vertical effective stress, the back pressure was adjusted to 50 kPa at both drainage outlets and this was maintained throughout the next consolidation stage.

4.3 EVALUATION OF PERMEABILITY

Permeability of clay/sand mixtures from various tests can be calculated directly or indirectly as follows

4.3.1 Direct evaluation permeability from constant flow rate test

In a constant flow rate test with an imposed flow rate (Q/t), the permeability k, can be determined from the resulting pressure difference Δp, by a direct application of Darcy's law

$$k = \left(\frac{Q}{t}\right)\left(\frac{\gamma_w 2H}{\Delta p}\right)\left(\frac{1}{A}\right) \qquad (4.8)$$

Where Q = volume of flow of water

t = elapsed time

Δp = pressure difference between drainage boundaries

2H = height of the sample

γ_w= unit weight of water

A= cross section area of sample normal to the direction of the flow

The term (Q/t), represents a controlled constant flow rate imposed on the sample (which depends on the Ramp 'R' specified for the GDS) and the steady state pressure difference induced is Δp. The digital pressure controllers used in this study produce a constant flow rate of 0.5 mm^3/s for a ramp of 1 s. Thus the relationship between (Q/t) and R is given by

$$\frac{Q}{t} = \frac{0.5}{R} mm^3 / s \qquad (4.9)$$

Where R is the ramp in seconds.

The permeability in constant flow tests obtained from Eq.4.8 & 4.9 and for the particular dimensions of the oedometer used for the experiments (Fig.3.2) is

$$k = (\frac{10^{-6}}{930})(\frac{1}{R})(\frac{2H}{\Delta p}) \quad m/s \qquad (4.10)$$

where 2H is height of sample in mm, R in s and Δp in kPa.

4.3.2 Indirect evaluation of permeability

Permeability can also be evaluated indirectly from one dimensional consolidation test results or from the transient phases of flow pump test data.

4.3.2.1 Permeability from one dimensional consolidation

From consolidation test data, permeability is calculated indirectly from Eq.3.2 provided the two consolidation properties c_v and m_v are known. The permeability follows from Eq.3.2 :

$$k = c_v m_v \gamma_w \qquad (4.11)$$

In terms of the experimental data, the coefficient of consolidation c_v is obtained, from Eq.3.6

$$c_v = \frac{0.848\ H^2}{t_{90}} \qquad (4.12)$$

Adopting the following units c_v (m^2/yr), H (mm) and t_{90} (min) with double drainage

$$c_v = \frac{0.446\ H^2}{t_{90}} \qquad m^2/yr \qquad (4.13)$$

Once c_v has been calculated, the permeability, k can be obtained from Eq. 4.11 if the other soil characteristic m_v is known. If σ'_v is measured in kPa, m_v from Eq.3.7 is

$$m_v = \frac{-\delta v \times 1000}{v \delta \sigma'_v} \qquad m^2/MN \tag{4.14}$$

4.3.2.2 Permeability from transient phases of a flow pump permeability test

The characteristic pressure responses observed during the transient phases of the flow pump permeability test have been examined theoretically by Morin and Olsen (1987). The analysis is similar to that of Al-Dhahir and Tan (1968), who determined the coefficient of consolidation c_v, from initial transient phase of a constant head permeability test based on Terzaghi's (1943) one dimensional consolidation Eq.3.3 with boundary and initial conditions as shown in Fig.4.2. The solution to this model is presented by Carslaw and Jaeger (1959) for an analogous application of conduction heat transfer. The distribution of hydraulic head within the specimen as a function of time is described by the general diffusion equation:

$$c_v \frac{\partial^2 h}{\partial z^2}(z,t) = \frac{\partial h}{\partial t}(z,t) \tag{4.15}$$

and the solution to the above equation is

$$h = \frac{Q'L}{kA}\left[1 - \frac{8}{\pi^2}\sum_{n=0}^{\infty}\frac{\exp(-c_v(2n+1)^2\pi^2 t/4L^2)}{(2n+1)^2}\right] \tag{4.16}$$

Where

h = differential head across the sample

A = cross sectional area of sample

L = length of specimen

Q′ = constant flow rate

z = vertical distance from top of specimen

t = elapsed time since pumped flow started

k = permeability

Morin et al. (1989) developed a graphical method from the theoretical formulation (Eq.4.16) to determine coefficient of consolidation, and permeability from the transient phases of a flow pump permeability test. In terms of head ratio $\overline{H}$ and time factor T_v, the analytical solution gives the familiar Terzaghi solution for $\overline{U}$ (Eq.3.3), the average degree of consolidation:

$$\overline{H} = 1 - \frac{8}{\pi^2} \sum_{n=0}^{n=\infty} \frac{1}{(2n+1)^2} \exp\left[\frac{-(2n+1)^2 \pi^2 T_v}{4} \right] \quad (4.17)$$

where $\overline{H} = \frac{hkA}{Q'L}$ (4.17a)

$$T_v = \frac{c_v t}{L^2} \quad (4.17b)$$

To obtain a graphical solution, Eq.4.17 is plotted on Fig.4.3a with logarithmic scales, to produce a unique type curve solution for the model in Fig.4.2. By matching experimental curves generated from a constant flow rate permeability test onto the type curve (Fig.4.3a), a match point, A is arbitrarily chosen on Fig.4.3b. The location of this point needs to be somewhere near the two solution curves. Thus at the match point A,

$$c_V = \frac{L^2}{t_A} T_{VA} \quad (4.18)$$

$$k = \overline{H}_A \frac{Q'L}{h_A A} \quad (4.19)$$

where t_A and h_A are actual time and head difference on the dimensional axes of the experimental curve corresponding to the match point values of $A(T_{VA}, h_A)$ on the unique type curve.

The important requirement of the curve matching technique is that the experimental curve and type curve have to be plotted on log-log graphs that have identical cycle scales and the co-ordinate axes of the two plots must be parallel to each other. This graphical method of matching an experimental curve with an analytical type curve is called Theis method (e.g.Todd 1980) and was originally developed for analysing time-drawdown data from pumped well aquifer tests.

4.4 RESULTS AND DISCUSSION

4.4.1 Permeability test data

The characteristics of the data obtained during permeability measurements with constant flow rate test are shown in Fig.4.4a and Fig.4.4b. These figures show the induced pressure differences with time for six flow rates imposed on the samples of M100 and M30 mixtures which has experienced a

consolidation pressure of 320 kPa. The positive pressure difference indicates an upward flow through the sample from bottom to top while a negative value indicates a downward flow from top to bottom. The principal features of the data in Fig.4.4a and Fig.4.4b are: The induced pressure difference in upward flow is almost equal to downward flow. The interval of time which elapses after the flow rate is changed before the induced pressure difference reaches to a steady state value is called the response time. Small variations occur in the steady state pressure difference values which reflect fluctuations in the constancy of the imposed flow rate and stability of the recording system. These features of the data in Fig.4.4a & Fig.4.4b are identical with those reported by Olsen (1966); Olsen et al. (1985); Aiban and Znidarcic (1989); and Hamidon (1994). The time responses of the induced pressure difference for upward and downward flow are approximately the same at different flow rates.

Fig.4.5a & Fig.4.5b show the plots of average steady state pressure difference against flow rate for the data of Fig 4.4a &b respectively. Clearly the relationships between induced pressure difference and flow rate in Figs.4.5a &b are linear and Darcy's law seems to be obeyed.

Permeability of the sample at this consolidation stage is given by Eq.4.10:

$$k = (\frac{10^{-6}}{930})(\frac{1}{R})(\frac{2H}{\Delta p}) \text{ m/s}$$

With slight modification,

$$k = \frac{10^{-6}}{930}(\frac{2H}{S}) \text{ m/s} \qquad (4.20)$$

where

$$S = \frac{\Delta p}{(1/R)}$$

S is the slope of the line in Fig 4.5a & b and 2H is the height of the sample in mm.

Pressure difference against flow rate relationships for different consolidation stages for different clay-sand mixtures are shown in Fig.4.6a to Fig.4.6j. In these figures 'U' stands for unloading stage corresponding to an overconsolidated state. Some lines in Figs.4.6 show a small intercept, which may relate to the hydraulic resistance of the connecting pipe network (e.g. Hamidon 1994). According to Olsen (1985), osmosis causes an intercept in flow rate

versus hydraulic gradient relationships. Olsen also suggested that osmosis can be generated within a specimen by chemical reactions such as those involved in ageing effects. If osmosis is present in the specimen and in the absence of seepage induced deformation, the validity of Darcy's law does not require (according to Olsen) direct proportionality in the flow rate versus hydraulic gradient relationships. It only requires continuous relationships which shows a finite flow rate intercept at zero hydraulic gradient and also a finite hydraulic gradient intercept at zero flow. Figs.4.6 a to j illustrates this phenomenon i.e. continuous linear flow rate versus induced pressure relationships which may be displaced either upwards or downwards. However, interpreting these effects as secondary it may be deduced that Darcy's law was obeyed for all clay/sand mixtures M100 to M10 up to 90% sand at different void ratios and consolidation pressures. The slopes S of the lines in Figs.4.6 are obtained by linear regression through the appropriate points and the corresponding slopes are used for the calculation of permeability with Eq.4.20. The relationships between permeability and void ratio will be presented in the following section.

4.4.2 Permeability and void ratio

The variation of the permeability with void ratio is shown on a double logarithmic plot in Fig.4.7 for different clay sand mixtures. It can be seen in Fig.4.7 that the permeability decreases with decreases in void ratio and increases with the sand content. For each mixture the variation is approximately linear in this double logarithmic plot following a relationship of the form

$$k = Xe^{Y} \tag{4.21}$$

where X, Y are experimentally determined constants depending on the type of the mixture.

The above results indicate the general trend but do not show clearly any correlation between the permeability and composition of different clay/sand mixtures and do not illustrate the extent to which the clay phase is controlling the permeability. The results are replotted with clay void ratio in a double logarithmic plot in Fig.4.8. It can be seen that the logk-loge_c curves for different mixtures up to a sand content of 70% converge to a narrow band. It is only for higher sand contents that the unique relationship breaks down and indeed for higher sand contents of 80% and 90%, the permeability will tend to be so high that a technique of permeability determination devised for clays will not be appropriate.

A least square fit to all the data points of different clay sand mixtures from M00 to M70 produces the following relationship:

$$k = 4.66\, e_c^{3.18} \times 10^{-10} \text{ m/s} \qquad (4.22)$$

which is shown by the solid line in Fig.4.8.

Various relationships for the variation of permeability of clays have been proposed in the literature. Relationships considered here are Eq.4.6 (Tavenas et al. 1983-b), Al Tabbaa and Wood (1987) and Hamidon (1994). Tavenas et al. relation (Eq.4.6) suggest a linear relationship between the logarithm of permeability and void ratio. Fitting Eq.4.6 to the data of Fig.4.8 using e_0= 2.81 and its corresponding $k_o = 1.32 \times 10^{-8}$ m/s and plotting the results on a logk and loge plot shows that the results can be averaged by the following linear relationship:

$$k = 4.44\, e^{3.15} \times 10^{-10} \text{ m/s} \qquad (4.23)$$

which is shown in Fig.4.9 along with other relationships for comparison. This plot clearly indicates that the expression obtained is similar to the relations obtained by others. But this expression is in terms of clay void ratio and this can be useful to predict permeability changes even with a sand content as high as 70%.

4.4.3 Effect of overconsolidation on permeability

Investigation of permeability of clay/sand mixtures during unloading in the oedometer was carried out using constant flow rate tests. The values of permeability obtained in the overconsolidated state for different mixtures are plotted against clay void ratio e_c in double logarithmic scale in Fig.4.10. The straight line of the expression 4.22 from the tests on normally consolidated clay sand mixtures is shown as a solid line. Within the narrow ranges considered, it can be deduced that the expression (4.22) for normally consolidated clay/sand mixtures provides a reasonable fit to the data for overconsolidated mixtures up to a sand content of 60%. At a sand content of 70% the permeability starts to deviate from Eq.4.22. This suggests that Eq.4.22 devised for clay phase is primarily dependent on the clay void ratio and independent of the overconsolidation ratio and is valid up to a sand content of 60% in the clay sand mixtures.

4.4.4 Evaluation of permeability from indirect methods

4.4.4.1 Permeability from consolidation tests

The results of consolidation tests were plotted in terms of vertical settlement against the square root of time $\sqrt{t}$ and t_{90} was determined using Taylor's curve fitting method. Some typical results for consolidation of the M70 mixture are shown in Fig.4.11 for different effective stress levels. Values of coefficient of consolidation were calculated using Eq.4.13. The values of c_V for different mixtures are shown in Fig.4.12 plotted against the vertical effective stress. It is clear that the values of c_V are not constant over the wide range of vertical effective stress, but increase as σ'_v becomes larger. It is also found that the pressure dependency of c_V varies according to the clay content of the mixture and becomes smaller for high values of clay content. Fig.4.13 shows the correlation between the ratio of the values of c_V at σ'_v = 480 kPa and σ'_v = 10 kPa and clay content. As shown in Fig.4.13, the variation of c_V with vertical effective stress tends to increase as the clay content becomes smaller.

Values of the coefficient of compressibility of clay m_V are obtained from the plot of specific volume against vertical effective stress (Fig.3.11) using Eq.4.14. Typical results for various clay/sand mixtures are presented in Fig.4.14.

Knowing the values of c_V and m_V, the permeability values were calculated using Eq.4.11. The calculated permeability values are plotted against the average clay void ratio for the load increment in double logarithmic plot as shown in Fig.4.15. The results obtained from Eq.4.22 are shown in Fig.4.15 by solid line and can be used as a reference. The calculated permeability based on Terzaghi's consolidation theory is almost always less than the directly measured permeability by 0-50%. The problems associated with the application of Terzaghi's theory to soils have been pointed out by Olson (1986) and Tavenas et al. (1983-a); Hamidon (1994) has shown that it often greatly underestimates values of permeability.

4.4.4.2 Permeability from transient phases

The theory briefly presented in section 4.3.2.2 provides a basis for evaluating c_V and k from the initial transient phase of a flow pump test. The method outlined in section 4.3.2.2 is applied to the test results in Fig.4.4a for the mixture M100 at a vertical consolidation stress of 320 kPa. The absolute values of induced pressure difference, $|\Delta p|$ in Fig.4.4a are replotted against time on a double logarithmic scale as shown in Fig.4.16 with the same axes as for the type curve, (Fig.4.3a). Six sets of experimental data points are shown in Fig.4.16 for 6

constant flow rates imposed in 6 tests i.e. 3 upward and 3 downward flows. The observed time response - induced pressure difference data are superimposed on the type curve, keeping the co-ordinate axes of the two curves parallel and adjusted until a position is found by trial and error where most of the plotted points of the observed data fall on a segment of the type curve as shown in Fig.4.17. This is accomplished by printing the type curve on a transparency and moving it over the experimental graph, Fig.4.16. Any convenient match point is then selected and the co-ordinates of this match point are recorded such as match point A in Fig.4.17 which gives the following sets of readings for upward flow with Ramp 3 for mix M100 at $\sigma'_v = 320$ kPa

$T_V = 0.8$ $\quad t = 6$ min

$\overline{H} = 0.5$ $\quad \Delta p = 2$ kPa

From Eq.4.17b

$$c_v = \frac{T_v H^2}{t}$$

$$c_v = \left[\frac{365.25 \times 24 \times 60}{10^6}\right] \frac{T_v H^2}{t} \text{ m}^2/\text{yr} \qquad (4.24)$$

where t is in minutes, H is half height of the sample in mm and T_V is a non dimensional time factor.

Also from Eq.4.17a and with the relations Q' = 1/(2R) and h, differential head = $\Delta p/\gamma_W$

$$k = \frac{H \overline{H} \gamma_w}{2 \Delta p A R}$$

$$= \left[\frac{98070}{2}\right] \frac{H \overline{H}}{\Delta p A R} \times 10^{-10} \quad \text{m/s} \qquad (4.25)$$

where Δp is in unit of kPa and A is cross section area (Fig.3.2) in mm^2 (i.e A = 4560 mm^2), H is half height of the sample in mm, $\overline{H}$ is a dimensionless head factor and R is the ramp in second.

The above value of T_V, t, $\overline{H}$, Δp, 2H = 14.31 mm and R = 3 s give c_V value of 3.59 m^2/yr and k = 6.41 x 10^{-10} m/s.

A similar exercise can be performed with other time - pressure difference data at different flow rates in Fig.4.16 so that the profile coincides with the type curve. Some results derived from this curve matching procedure at σ'_v= 320 kPa for different clay/sand mixtures are listed in Table 4.1. Typical average values of k and c_v were obtained from transient phase for 6 constant flow rates imposed across the sample (3 upward and 3 downward flows). Inspection of these values indicates that permeability k from the transient curve matching technique estimates is consistently less than the corresponding steady state value by around 50%. The c_v values listed in the table are quite significantly smaller than the c_v values deduced from the square root of time method by about 50% to 86%..

Permeability values evaluated by curve matching method for different clay/sand mixtures at different stress levels are presented in Fig.4.18. The permeability relationship (Eq.4.22) obtained from steady state values is considered as a reference and is shown in Fig.4.18 as a solid line. The figure shows that permeability values obtained from transient records are almost half of the steady state values, whereas k deduced from consolidation results as shown in Fig.4.15 usually underestimated the steady state values by less than 50%. Hamidon (1994) has shown that permeability values calculated from transient phase are always within a factor of 2 of steady state values. This can be explained by the fact that the permeability values evaluated from the transient records use Terzaghi's one-dimensional consolidation solution (Eq.3.3) whereas the permeability values obtained from the steady state conditions were computed using Darcy's law with no further assumptions about soil behaviour.

4.5 CONCLUSION

Permeability of clay/sand mixtures have been deduced by three techniques:

a) by direct measurement using constant flow tests

b) by interpretation of the consolidation stages of the oedometer tests

c) by interpretation of the transient stages of the constant flow tests.

The direct measurements of permeability are regarded as the most reliable. For a given void ratio the permeability obtained by methods b and c are up to 50% lower with the interpretation of the transient stage tending to give lower values that those obtained from interpretation of the consolidation.

When plotted as a function of clay void ratio it is found that the relationship between permeability and clay void ratio for the clay/sand mixtures is unique for loading and unloading for clay contents down to 40%.

Table 4.1 Summary of curve matching results at σ'_v = 320 kPa for M100

Mix	k- transient data m/s	k-steady state value m/s	% error in k	c_v from transient data, m2/yr	c_v from square root time, m2/yr	% error in c_v
M100	6.37E-10	1.19E-09	-46.5	2.66	5.45	-51.2
M90	7.06E-10	1.29E-09	-45.4	1.40	6.00	-76.7
M80	7.21E-10	1.28E-09	-43.7	3.40	8.46	-59.8
M70	6.78E-10	1.23E-09	-45.1	4.84	9.53	-49.2
M60	7.20E-10	1.32E-09	-45.6	4.38	9.65	-54.6
M50	6.75E-10	1.20E-09	-44.0	4.19	10.31	-59.4
M40	6.72E-10	1.43E-09	-52.9	7.71	15.91	-51.5
M30	6.72E-10	1.43E-09	-52.9	6.23	44.94	-86.1

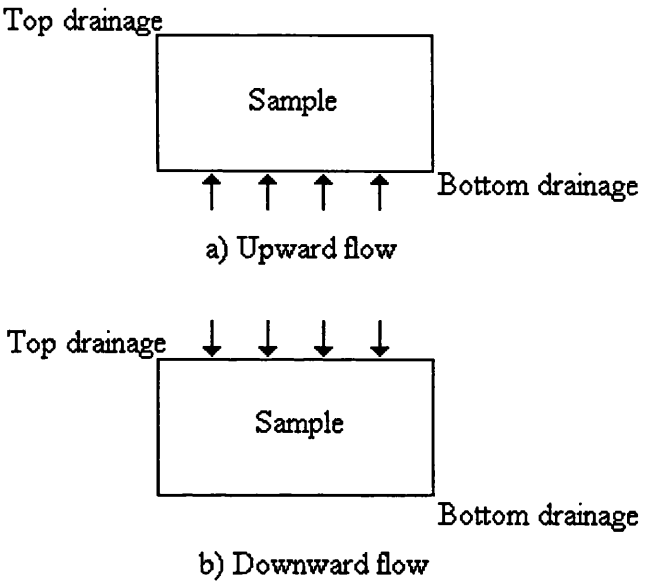

Fig.4.1 Flow direction

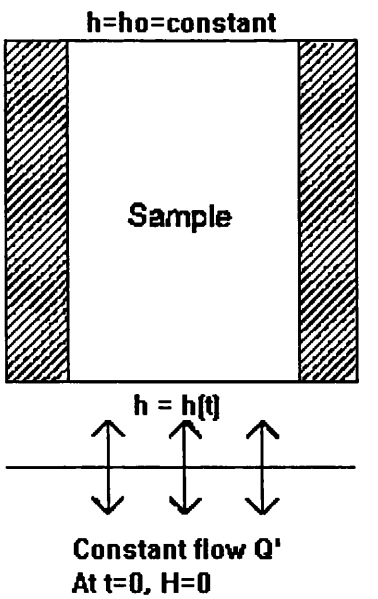

Fig.4.2 Boundary and initial conditions (Morin et al. 1989)

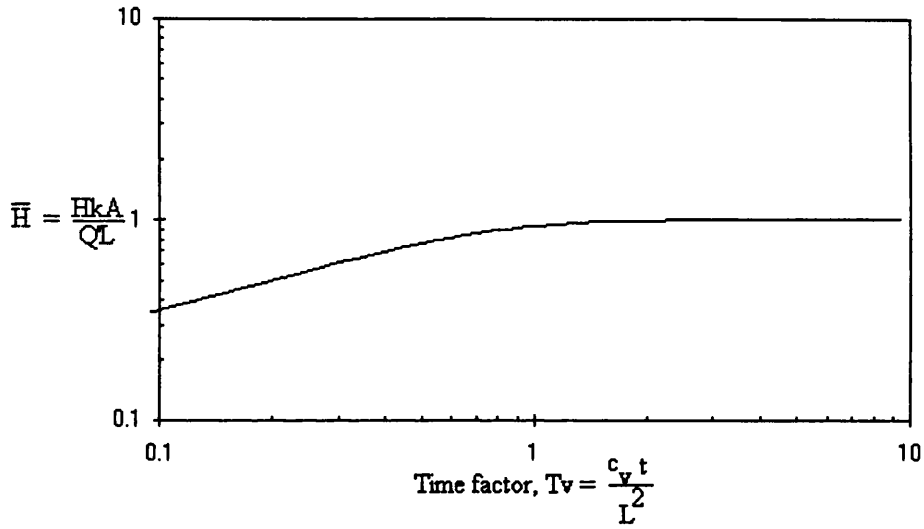

(a)

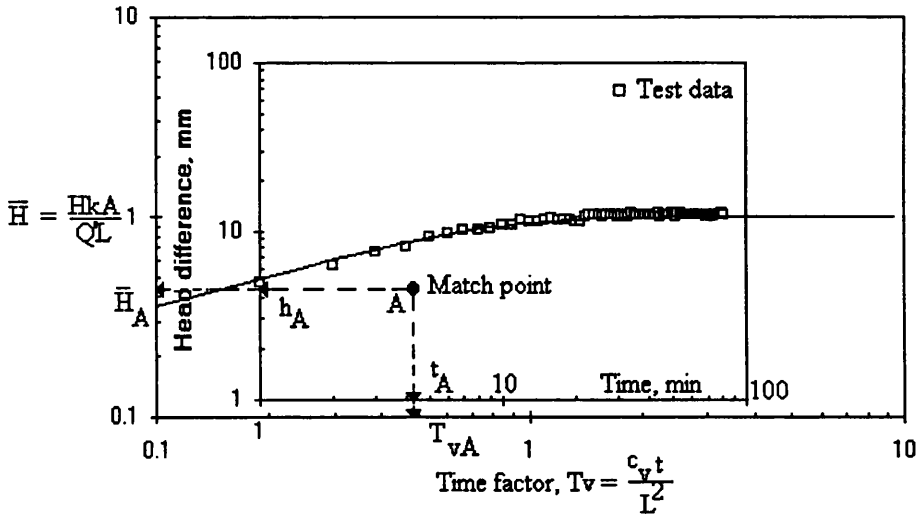

(b)

Fig.4.3 (a) Type curve of Eq.4.16; (b) Curve matching of constant flow rate test data (Morin et al. 1989)

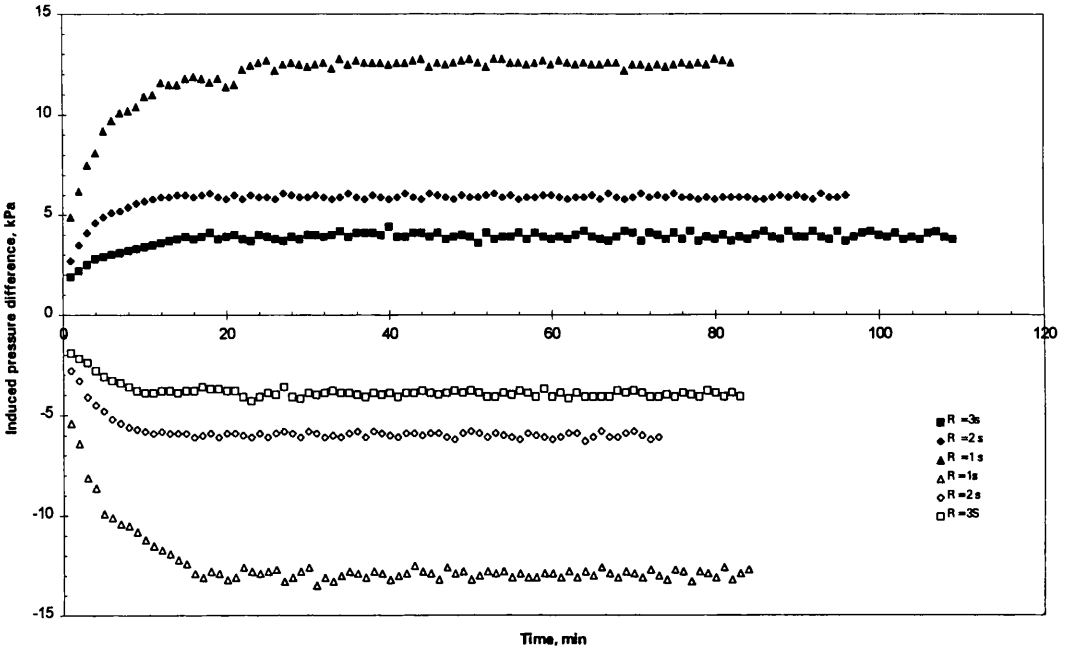

(a)

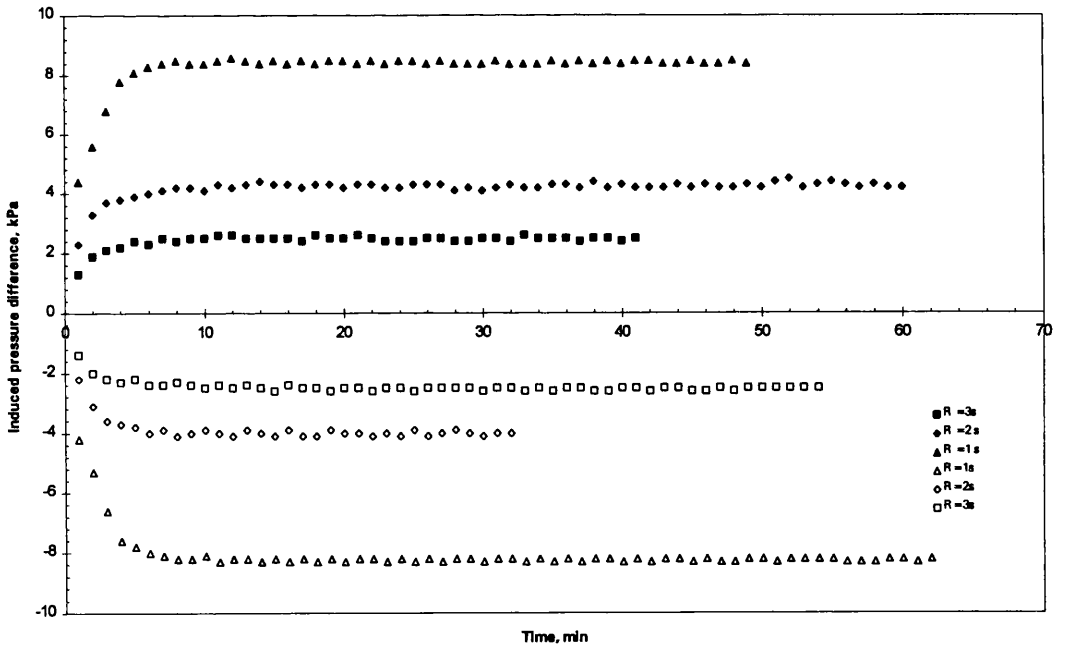

(b)

Fig.4.4 Typical data for permeability measurements.
Fig.4.4a. Induced pressure difference versus time across M100 at 320 kPa.
Fig.4.4b. Induced pressure difference versus time across M30 at 320 kPa.

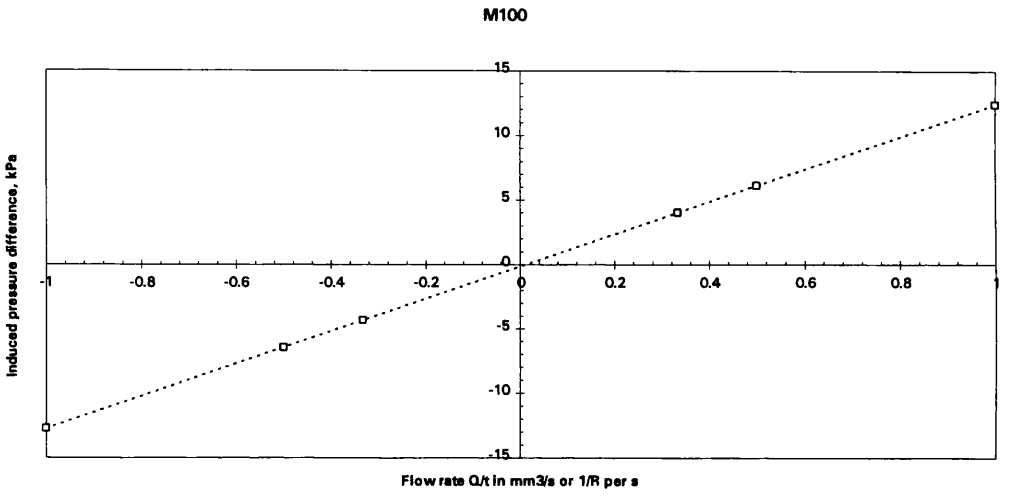

(a)

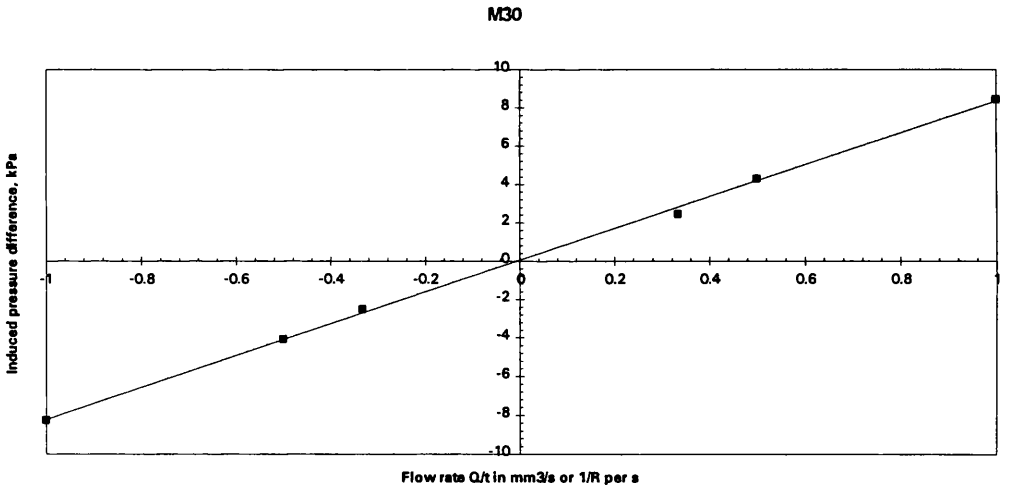

(b)

Fig.4.5 Relations between steady state induced pressure difference and flow rate

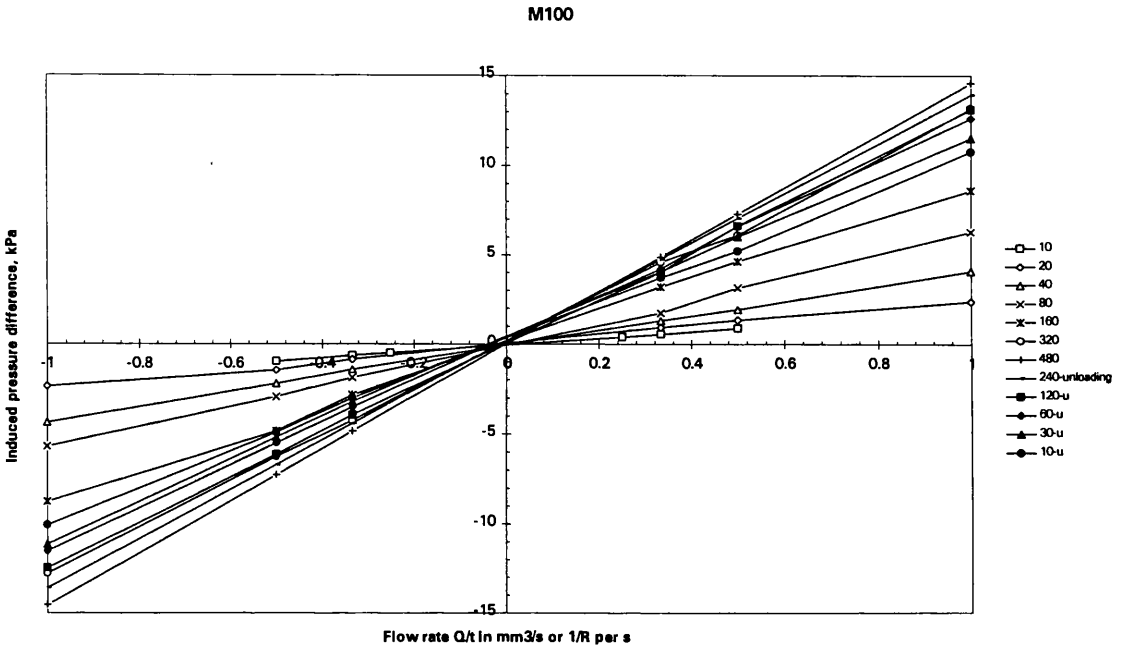

(a)

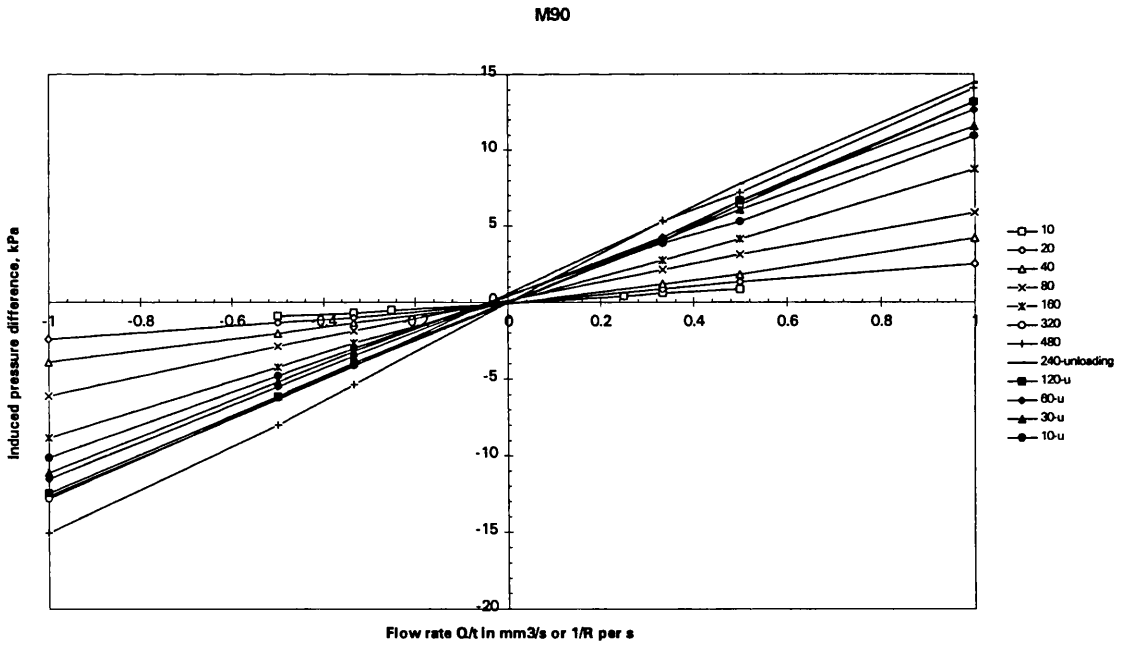

(b)

Fig.4.6 Induced pressure difference- flow rate relationships at different consolidation stages

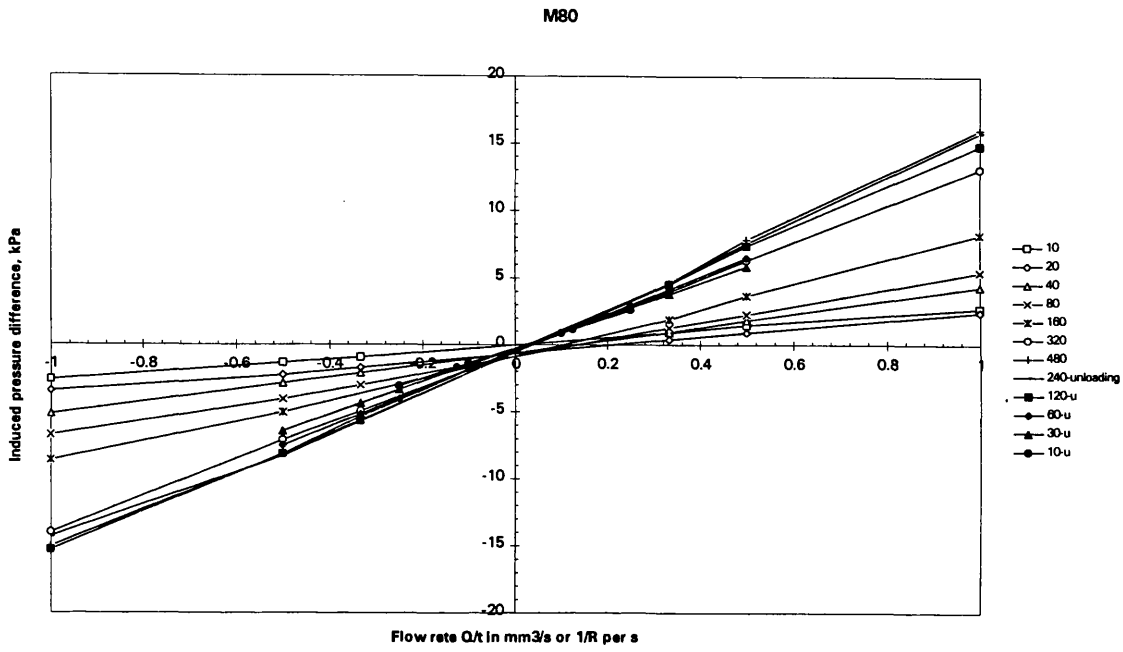

(c)

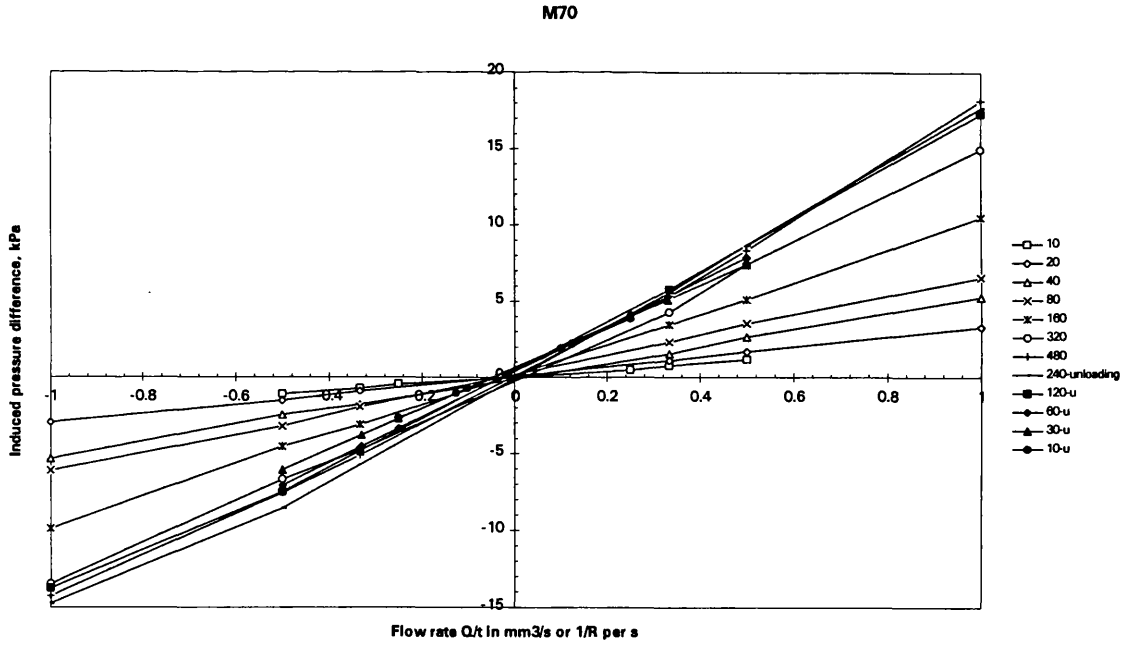

(d)

Fig.4.6 Induced pressure difference- flow rate relationships at different consolidation stages

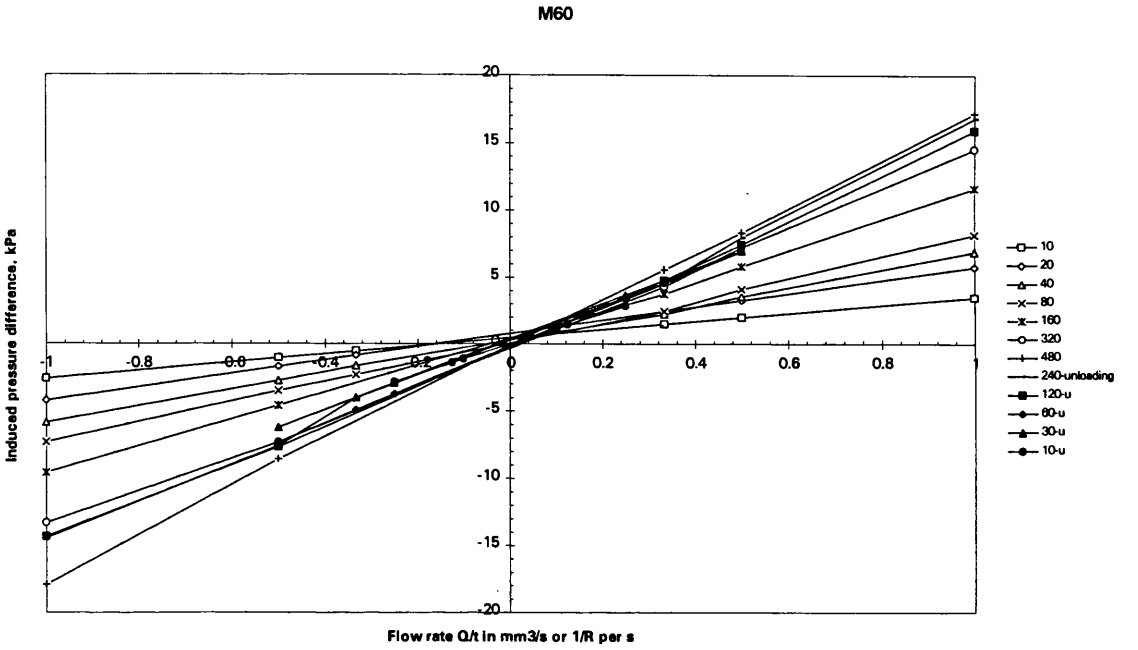

(e)

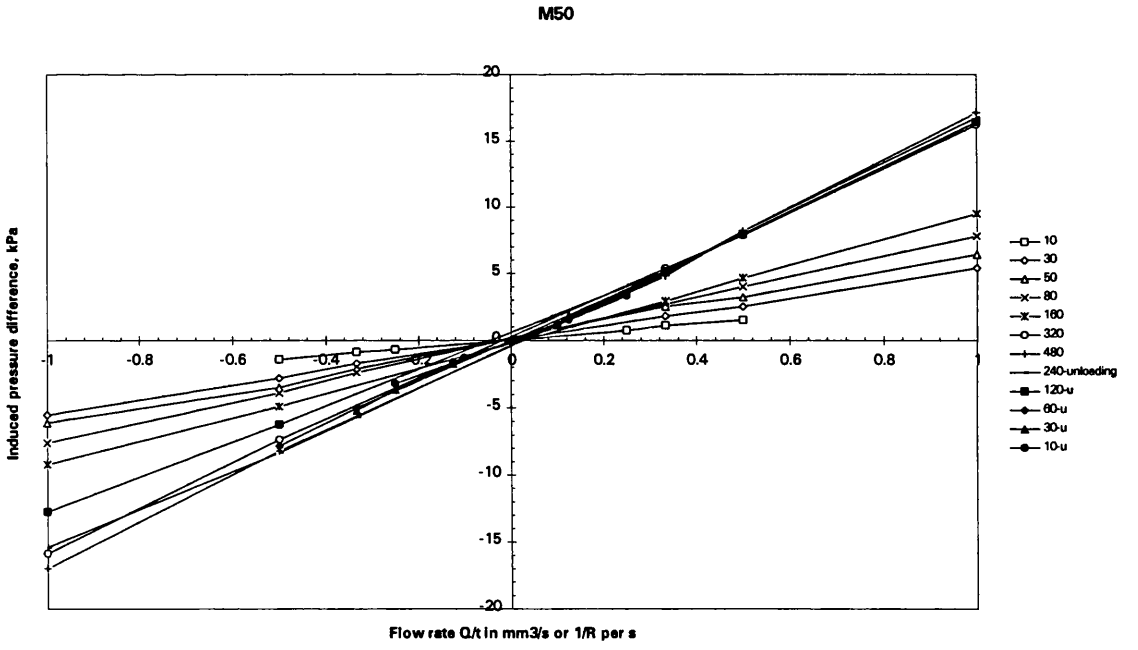

(f)

Fig.4.6 Induced pressure difference- flow rate relationships at different consolidation stages

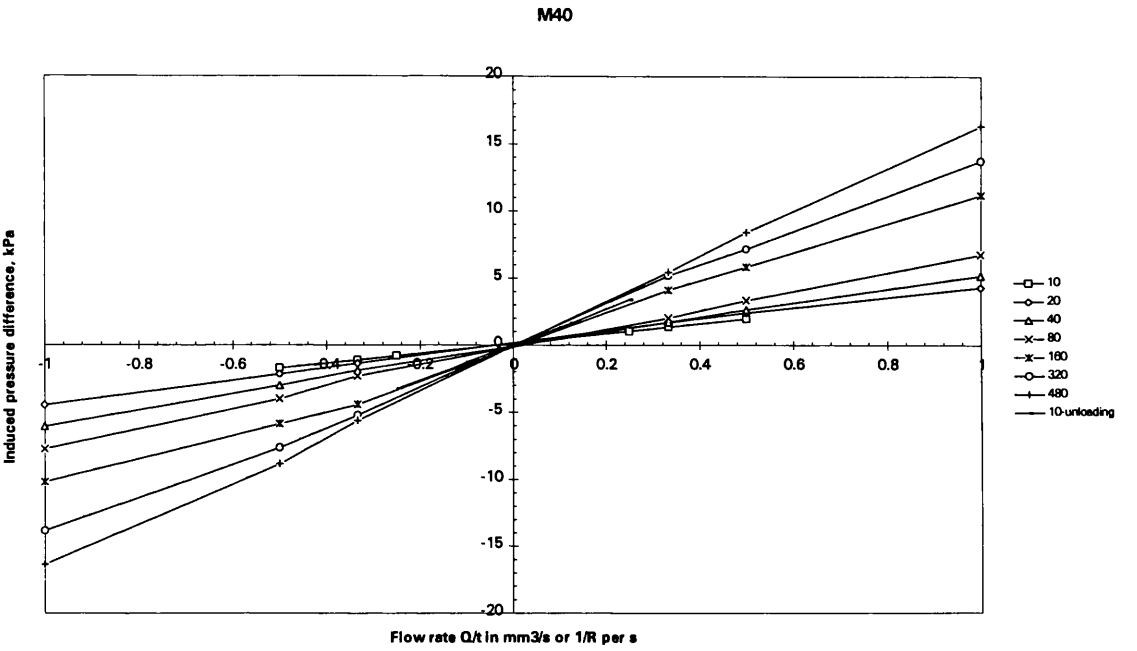

(g)

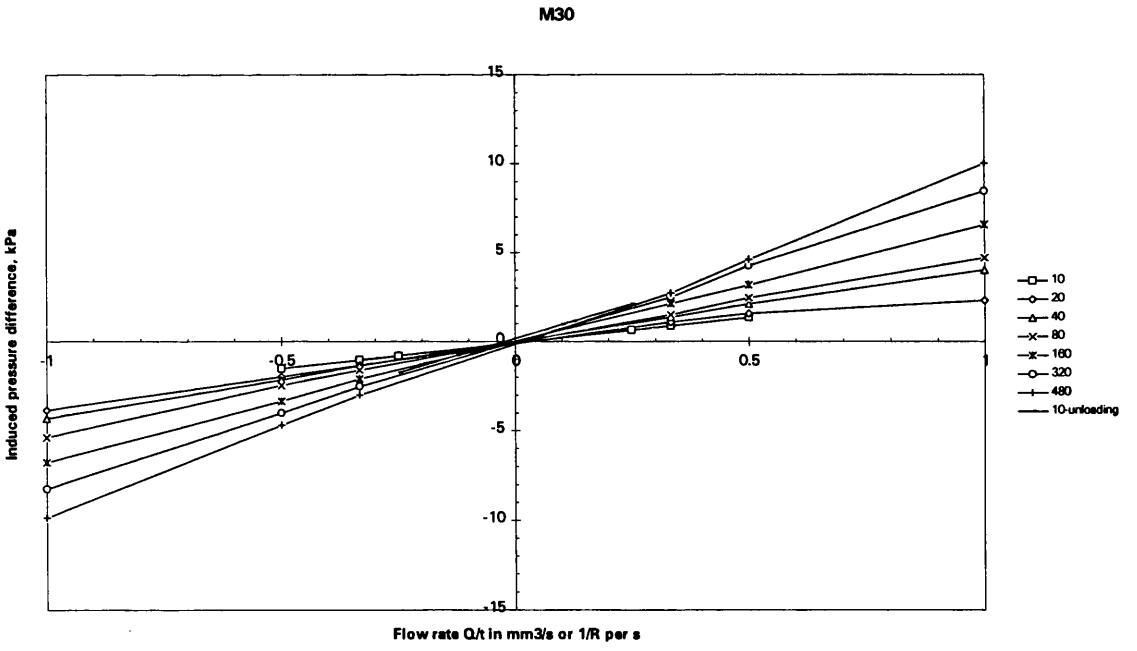

(h)

Fig.4.6 Induced pressure difference- flow rate relationships at different consolidation stages

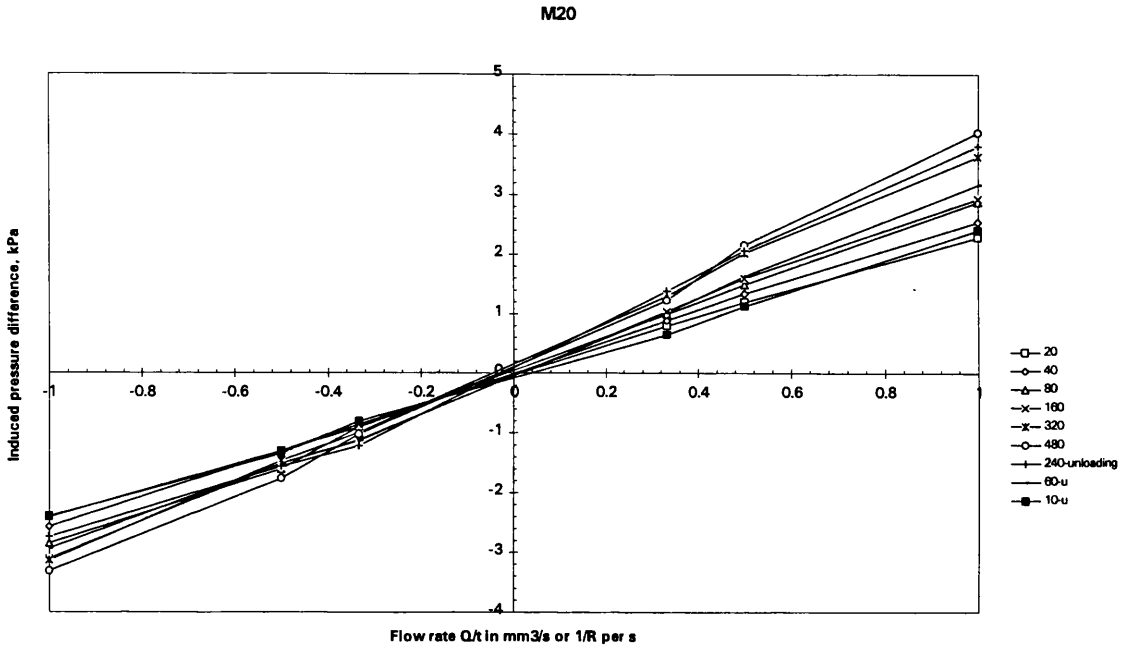

(i)

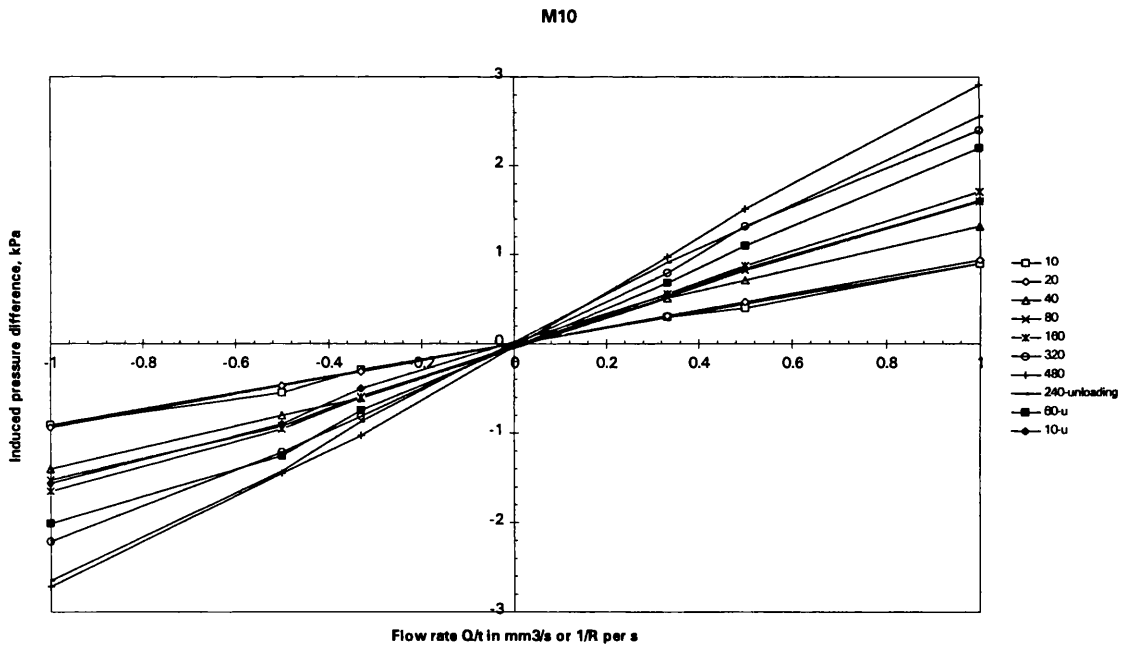

(j)

Fig.4.6 Induced pressure difference- flow rate relationships at different consolidation stages

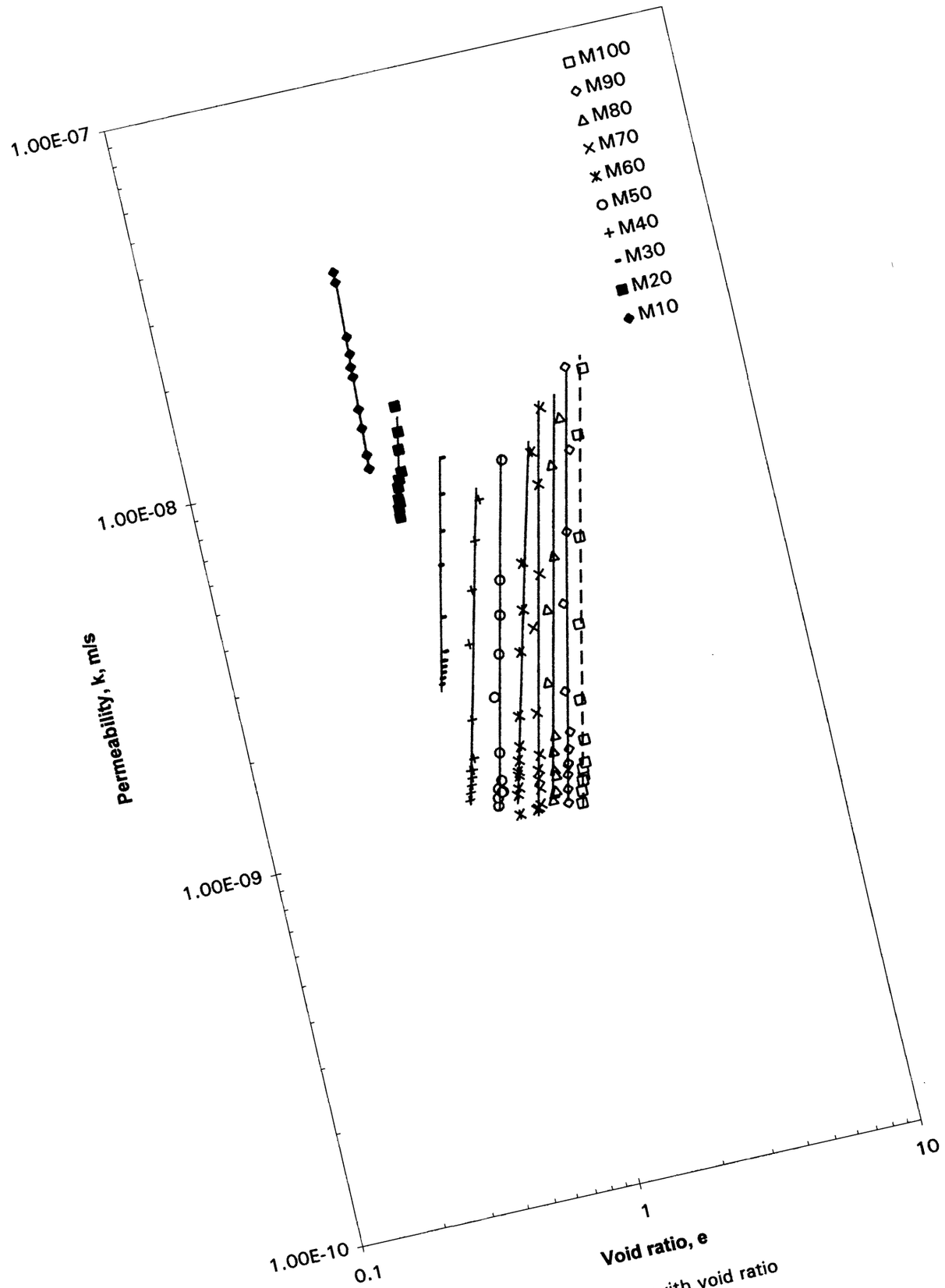

Fig.4.7 Variation of permeability with void ratio

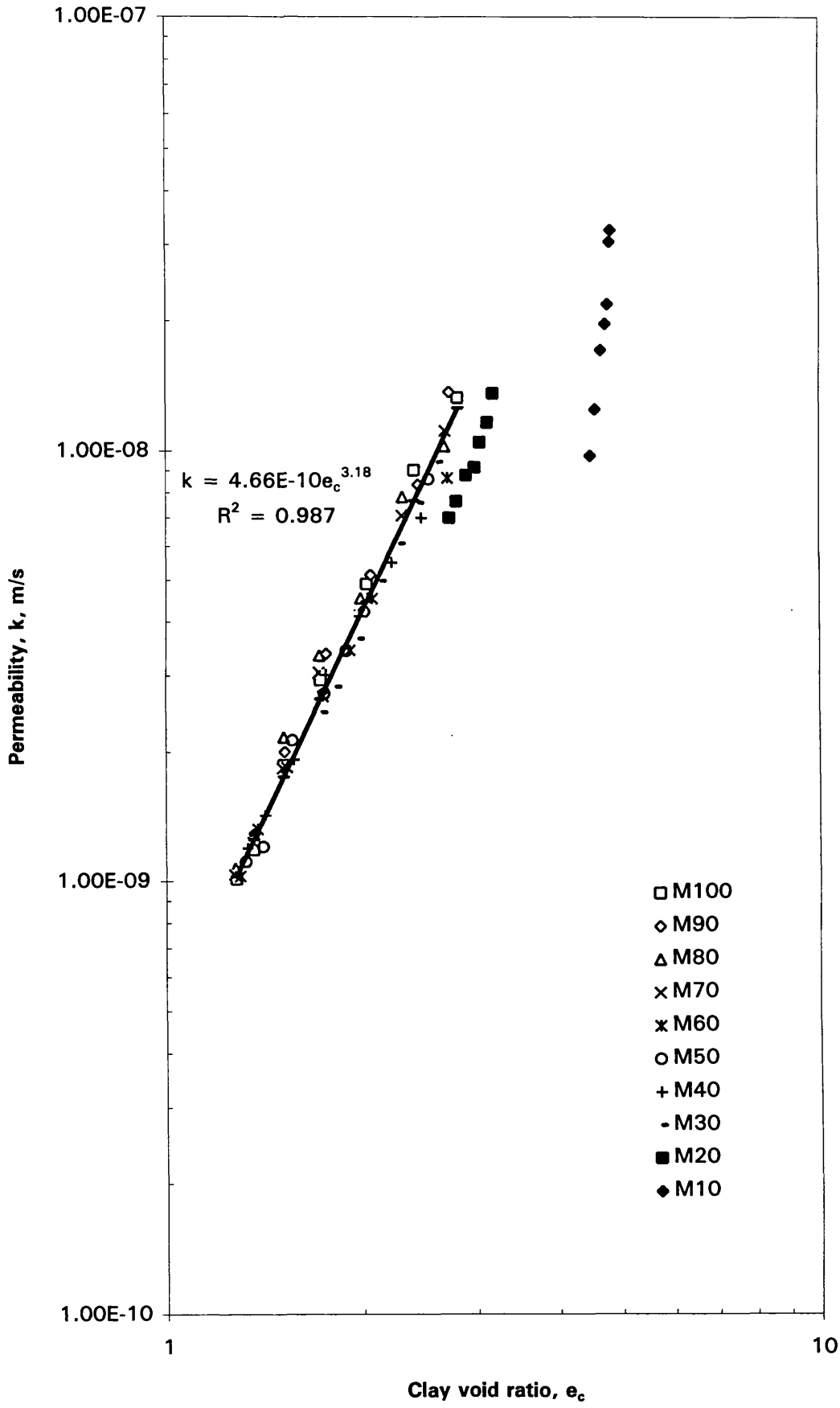

Fig.4.8 Variation of permeability with clay void ratio

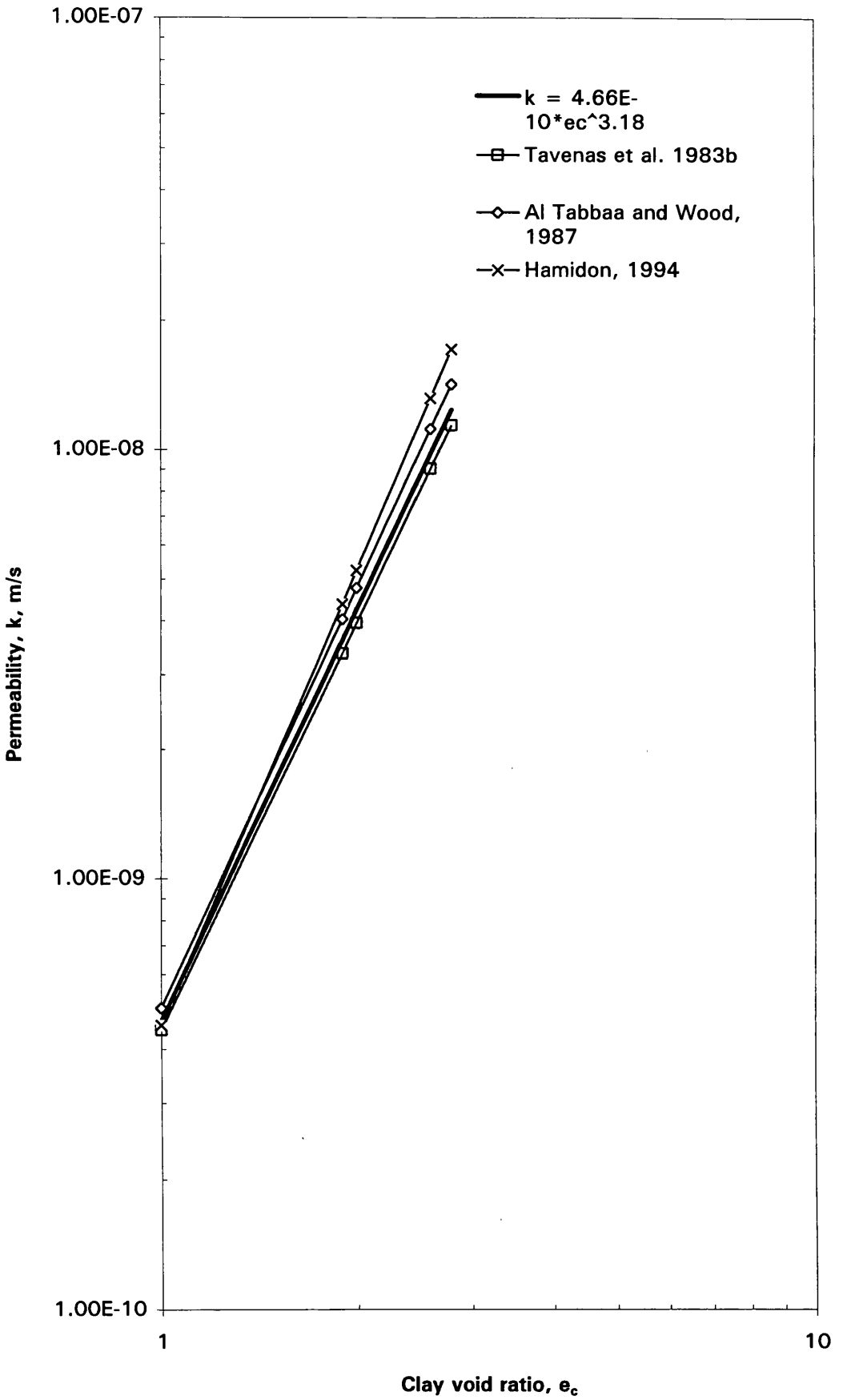

Fig.4.9 Vertical permeability obtained by various research workers

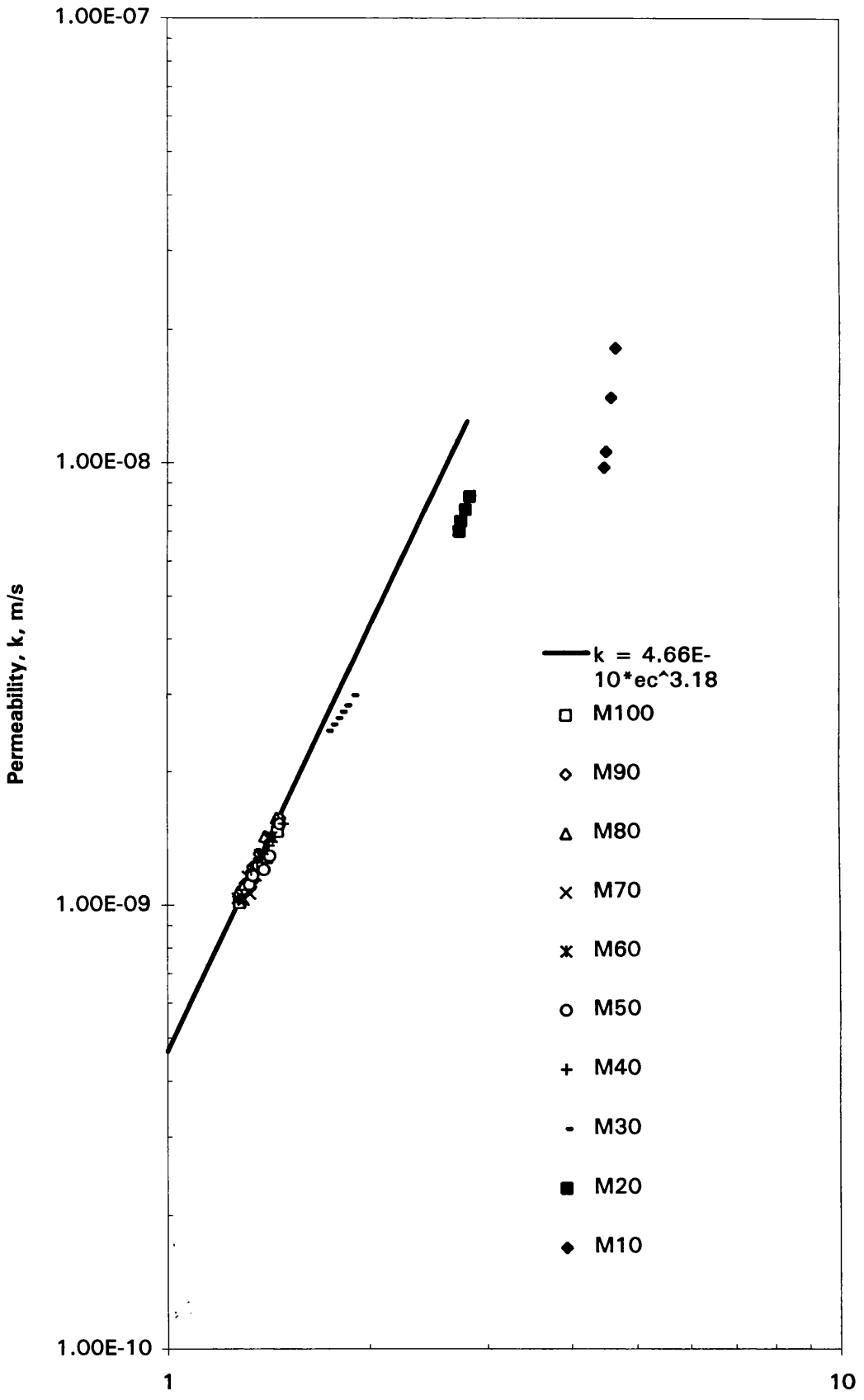

Fig.4.10 Variation of permeability with clay void ratio during unloading in odeometer

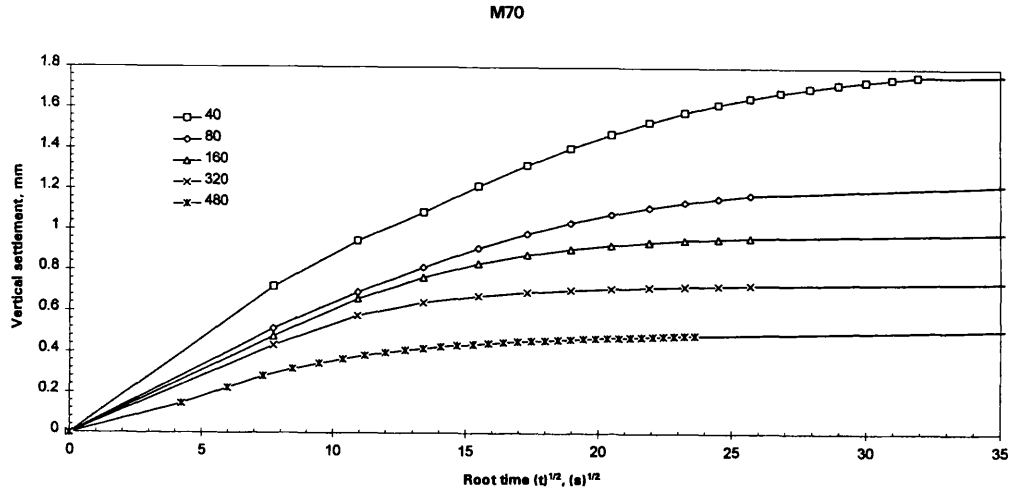

Fig.4.11 Settlement - square root of time

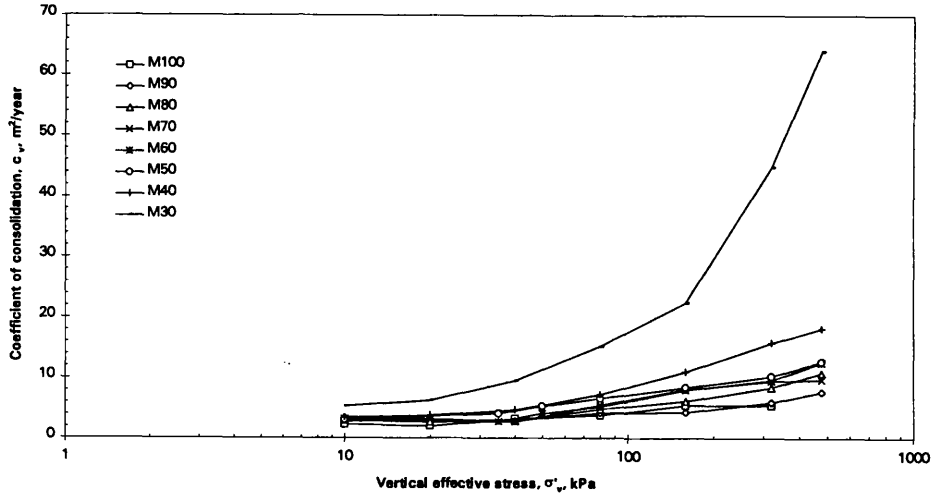

Fig.4.12 Variation of c_V with vertical effective stress

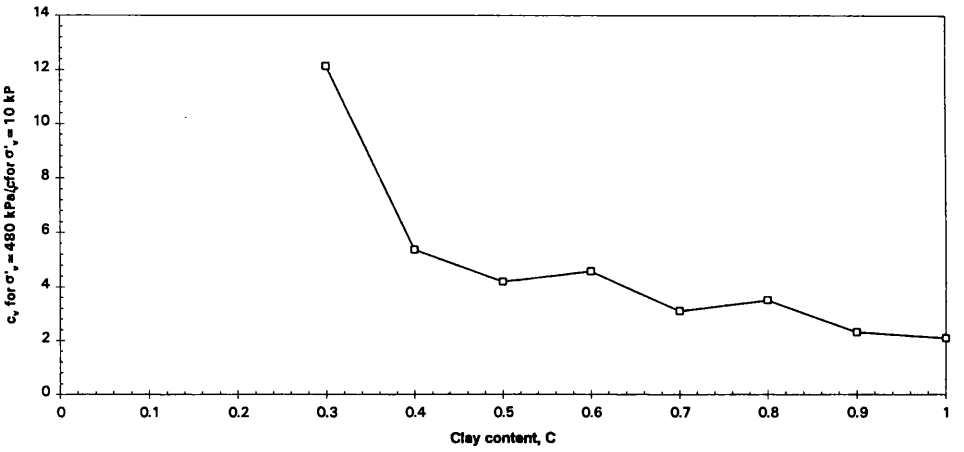

Fig.4.13 Relationship between c_V ratio and clay content

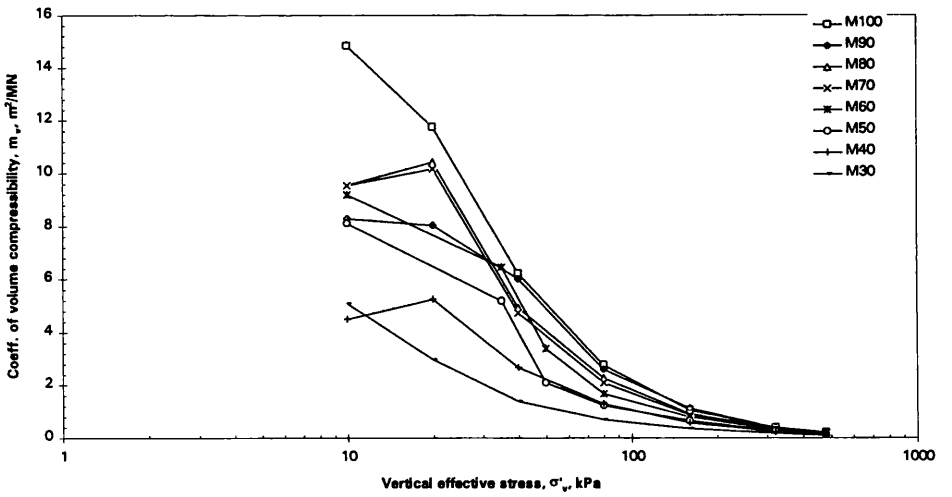

Fig.4.14 Variation of m_V with vertical effective stress

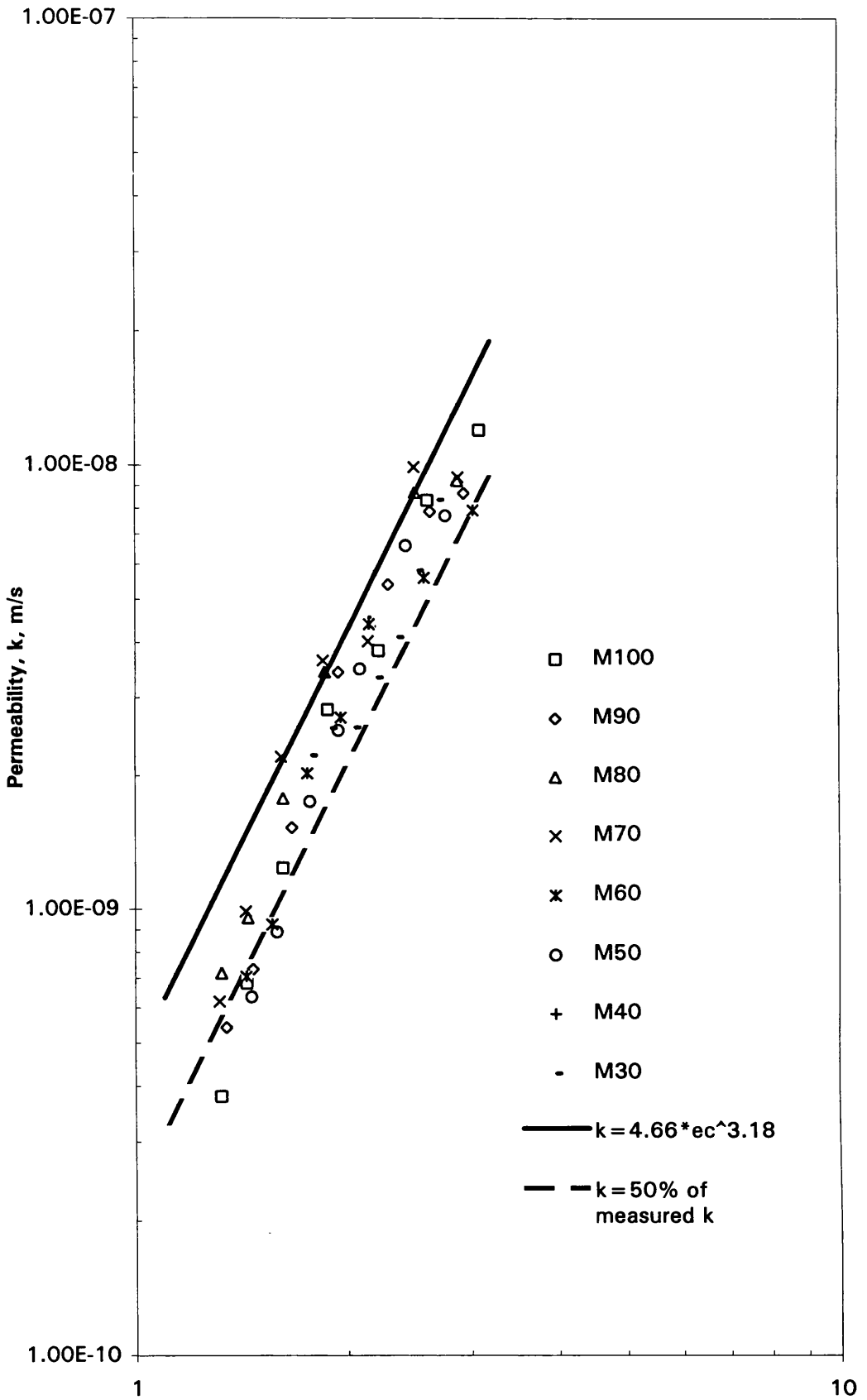

Fig.4.15 Comparison of permeability obtained from 1-D consolidation theory

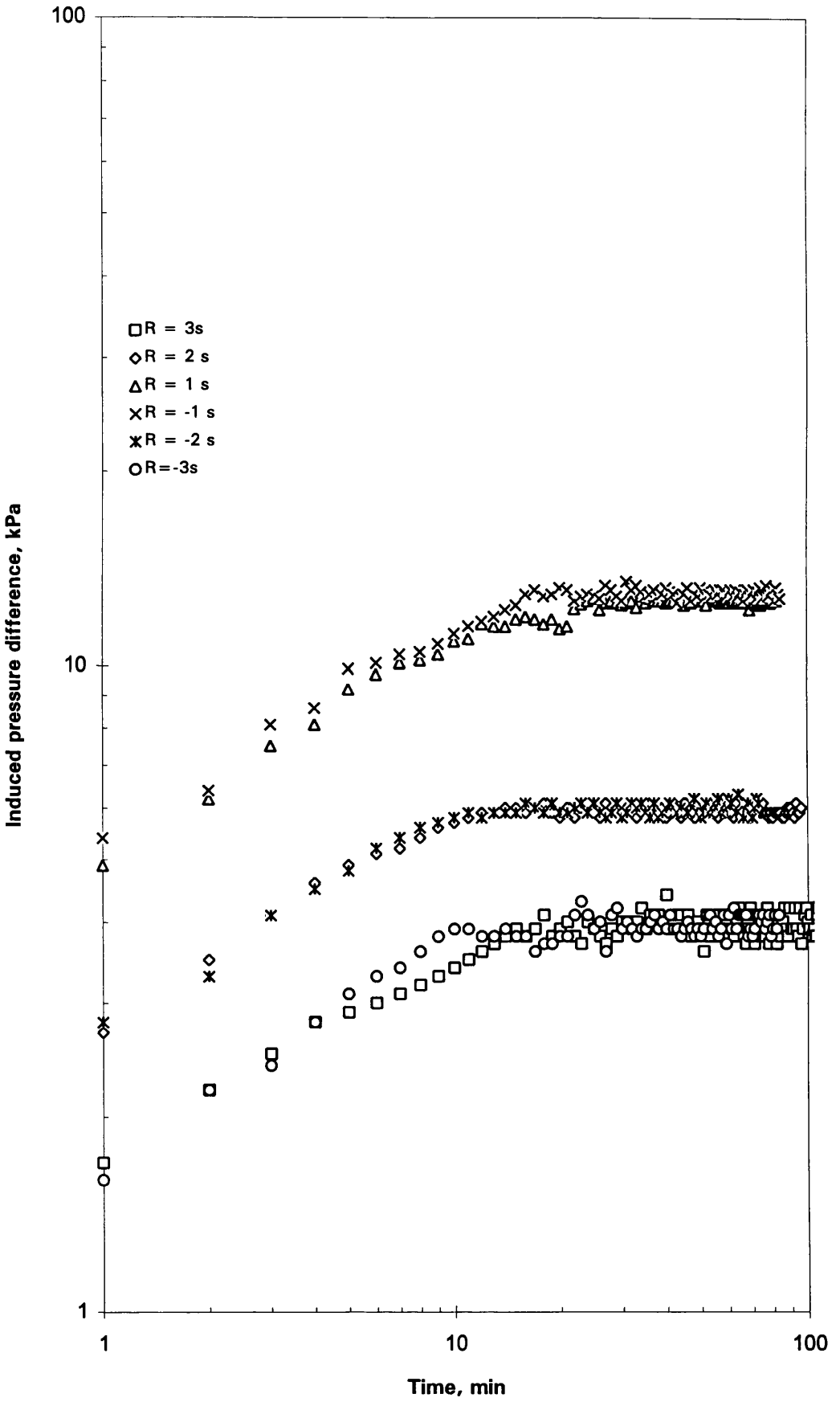

Fig.4.16 Pressure difference - time for M100 at vertical stress of 320 kPa

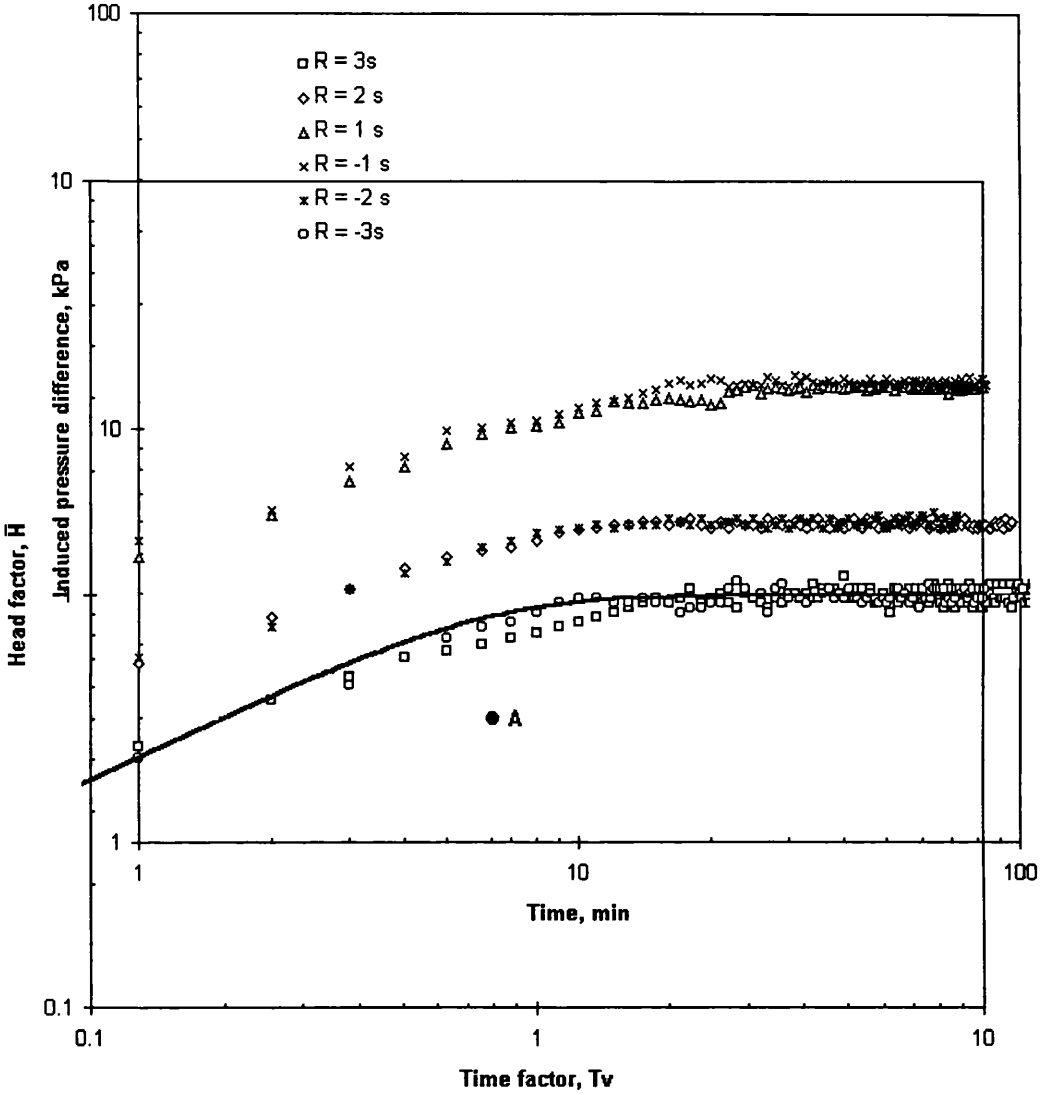

Fig.4.17 Curve matching of experimental data to type curve for M100 σ'_v = 320 kPa

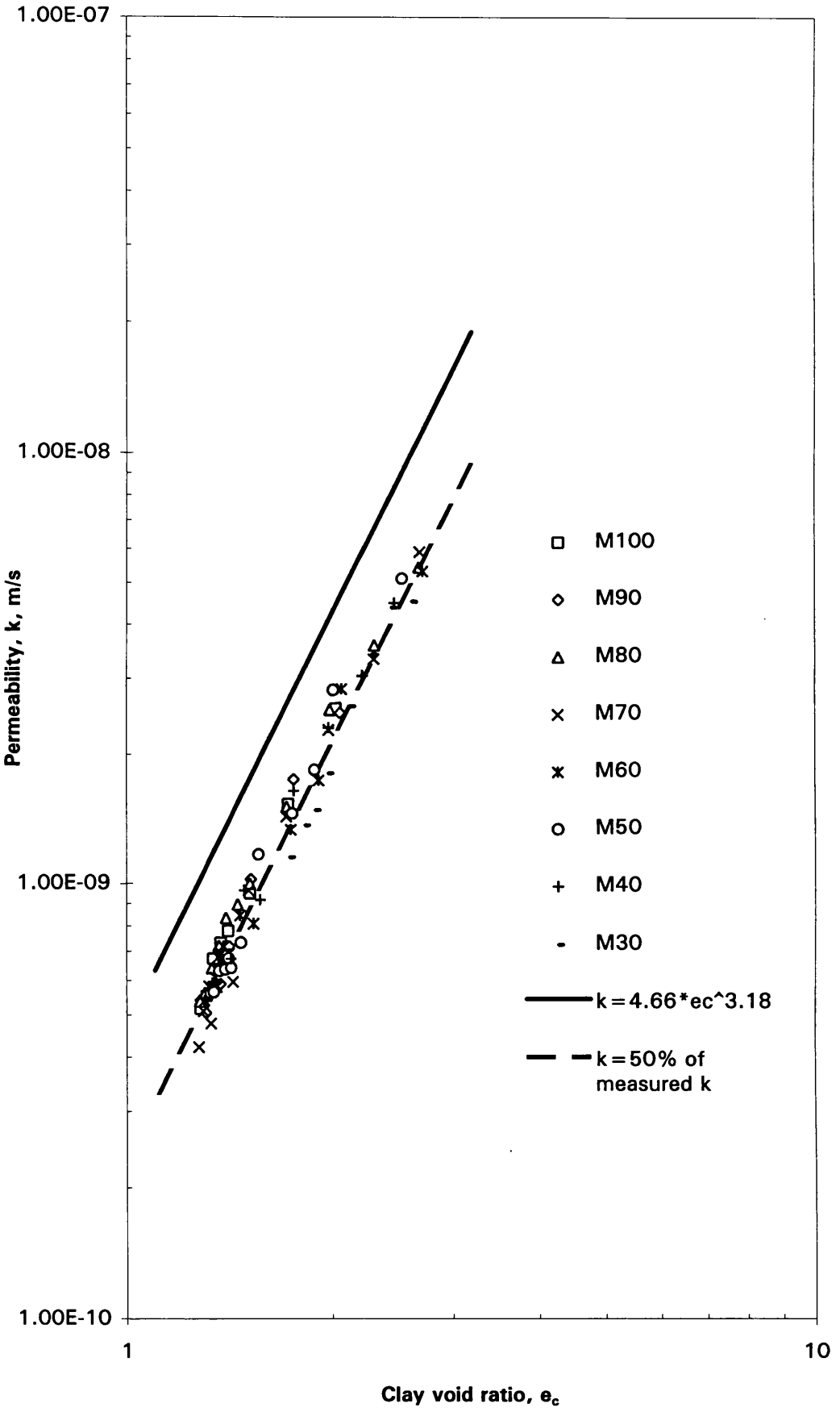

Fig.4.18 Comparison of permeability from transient data

CHAPTER 5

STRESS : STRAIN BEHAVIOUR

The shear behaviour of soils is an important aspect in many foundation engineering problems such as the bearing capacity of shallow foundations and piles, the stability of the slopes of dams and embankments, and lateral earth pressure on retaining walls. The analysis of these structures is carried out by performing settlement and stability calculations. They are concerned with stiffness and strength at failure of soils under applied loads. Stability calculations are usually performed in terms of either total stresses or effective stresses. Total stress analyses are usually performed for situations in which undrained loading response is of interest and a single undrained shear strength will be directly relevant to the behaviour of soil. For drained loading conditions where all excess pore pressure has dissipated, stability analyses must be carried out in terms of effective stress using drained shear parameters. Effective stress analyses can also be used in undrained situations where pore pressure can be reliably estimated. The test data required for settlement and stability analyses can be obtained conveniently with triaxial apparatus (e.g. Bishop and Henkel 1962). For economic design of engineering structures, it is vital to understand the stress:strain behaviour of soils and this chapter describes a laboratory investigation aimed at a detailed study of undrained and drained behaviour of clay/sand mixtures to identify the extent to which the clay controls the shear behaviour of mixtures at different overconsolidation ratios.

5.1 TRIAXIAL APPARATUS AND EXPERIMENTAL PROCEDURE

5.1.1 Description of the triaxial apparatus

A schematic arrangement of the triaxial apparatus is shown in Fig.5.1. The equipment used for testing was similar to that described by Bishop and Henkel (1962). The triaxial machine used in all strength tests in this study was a constant rate of strain machine manufactured by Wykeham Farrance, England. The strain is applied by a mechanical jack operated by a motorised gearbox. The motor applies continuous strain with the rate of strain depending upon the gear setting.

The cell pressure and back pressure were maintained constant during testing using an air/water pressure system with a pressure regulator in the air line.

This system provides a pressure range of 0-650 kPa with maximum fluctuations of about ±5 kPa.

The cell pressure, back pressure, and pore pressure were measured using Bell and Howell pressure transducers. Each test was began with isotropic consolidation and during this stage, drainage was allowed from the top of the specimen. In all stages of the test, pore pressure was measured at the base of the specimen. During undrained shearing pore pressure was also measured at the top with a transducer in the back pressure line. The pressure transducers were calibrated using a dead weight pressure tester. The maximum error in the transducer measurement is about ±3 kPa.

The axial load was measured by a submersible load cell fitted on the lower end of the loading plunger. This internal measurement of axial load eliminated the effects of shaft friction. The capacity of this transducer was 4.5 kN. The load cell was also calibrated using a dead weight tester.

The axial deformation of the sample was measured using a linear variable differential transformer (LVDT) which recorded the vertical movement of the loading ram with a range of 50 mm. The LVDT was calibrated against a micrometer and is accurate to ±1.6 μm.

The volume changes during saturation, consolidation, and during drained tests were measured using an automatic volume change apparatus (manufactured by Wykeham Farrance, England) connected to the back pressure system. The displacement capacity of the device is 80 cm^3, but this can be extended by using push-pull flow reversing valves. This device can be used at back pressures up to 1000 kPa with a resolution of about 0.025 cm^3 but it is very sensitive to pressure fluctuations.

The outputs from the above transducers were monitored by a Solartron Orion data logger, which also provides a constant voltage source to energise each transducer.

The compression behaviour of samples tested in the triaxial apparatus is influenced by the frictional restraint imposed at the ends of the sample. Rowe and Barden (1964) have discussed the effect of sample geometry (ratio of height to diameter) and the effect of providing frictionless ends (by lubricating enlarged smooth end platens) on the stress:strain response. Barden and McDermott (1965) tested compacted clay as well as remoulded normally consolidated and overconsolidated clay with lubricated and nonlubricated platens and concluded that the effective strength parameters were not altered when the results were compared with samples with a length to diameter of 2:1 between ordinary platens. Bishop and Green (1965) tested sand and reached the same conclusion

regarding the maximum angle of shearing resistance. Lubricated ends have relatively little effect (Head 1985) on the behaviour of samples of conventional length and hence conventional 38 mm diameter end platens with ratio of sample height to diameter 2 were used in this study. However contact between the top cap and the load cell was improved so that no tilting will occur while shearing the specimen at large strains. Tilting was prevented by eliminating rotation of the cap and this was done by clamping the top cap into the load cell. Details of this top cap are shown in Fig.5.2

5.1.2 Triaxial tests on clay/sand mixtures

5.1.2.1 Sample preparation

Specimens for testing were prepared from clay-sand slurry consolidated in the consolidation tube shown in Fig.3.5. The method of setting up of samples in the consolidation tube is identical to that used for the study of the consolidation characteristics of clay/sand mixtures at higher vertical stresses which was discussed in section 3.1.2 in Chapter 3. Slurry was put in the tube up to a height of 180-190 mm so that enough material should be left after trimming to 80 mm in height for water content and density evaluation. After placement of the slurry was completed, the triaxial cell for 38 mm diameter specimens was fitted to the base pedestal and filled with de-aired water. The plumbing arrangements for the consolidation tube enclosed in the triaxial cell are shown in Fig.5.3. Increments of consolidation pressure were provided by the cell pressure. In the consolidation tube, the clay-sand slurry was consolidated one-dimensionally to a vertical pressure of 400 kPa. This was achieved by applying cell pressure increments of 10, 25, 50, 100, 200 and 400 kPa. During the consolidation, drainage was permitted at top and bottom through porous Vyon plastic discs. Volume changes occurring in the sample were recorded with twin burette gauges connected to the drainage lines. The piston connected to the top cap also enabled vertical movement to be measured using a dial gauge. A Time interval of about 24 hours was left between each load increment to allow complete consolidation.

At the end of consolidation, the bottom and top drainage valves were closed and the triaxial cell was carefully removed. Then the cell base was clamped to the compression machine as shown in Fig.5.4 in order to remove the top cap. To pull out the top cap, a rod assembly (Fig.5.4) guided through a rigid stabilising support was used. The end of the rod assembly was connected to the top cap and by turning the triaxial apparatus handle in an anti-clockwise direction

the top cap was gradually pulled up. After removing the top cap, the consolidation tube was carefully removed from the base and the specimen was extruded with a hand operated hydraulic jack and trimmed with wire saw. The general arrangement is shown in Fig.5.5. The presence of sand presented a problem when trimming the excess soil. If pieces of sand broke the trimmed plane at the top of consolidometer, they were removed during trimming, which left voids in the surface of the sample. After trimming the sample to a height of 80±2 mm, these voids were carefully filled with clay or sand in an attempt to replace the voids with the material removed during the trimming.

5.1.2.2 Selection of shearing rate

Before the first test began, a displacement rate had to be selected. The maximum rate was controlled by the time required for equalisation or dissipation of the pore pressure within the sample.

A fully drained test must be run slowly to allow excess pore pressure to dissipate by the provision of drainage before failure is reached. In an undrained test the excess pore pressure is allowed to build up and enough time must be allowed to enable the pore pressure to equalise throughout the sample if true measurements of pore pressure are to be made at the boundary of the sample and the deformation of the sample is to be uniform.

Bishop and Henkel (1962) gave a theoretical relationship for pore pressure dissipation during a drained test in which the sample is sheared between rigid ends. For 95 % dissipation with drainage from one end the time required to reach failure is given by

$$t_f = \frac{80h^2}{3c_v} \tag{5.1}$$

where c_v is the coefficient of consolidation determined from the consolidation stage, t_f is the time to failure, h is the half height of sample.

The time required to reach failure in an undrained test based on 95% pore pressure equalisation within the sample was given by Blight (1963) as

$$t_f = \frac{1.6h^2}{c_v} \tag{5.2}$$

Bishop and Henkel (1962) described how the value of c_v can be determined during the consolidation stage of the test by plotting volume change against the square root of the elapsed time from the beginning of the

consolidation stage (Fig.5.6). The initial linear portion of this curve is extended to intersect the line representing 100% consolidation. The time intercept of this point, converted to an arithmetic scale is termed t_{100} and c_v is

$$c_v = \frac{\pi h^2}{t_{100}} \tag{5.3}$$

For kaolin at 400 kPa, from Fig.5.6, t_{100} = 139.28 min and c_v from Eq.5.3 is 32.6 mm^2/min. Insertion of this value of c_v in Eq.5.2 and Eq.5.1 along with a sample half height 38 mm gives times of about 71 and 1181 min for 95% equalisation and dissipation respectively. This would correspond to a strain rate of 4.3%/hr for undrained tests with a failure strain of 5% and 1.0%/hr for drained tests with a failure strain of 20%.

Various strain rates have been used by a different research workers for performing triaxial tests on kaolin: e.g. Amerasinghe and Parry (1975) used a axial strain rate of 0.2%/hr for drained and undrained tests, Al-Tabbaa (1987) used 0.1%/hr for drained and undrained tests. After some consideration, all undrained test were conducted at an axial strain rate of 0.47%/hr and drained tests were performed at a rate of 0.1%/hr. These rates were 10 times lower than the values obtained from Eq.5.2 & 5.1.

5.1.2.3 Test procedure

Before setting up the sample, the triaxial cell base was de-aired by flushing water through it. The triaxial cell top cap was flushed with water and was also saturated by temporary connection to rubber tubing and filling the whole length with water. The end of rubber tubing was clipped to stop water escape. A layer of silicon grease was smeared round the base pedestal and top cap. The porous stones were saturated by boiling them for an hour and keeping them immersed in water at all time.

The trimmed consolidated specimen of 80 mm height and 38 mm diameter was carefully mounted on the bottom pedestal of the triaxial base. Before this, a conventional 38 mm diameter porous stone was placed on the bottom pedestal and a water soaked filter paper was placed on the top of the porous stone. A water soaked filter paper was also placed on top of the sample and a de-aired 38 mm diameter porous stone placed on top of it. The triaxial top cap was placed on top of the porous stone. Then a rubber membrane was released around the sample and sealed at each end with two rubber o-rings. The temporary rubber tubing connected to the top drainage lead for saturation was carefully

removed from the drainage line under water and quickly connected to the triaxial base by tightening the screw connection.

The top part of the triaxial cell was lowered and screwed tightly in position. The ram was carefully lowered into the top cap avoiding any contact with it and the cell was filled with de-aired water. The LVDT was clamped in position. The sample was then ready for testing.

Complete saturation of the sample can be achieved by subjecting the sample to a large back pressure to dissolve all the air trapped in the sample using increments of back pressure as described by Head (1985). This was however limited by the capacity of the air/water pressure system. The minimum back pressure used in the test series was 190 kPa. The degree of saturation was checked by performing a B-test. In these tests the cell pressure was increased by an increment of about 50 kPa while drainage was prevented. The rise in the pore water pressure in the sample due to the rise in the cell pressure depends on the degree of saturation of the sample. A degree saturation of 100% gives a B value of 1.0. B-tests carried out using a back pressure of 190 kPa for 24 hours gave an average value of 0.97. Saturation is generally accepted as being complete when B value reaches about 0.96 (Black and Lee 1973) which corresponds to a degree of saturation of 99%.

After saturation, all samples were isotropically consolidated to an effective stress of 400 kPa (p'_c). This was achieved by raising the cell pressure to 600 kPa and back pressure to 200 kPa. The consolidation stage was started by opening the top drainage valve and recording the output of the pore pressure, back pressure and volume change transducers using the data to the data logger at a preselected time interval, typically 1 min in the initial stages. The consolidation stage was terminated when 95%-98% dissipation was reached. Over consolidated specimens were allowed to swell isotropically to p'_c/OCR, where OCR is overconsolidation ratio in the range of 1.0-4.0. Fig.5.7 represents schematically the effective stress path employed in this study.

After bringing a specimen to its predetermined consolidation condition, it was sheared to failure in either undrained or drained compression under displacement control. All the undrained and drained tests were conducted at axial strain rates of 0.47 and 0.1 % per hour respectively as noted above. Readings during shearing were initially taken at 40s intervals and this interval was increased to 3 minutes later in the test. All the tests performed are listed in Table 5.1

At the end of a test, when the sample had reached approximately 20% axial strain, the machine was unloaded. The pore pressure and back pressure lines

were closed. The cell pressure was reduced to zero and the triaxial apparatus was dismantled after draining the water from the cell. The weight of the specimen was determined and specimens were divided into three parts for water content and sand content determination.

The initial water content of a specimen was determined from trimmings and the final water content was obtained from the entire specimen after the compression test. Theoretically, the final water content should have the same value as that determined from the initial water content and volume change readings during saturation, consolidation and shearing. However, it was most difficult to obtain such ideal agreement. Maximum variation of ±.0.8-1.2% was observed in this study and the final water content at the end of shearing has been used in determination of specific volume in data analysis.

The dimensions of the specimens, the height and diameter after saturation and consolidation, were computed from the initial measured sizes and the volume change readings by assuming isotropic volume changes. In the calculation of axial stresses during shearing the current cross sectional area of the sample was calculated from the measured axial and volumetric strains making the usual assumption that the sample maintains a right cylindrical shape. In the present study, shearing of samples have been taken up to an axial strain of 20%. Most of the samples, therefore showed distinct barrelling and slip failure plane (see Table 5.1) during shearing, introducing some uncertainty into the calculation of axial stress. The axial strain at which barrelling or slip failure initiated was not recorded during the tests because the tests were going on 24 hr/day and the author was not usually present to observe failure.

The measurements of axial strains, volumetric strains and deviator stresses were carefully calibrated to take account of the compliance of the apparatus and to check repeatability by running duplicate undrained and drained tests at OCR 1 using pure clay samples.

5.1.3 Triaxial tests on sand

The triaxial tests on sand were performed with the intention to determine the critical state friction angle of the sand used in the present study. A total of four drained tests was performed as follows:

The sand sample preparation technique used in the present study is based on that described by Bishop and Henkel (1962) for the preparation of triaxial specimens of saturated sand.

The specimens were prepared in split mould fitted with a vacuum connection, enclosing a rubber membrane clamped to the base pedestal of the

triaxial cell (Fig.5.8). Before this, the base pedestal is covered by a porous stone which has been saturated by boiling in water, and by a layer of filter paper. The rubber membrane was rolled over the top of the split mould and a small vacuum was applied through the mould to hold the membrane tight against its inside. A rubber bung and funnel are fitted into the top of the split mould as shown in Fig.5.8. A burette is connected to the outlet on the cell base and water was allowed to enter the mould until the funnel is about half filled. Then the rubber stopper on the end of a glass rod is inserted in the mould of the funnel. The cell valve to the burette fitted to the base pedestal is closed.

The quantity of dry sand required to fill the specimen mould is weighed out and mixed in a beaker with enough water to just cover the sand and the mixture is boiled to remove air. Then the sand is transferred to the funnel with a spoon. The specimen is formed by displacing the stopper so that the sand flows steadily, but fairly rapidly into the mould. Excess water is siphoned from the funnel, enabling the funnel, bung connection to be removed. After the sample is prepared and before connecting the top cap, a porous stone and a layer of filter paper are placed on the carefully levelled top surface of the specimen. The membrane is next fixed to the top cap with O-rings and the top drainage line is connected from the top cap to the cell base. Then a small negative pore pressure is applied to the base of the specimen by lowering the burette (Fig.5.9) to give it sufficient strength to stand while the split mould is removed. The specimen height and diameter are carefully measured and the cell body is fitted. After the cell is filled, the sample is saturated by using conventional back pressure technique as described in section 5.1.2.3. Once a high B-value ($\approx$ 0.99) is achieved, the sample is isotropically consolidated. After consolidation, the specimen is sheared at an axial strain rate of 5.2% per hour.

A total of 4 drained tests were conducted as shown in Table.5.2. Out of four tests two tests were performed with the triaxial set up shown in Fig.5.1. The other two tests were conducted with conventional proving ring and dial gauge, but the volume changes were recorded through the GDS pressure controller. Care was taken to calibrate the proving ring and load cell; and the GDS device and volume change transducer against each other.

5.2 ANALYSIS OF TEST DATA

The test results were analysed using deviator and mean effective stress variables q and p' given by

$$q = \sigma'_a - \sigma'_r = \frac{F}{A} \qquad (5.4)$$

$$p' = \frac{\sigma'_a + 2\sigma'_r}{3} \tag{5.5}$$

where σ'_a and σ'_a are the axial and radial effective stresses on a cylindrical triaxial sample; F and A are the force in the ram measured by load cell and cross-sectional area of the sample. The stress ratio, q/p' is denoted by η.

The corresponding shear ($\delta\varepsilon_q$) and volumetric ($\delta\varepsilon_p$) strain increments are

$$\delta\varepsilon_q = \frac{2(\delta\varepsilon_a - \delta\varepsilon_r)}{3} \tag{5.6}$$

$$\delta\varepsilon_p = \delta\varepsilon_a + 2\delta\varepsilon_r \tag{5.7}$$

where $\delta\varepsilon_a$ and $\delta\varepsilon_r$ are the axial and radial strain increments.
For undrained tests $\delta\varepsilon_p = 0$ and hence $\delta\varepsilon_q = \delta\varepsilon_a$.

The strain increments $\delta\varepsilon_a, \delta\varepsilon_r, \delta\varepsilon_q, \delta\varepsilon_p$ can be related directly or indirectly to the quantities measured during a triaxial test: change of length of the sample δl and change in volume of sample δV:

$$\delta\varepsilon_a = -\frac{\delta l}{l} \tag{5. 8}$$

$$\delta\varepsilon_r = \frac{-\delta V / V + \delta l / l}{2} \tag{5.9}$$

$$\delta\varepsilon_p = -\frac{\delta V}{V} \tag{5.10}$$

$$\delta\varepsilon_q = -\frac{\delta l}{l} + \frac{\delta V}{3V} \tag{5.11}$$

In previous chapters, the volumetric variable e_c has been found to be very useful for identifying the influence of clay phase on consolidation and permeability characteristics. However, in analysing stress:strain response it is often useful to work in terms of volumetric strains. To correspond with previous use of clay void ratio or clay specific volume, an increment of clay volumetric strain $\delta\varepsilon_{pc}$ can be defined as

$$\delta\varepsilon_{pc} = -\frac{\delta V}{V_c + V_w} \tag{5.12}$$

where δV is change in volume and V_c is clay volume in the mixture as shown in Fig1.1. This definition assigns all the volumetric strain to the clay matrix treating the sand particles as rigid material which plays no part in the deformation.

From Eq. 5.10

$$\delta\varepsilon_{pc} = \frac{V}{V_c + V_w}\delta\varepsilon_p \tag{5.13}$$

From Fig.1.1

$$\begin{aligned}\delta\varepsilon_{pc} &= \frac{V}{V - V_g}\delta\varepsilon_p \\ &= \frac{\delta\varepsilon_p}{1 - \frac{V_g}{V}}\end{aligned} \tag{5.14}$$

From Eq.1.7

$$\frac{V_g}{V} = \frac{1-C}{1+e} \tag{5.15}$$

$$\delta\varepsilon_{pc} = \frac{1+e}{e+C}\delta\varepsilon_p \tag{5.16}$$

In terms of e_C and C from Eq.1.4

$$\delta\varepsilon_{pc} = \frac{1+e_C C}{C(1+e_C)}\delta\varepsilon_p \tag{5.17}$$

In correct association of increment of clay volumetric strain $\delta\varepsilon_{pc}$; an increment of clay axial strain $\delta\varepsilon_{ac}$ can be defined as

$$\delta\varepsilon_{ac} = -\frac{\delta l}{l_{cm}} \tag{5.18}$$

where δl is change of length of sample and l_{cm} is equivalent length of clay matrix (clay mineral + water) in the mixture.
It is straightforward to show from Eq.5.8, Eq.5.18 and Eq.1.7 that

$$\delta\varepsilon_{ac} = \frac{1+e}{e+C}\delta\varepsilon_a \qquad (5.19)$$

assuming that the ratio of lengths of clay matrix and total length is

$$\frac{l_{cm}}{l} = \frac{V_c + V_w}{V}$$

5.3 RESULTS

5.3.1 Undrained test results

5.3.1.1 Stress:strain characteristics

Values of deviator stress q are plotted against axial strain for undrained tests on various clay/sand mixtures in Fig.5.10. Fig.5.10a shows stress-strain curves for samples isotropically consolidated to p_c' = 400 kPa and Fig.5.10b & c shows stress-strain relations for samples isotropically consolidated to p_c' = 400 kPa and swelled isotropically to overconsolidation ratios (OCRs) of 1.33 and 4 respectively. Visual examination of the data indicates that the response curves for the mixtures with clay contents 40 to 100% are very similar up to a shear strain of 9-10%, whereas mixtures with clay content 30% show a considerable increase in strength at each of the different OCRs. At large strain in the tests with clay contents 40 to 100%, most of the samples failed (Table 5.1) on a distinct slip plane and there was a drop in deviator stress after a peak value was attained. It was unclear whether initiation of the slip plane coincided with the peak deviator stress or occurred at a higher strain.

The stress:strain behaviour of the mixture with clay content 30% is different from the other mixtures. For instance, at OCR 1 (Fig.5.10a), the curve rises steeply to 200 kPa at very low strain of 0.5%, but then falls slightly to a axial strain of 4%. From here the curve rises gently again. Surprisingly the deviator stress is increasing even at 20% strain. Similar trends can be seen in Fig.5.10b for the mixture with clay content 30% at OCRs 1.33 and OCR 4 (Fig.5.10c) shows no fall beyond initial peak. It has to be noted that the fall is negligible in Fig.5.10b.

5.3.1.2 Pore pressure: strain relations

Fig.5.11 presents pore pressure - strain responses of the different mixtures during shearing of samples prepared with OCRs 1, 1.33 and 4. Visual

examination of the data indicates that the response curves for the mixtures with clay contents from 40 to 100% are similar in shape with the following features:

- For OCRs 1.0 and 1.33 (Fig.5.11 a & b) mixtures show a tendency to compress with pore pressure increasing through to the end of the shearing. At OCR 1.33 positive change in pore pressure is less than in tests on normally consolidated samples.
- The rate of pore pressure change falls just before maximum shear stress is reached for OCRs 1 and 1.33. However, the pore pressure continues to increase very slowly until the test end. Bjerrum and Simons (1960) and Leroueil et. al. (1990) have observed similar behaviour.
- For OCR 4.0 (Fig.5.11c) the pore pressure is initially positive, but soon becomes negative with zero pore pressure seen at a strain range of about 4-4.5%.

It can be seen in Fig.5.11 that the mixtures with 30% clay content at different OCRs, show very high pore pressure responses when compared with other mixtures. At OCR 1 pore pressure developed more rapidly in the early stages of testing and a value of 290 kPa was reached at an axial strain of 3.25%. The pore pressure remained essentially constant thereafter up to 10% strain. There is a slight tendency for a subsequent decrease in pore pressure at high strains. The pore pressure response of the mixture at OCR 1.33 is basically the same as OCR 1; any difference is in magnitude rather than nature.

The qualitative picture that emerges from Fig.5.11a & b is that at OCR 1 and 1.33 all clay/sand mixtures show a tendency to contract when they are sheared (and hence develop positive pore pressures) whereas at OCR 4 (Fig.5.11c) the mixtures with clay content 40 to 100% generated negative pore pressure showing a tendency to expand. This change in pore pressure responses pattern is not seen so drastically for the mixture with clay content 30% at OCR 4 shown in Fig.5.11c. The pore pressure is steadily increasing up to a strain 7% and then shows a slight tendency to decrease, but does not reach a negative value. In contrast, samples with other clay contents end up with negative pore pressure at the end of shearing.

5.3.1.3 Pore pressure parameters

The pore pressure parameter B in the present series of mixtures was found to be practically equal to unity, because of the high degrees of saturation. The smallest value of B measured in the present experiment was 0.97 (section 5.1.2.3). The pore pressure parameter A (Skempton 1954), on the other hand is known to change with stresses and strains. Its value may be quoted at failure or at

maximum effective stress ratio as a representative value. Pore pressure parameter at failure A_η in conventional triaxial tests is expressed as

$$A_\eta = \frac{u_\eta - u_o}{q_\eta - q_o} \tag{5.20}$$

Where u_η is pore pressure at maximum stress ratio and u_o is non zero back pressure, q_o and q_η are principal stress difference at the beginning of the test and at maximum stress ratio respectively.

The values of A_η at the maximum stress ratio obtained in the present experiments are plotted against clay content in Fig.5.12. It can be seen in Fig.5.12 that for each OCR the A_η values are almost constant for clay contents above 40% but that the value of A_η increases rapidly for a clay content of 30% at all OCRs. The value of A_η falls with increasing OCR irrespective of clay content of the mixture confirming the general pattern found in other soils (e.g. Henkel 1956).

5.3.1.4 Effective stress paths

The effective stress paths (ESPs) of the mixtures sheared after being prepared at overconsolidation ratios of 1, 1.33 and 4 are shown in Fig. 5.13a, b, & c. The ESPs of all the clay/sand mixtures with clay contents between 100 and 40% are presented in Fig.5.14 for comparison. The ESPs of the mixtures with clay content 30% at different OCR are presented in Fig.5.15. The dashed lines in Fig.5.14 & 5.15 correspond to shear strain contours and will be considered in the subsequent section.

Considering shear behaviour of mixtures having clay content from 40 to 100% (Fig.5.14) shows that the ESPs at each value of OCR are practically identical. All the ESPs have shown sharp drop in deviator stress after failure. The so-called softening or drop in deviator stress observed in all the tests is not a true material behaviour, but simply a result of non-homogeneous deformation such as barrelling and formation of slip plane etc. (e.g. Vaughan 1994). How much the drop in stress is a function of experimental errors such as area correction and how much of it reflects actual behaviour is unknown.

The points of maximum deviator stress can be used according to Leroueil et al. (1990) to define a failure envelope through the origin for normally consolidated soils. End of shear data from the mixtures with clay content 40 to 100% at OCR 1 produced a well defined failure point implying a failure envelope with a slope of 0.8.

Considering the data for triaxial compression of the mixture with clay content 30 % at different OCRs (Fig.5.15) shows many interesting features:

The shapes of the ESP for the mixture with 30% clay content are very different from the other mixtures. Such a shape is unusual for clays, but has been observed for some soils such as sands (e.g. Been and Jefferies 1985) and clayey sands with small amount of clay as shown in Fig.1.8 (Georgiannou et al. 1990). Considering test at OCR 1 (Fig.5.15) in detail, from the initial isotropic state X, the path is initially compressive to point Y, that is increase of pore pressure was measured. At the point Y descent of ESP is arrested and the path shows a tendency of the soil to dilate. After maximum stress ratio, the ESP follows the same failure line up to the point Z where the test was ended at shear strain of 20%. How much of final part of path is result of barrelling in not known. In marked contrast, other clay/sand mixtures did not exhibit any dilatant behaviour during normal compression.

Similar behaviour can be seen at OCR 1.3 in Fig.5.15. At OCR 4 the decrease in p' up to failure is not very clear, but increase in p' can be seen distinctly to reach common failure envelope. The failure line in Fig.5.15 has a gradient of 1.2.

5.3.1.5 Shear strain contours

Shear strain contours are superimposed in q-p' space in Fig.5.14 for the mixtures with clay content from 100 to 40% and in Fig.5.15 for the mixture with clay content 30%. The contours shown are average lines through the data points. For all the mixtures the equal strain contours tend to be concave with respect to the q = 0 axis, this tendency increasing as failure is approached. Similar observations have been made by Parry and Nadarajah (1974) for tests on isotropically consolidated kaolin.

5.3.1.6 Undrained stiffness

The stiffness characteristics of mixtures at different OCRs are examined in Fig.5.16 by plotting secant shear stiffness G, normalised with respect to mean effective stress p'_o at the start of shearing, against the axial strain. Logarithmic strain axes have been used to allow the very stiff initial response of the mixtures to be observed. The secant shear stiffness is given by

$$3G = \frac{\Delta q}{\Delta \varepsilon_q} \qquad (5.21)$$

which is the gradient of the secant to the stress:strain curve and the increments of q and ε_q are measured from the start of the shearing. The use of secant shear stiffness is not meant to imply that the behaviour of the mixture is strictly elastic, and has merely been taken as a convenient way of characterising shear response.

In the present study axial strain determinations were based on external measurements of displacement and the local strain measuring techniques (e.g. Jardine et al. 1984) have not been used to measure very small strains. Nevertheless the stiffness - strain curves shown in Fig.5.16 are typical of those commonly found for soils in which very small strains are carefully measured and they indicate highly non-linear stiffness properties (Jardine et al. 1986). They indicate a high initial stiffness that degrades rapidly with increasing strain. The variation of clay content in the mixtures from 100 to 40% does not appear to have a significant effect on the measured stiffness for normally consolidated mixtures in Fig.5.16a. However, there is marked increase in the stiffness for mixture with 30% clay content particularly at low strains. Similar trends can be seen in Fig.5.16b & c at OCRs 1.33 and 4. It has to be noted that because of the measuring techniques used the accuracy of strain measurement is not great for strains less than 0.01%.

The influence of clay content on G/p_o' at different strain levels from 0.01 to 5% for OCRs 1, 1.33 and 4 are presented in Fig.5.17a, b, & c respectively. At small strains up to 1%, G/p_o' is almost constant up to clay content 40% and an abrupt increase in the stiffness can be observed at clay content 30% at different OCRs.

5.3.2 Drained test results

5.3.2.1 Stress:strain behaviour

Fig.5.18 presents stress-strain relations of various mixtures from drained compression tests. Data are shown for normally consolidated specimens and for overconsolidated specimens with OCRs 1.33 and 4. Fig.5.18a & b also presents shear response of sand isotropically consolidated to 400 kPa and 300 kPa respectively. The plots in Fig.5.18a, b & c illustrate the following points:

- Irrespective of OCR, the shapes of the curves are similar for mixtures with clay content 40 to 100% but a marked increase in q can be observed for the mixture with clay content 30%.
- Well defined peaks were not observed in any of the stress-strain curves in Fig.5.18a & b at OCRs 1 and 1.33. In contrast at OCR 4 (Fig.5.18c), the mixtures with clay content 40 to 100% have shown peak values before the

ultimate state is reached whereas the mixture with 30% clay content shows continued slight increase in strength with strain.

- At larger strains deviator stress q of pure sand (Fig.5.18a & b) is almost equal to the mixture with clay content 30% at that stress level.

5.3.2.2 Volume change behaviour

Fig.5.19 summarises the volumetric strain and axial strain relationships measured during drained tests at OCR 1, 1.3 and 4.

At OCR 1 & 1.33 (Fig.5.19a & b) all the specimens, regardless of clay content exhibited steady increase in volumetric strain reaching steady values at large strains. This could be expected as positive pore pressure developed in the corresponding undrained test specimens (Fig.5.11a & b). At a given strain, the magnitude of the volumetric strain is decreasing with decrease in the clay content up to 40% but an increase in volumetric strain can be observed in Fig.5.19a & b at OCRs 1, 1.33 in the mixture with clay content 30%. In Fig.5.19a &b volumetric strains of sand are smaller than the mixture with clay content 30%.

The volumetric strain curves for OCR 4 samples shown in Fig.5.19c are distinctly different from those observed at OCR 1 and 1.33. The clay/sand specimens with clay content from 100 to 40% were initially found to show positive volumetric strain. However, with an increase in strain the volumetric strain soon became negative. The magnitude of the volumetric strain seems to be very different for all the specimens. In contrast, the specimen with 30% clay shows steady increase in volumetric strain up to an axial strain of 8.5% followed by a slight tendency to decrease, but not sufficient to reach a negative value.

The data in Fig.5.19 are not showing the way in which the clay phase controls the volumetric behaviour at different OCRs. So the data in Fig.5.19 were replotted in terms of clay volumetric strain (see section 5.2, Eq.5.17) and clay axial strain (see section 5.2, Eq.5.19) as shown in Fig.5.20. In Fig.5.20a & b the normalisation process appears to be remarkably successful in collapsing the volumetric stain data of mixtures with clay content from 100 to 40% onto a single curve for each of the different OCRs 1 and 1.33. But at OCR 4 (Fig.5.20c), the simple model is unable to collapse the data into a unique curve. So the data in the Fig.5.19 were replotted in terms of clay volumetric strain and conventional shear strain as shown in Fig.5.21. The consistency of the data for clay contents 40-100% is remarkable. It may be concluded from Fig.5.21 that the clay matrix controls the volumetric behaviour of the clay/sand mixtures for clay contents down to 40% but that the presence of the sand does not affect the shear strains. It can also be seen that the clay volumetric strains of the sample with 30% clay are

distinctly different: the mixtures have higher clay volumetric strains at all OCRs. The sand particles are evidently interacting to give an extra contribution to the observed volumetric strains.

5.3.2.3 Effective stress paths

ESPs of mixtures at different OCRs with clay content from 100 to 40% and 30% are presented in Fig.5.22a &b respectively. At OCRs 1 and 1.33 in Fig.5.22a & b, the ESPs of the mixtures rise steadily to the maximum value of q. However at OCR 4 in Fig.5.22a, the ESPs of the mixtures with clay content from 100 to 40% rise to a maximum value of q and then return to a lower value. This corresponds to the peak deviator stress and strain softening observed in Fig.5.18c. In contrast the ESP of the mixture with clay content 30% in Fig.5.22b is steadily rising to a maximum value. The corresponding stress:strain curve in Fig.5.18c shows a steady increase in q with strain.

Straight line envelopes can be drawn through the origin and through the end points of the tests in Fig.5.22a & b. The failure envelope for the mixtures with clay contents from 100 to 40% is well defined (Fig.5.22a) and has slope of 0.8. The failure envelope for the mixture with clay content 30% is different with slope of 1.2 as shown in Fig.5.22b. The failure lines from undrained test in Fig.5.14 & 5.15 are superimposed in Fig.5.22a & b respectively. The failure data from drained and undrained tests are consistent with a single failure lines through origin with slope 0.8 for mixtures with clay content 40-100% and 1.2 for mixture with clay content 30%.

5.3.2.4 Drained shear stiffness

The secant shear stiffnesses deduced from Eq.5.21 are normalised with mean effective stress at the start of shearing, p'_o. These values are plotted in Fig.5.23 against the logarithm of shear strain. Data are given for different OCRs. It is evident from the form of the curves that the drained stiffness of clay/sand mixtures is strongly non-linear and degrades rapidly with increasing shear strain. From Fig.5.23a it can be seen that G/p_o' characteristics of normally consolidated mixtures with clay content from 100 to 40% are very similar for strains above about 0.1%. The mixture with 30% clay content shows higher stiffness when compared with other mixtures particularly at low strain. Similar trends can be noted at OCR 1.33 and 4 in Fig.5.23 b & c.

The limits of the data in Fig.5.23 correspond to shear strain of 0.1% and this represents the limits of reliability for measurements of volume change behaviour in the present experimental set up. In the calculations of shear strains

(Eq.5.7 & 5.11) in drained tests, volumetric strains are required, but not in undrained tests. Theoretically, shear modulus is independent of drainage conditions and hence the shear modulus values from drained and undrained tests should be equal. Fig.5.24 shows values of shear stiffnesses for drained and undrained test at different shear strain levels from 0.1 to 5%. At OCR 1 and 1.33 (Fig.5.24a & b), there is little difference between stiffnesses for drained and undrained tests, but at OCR 4(Fig.5.24c) the agreement is reasonable only after shear strain of 1%. The reason for the discrepancy between the values of drained and undrained stiffnesses is because of the accuracy of the volume change readings.

5.4 SYNTHESIS OF DATA

5.4.1 Critical state

The critical state concept developed by Roscoe and his co-workers at Cambridge during 1950s and 1960s provides a framework for understanding the behaviour of soils. Critical states (see for e.g. Muir Wood 1990) can be defined as states where deformation can continue to occur without change in q, p', and v. The mathematical definition of critical state is given by Eq.5.22.

$$\frac{\partial p'}{\partial \varepsilon_q} = \frac{\partial q}{\partial \varepsilon_q} = \frac{\partial v}{\partial \varepsilon_q} = 0 \tag{5.22}$$

Typically critical states have been found with a constant effective stress ratio

$$\frac{q_{cs}}{p'_{cs}} = M \tag{5.23}$$

The frictional constant M is related to angle of internal friction ϕ' in compression by

$$M = \frac{6\sin\phi'}{3-\sin\phi'}$$

or

$$\sin\phi' = \frac{3M}{6+M} \tag{5.24}$$

The critical state concepts were originally developed to explain behaviour of clays (e.g. Roscoe et al. 1958), but have also been applied to sands (e.g. Been et. al. 1991). The following section attempts to consider the shear behaviour and failure of clay/sand mixtures within the critical state framework and attempts to identify the influence of clay phase.

5.4.1.1 Stress ratio:shear strain relationships

Stress ratio and strain relationships for all undrained and drained tests at different OCRs are plotted in Fig.5.25 and 5.26 respectively as q/p' against shear strains. Fig.5.10 and 5.25 contain the same undrained test data, but stress ratio curves in Fig.5.25 are supposed to reveal critical states which are not shown in the corresponding stress:strain curves in Fig.5.10. Fig.5.26 shows stress ratio:strain relations for drained samples shown previously in Fig.5.18. Fig.5.26a & b also shows data obtained from the tests with sand at different void ratios tested isotropically consolidated at 400 kPa and 300 kPa.

Normally consolidated and OCR 1.33 samples with clay content from 100 to 40% generally reached states at which they appear to strain uniformly up to shear strains approximately equal to 10-11% and 15% in undrained and drained tests respectively. After these strains, it is clear that the testing difficulties have prevented the sample from shearing at constant stress ratio. On the other hand, at OCR 4 mixtures with clay content 100 to 40% exhibited a peak stress ratio and there was some uncertainty whether the post-peak stress ratio represented a fall towards a critical state value or towards a lower value. This discrepancy can be explain in part by the development of slip planes observed in the samples. This localisation of deformation is commonly observed in laboratory tests on highly overconsolidated clays and has been linked to the high rate of dilation at stress ratios which are higher than critical conditions (e.g. Muir Wood 1990) and to non-uniform specific volumes which occur in the rupture zones (Atkinson and Richardson 1987). The concept of critical states seems to be satisfied in Fig.5.25 & 5.26 with some reservations, but as an idealisation, it would not be unreasonable to say that the mixtures with clay content 100 to 40% have reached a critical state stress ratio of 0.8.

In Fig.5.25a the normally consolidated undrained mixture with clay content 30% reached a constant stress ratio line, although measured deviator stresses (Fig.5.10a) continued to change with shearing and did not show any tendency to reach a constant value. Even the effective stress paths approached, asymptotically, a constant failure line as shown in Fig.5.15. To satisfy the definition of a critical state (Eq5.22), both the stresses and pore pressures have to

approach constant values. Similar patterns can also observed in Fig.5.25b & c at OCR 1.33 and 4. A critical state was not reached via an undrained path in the present series of tests with 30% clay content. Consequently, the use of undrained test data in this study to measure the critical state parameters of the mixture with clay content 30% may be questionable. In contrast drained test data for mixtures with 30% clay shows a definite trend towards a constant volume state (Fig.5.19a &b) and correspondingly, towards a constant deviator stress (Fig.5.18a & b) at OCRs 1 and 1.33. Correspondingly in Fig.5.26a & b drained tests on mixtures with 30% clay content reached a well-defined constant stress ratio of 1.2. Drained test data at OCR 4 (Fig.5.19c) do not show a constant volume state although the stress ratio reaches a constant value of 1.2 in Fig.5.26c. For the purpose of the present study the critical state for the mixture with clay content 30% was assumed to correspond to value of q, v and p' at which stress ratio had reached a reasonable constant maximum value which is 1.2. The data in Fig.5.26a indicate that the stress ratio:strain relation of sand is almost similar to the mixture with clay content 30%. Similar trends can be seen in Fig.5.26b. The curves in Fig.5.26a & b suggest that the critical state value for sand and for the mixture with clay content 30% is the same. In an earlier study on kaolin and Ham medium sand with clay content 6 to 30% (Fig.1.8), Georgiannou et al. (1990) showed that the critical state friction angle of the mixtures in compression is equal to that of pure Ham river sand. They reported angle of internal friction 32.6° (in compression) which is similar to the value of 30° obtained in this study for the mixture with clay content 30% and sand.

5.4.1.2 Failure data

The critical states reached by samples in undrained and drained tests are shown in the stress plane and the compression plane in Fig.5.27 & 5.28.

In Fig.5.27, it can be seen that the critical state points from undrained and drained tests on the different mixtures are falling on two distinct straight lines passing through the origin. The most interesting aspect of this plot is that the locus of all the test data of mixtures with clay content from 100 to 40% is unique and locus of the test data with mixture with clay content 30% is distinctly different with slope about 1.3 times higher. These critical states lines can be characterised with an equation given by

$$q = Mp' \qquad (5.25)$$

where M = 0.8 for mixtures with clay content from 100 to 40% and M = 1.2 for mixture with clay content 30%. From Eq.5.24, the above M values correspond to the angles of internal friction 20.67° and 30° respectively.

The angle of internal friction of sand obtained from Fig.5.26a, & b with Eq.5.24 is equal to 30°. The agreement between the critical state friction angles in the mixture with 30% clay content and sand alone supports the view that, for this mixture (with 30% clay content), the applied load at failure is taken entirely by the sand skeleton. Similar findings were reported by Georgiannou et al. (1990). It is interesting that this indicates that granular void ratio alone is not enough - undrained tests start at same granular void ratio as drained tests but the value does not change whereas the drained value does. So the shear strains must be bringing the particles into contact (or at least interaction) in a more dramatic way - and shear strains to critical state stress ratio in undrained tests is smaller than in drained tests. From this result it is reasonable to assume that at failure in the mixture with 30% clay content, that load is taken by the sand grains structure and clay and water present in the voids or interstices is insufficient to separate any grains of sand skeleton.

In the semi-logarithmic compression plane, (Fig.5.28), the data are presented in terms of clay specific volume v_c, rather than overall specific volume v, to facilitate comparisons between clay/sand mixtures with different proportions of clay present. The figure also shows the average normal one-dimensional compression lines obtained from Fig.3.14 & 3.15 in high stress ranges, plotted in v_c: $\ln\sigma_v'$ space. All the data points of the mixtures with clay content from 100 to 40% fall close to one unique critical state line represented by the line AA. Data from the mixture with clay content 30% give line BB which deviates significantly from AA. The resulting critical state line BB has higher v_c values than the critical state line AA. The critical state lines in v_c: lnp' plane may be described by

$$v_c = \Gamma - \lambda_c \ln p' \qquad (5.26)$$

where Γ is the value of v_c corresponding to p' = 1 kPa on the critical state line; λ_c is the slope of the critical state line. The values of Γ, λ_c of the critical state lines AA, BB are presented in Table5.3 together with the slopes of one-dimensional normal compression lines and reference values of clay specific volume (A_c) at σ'_v = 1 kPa on the 1-D normal compression lines. It can be seen that the slopes of these critical state lines turn out to be the same as the corresponding 1D normally compression lines.

The data in Fig.5.27 & 5.28 present more convincing evidence for the existence of a line of values of p', q and v towards which all the tests have headed, irrespective of clay content and consolidation history.

5.4.1.3 State boundary surface

It is helpful to display the information about triaxial states in q:p':v_c space rather than simply in separate stress:strain relationships, stress planes and compression planes as discussed in the previous section. One of the basic assumptions of the critical state models for the stress-strain behaviour of soils is that there is a unique state boundary surface in v:q:p' space outside which the 'state' of a sample - defined as its current specific volume and applied stress state - cannot lie (e.g. Atkinson 1993; Muir Wood 1990). To get a better idea of what the state boundary surface might look like, two different plotting techniques are usually used to present two-dimensional views of the three dimensional information (e.g. Muir Wood 1990): 1) stresses normalised with critical pressure p'_{cs} and 2) results presented in terms of stress ratio η and equivalent specific volume, $v_{c\lambda}$.

Equivalent critical pressure, p'_{cs} for a state 's' shown in Fig.5.29 is defined as the corresponding mean effective stress on an appropriate critical state line at the same clay specific volume. It is given by

$$p'_{cs} = \exp\left(\frac{\Gamma - v_s}{\lambda_c}\right) \tag{5.27}$$

In Fig.5.29, p'_e is the equivalent pressure on the isotropic normal compression line which is often used (e.g. Wroth and Loudon 1967) as a normalising parameter for test data. In this study p'_{cs} is used here because the critical state line is better defined (isotropic compression data not available), but since other lines such as one dimensional normal compression lines or isotropic normal compression lines are expected to be parallel it does not matter which is used for normalisation (Muir Wood 1990).

The volumetric parameter, $v_{c\lambda}$ for a state s (Fig.5.29) is defined by

$$v_{c\lambda} = v_s + \lambda_c \ln p'_s \tag{5.28}$$

As shown in Fig.5.29 the parameter $v_{c\lambda}$ is the clay specific volume at p'=1 kPa on the line parallel to the critical state line or normal compression line through the point s in the v_c:lnp' plane.

A complete picture of the undrained stress paths of the mixtures with clay content from 100 to 40% is shown in Fig.5.30a & b. Fig.5.31a & b presents normalised drained stress paths for all the mixtures with clay content from 100 to 40%. The data of undrained stress paths for the pure clay (Fig.5.30a & b) were replotted in Fig.5.31a & b respectively. In Fig.5.30a & 5.31a the effective stresses are normalised with the critical state stress p'_{cs}. In Fig.5.30b & 5.31b the stress ratios η are plotted against equivalent specific volume $v_{c\lambda}$. Fig.5.32a & b show stress paths for the mixtures with clay content 30%. The values of p'_{cs} and $v_{c\lambda}$ are calculated from Eq.5.27 & 5.28 with values of soil parameters given in Table5.3.

In the q/p' vs $v_{c\lambda}$ plot : $v_{c\lambda} = N$, $\eta = 0$ represents the isotropic normal compression line and $v_{c\lambda} = \Gamma$, $\eta = M$ represents the critical state line.

In the plot q/p'_{cs} vs p'/p'_{cs} : $q/p'_{cs} = 0$, p'/p'_{cs} represent the isotropic normal compression line and $p'/p'_{cs} = 1$, $q/p'_{cs} = M$ represents the critical state line.

The normalised plots (Fig.5.30a & b, Fig.5.31a & b) for the mixtures with clay content 100 to 40% show a number of interesting features:

- All the undrained and drained stress paths migrate reasonably close to critical state C. All the stress paths have reached critical state C within ± 5-8% of the target value.
- It is clear from Fig.5.31a & b that in this two-dimensional plot the data of drained and undrained tests of different mixtures are brought together.
- The stress paths of the normally consolidated mixtures act as a boundary for the stress paths of the overconsolidated specimens defining a state boundary surface.
- The stress paths of over consolidated mixtures lie inside the unique state boundary surface for different mixtures.
- At OCR 4, the stress paths rise towards the Hvorslev line TC and curl over towards the critical state C.

Considering the stress paths for mixtures with clay content 30% shows many interesting features: The drained test data shown in Fig.5.32 indicate a clear boundary surface which resembles that of clay. The paths by migrate towards a common critical state within the range of experimental scatter. The undrained paths curve quickly towards the Hvorslev line. Even path at OCR 1 and 1.33 (which start wet of critical state) move away from the boundary surface of drained tests, passing below the critical state before reaching the Hvorslev line. In 1985 Gens reported drained data defining a state boundary surface further from the origin than undrained data for low I_p clays.

5.4.2 Critical state compression in relation to particle packing

In the above section, the contribution of clay phase is clearly identified and it is the mixture with clay content 30% which shows a sudden increase in shear resistance. It is difficult to argue whether the increase in strength is due to the sand particles coming closer or due to some interaction between clay and sand. To investigate this, consideration of volume packing of the sand particles may be useful.

The parameter granular specific volume v_g reflects changes in packing of the sand particles due to compression of the clay phase. The v_g values at critical state for different mixtures (Table 5.1) are plotted against clay content in Fig.5.33. It can be seen in Fig.5.33 that the v_g values of drained and undrained test are quite close and volume changes occurring in drained tests are not enough to produce much extra interaction. However, once v_g drops to around 2.2-2.4 sudden increase in deviator stress was observed in Fig.5.27. At v_g = 2.2, from Fig.1.3 the separation between sand particle s/d = 1.18 for hexagonal, 1.05 for cubical and is very small and this confirms that the strength increase is mainly from the results of the interaction between sand particles. It was postulated in Chapter 3 that the interaction between sand particles in one-dimensional compression was initiated around v_g =2.4-2.5. The shear test data in Fig.5.33 suggest that the granular interaction between sand particles begins at granular specific volume of 2.2-2.4 which is reasonably consistent with the conclusion, from the one-dimensional compression tests.

5.4.3 Critical state ϕ'_{cs} versus plasticity index

The ϕ'_{cs} values implied in Fig.5.27 are plotted against plasticity index (Fig.2.8) in Fig.5.34. The trend lines proposed by Mitchell (1976) and Nakase (1988) for natural soils; Rossato et al. (1992) for kaolin based mixtures are compared in Fig.5.34. The measured values for different mixtures are well below the two trend lines shown in Fig.5.34 for natural soils, but approximately close to the values for kaolin based mixtures proposed by Rossato et al. It should be noted that ϕ'_{cs} is weakly dependent on plasticity index and is more dependent on mineralogy etc. Example for Bothkennar soil (Allman and Atkinson 1992) the combination of low clay fraction and the presence of organic material results in high plasticity (34%) and shows ϕ'_{cs} = 32° which corresponds more closely to values for granular soils. Nevertheless, Fig.5.34 suggests that ϕ'_{cs} values in the present study are constant down to plasticity index 16.5% and a sudden increase in value can be seen at plasticity index 12.4%.

5.5 CONCLUSION

Drained and undrained triaxial compression tests on normally consolidated and overconsolidated clay:coarse sand mixtures have shown that the stress:strain and pore pressure response are independent of clay content for clay content down to 40% and that the volumetric strain in drained tests is unique if it is interpreted in terms of the volumetric strain occurring in the clay paste alone.

Plots of normalised paths have shown that the undrained and drained response fit into a coherent pattern and that a state boundary surface is defined reasonably well by the normally consolidated samples.

Samples with clay content of 30% show response which has more similarity to the response of pure sand than to the response of mixtures with higher clay contents.

Table 5.1 Summary of laboratory triaxial tests on clay/sand mixtures

Test	Clay content C	Specific volume v at critical state	Clay specific volume v_c at critical state	Granular void ratio v_g at critical state	Mean effective stress at critical state p'	Deviator stress q at critical state	Failure type
UM100A	1.0	2.310	2.310	∞	229.91	184.91	R.P
UM90A	0.9	2.175	2.305	21.745	233.37	187.40	R.P
UM80A	0.8	2.050	2.312	10.248	223.15	188.50	R.P
UM70A	0.7	1.910	2.300	6.367	226.63	183.70	R.P
UM60A	0.6	1.788	2.314	4.471	227.70	182.70	R.P
UM50A	0.5	1.657	2.313	3.313	231.10	186.60	Bulge
UM40A	0.4	1.526	2.315	2.543	229.40	187.20	R.P
UM30A	0.3	1.483	2.610	2.119	176.79	213.94	Bulge
UM100B	1.0	2.330	2.330	∞	210.57	171.50	R.P
UM90B	0.9	2.199	2.332	21.988	212.21	170.03	R.P
UM80B	0.8	2.063	2.329	10.316	212.20	169.79	R.P
UM70B	0.7	1.930	2.328	6.432	215.66	173.25	R.P
UM60B	0.6	1.800	2.334	4.501	212.60	171.01	R.P
UM50B	0.5	1.668	2.335	3.335	210.47	167.40	R.P
UM40B	0.4	1.534	2.336	2.557	210.50	168.00	Bulge
UM30B	0.3	1.490	2.633	2.128	155.70	187.52	Bulge
UM100C	1.0	2.389	2.389	∞	154.95	124.51	R.P
UM70C	0.7	1.979	2.398	6.595	154.32	124.80	R.P
UM60C	0.6	1.831	2.385	4.578	154.50	124.00	R.P
UM50C	0.5	1.697	2.394	3.394	153.95	123.29	R.P
UM40C	0.4	1.557	2.392	2.595	152.91	122.40	R.P
UM30C	0.3	1.510	2.700	2.157	115.78	140.00	Bulge
DM100A	1.0	2.123	2.123	∞	545.92	437.77	Bulge
DM70A	0.7	1.786	2.123	5.954	545.67	437.00	Bulge
DM60A	0.6	1.680	2.134	4.200	547.00	441.00	Bulge
DM50A	0.5	1.565	2.131	3.131	545.68	437.05	Bulge
DM40A	0.4	1.451	2.127	2.418	546.33	439.02	Bulge
DM30A	0.3	1.394	2.313	1.991	668.49	805.47	Bulge
DM100B	1.0	2.185	2.185	∞	409.08	327.40	Bulge

DM70B	0.7	1.834	2.192	6.115	409.57	328.70	Bulge
DM60B	0.6	1.716	2.194	4.290	409.23	327.70	Bulge
DM50B	0.5	1.595	2.190	3.190	408.92	326.70	Bulge
DM40B	0.4	1.473	2.182	2.454	409.23	327.70	Bulge
DM30B	0.3	1.413	2.377	2.019	500.33	601.00	Bulge
DM100C	1.0	2.423	2.423	∞	136.36	109.10	Bulge
DM70C	0.7	1.997	2.424	6.656	136.62	110.12	R.P
DM60C	0.6	1.848	2.414	4.621	138.11	110.70	R.P
DM50C	0.5	1.708	2.415	3.415	136.40	109.00	R.P
DM40C	0.4	1.565	2.412	2.608	136.52	109.20	R.P
DM30C	0.3	1.487	2.623	2.124	167.17	201.00	Bulge

U, Undrained test

D, Drained test

A, B, C, Overconsolidation ratio's at 1, 1.33 and 4 respectively

M, Mixture

The number following M represents clay content present in the mixture

Thus UM100A denotes undrained test on a mixtures with 100% clay content at overconsolidation ratio of 1

R.P Rupture plane

Table 5.2 Summary of laboratory triaxial tests on sand

Test	Initial specific volume v	Specific volume v at critical state	Mean effective stress at critical state p'	Deviator stress q at critical state	Failure type
SA (v-1.861)	1.861	1.832	668.39	805.19	Bulge
SA (v-1.854)	1.854	1.828	669.42	808.27	Bulge
SA (v-1.845)	1.845	1.821	667.09	801.28	Bulge
SB (v-1.860)	1.860	1.842	500.17	600.52	Bulge

SA Sand isotropically consolidated at 400 kPa - drained test

SB Sand isotropically consolidated at 300 kPa - drained test

SA (v-1.861) denotes drained test at p' = 400 kPa with initial specific volume of 1.861

Table 5.3 Critical state values in compression plane

Clay content C%	Line	Γ	λ_c	λ_c from 1D compression	A_c value at σ'_v=1 kPa
40-100%	AA	3.446	0.21	0.214	3.61
30%	BB	3.754	0.22	0.225	4.11

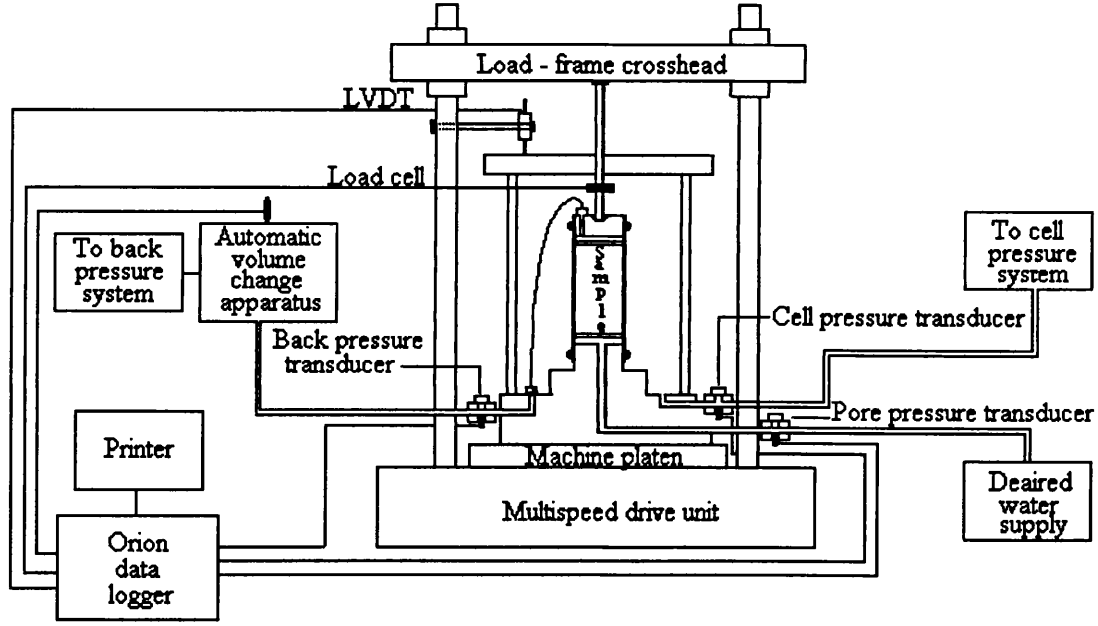

Fig.5.1 Schematic arrangements of triaxial apparatus

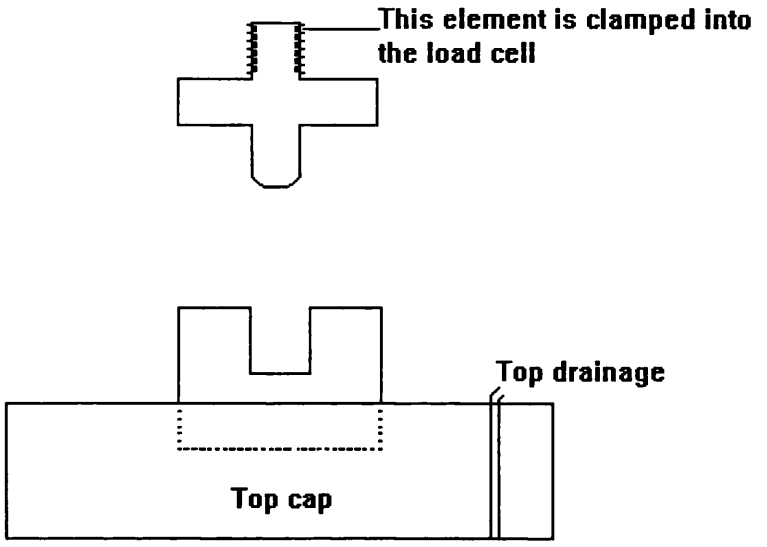

Fig.5.2 Details of top cap

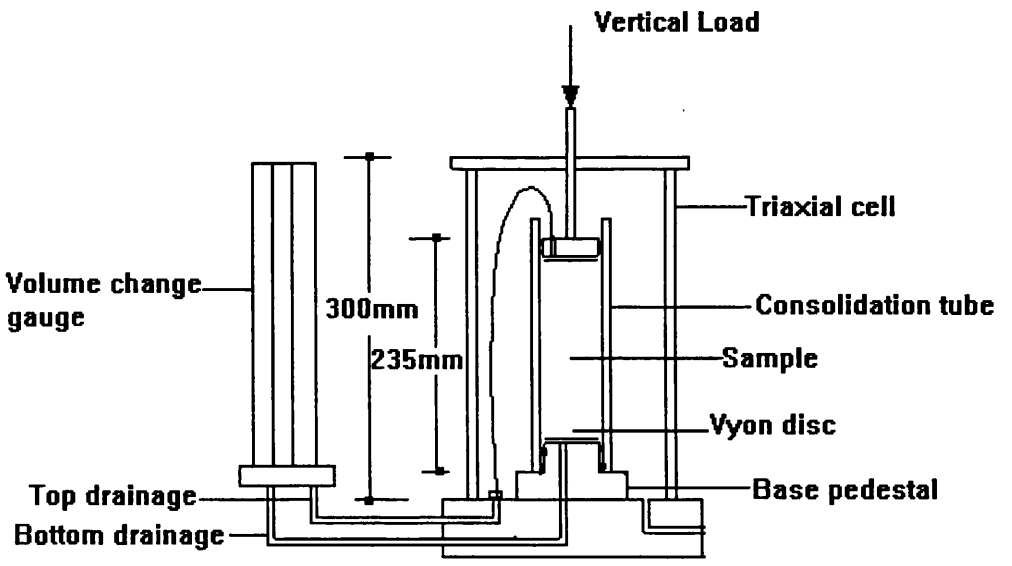

Fig. 5.3 Consolidation tube in use as located inside triaxial cell

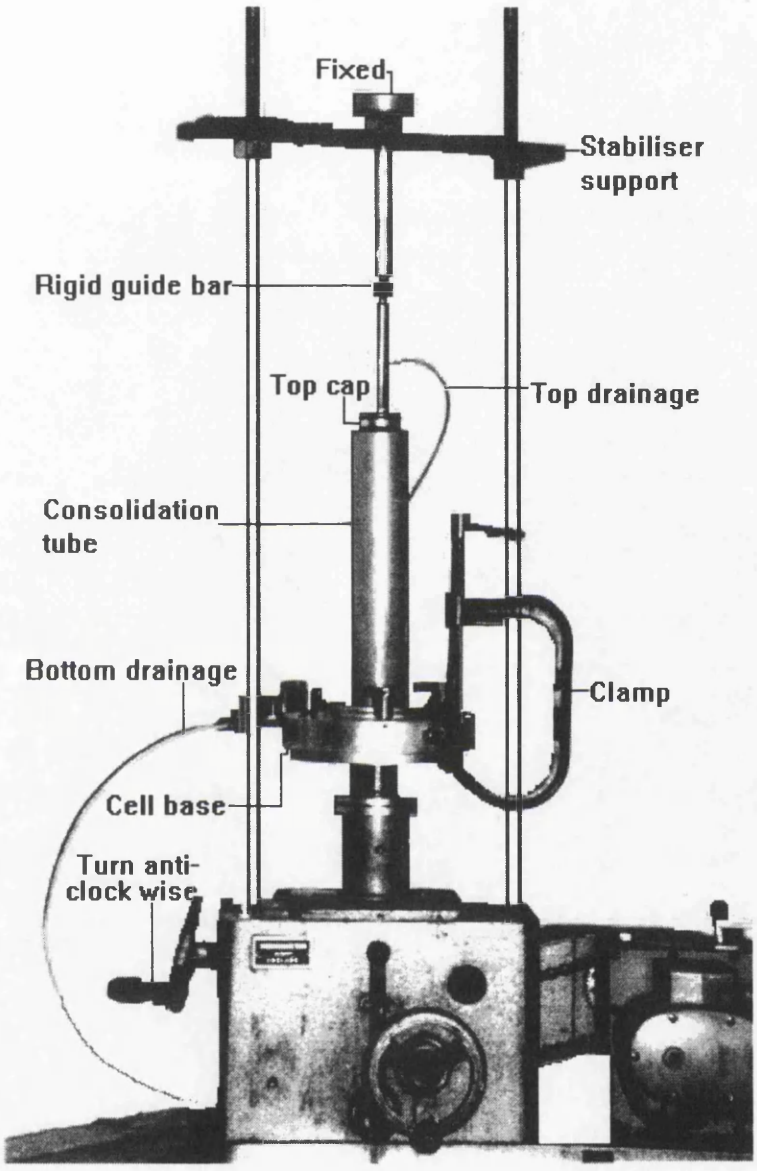

Fig.5.4 Removing top cap from the consolidation tube

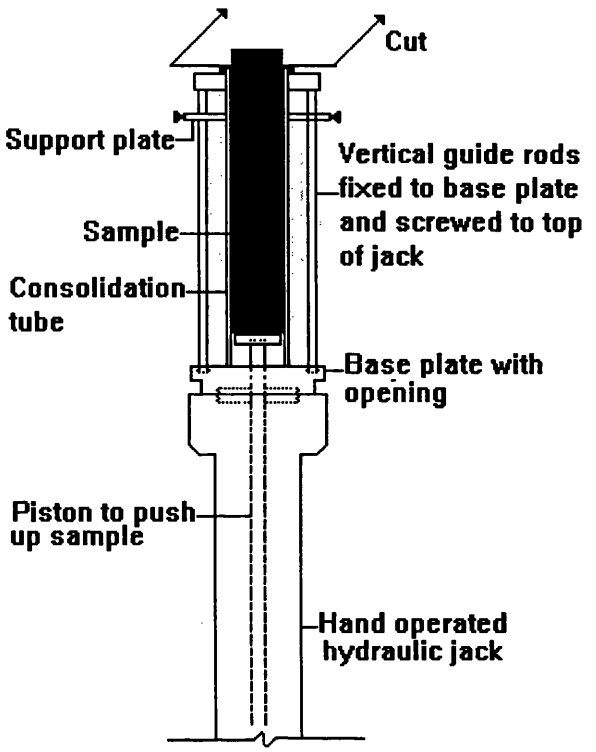

Fig.5.5 Arrangement for sample extrusion

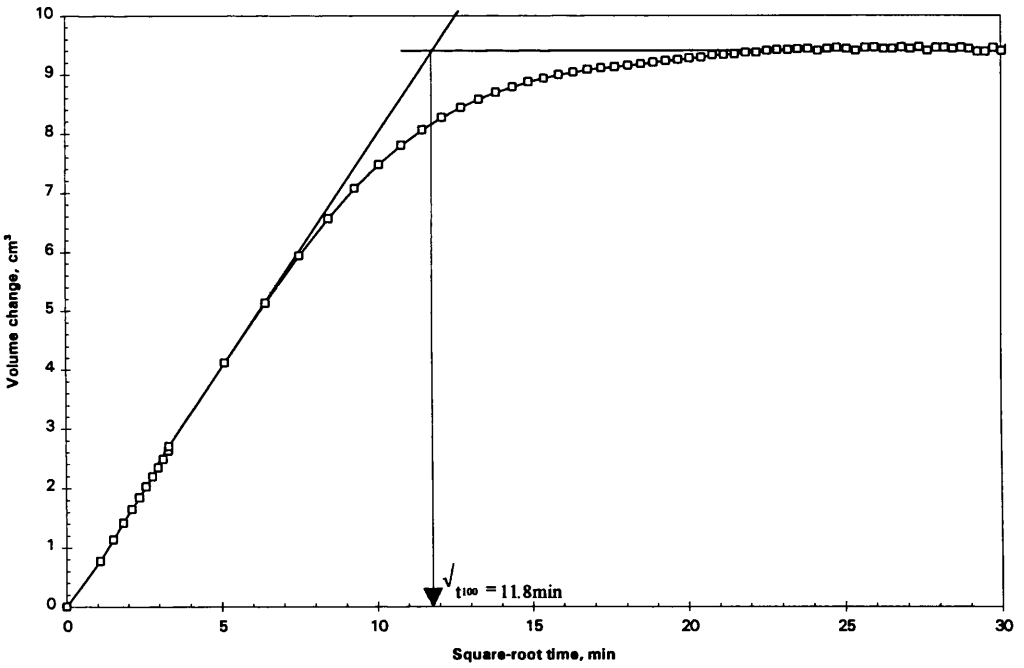

Fig.5.6 Triaxial consolidation stage of clay sample at 400 kPa: volume change against square-root time

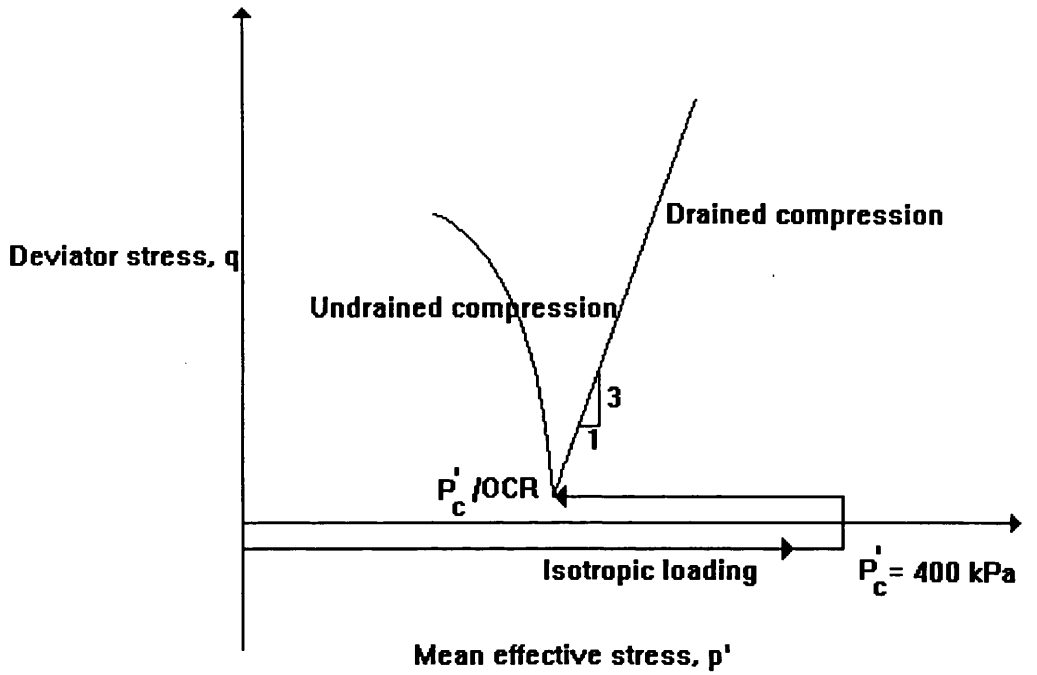

Fig.5.7 Schematic representation of the effective stress paths employed in this study

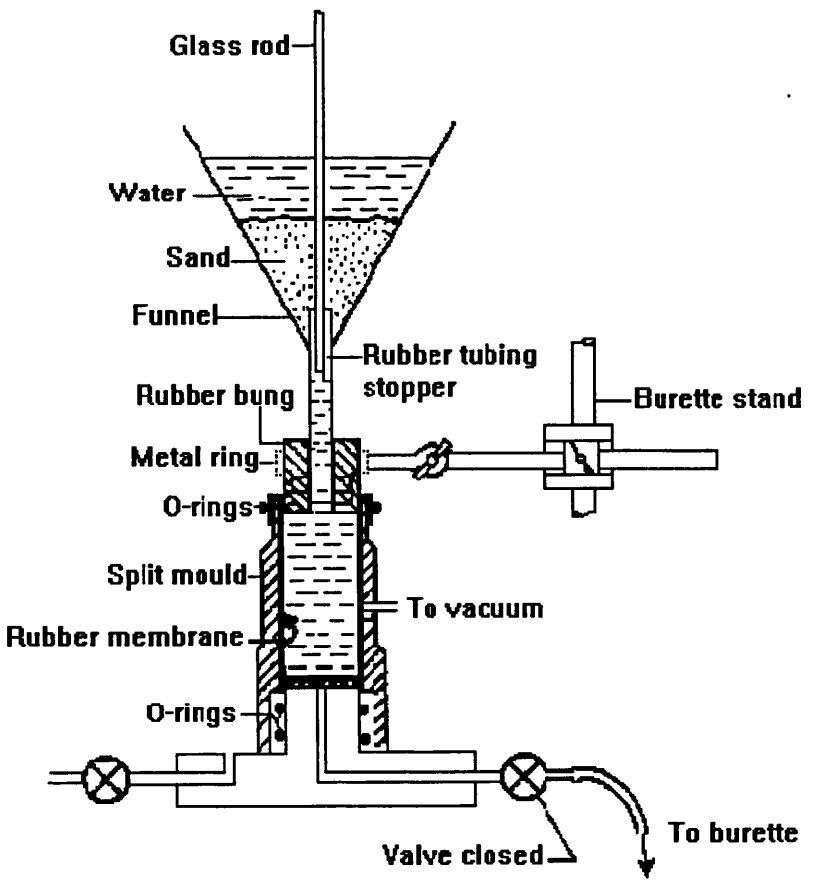

Fig.5.8 Preparation of triaxial specimen of saturated sand

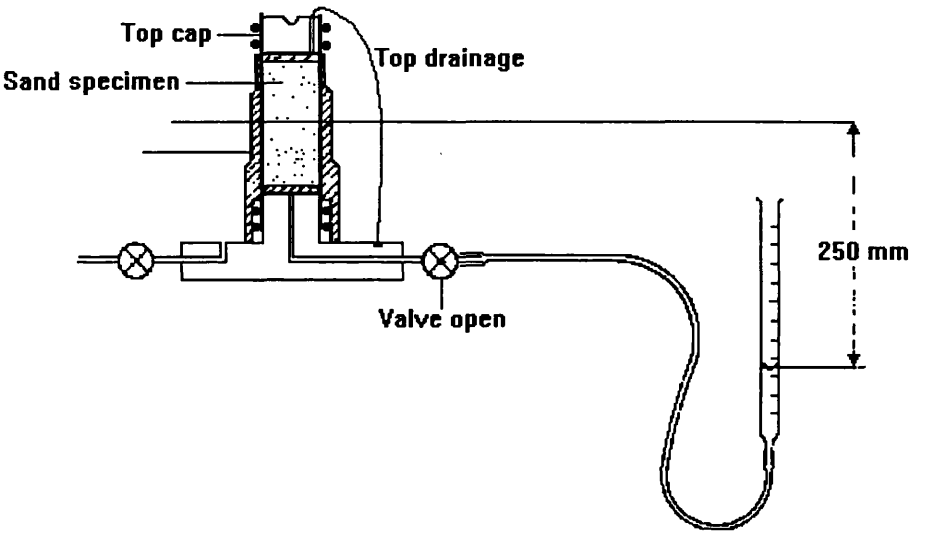

Fig.5.9 Application of suction to saturated sand specimen (Head 1982).

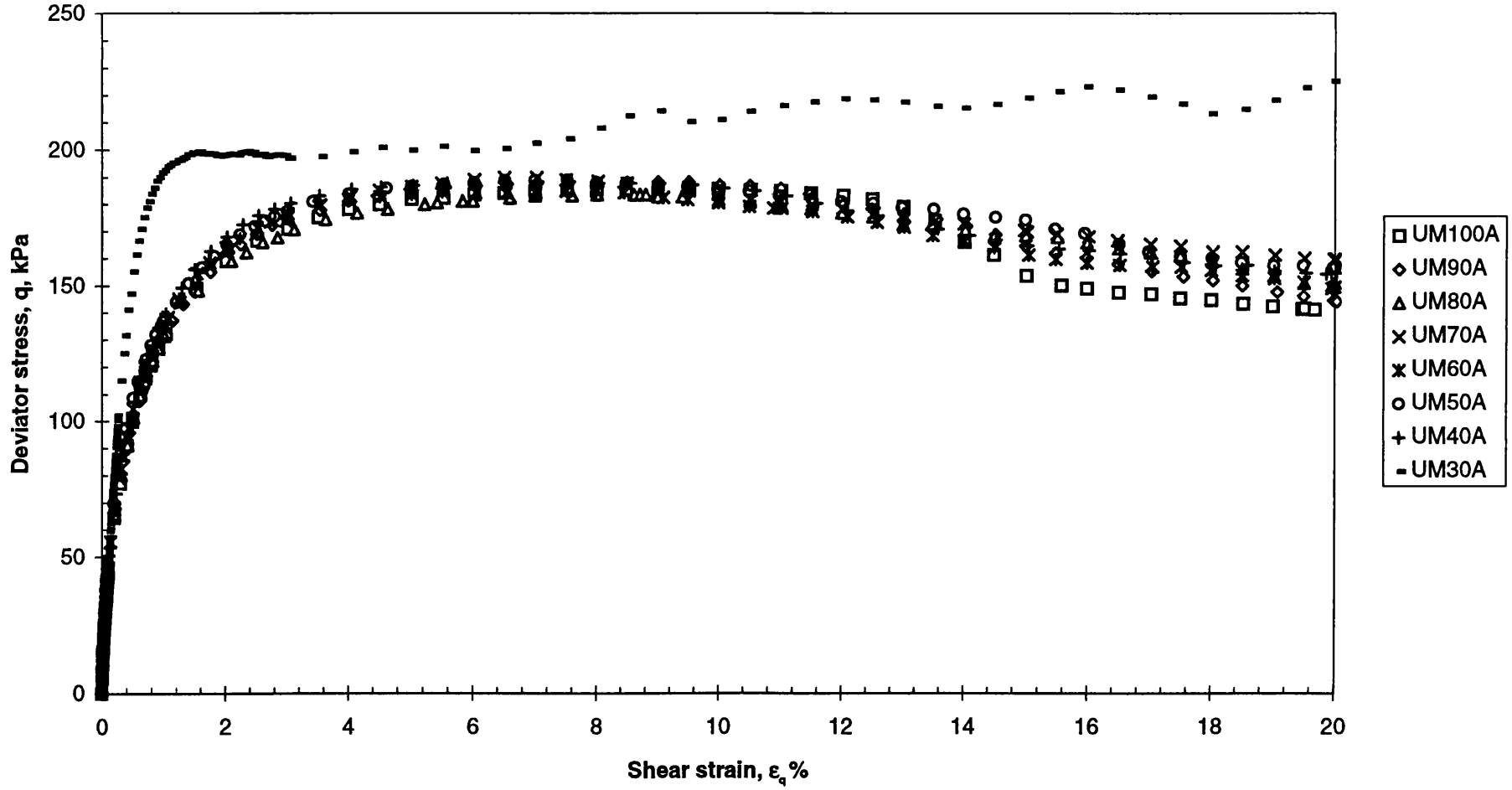

Fig.5.10a Undrained stress-strain response at OCR 1

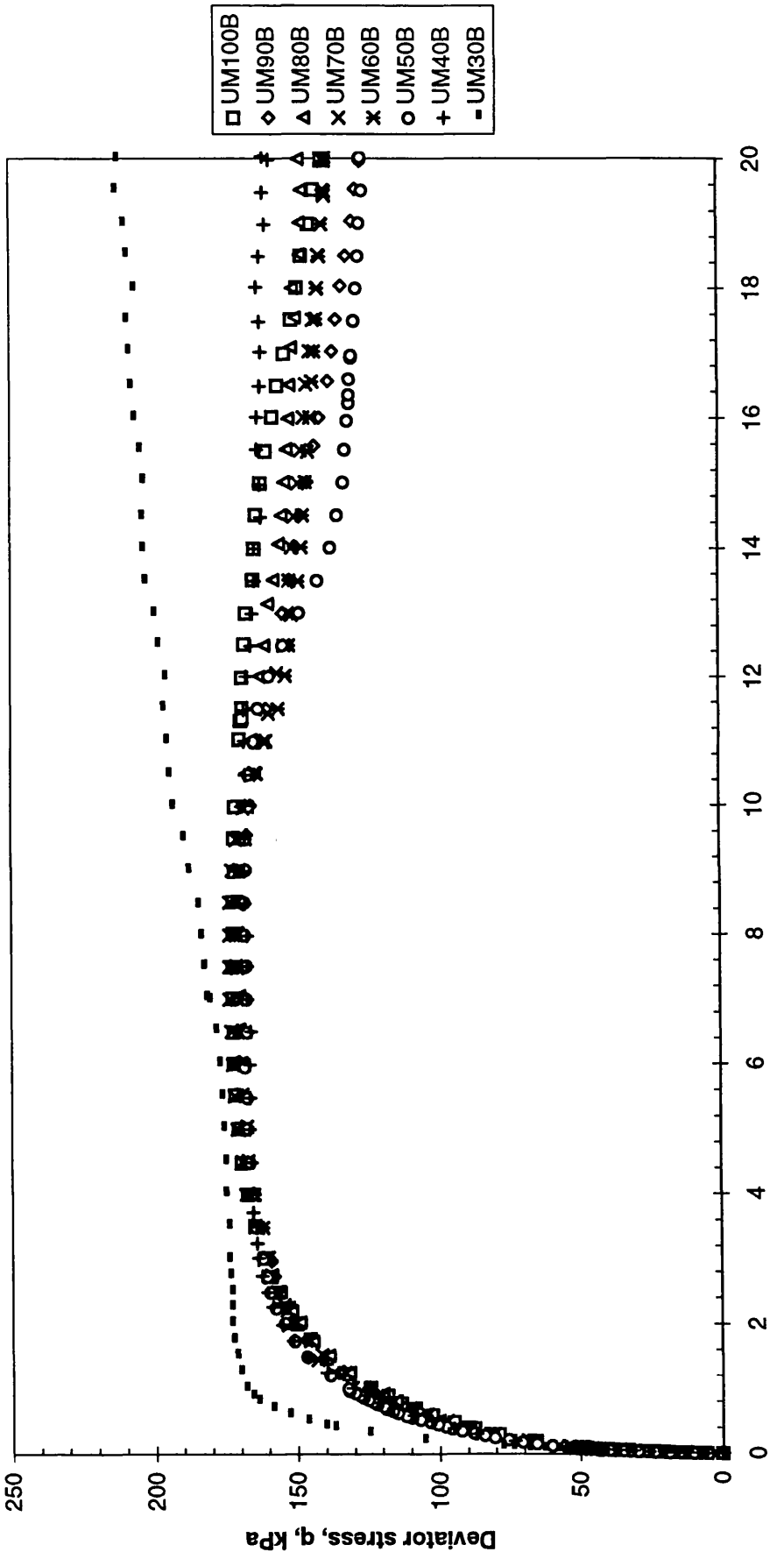

Fig.5.10b Undrained stress-strain response at OCR 1.33

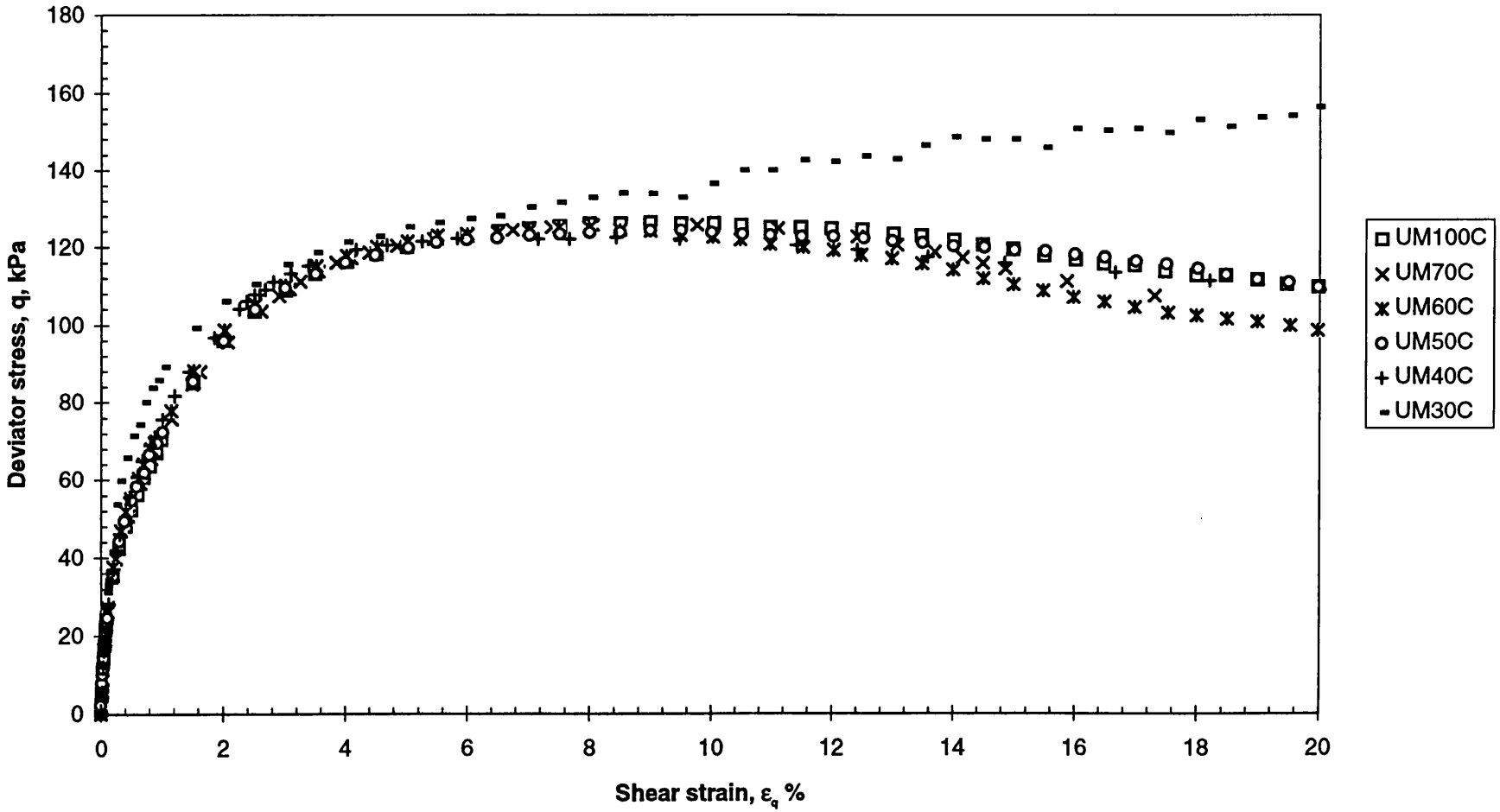

Fig.5.10c Undrained stress-strain response at OCR 4

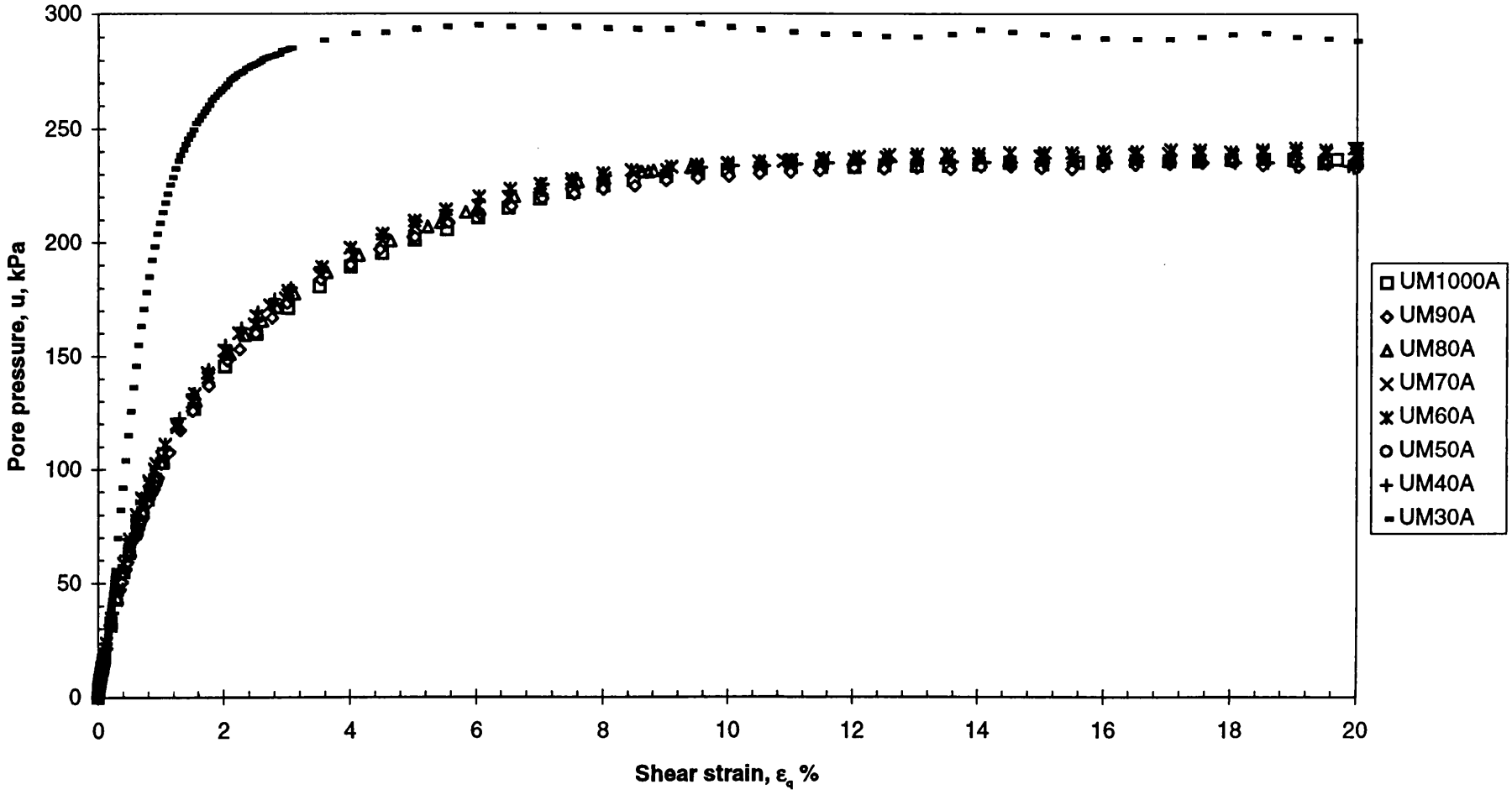

Fig.5.11a Undrained pore pressure-strain response at OCR 1

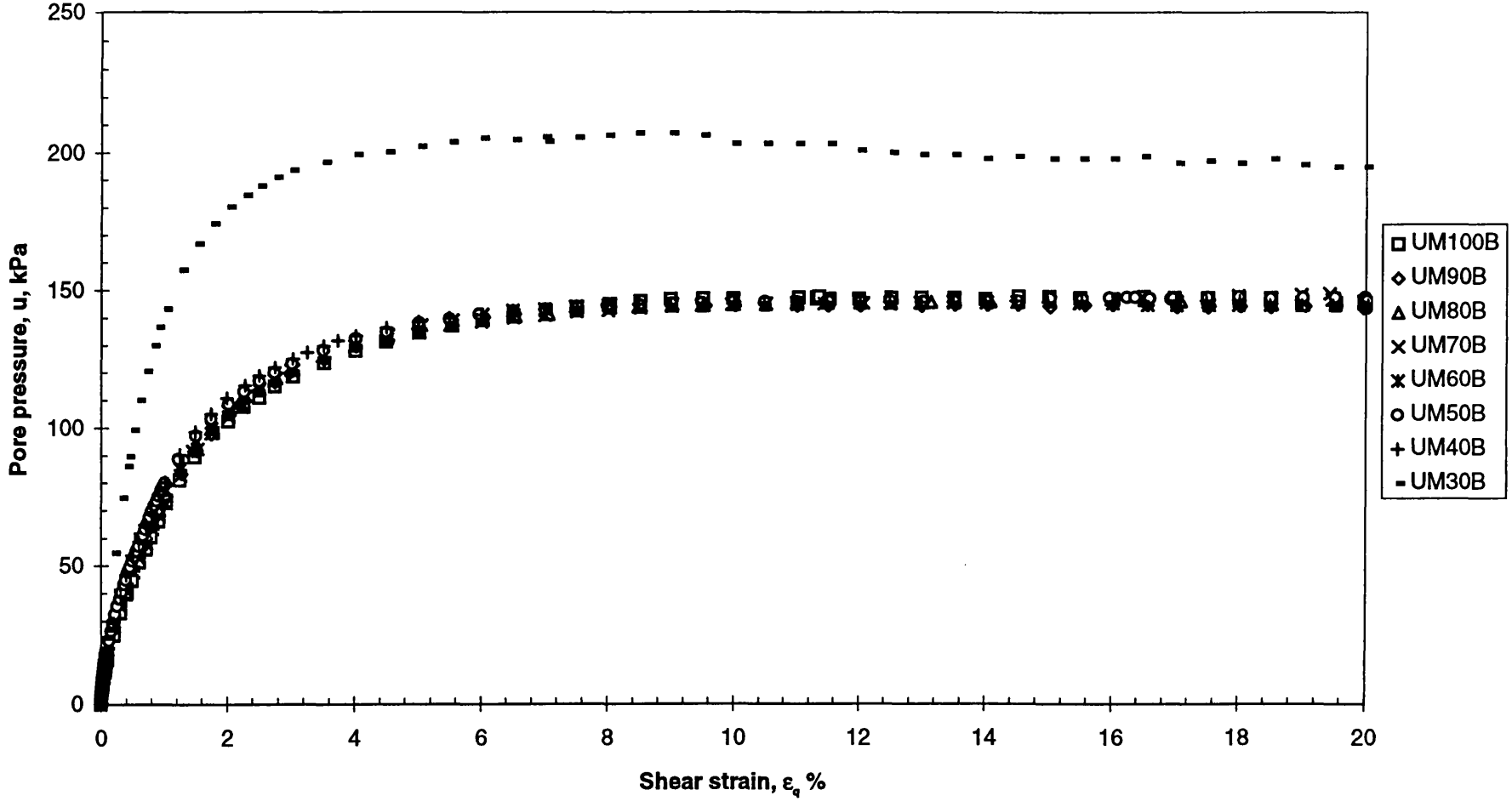

Fig.5.11b Undrained pore pressure-strain response at OCR 1.33

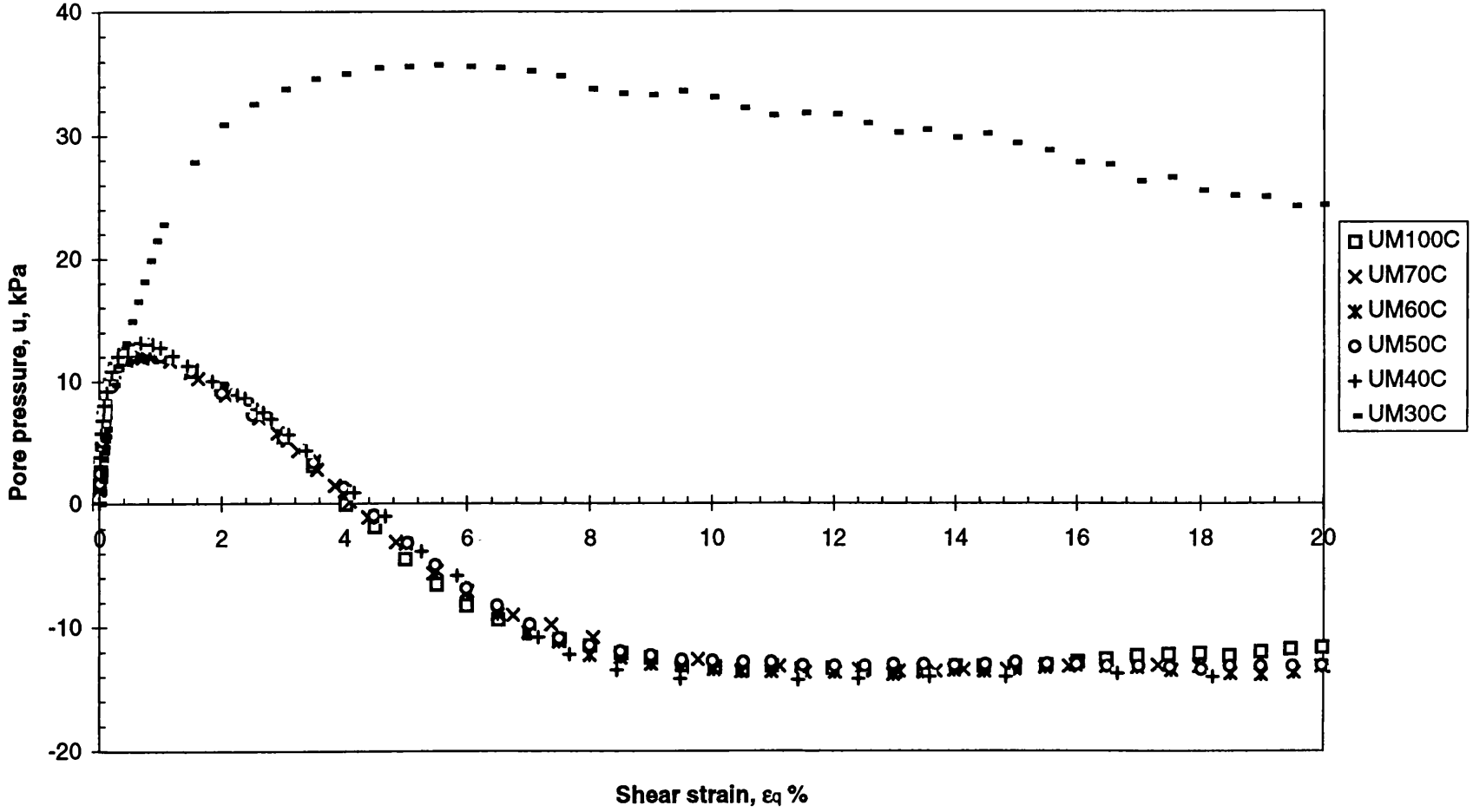

Fig.5.11c Undrained pore pressure-strain response at OCR 4

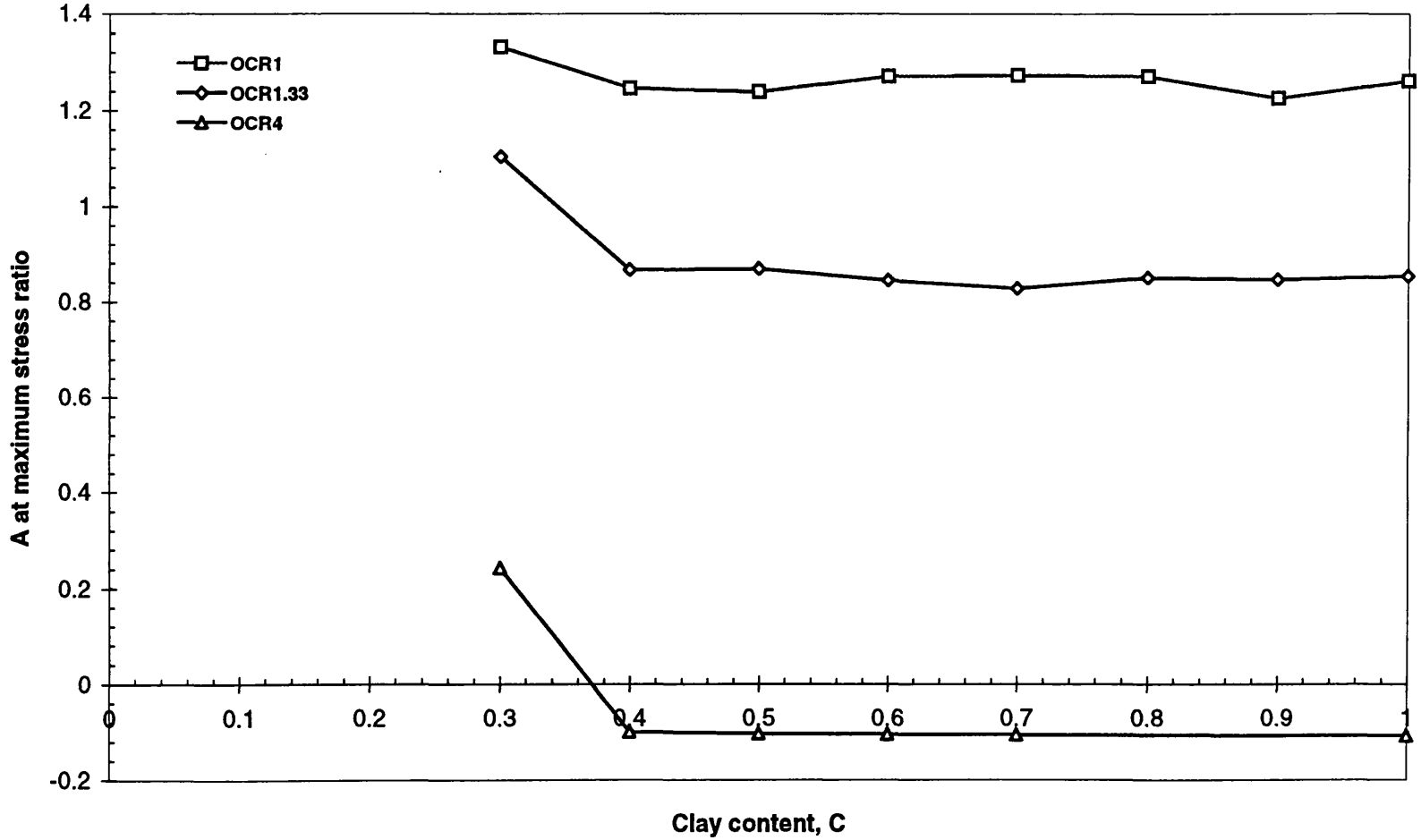

Fig.5.12 Variation of A values

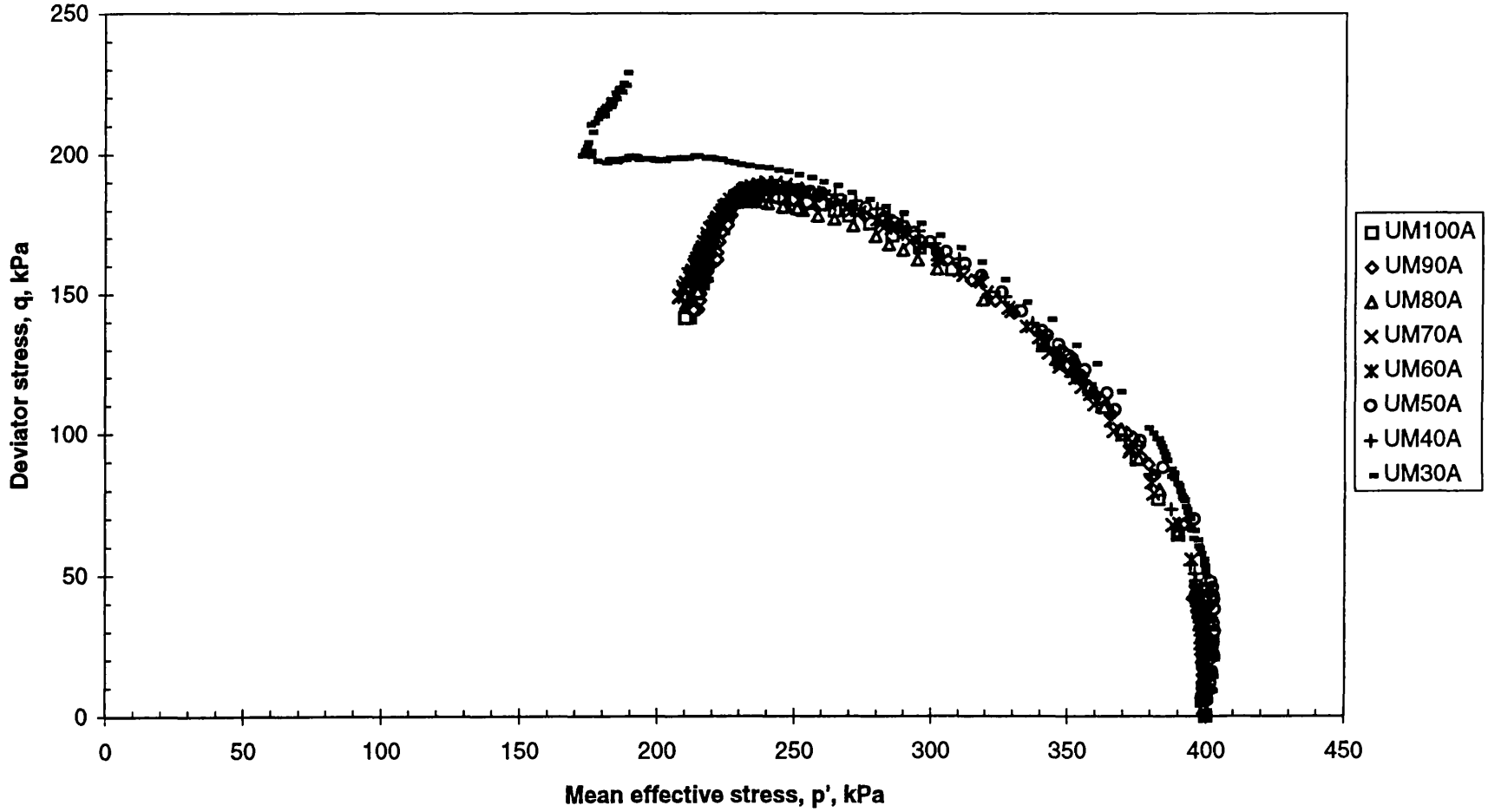

Fig.5.13a Undrained effective stress paths at OCR 1

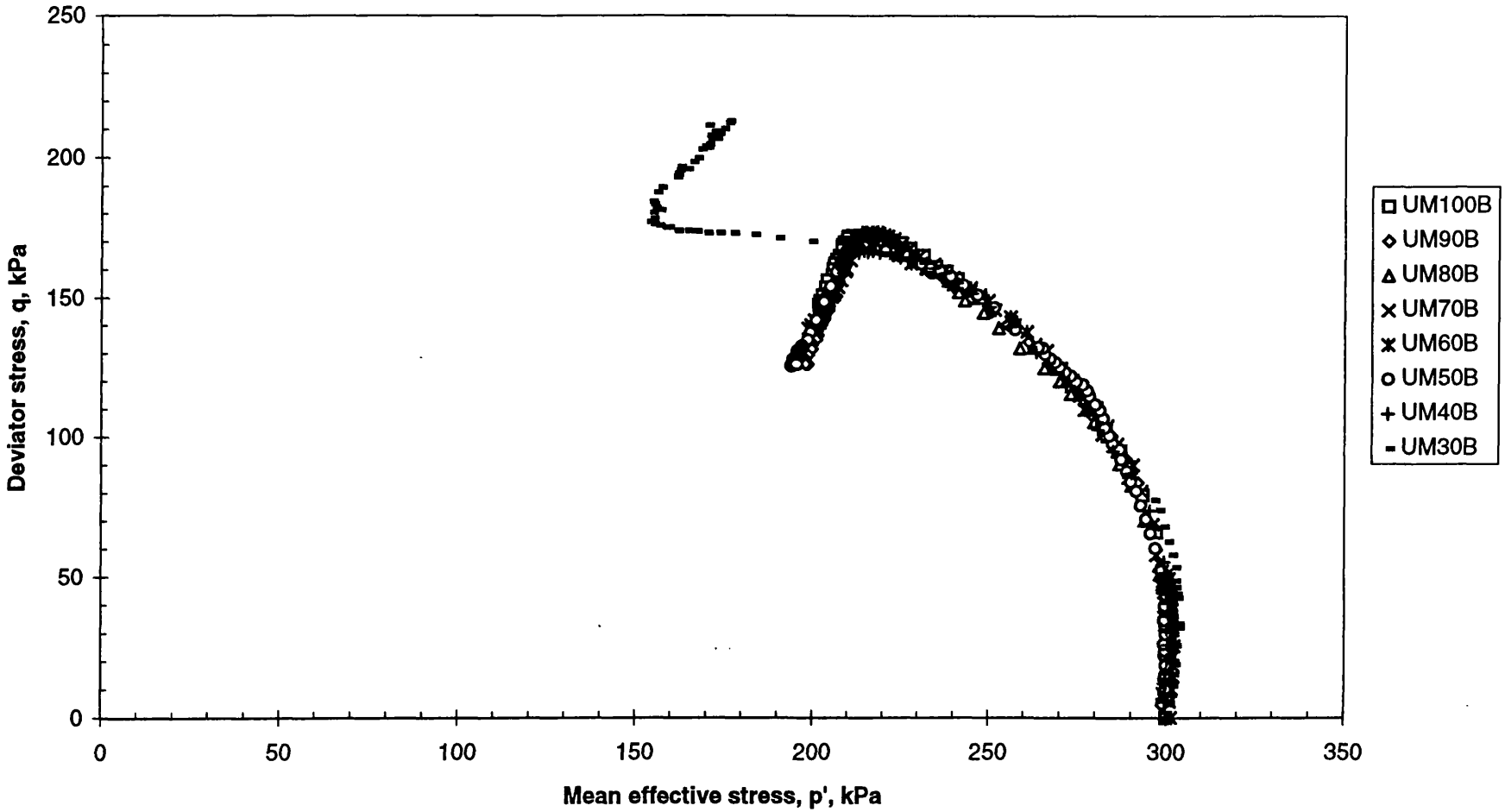

Fig.5.13b Undrained effective stress paths at OCR 1.33

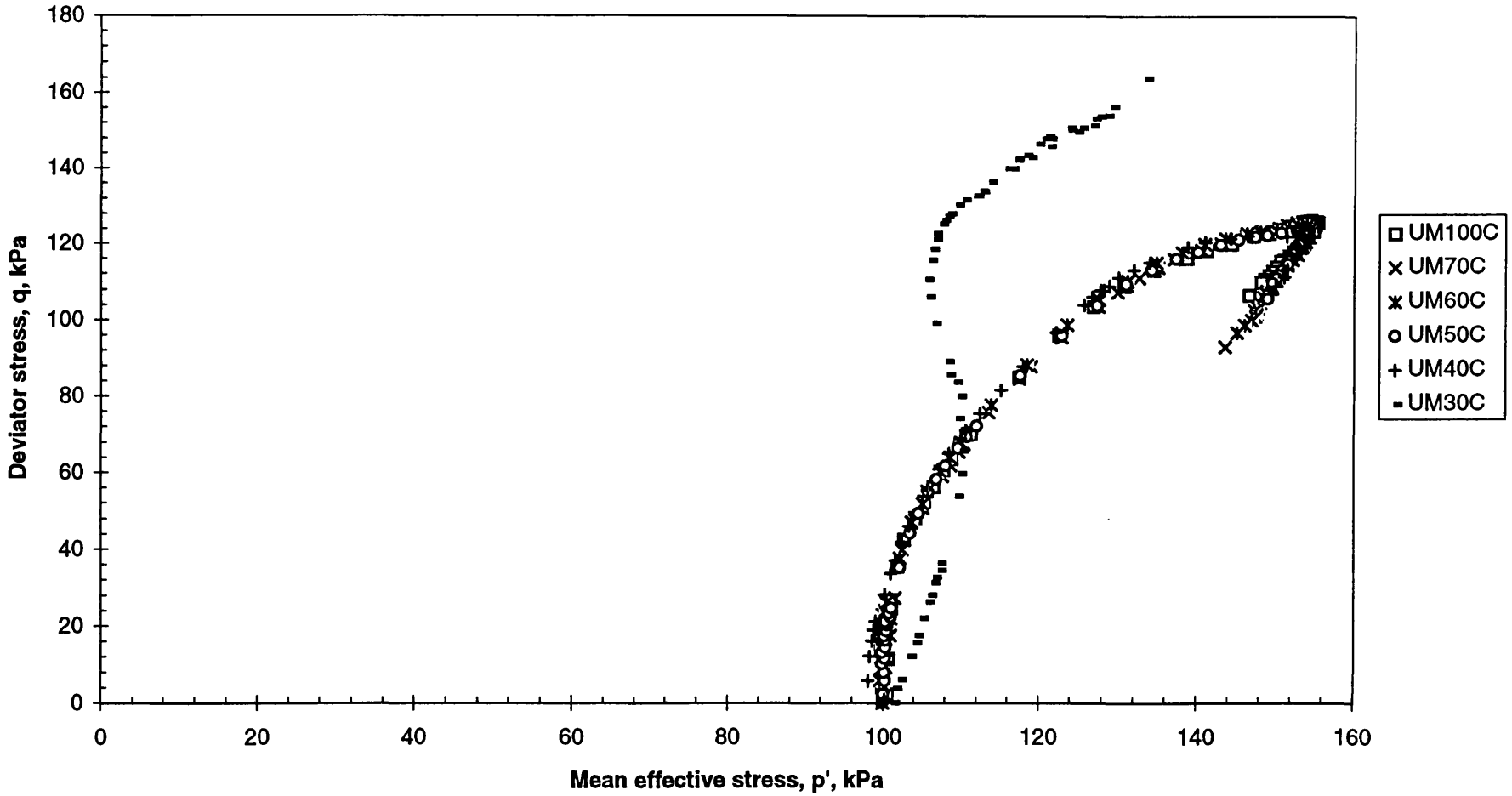

Fig.5.13c Undrained effective stress paths at OCR 4

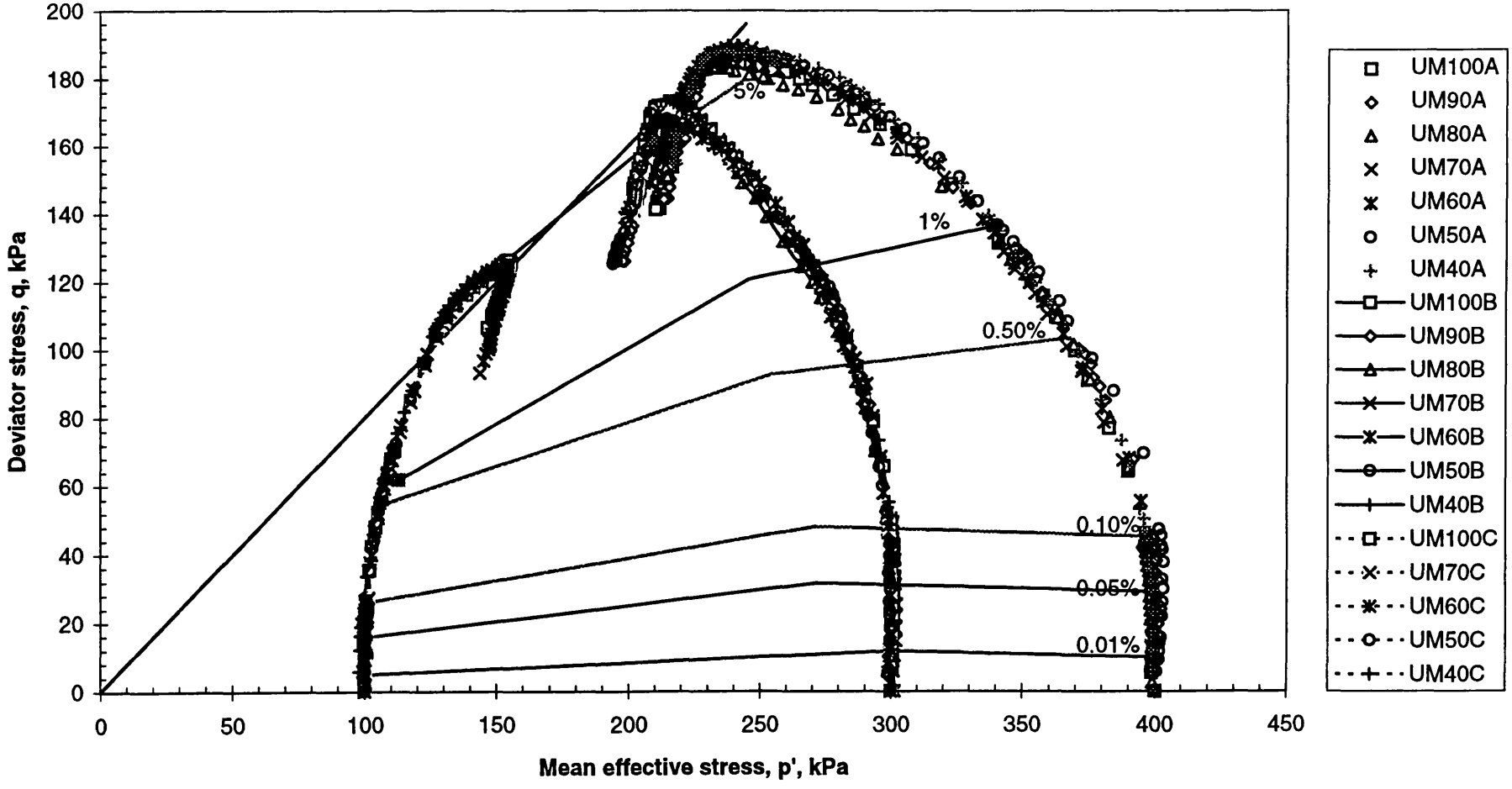

Fig.5.14 Undrained effective stress paths of mixtures with clay content from 40 to 100%

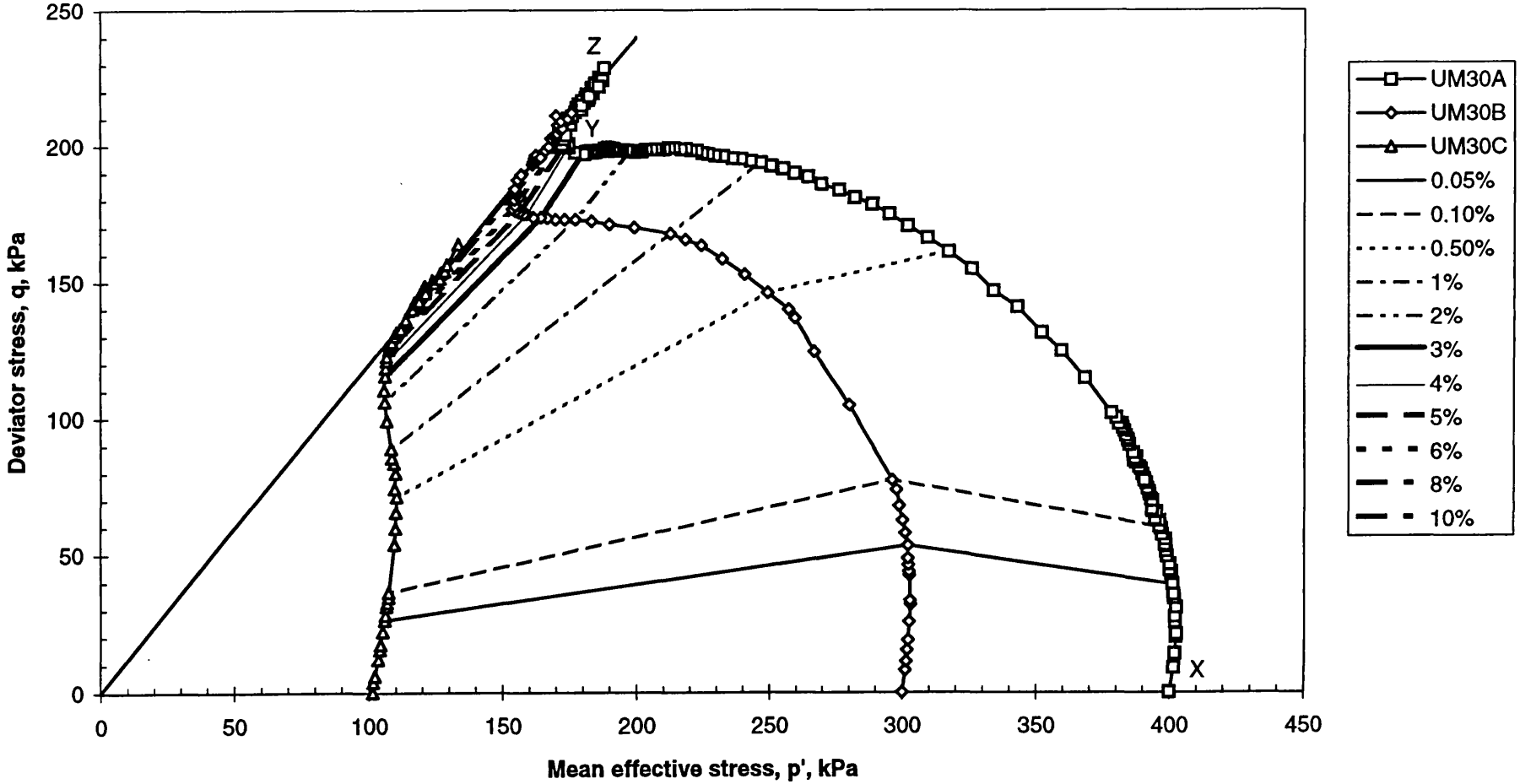

Fig.5.15 Undrained effective stress paths of mixture with 30% clay content

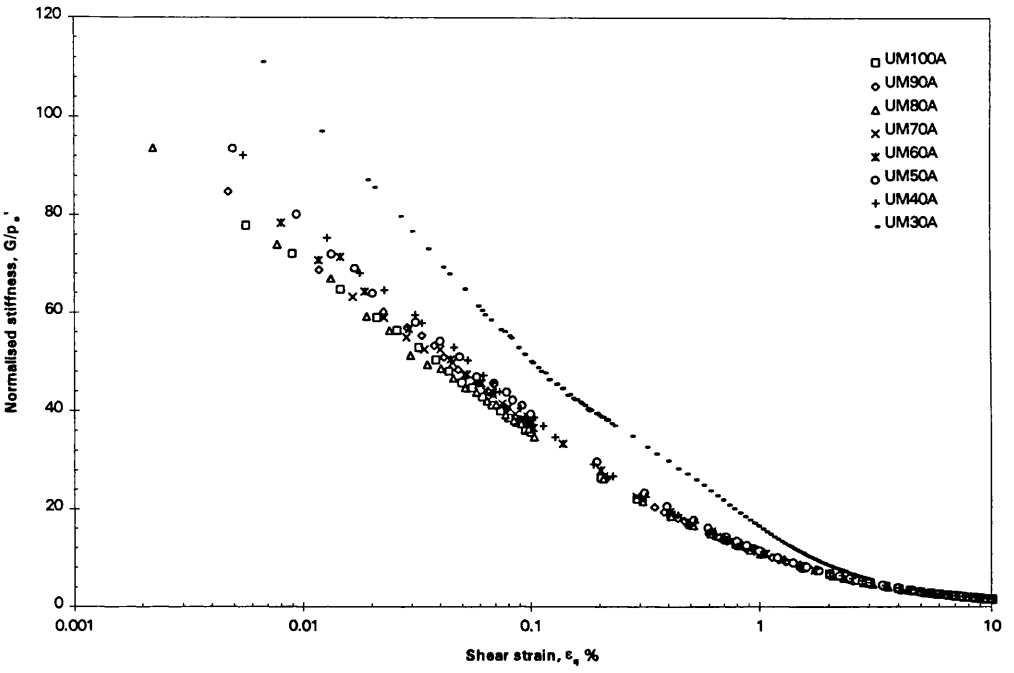

Fig.5.16a Variation of undrained shear stiffness at OCR 1

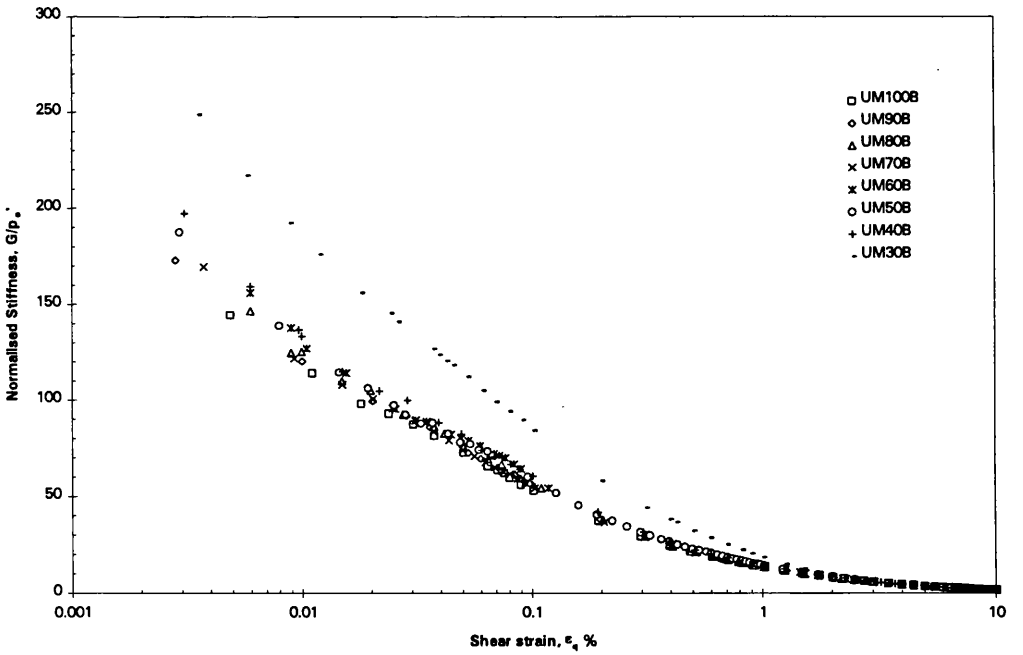

Fig.5.16b Variation of undrained shear stiffness at OCR 1.33

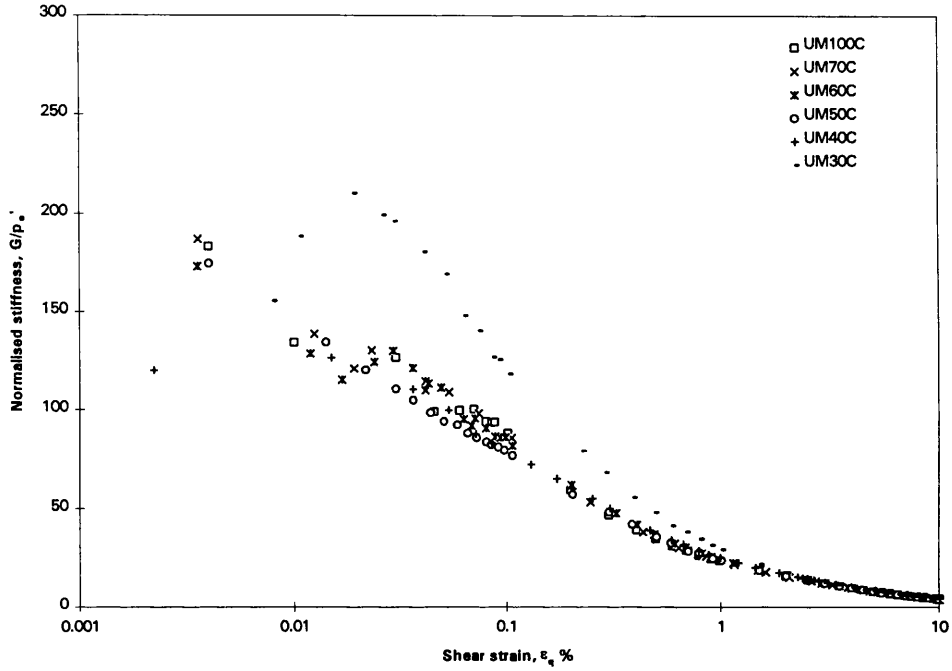

Fig.5.16c Variation of undrained shear stiffness at OCR 4

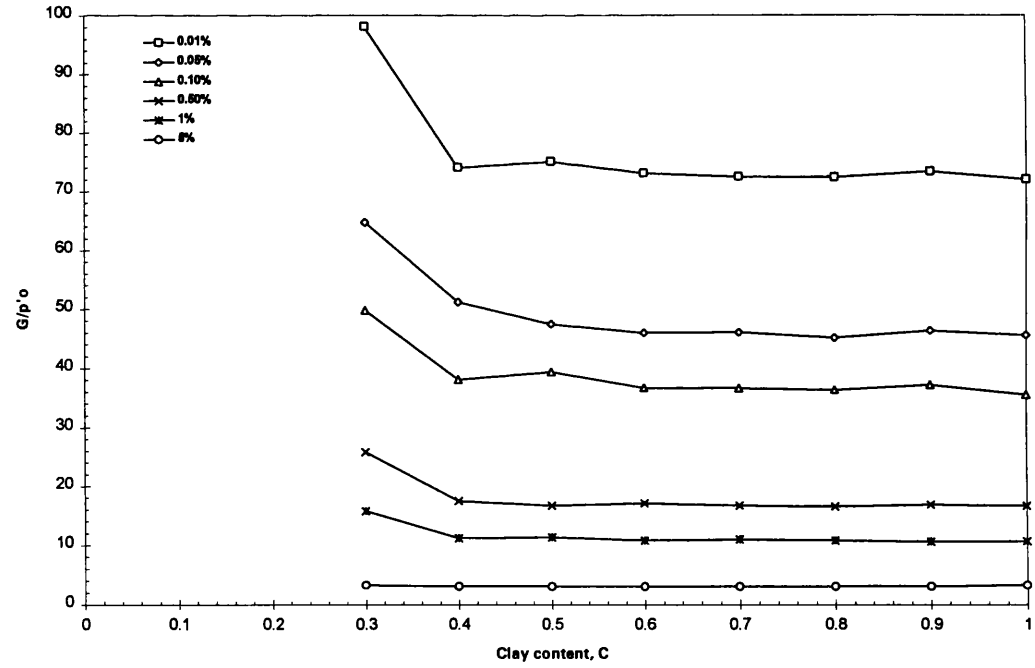

Fig.5.17a Variation of undrained G/p'_0 with clay content at OCR1

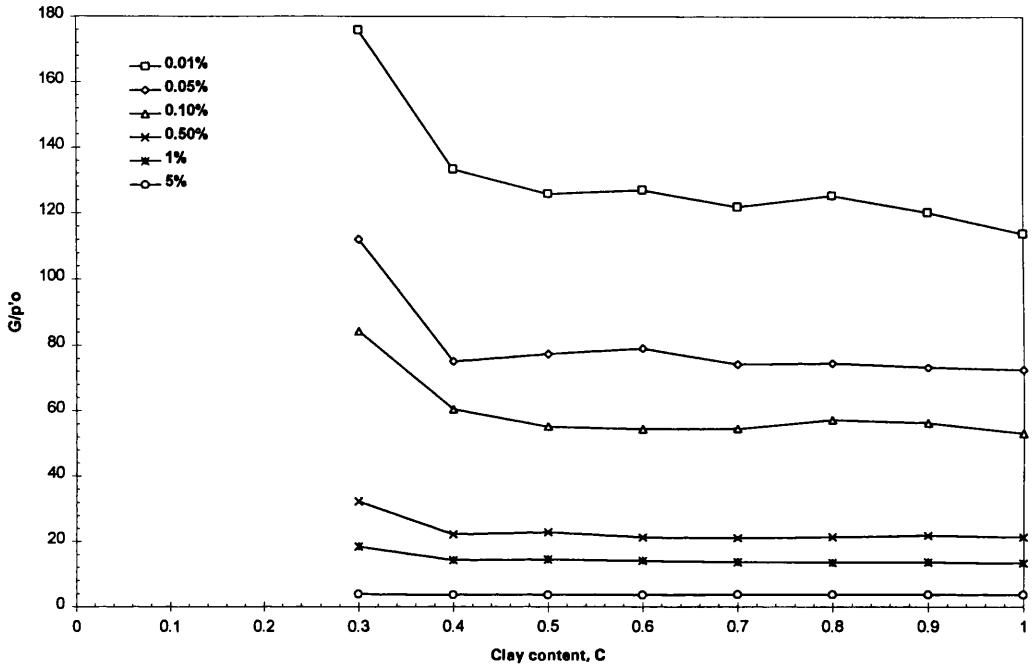

Fig.5.17b Variation of undrained G/p'_0 with clay content at OCR 1.33

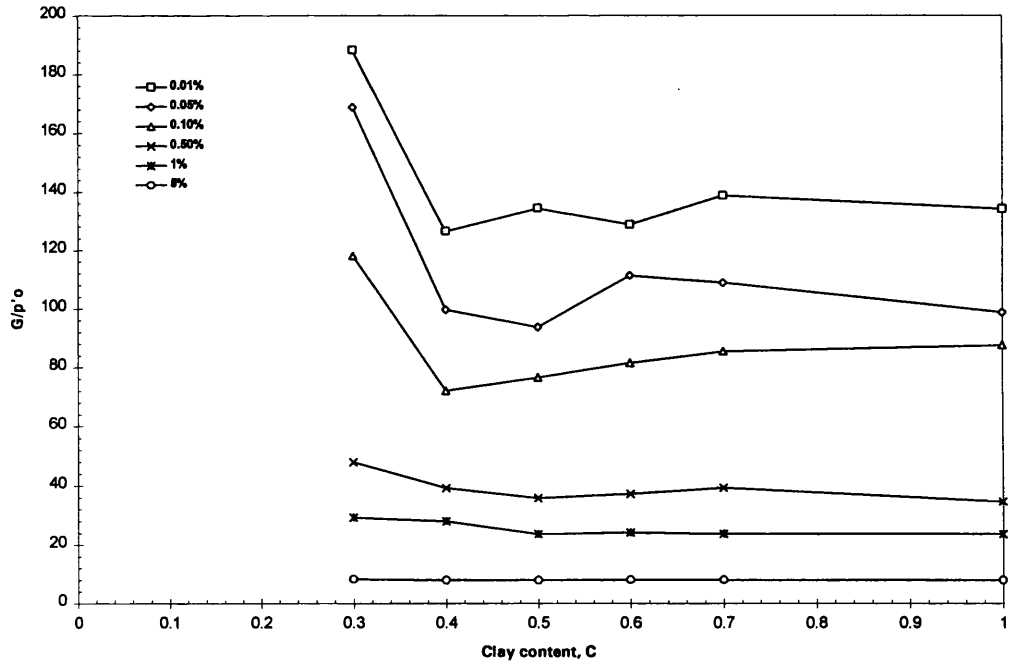

Fig.5.17c Variation of undrained G/p'_0 with clay content at OCR 4

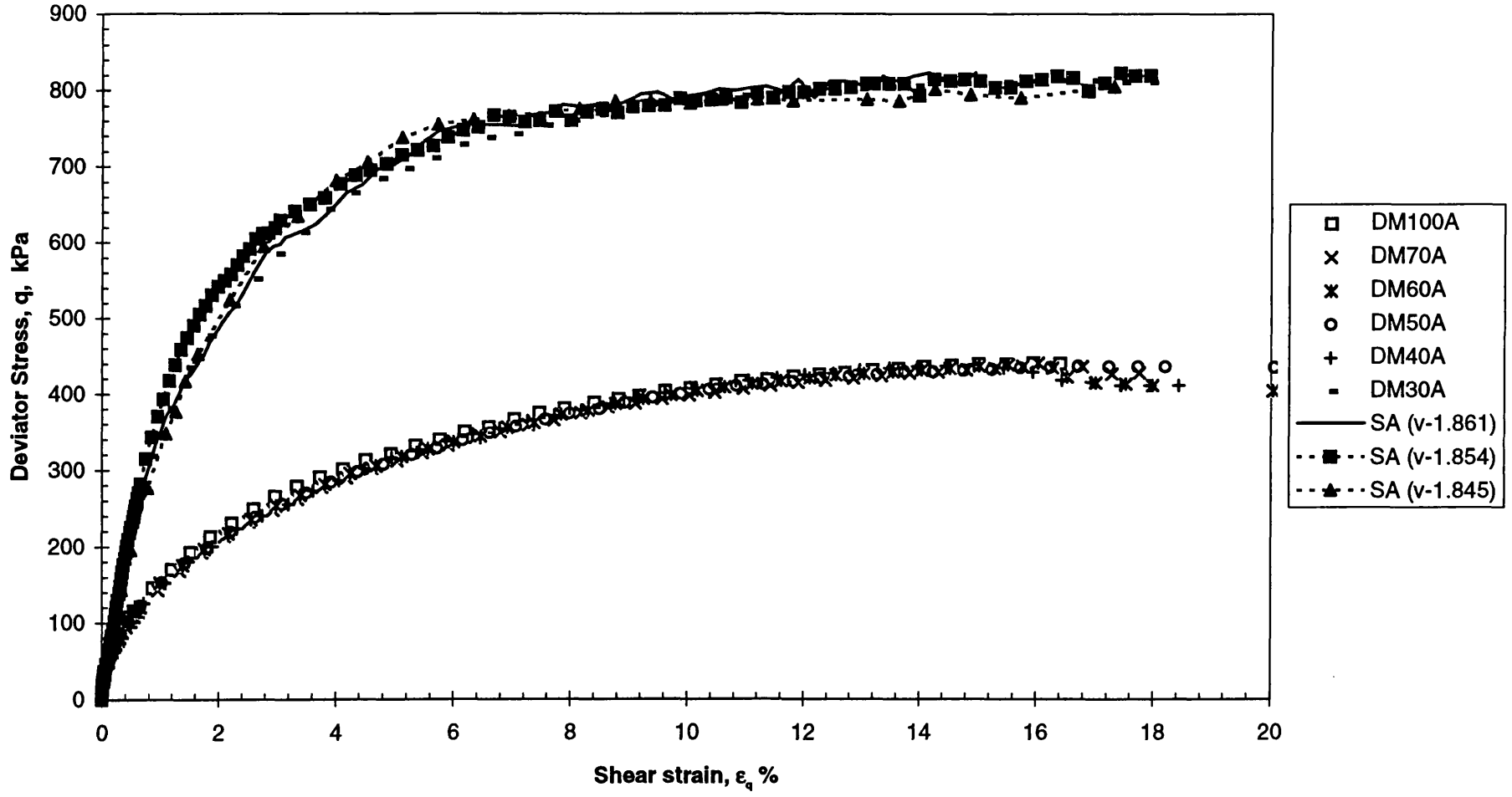

Fig.5.18a Drained stress-strain response at OCR 1

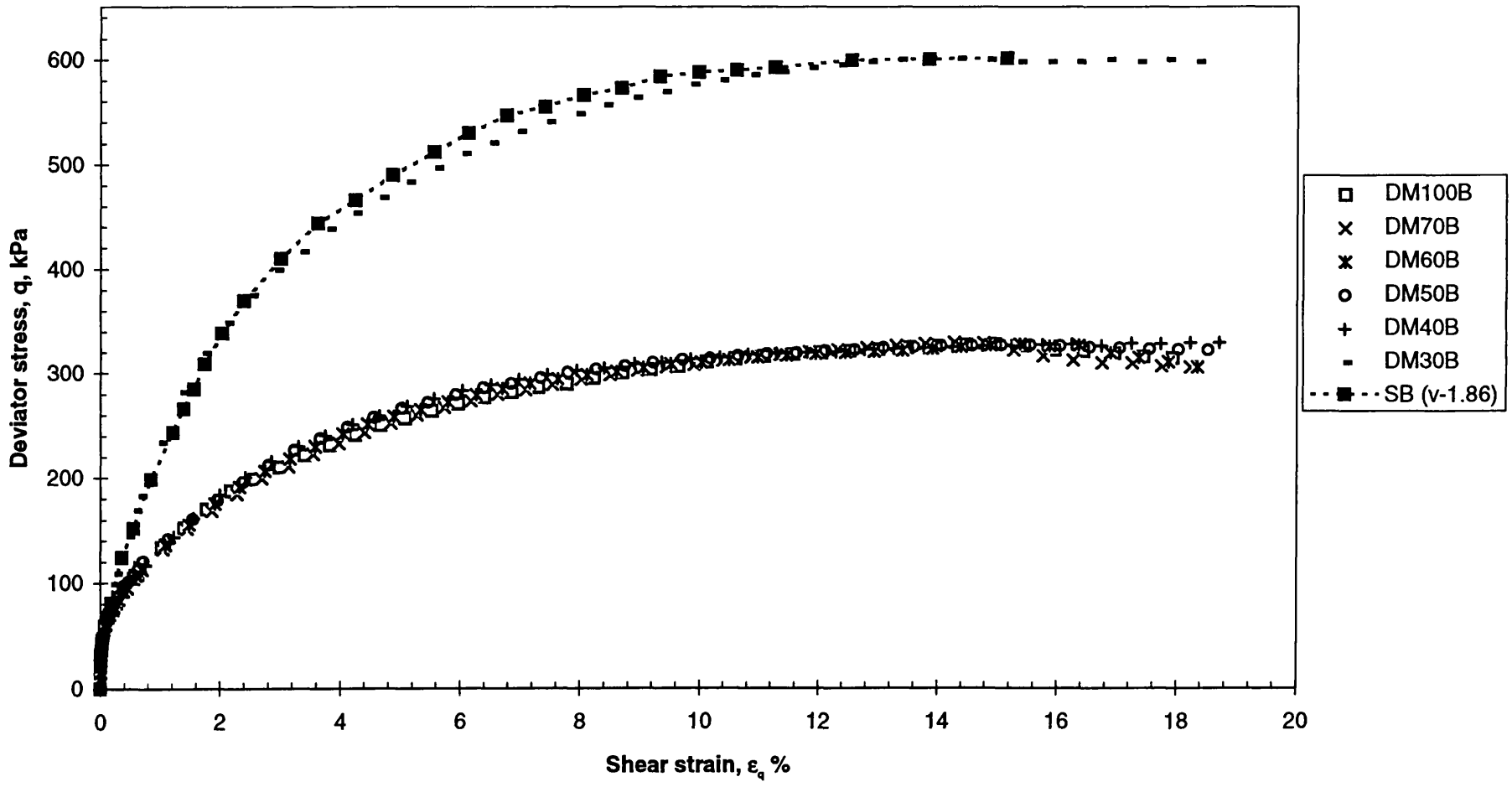

Fig.5.18b Drained stress-strain response at OCR 1.33

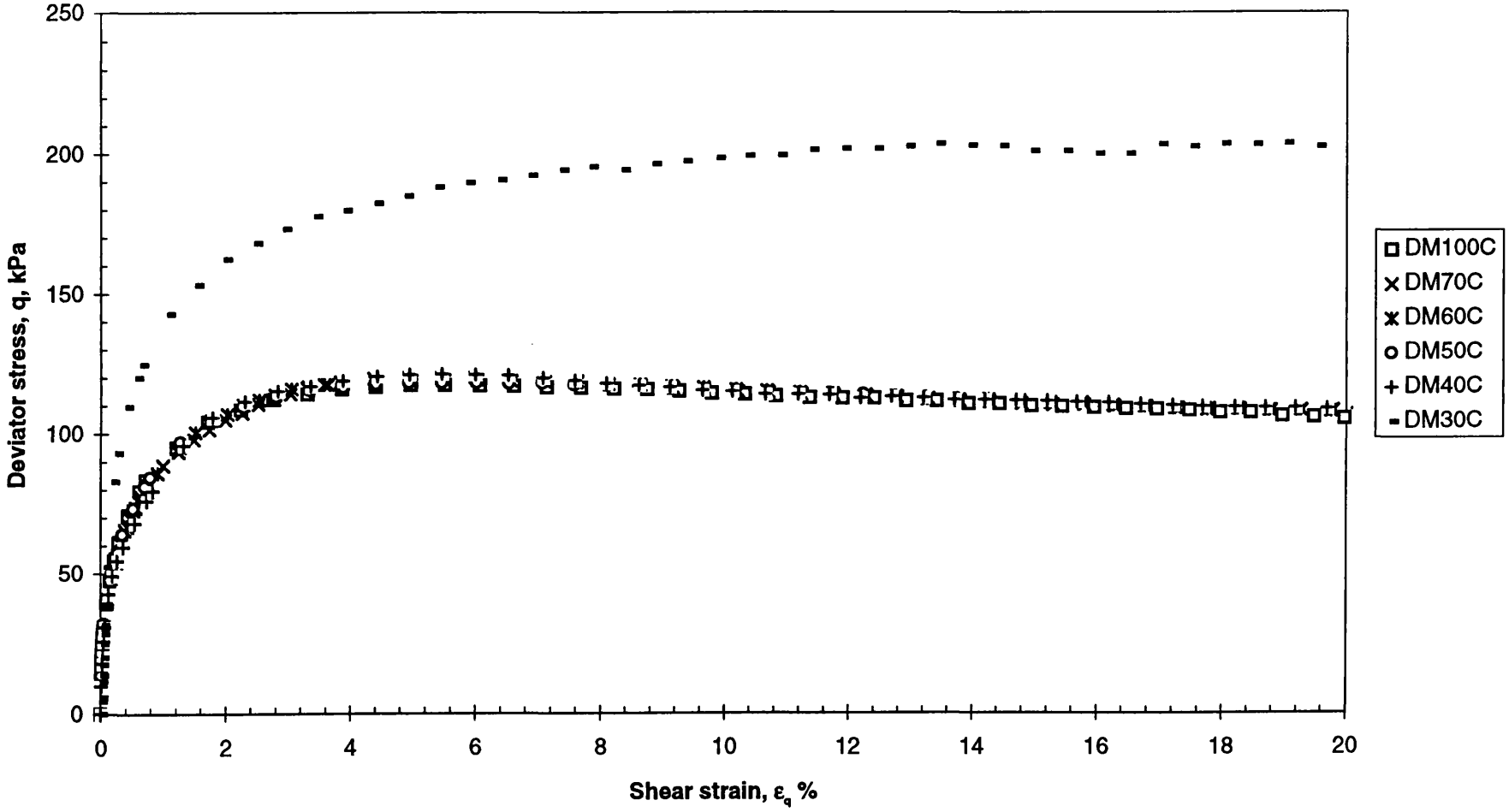

Fig.5.18c Drained stress-strain response at OCR 4

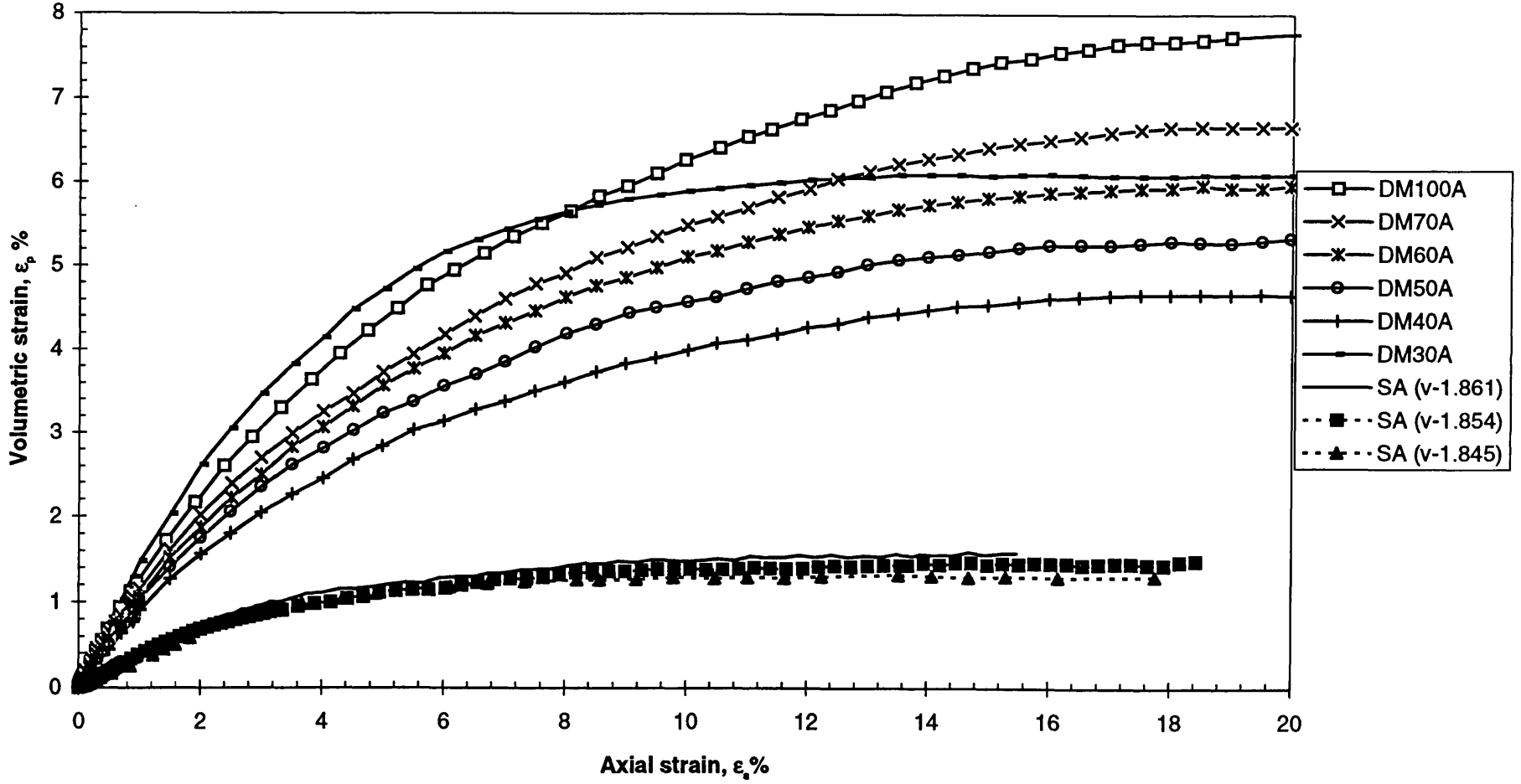

Fig.5.19a Drained volumetric strain - strain response at OCR 1

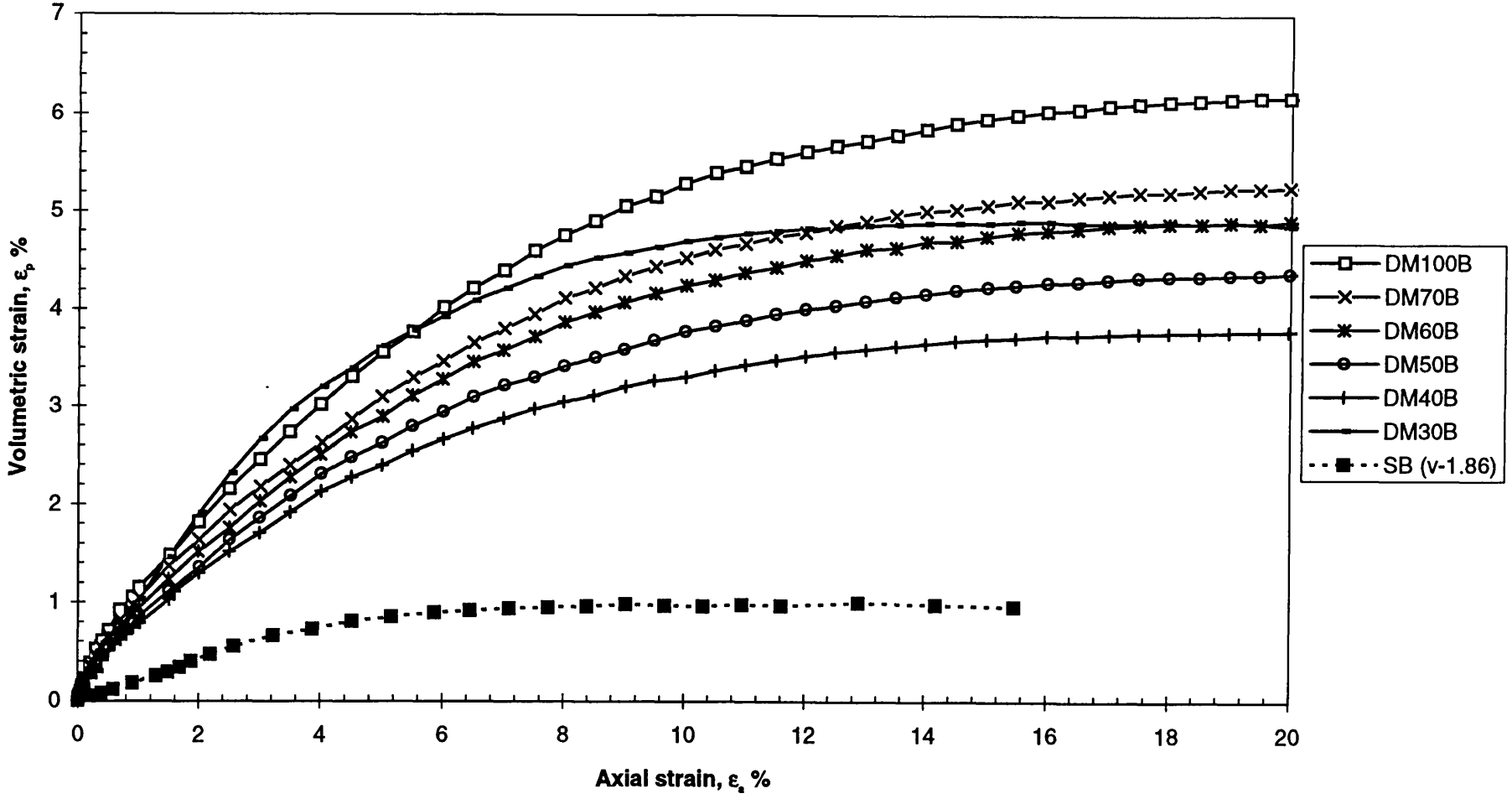

Fig.5.19b Drained volumetric strain: strain response at OCR 1.33

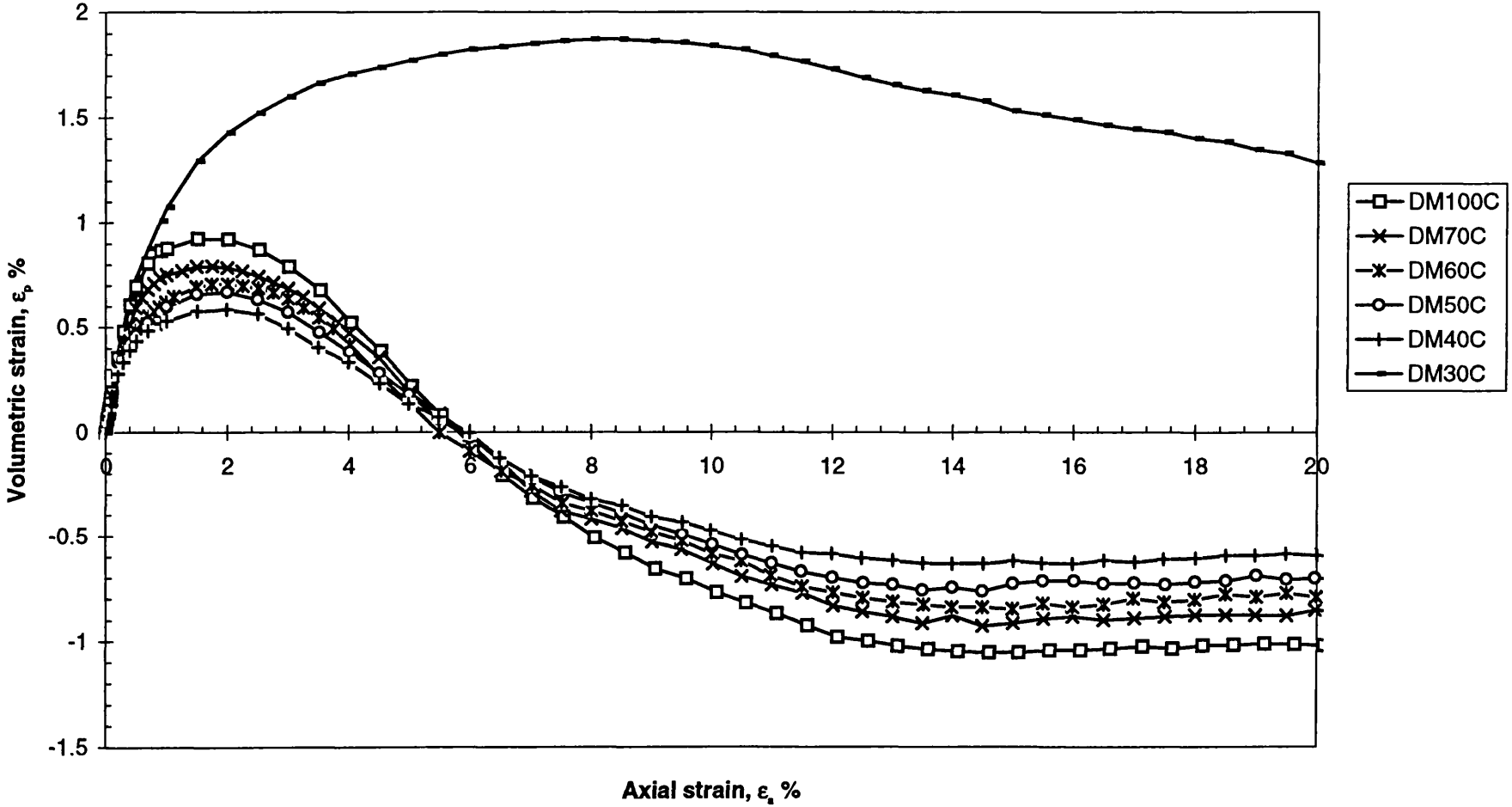

Fig.5.19c Drained volumetric strain: strain response at OCR 4

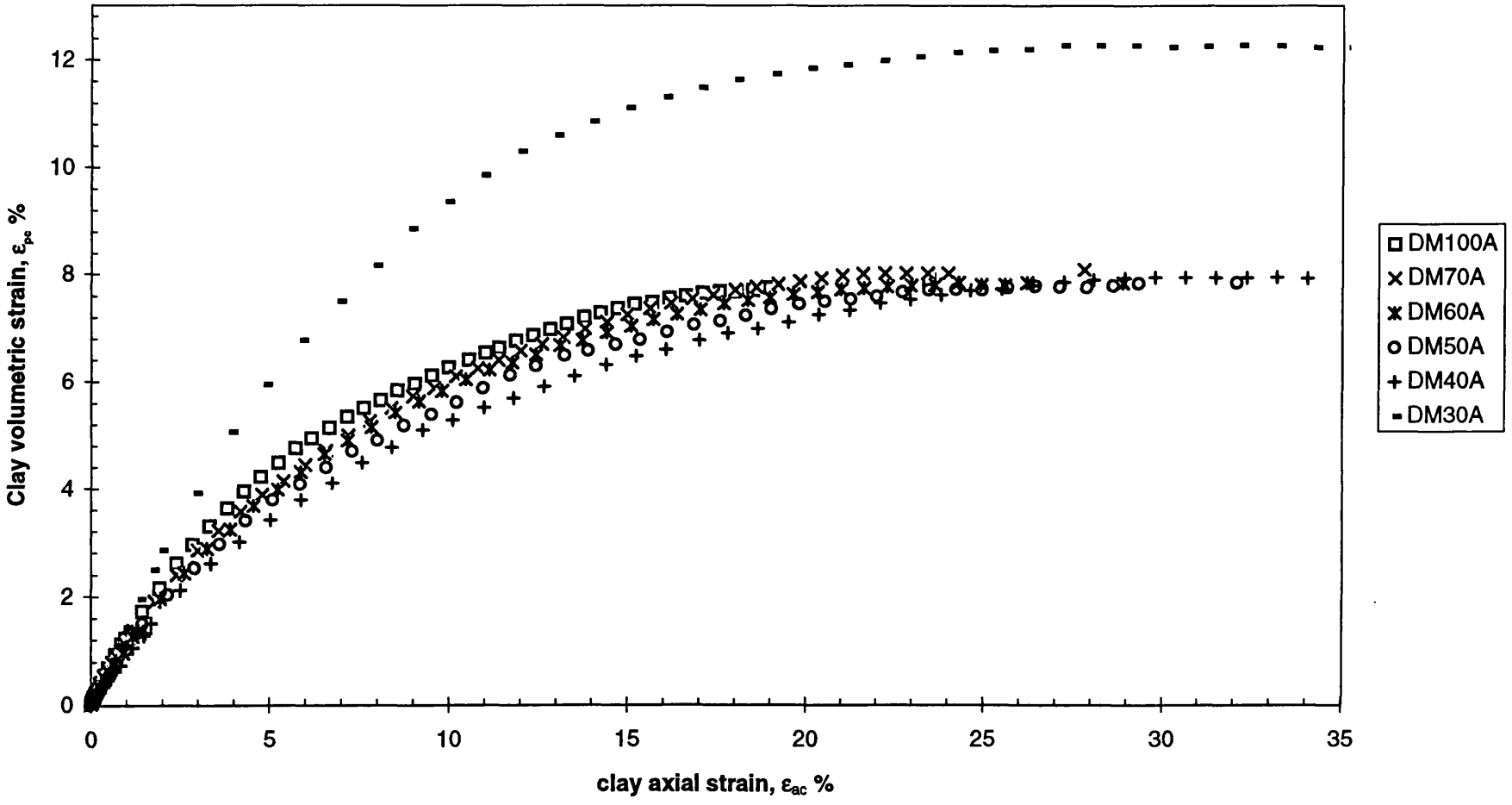

Fig.5.20a Clay volumetric strain - clay axial strains response at OCR 1

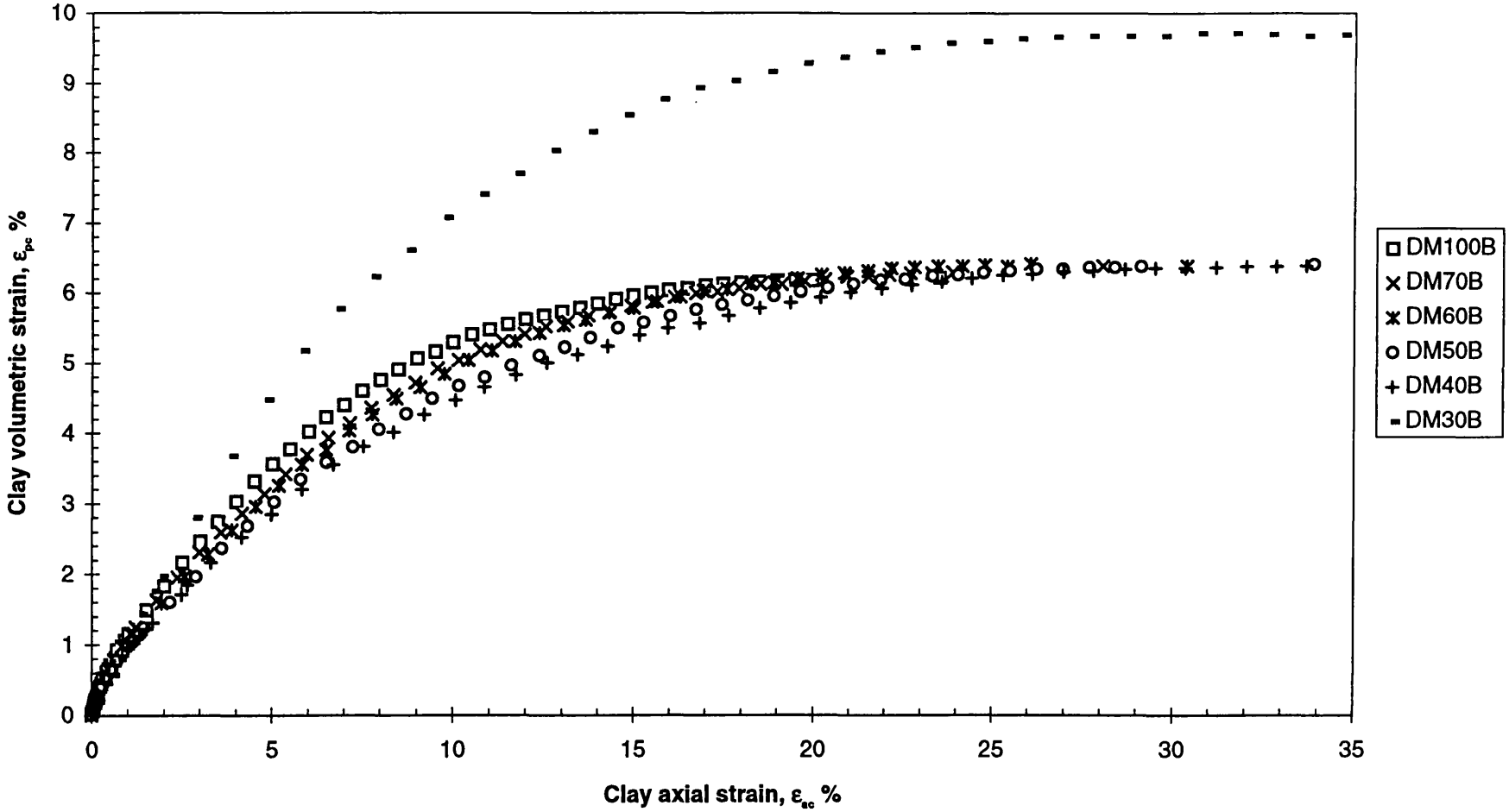

Flg.5.20b Clay volumetric strain - clay axial strain response at OCR 1.33

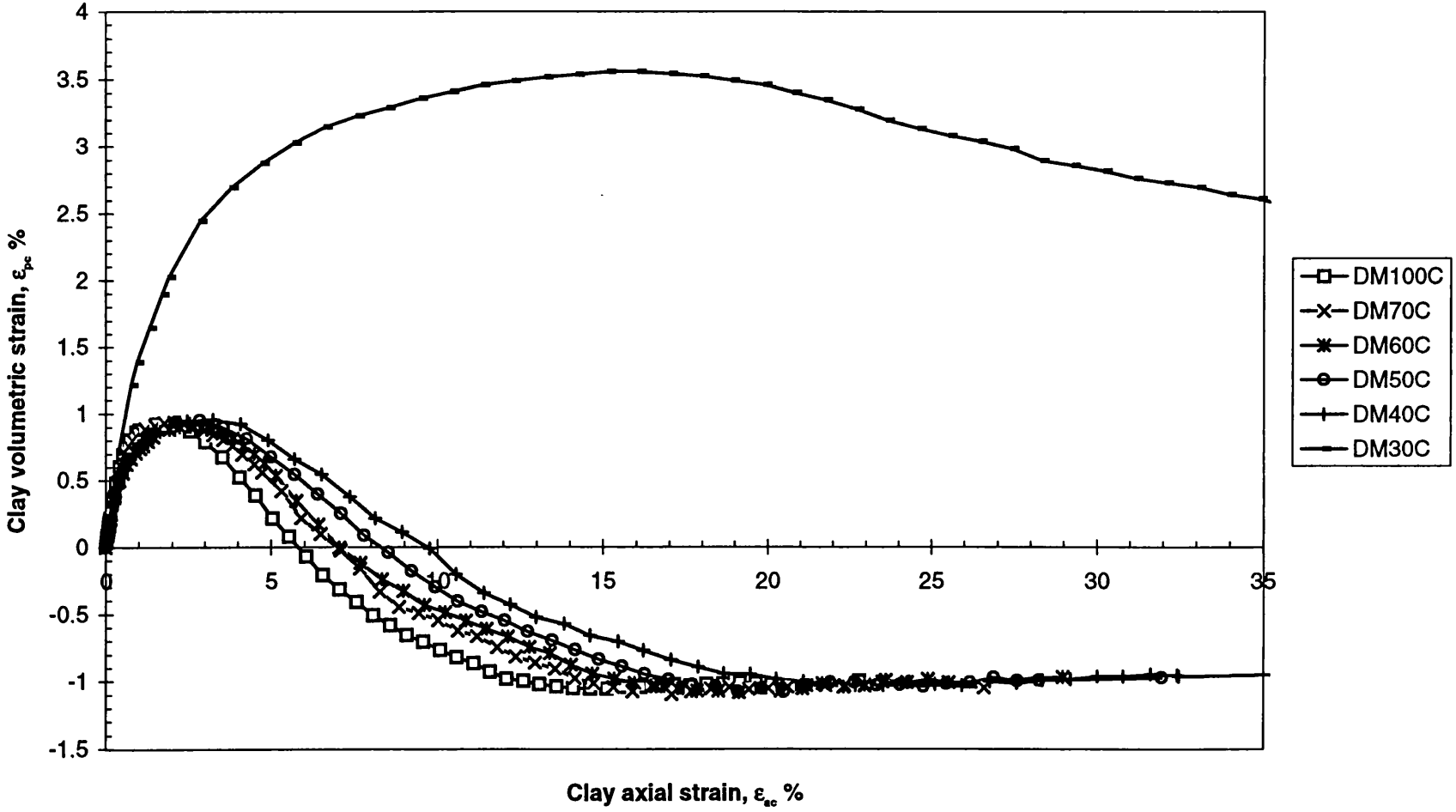

Fig.5.20c Clay volumetric strain: clay axial strain response at OCR 4

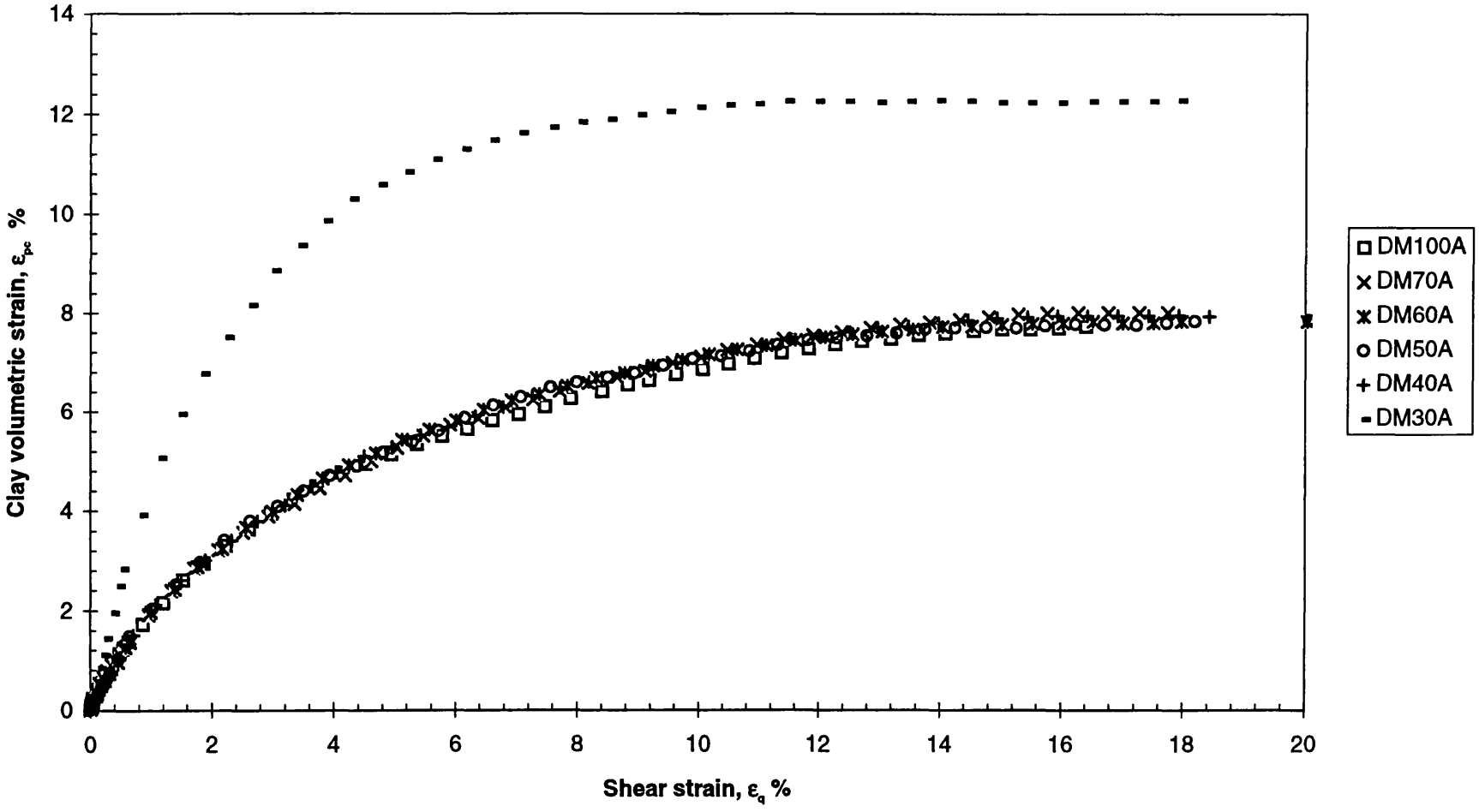

Fig.5.21a Clay volumetric strain : shear strain response at OCR 1

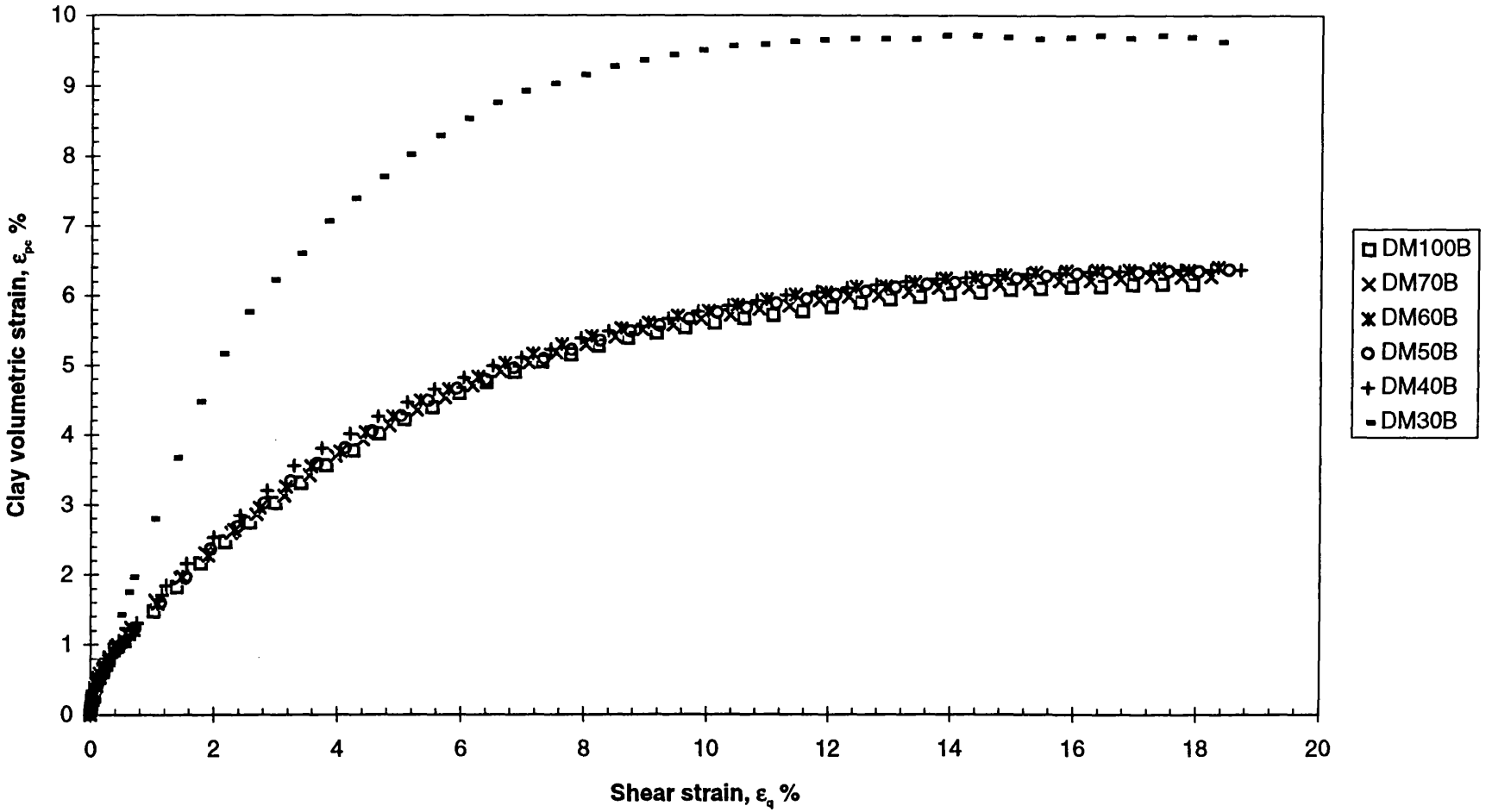

Fig.5.21b Clay volumetric strain: shear strain response at OCR 1.33

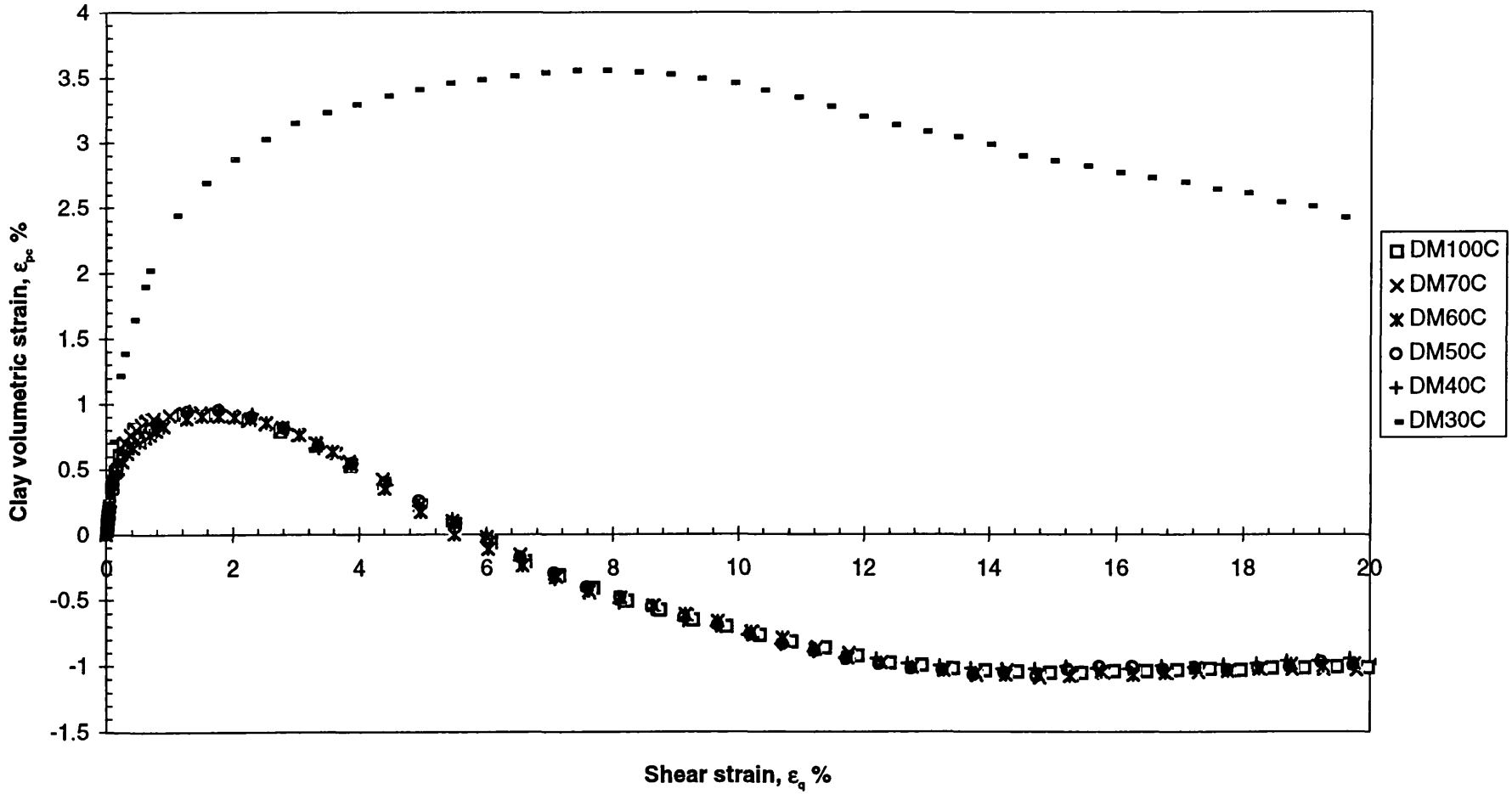

Fig.5.21c Clay volumetric strain : shear strain response at OCR 4

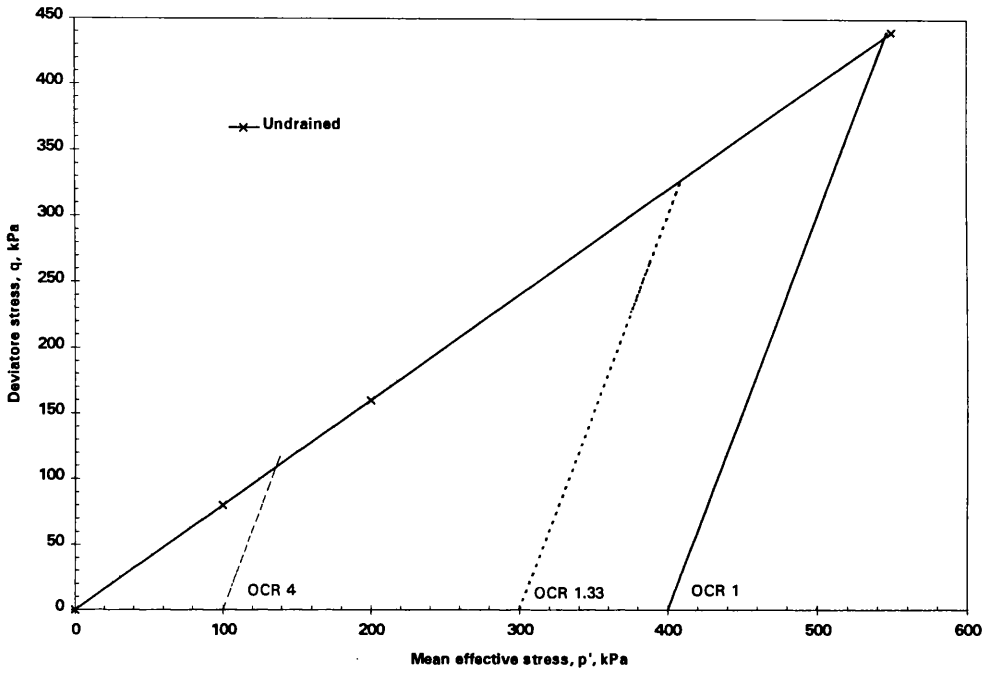

Fig.5.22a Effective stress paths of mixtures with C = 100 to 40% (Drained tests)

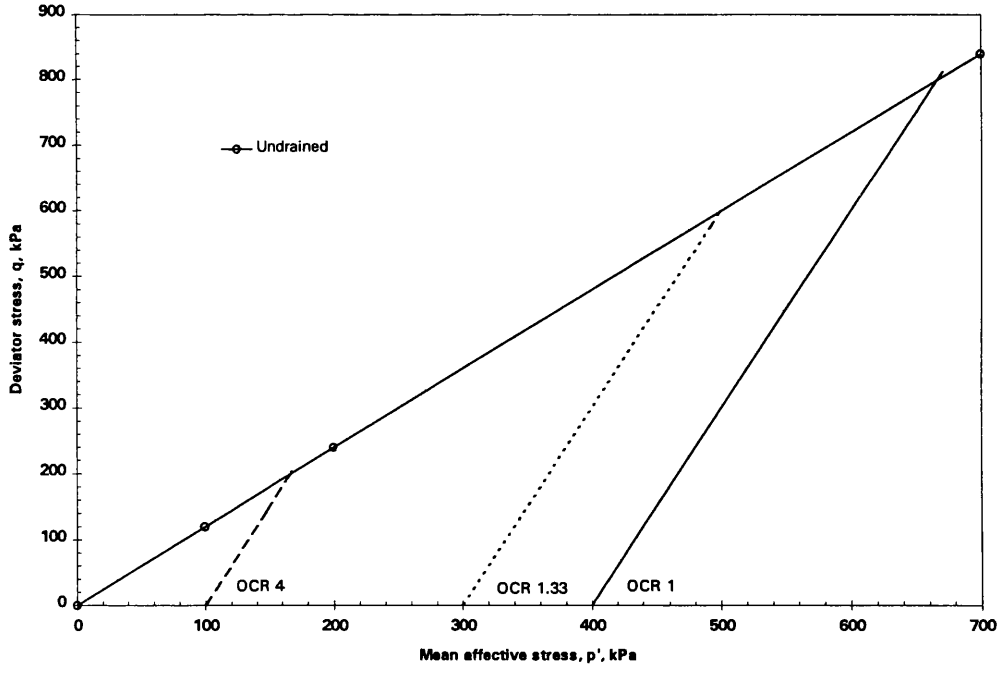

Fig.5.22b Effective stress paths of mixture with C = 30% (Drained tests)

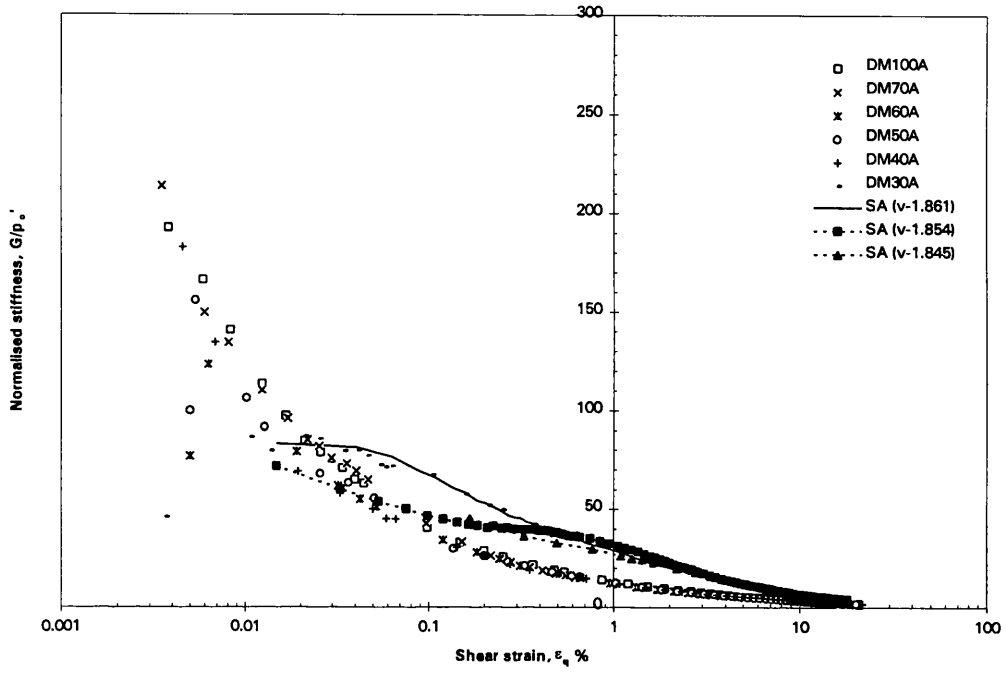

Fig.5.23a Variation of drained shear stiffness at OCR 1

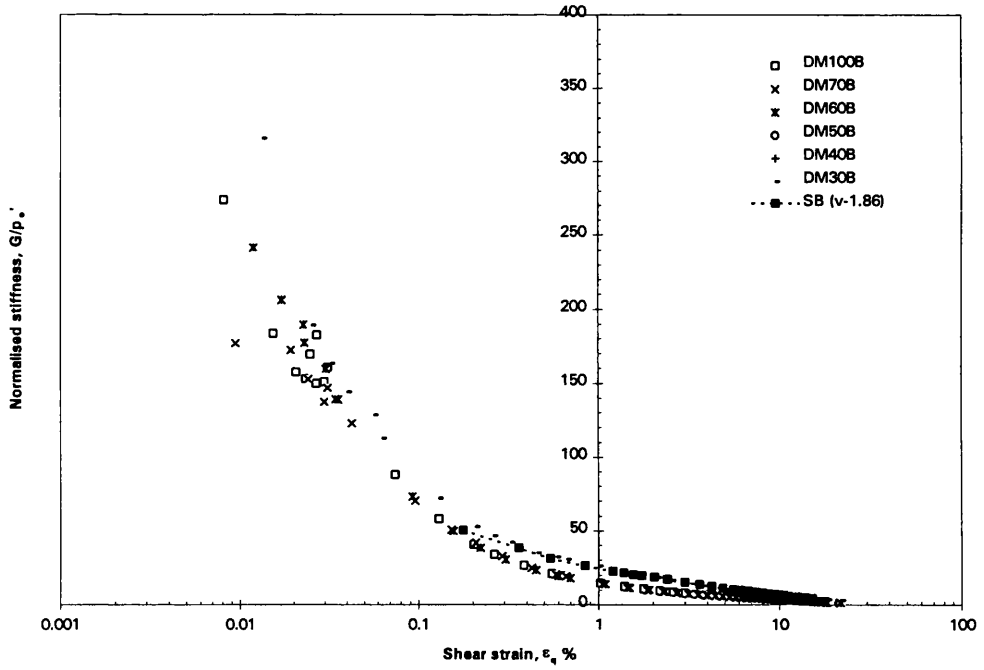

Fig.5.23b Variation of drained shear stiffness at OCR 1.33

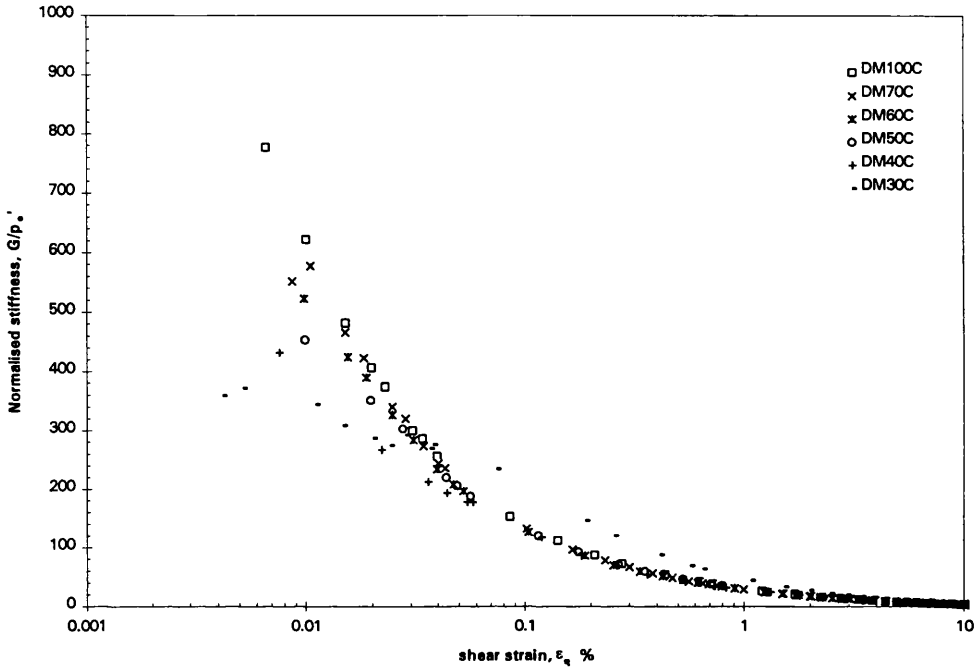

Fig.5.23c Variation of drained shear stiffness at OCR 4

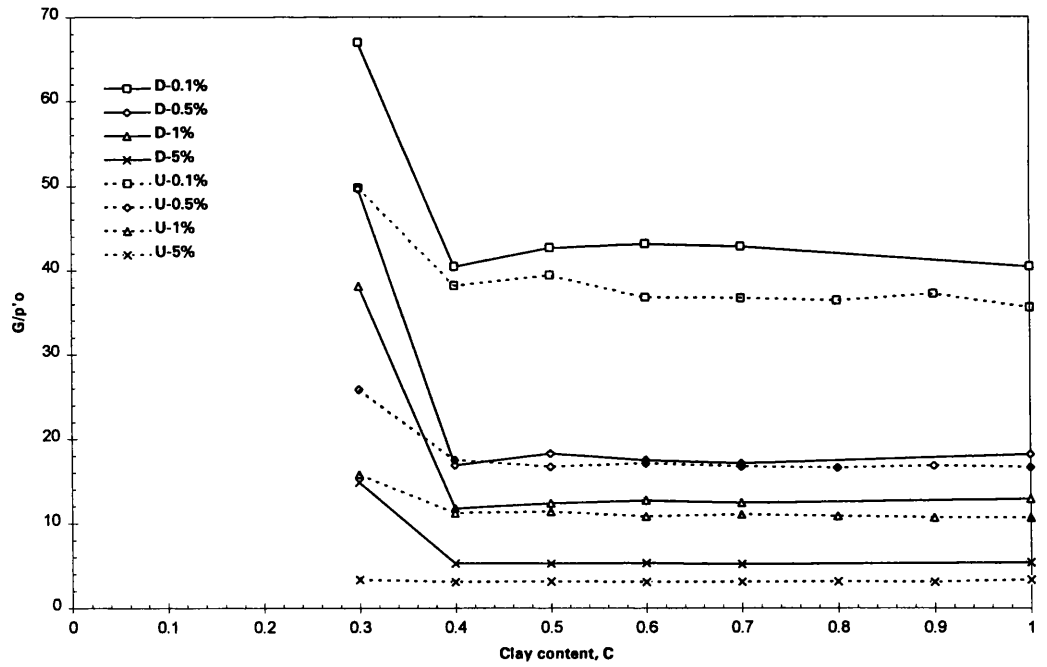

Fig.5.24a Drained and undrained stiffness against clay content at OCR 1

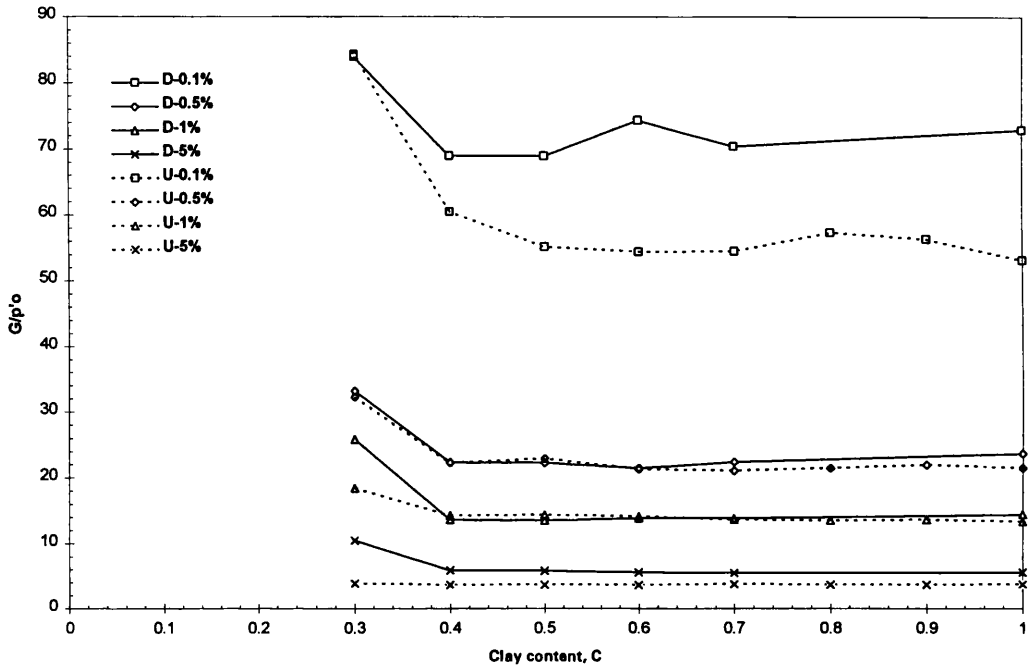

Fig.5.24b Drained and undrained stiffness against clay content at OCR 1.33

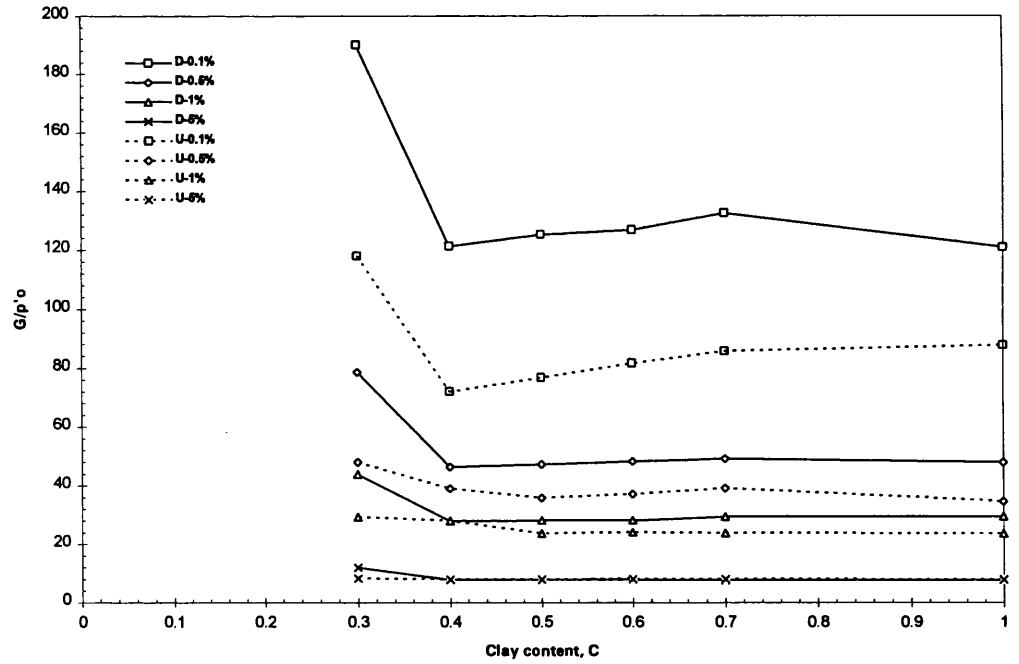

Fig.5.24c Drained and undrained stiffness against clay content at OCR 4

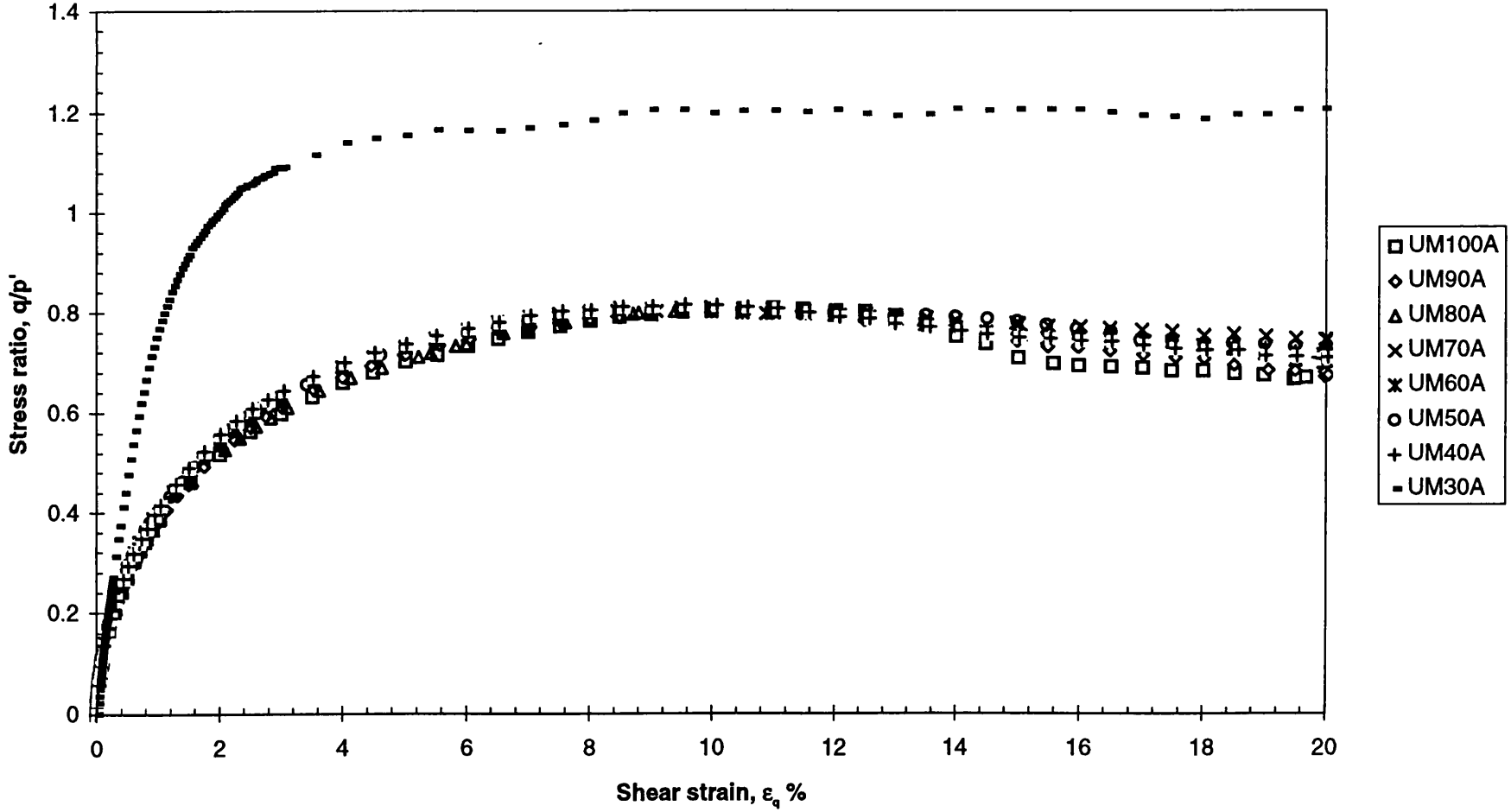

Fig.5.25a Undrained stress ratio: shear strain response at OCR1

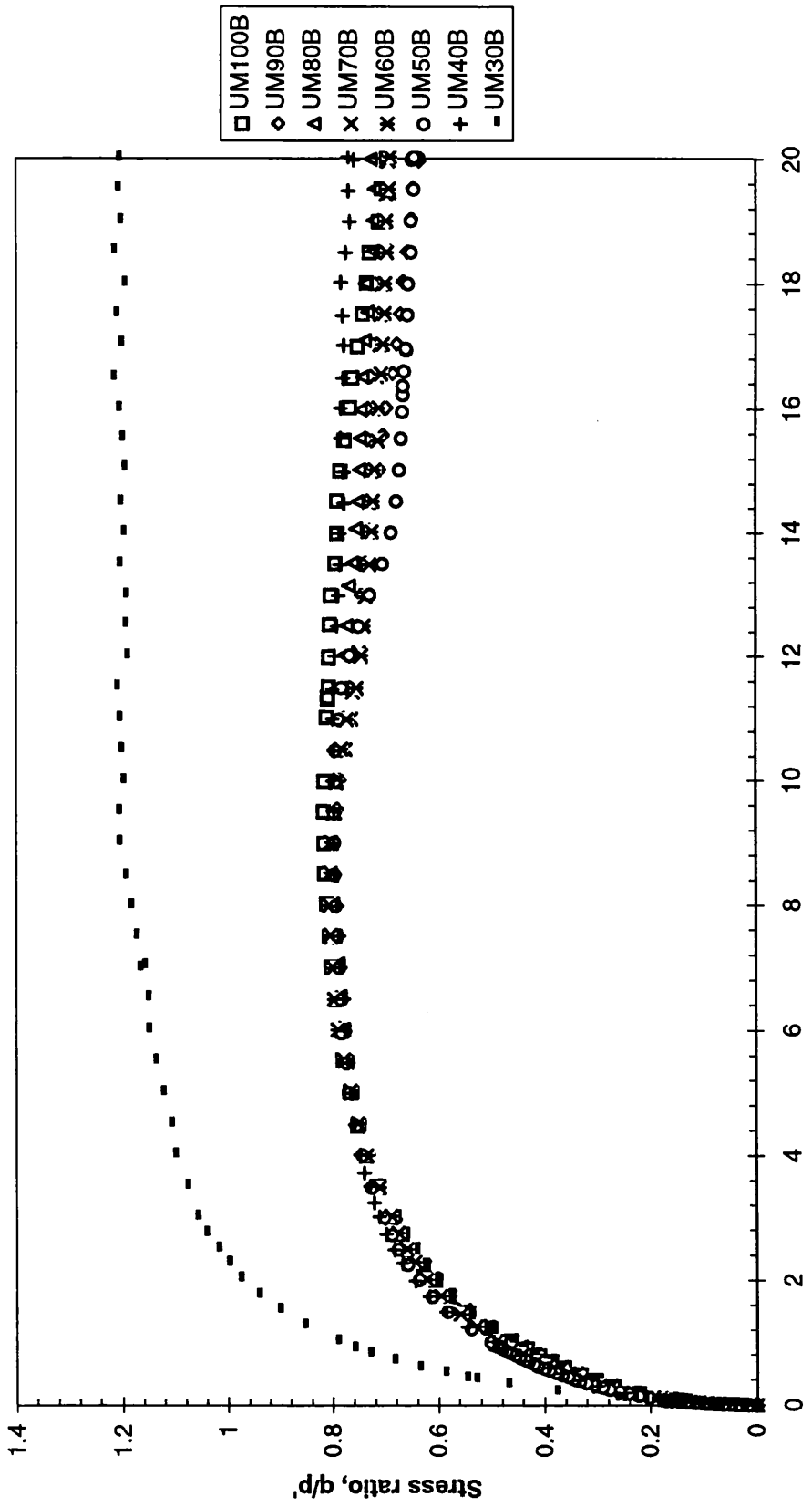

Fig.5.25b Undrained stress ratio: shear strain response at OCR 1.33

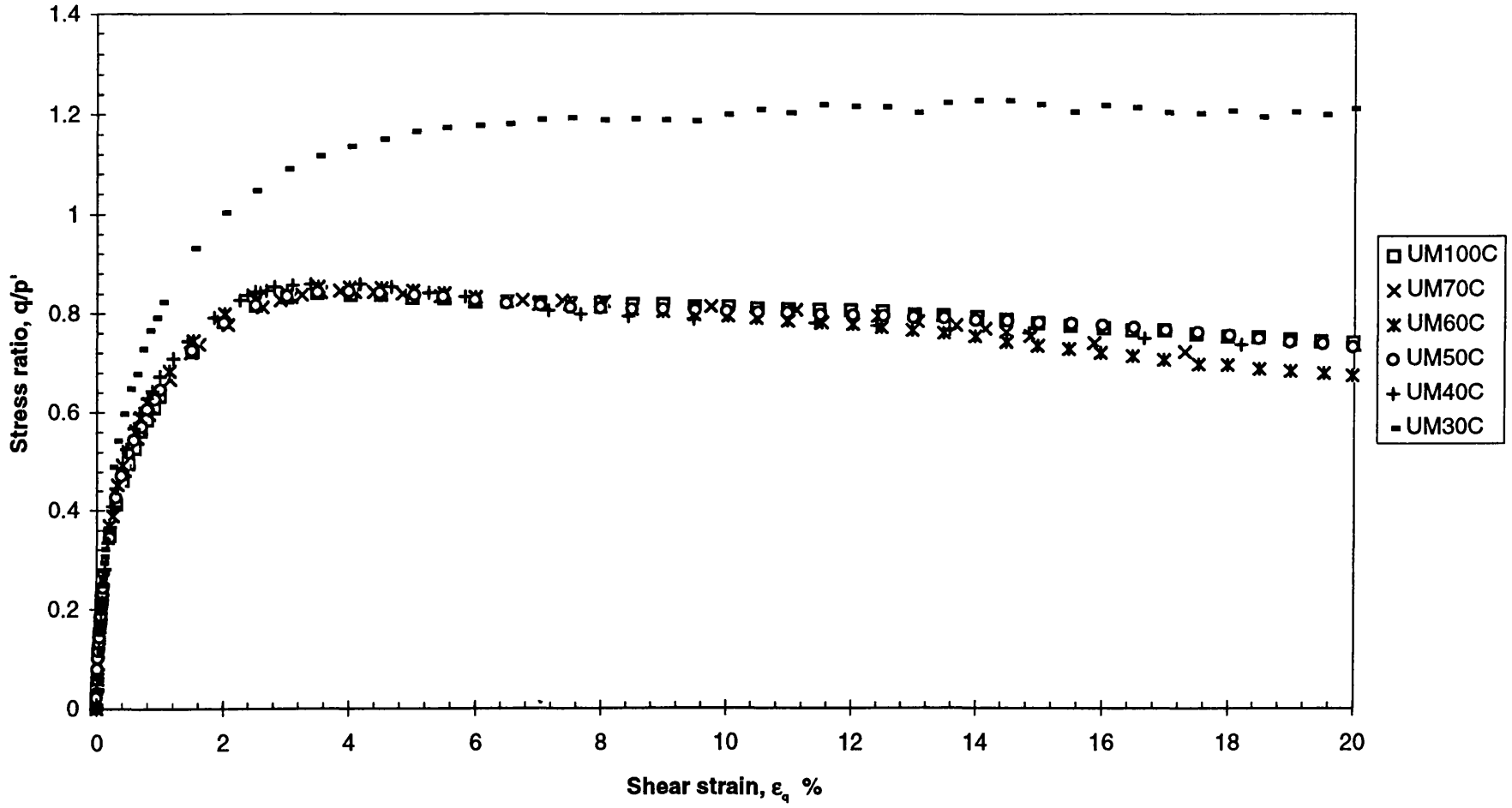

Fig.5.25c Undrained stress ratio: shear strain response at OCR 4

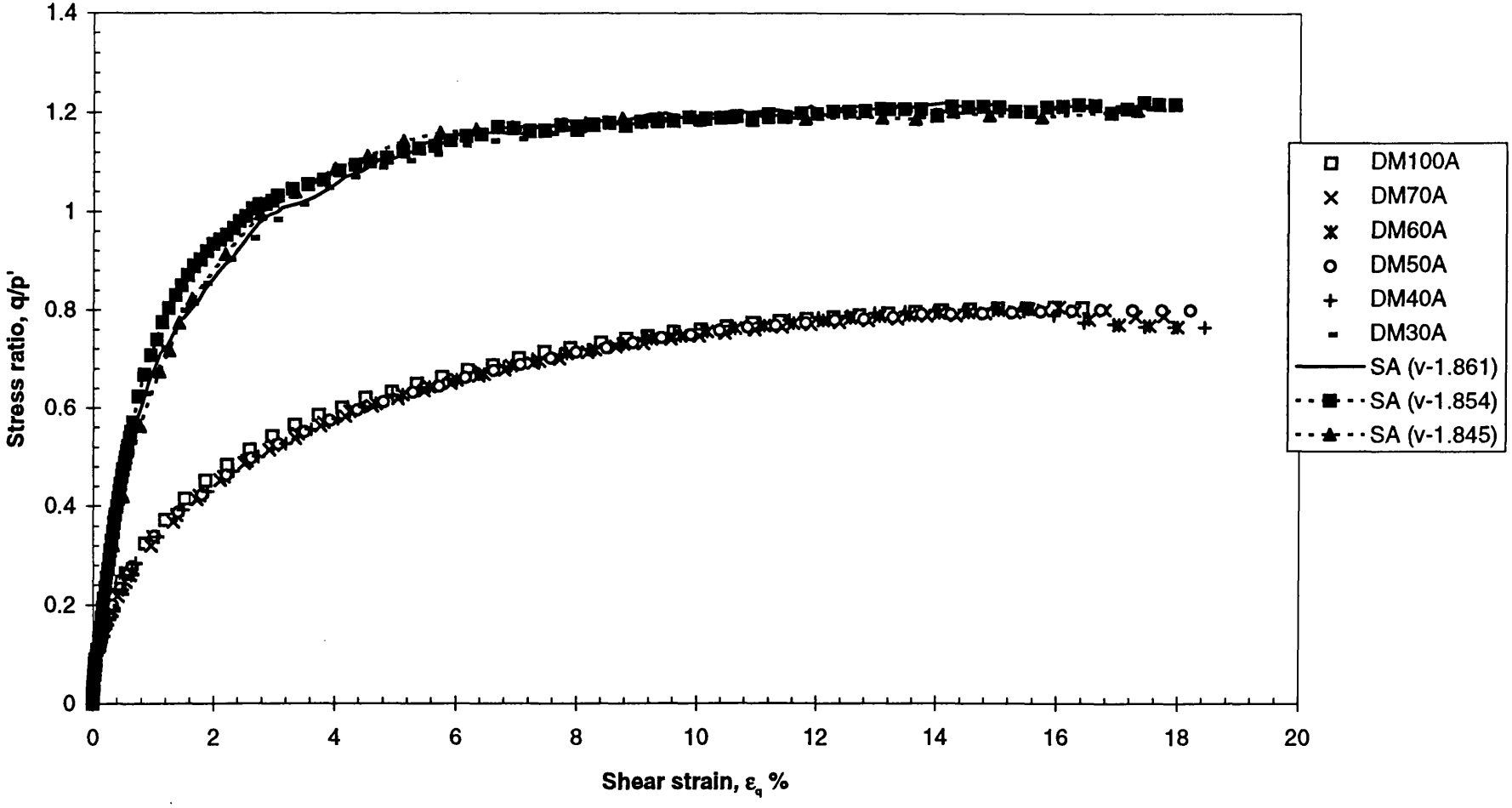

Fig.5.26a Drained stress ratio:shear strain relations at OCR 1

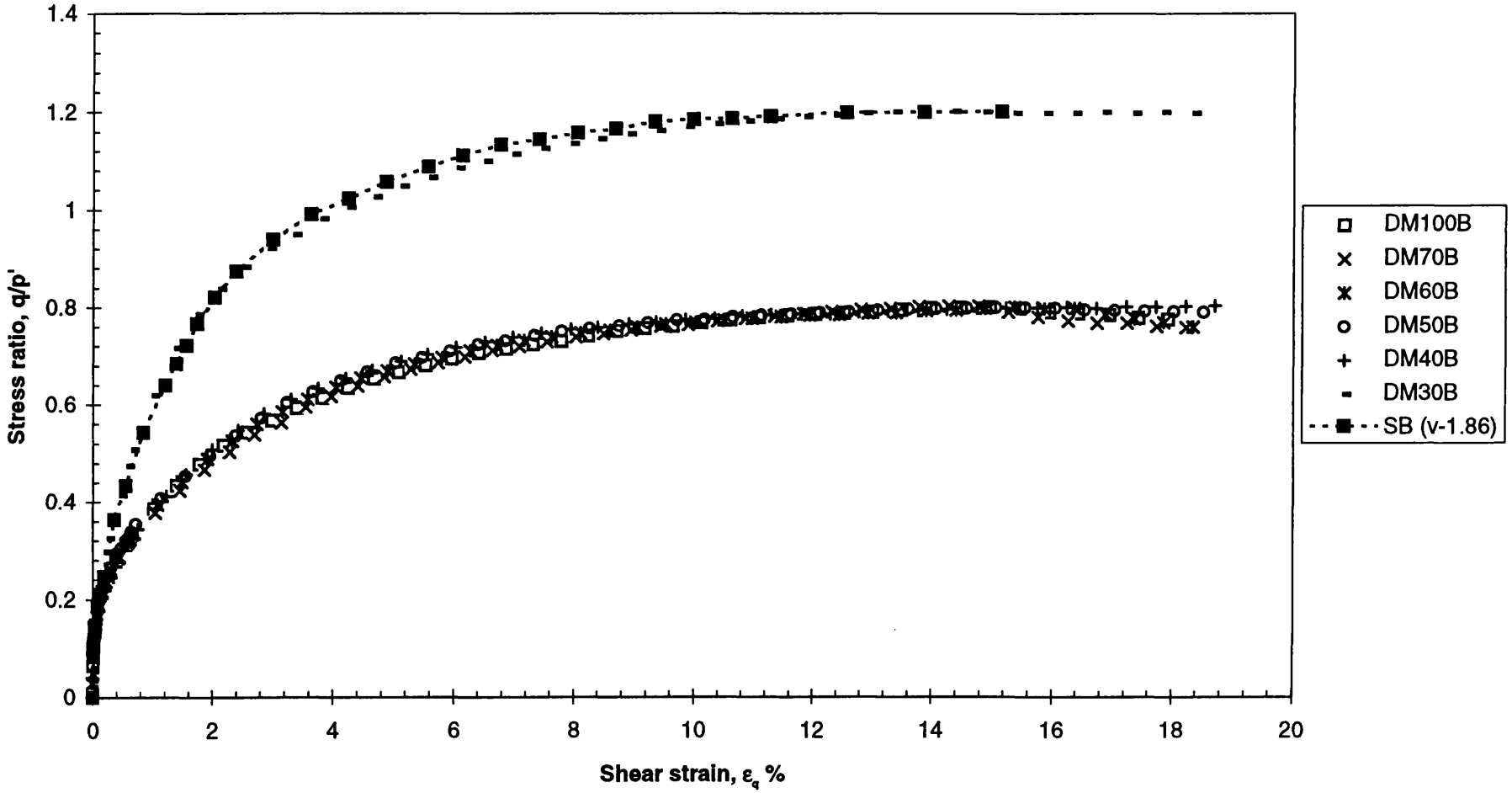

Fig.5.26b Drained stress ratio:shear strain relations at OCR 1.33

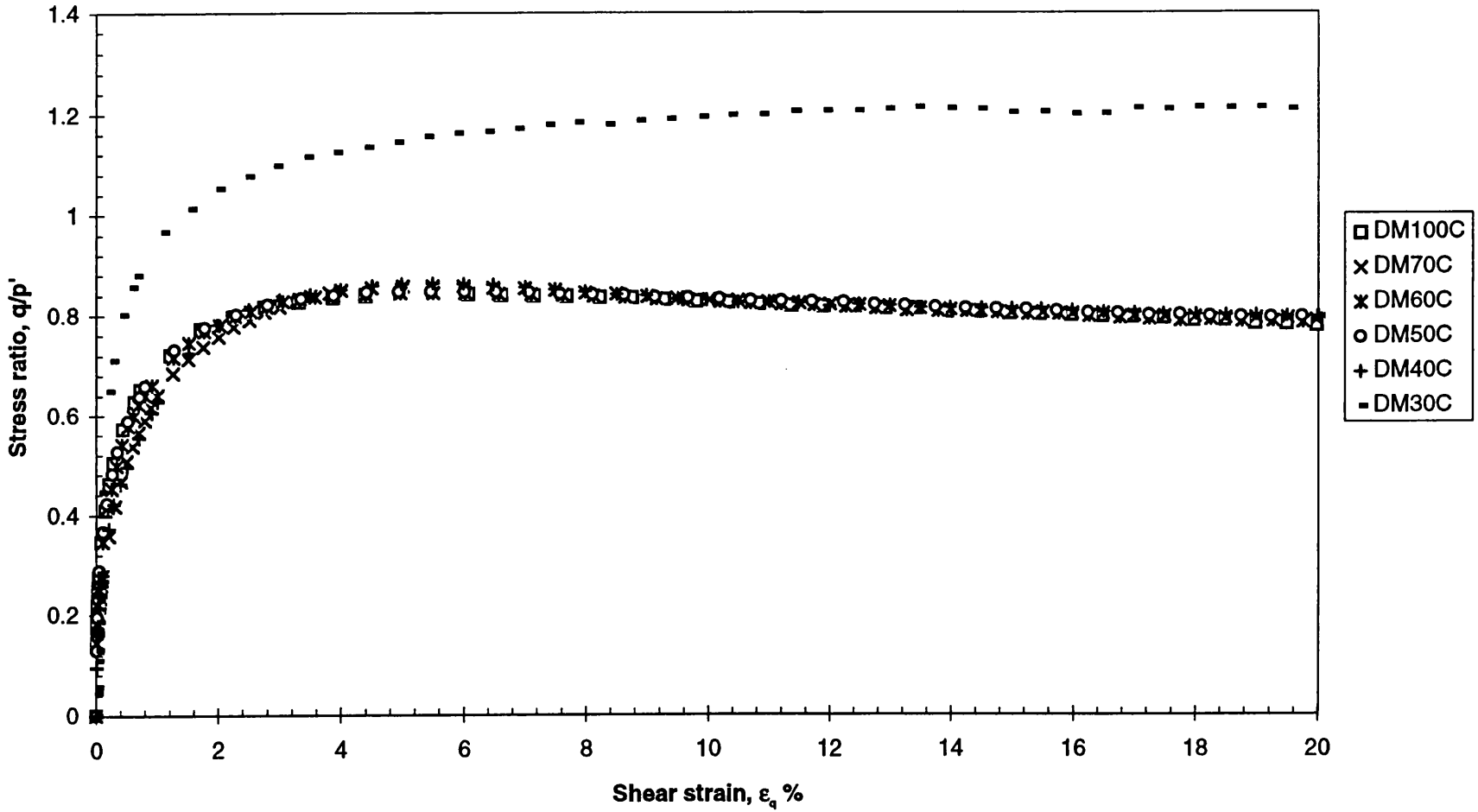

Fig.5.26c Drained stress ratio : shear strain relations at OCR 4

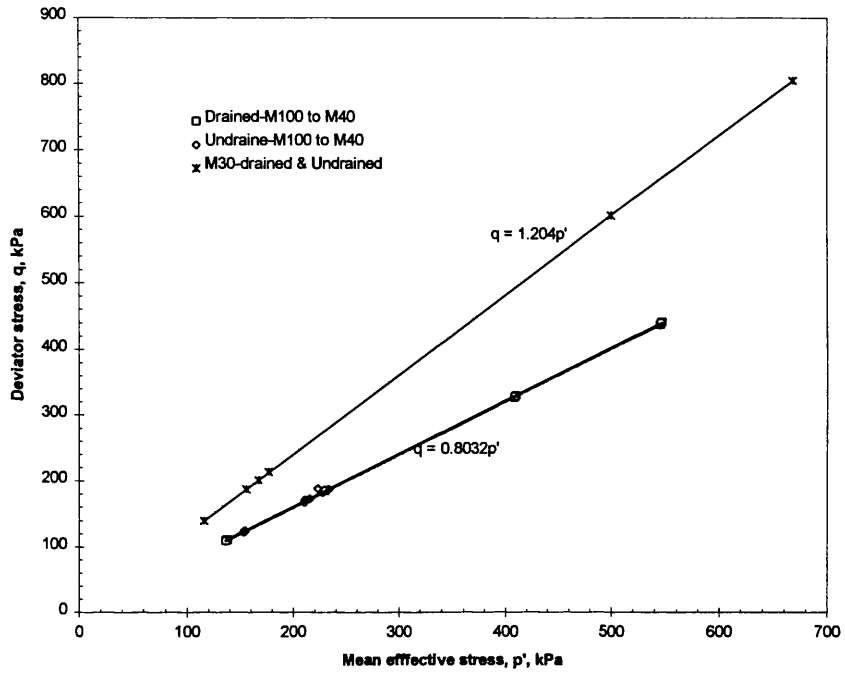

Fig.5.27 Critical state data (Failure data) in stress plane

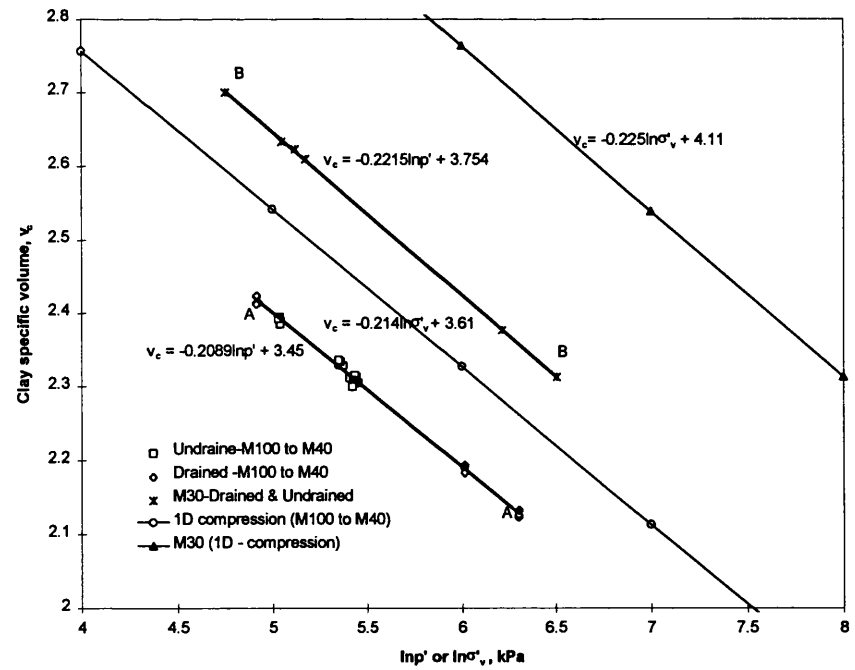

Fig.5.28 Critical state data in compression plane

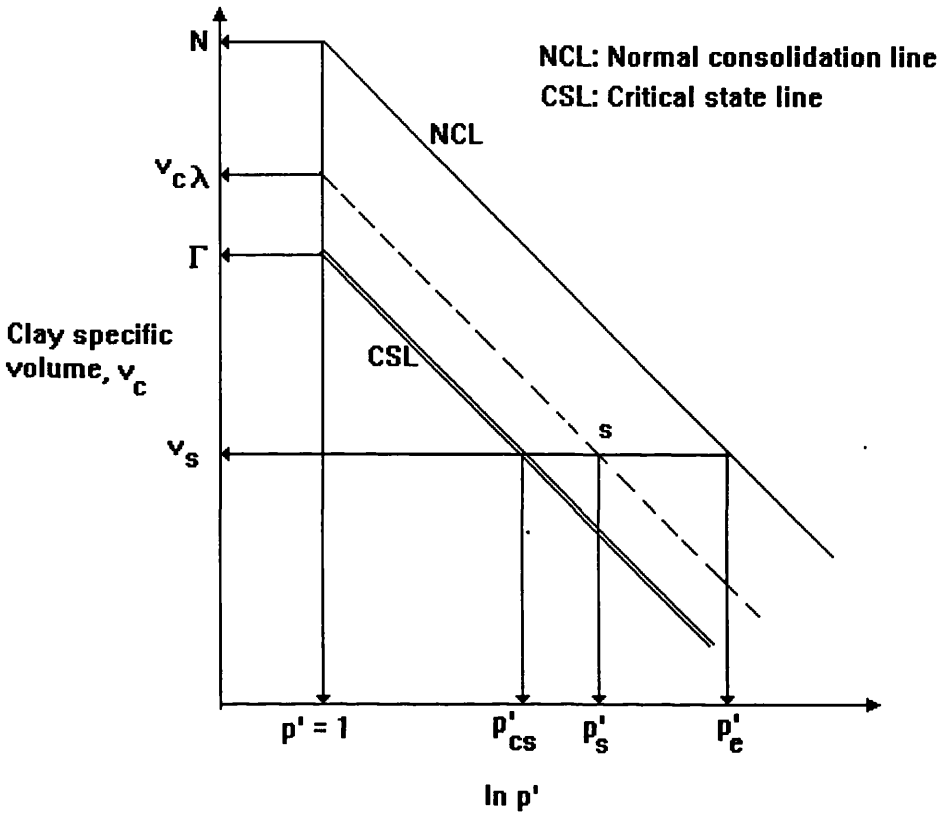

Fig.5.29 Parameters for normalising test results

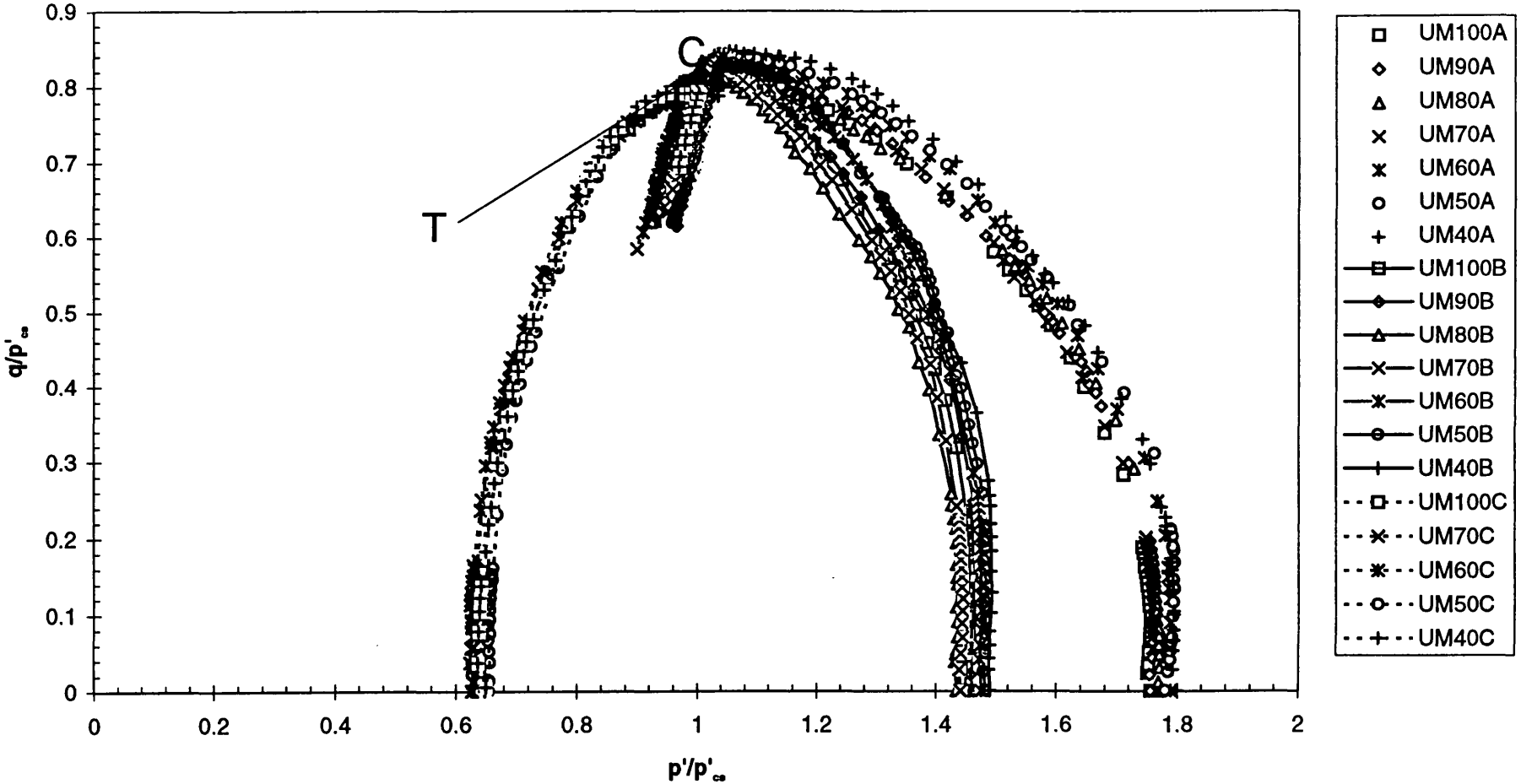

Fig.5.30a Undrained paths in non-dimensional effective stress space

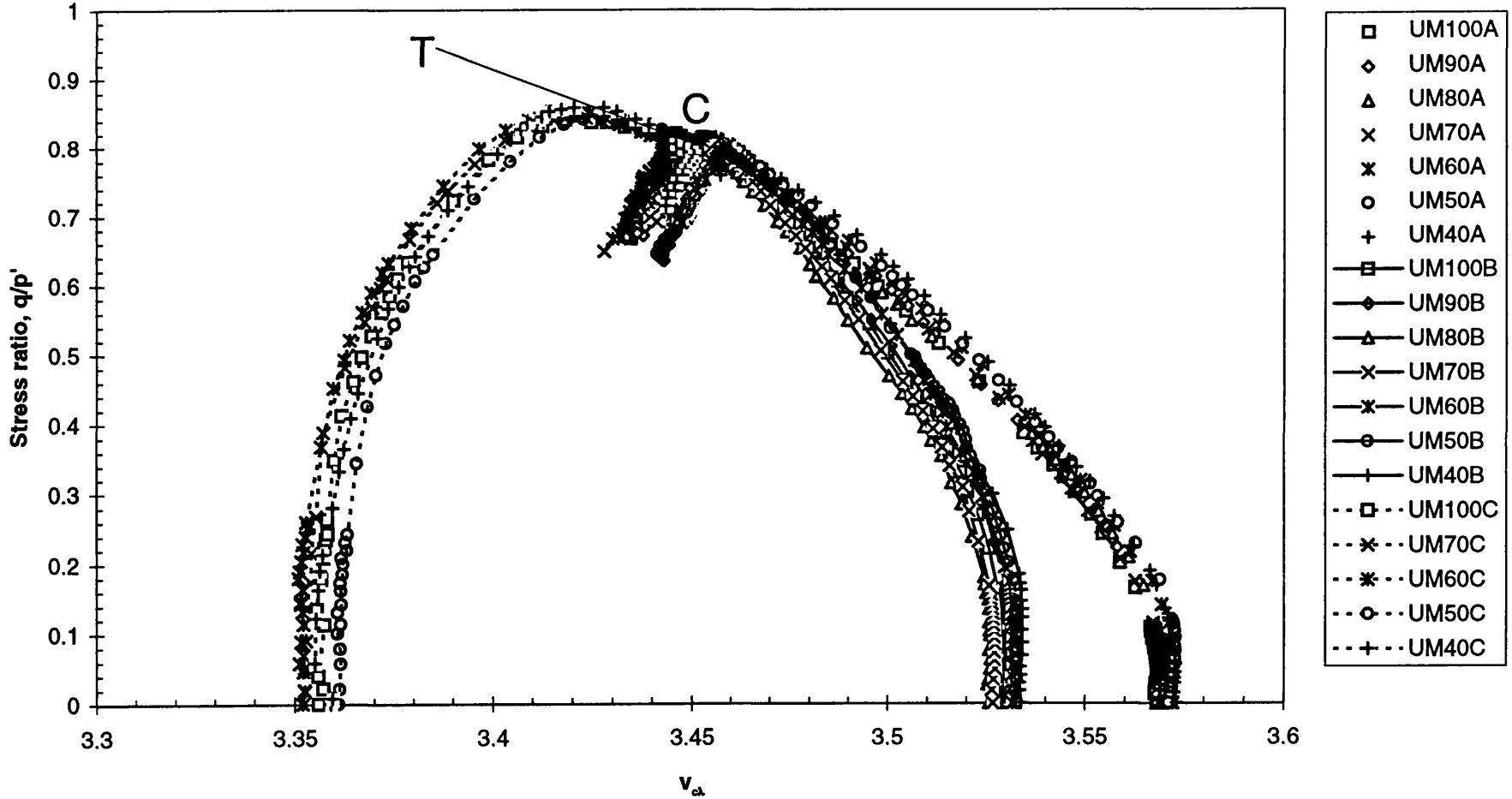

Fig.5.30b Undrained paths in terms of normalised volume and stress ratio

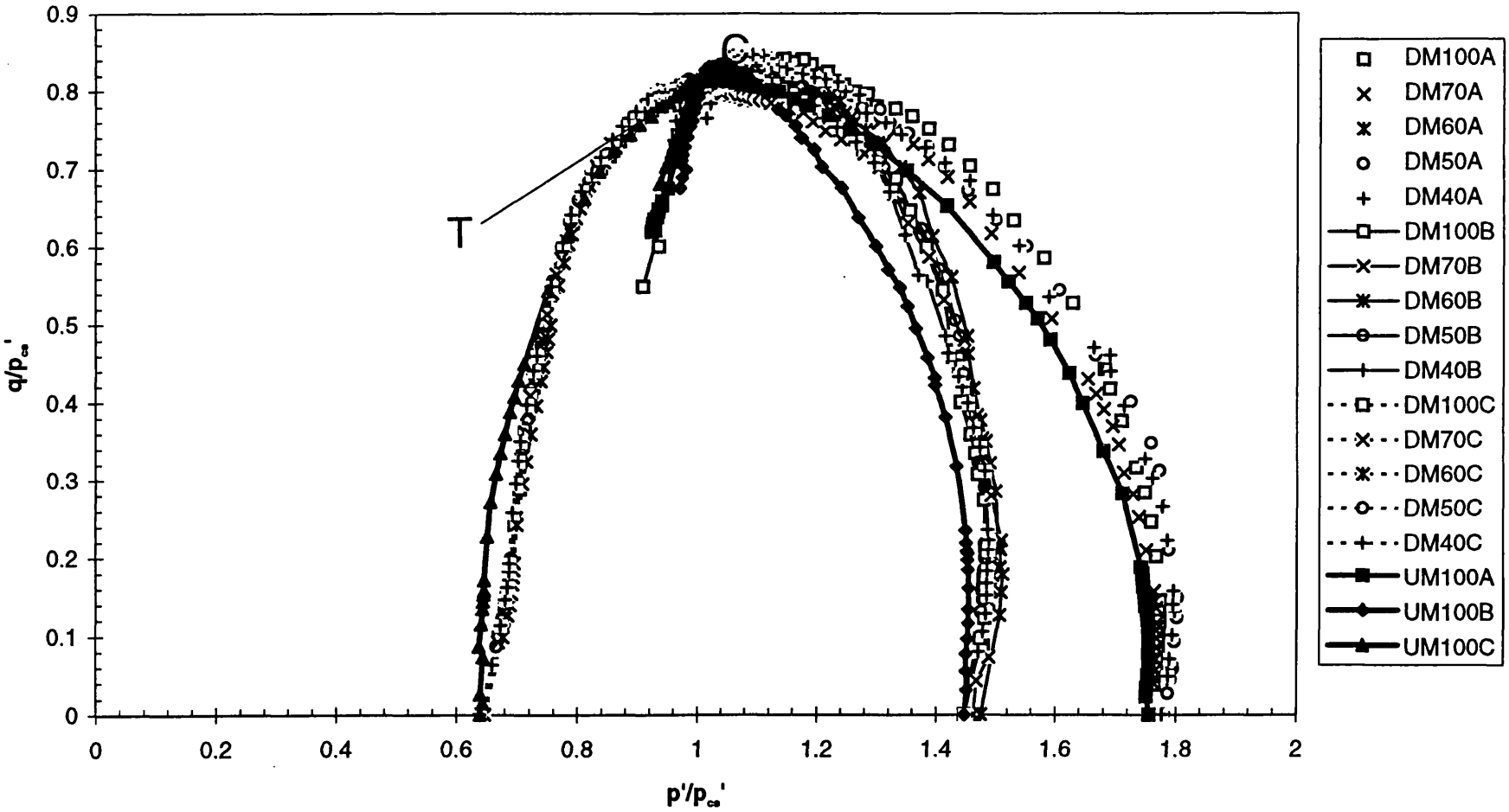

Fig.5.31a Drained paths in non-dimensional effective stress space

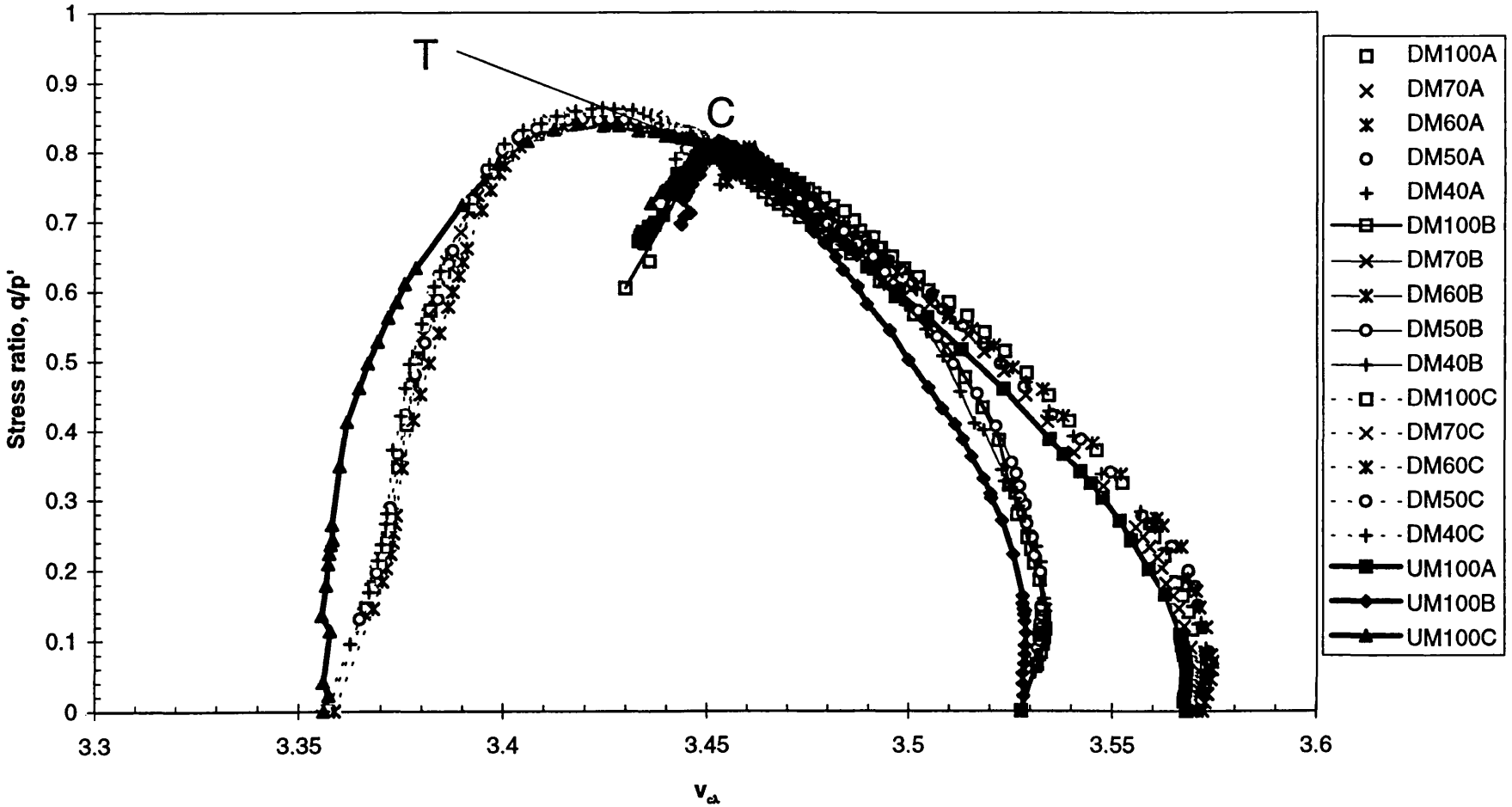

Fig.5.31b Drained paths in terms of normalised volume and stress ratio

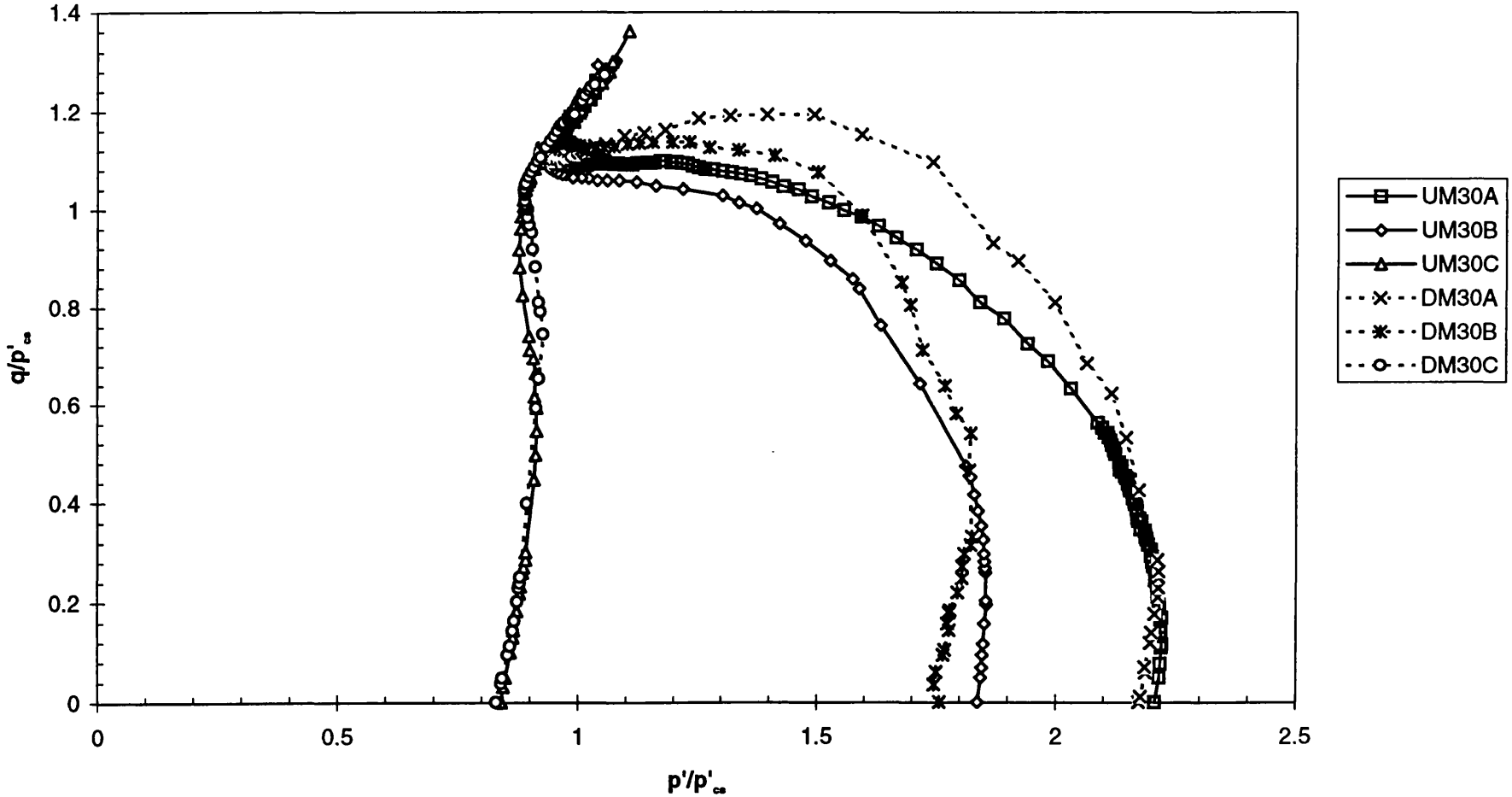

Fig.5.32a Undrained and drained paths of mixture with 30% clay - non dimensional effective stress space

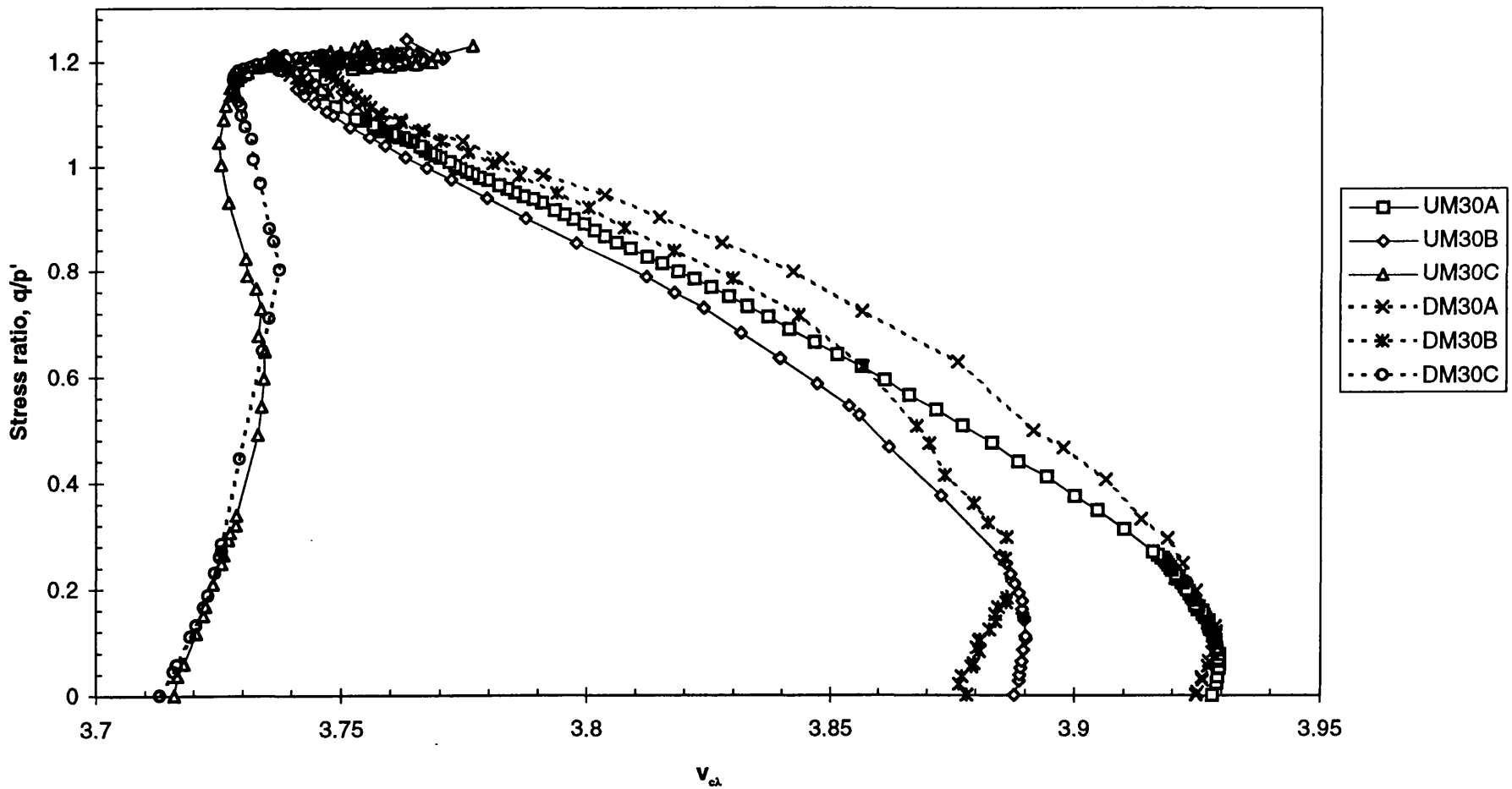

Fig.5.32b Undrained and drained paths of mixture with 30% clay - normalised volume and stress ratio

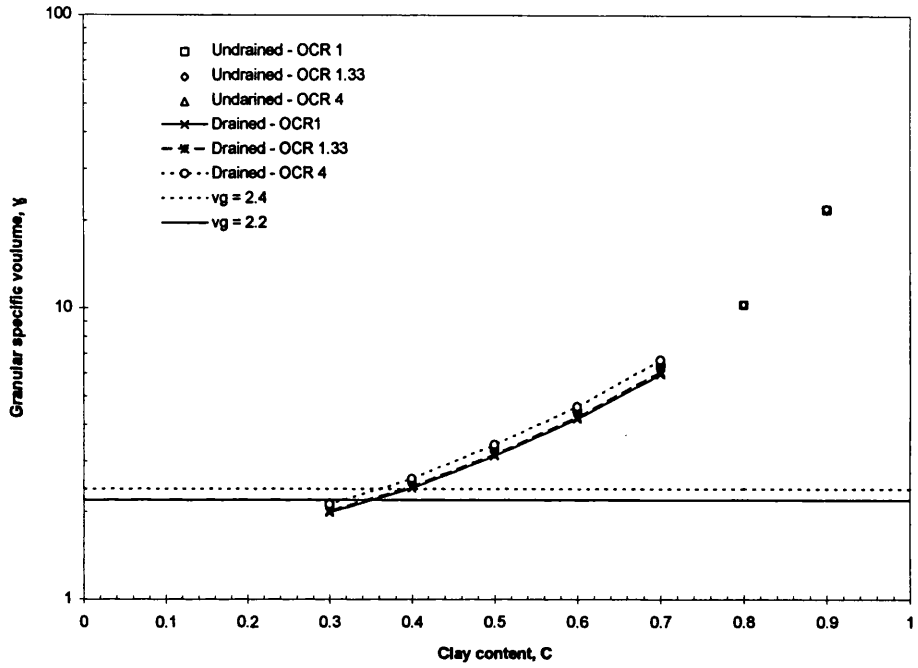

Fig.5.33 Variation of granular specific volume at critical state with clay content

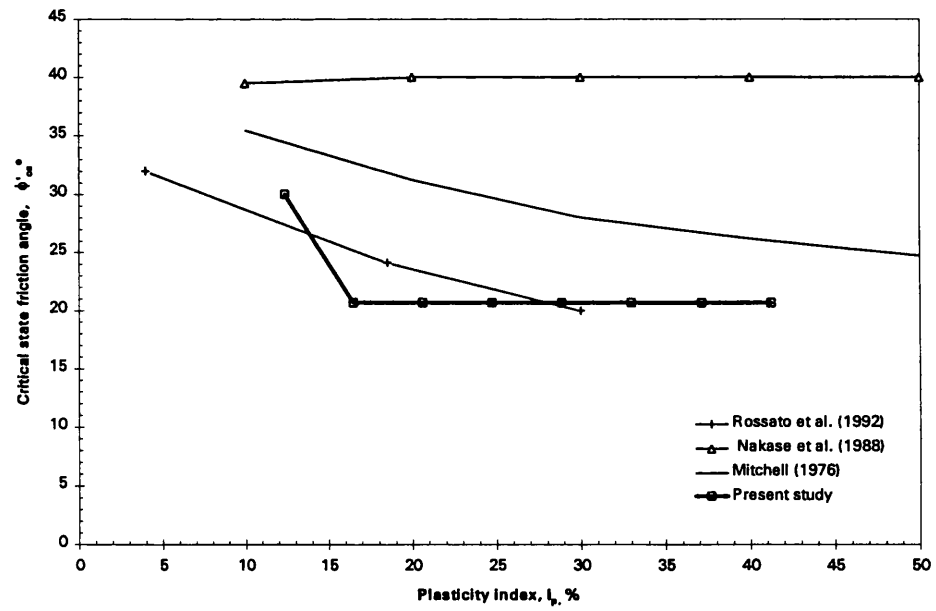

Fig.5.34 Critical state friction angle versus plasticity index

CHAPTER 6

NUMERICAL STUDIES : SHEAR BEHAVIOUR

This chapter describes finite element and theoretical analyses of shear behaviour of clay/sand mixtures. The analyses presented in this chapter are particularly relevant to the experimental work described in Chapter 5, because the primary objective of the experimental programme was to study the extent to which the clay matrix controls the undrained and drained shear behaviour of the mixtures. In this chapter numerical predictions were performed for a clay/sand composite model with an aim to throw light on the patterns of behaviour observed in triaxial experimental investigations. The discussion here on finite element analysis will be restricted to shear behaviour of normally consolidated mixtures. Theoretical predictions are attempted only for undrained normally consolidated material.

In the previous chapters the experimental mechanical behaviour of clay/sand mixtures was presented in terms of the clay content (see Eq.1.2) of the mixture. In order to carry out numerical experimentation, granular volume fraction f (i.e. the proportion of the total mixture volume that is taken up by sand) is a useful parameter and from Fig.1.1 this is

$$f = \frac{V_g}{V} \tag{6.1}$$

From Eq.1.7

$$f = \frac{1}{v_g} \tag{6.2}$$

Where v_g is granular specific volume.

In terms of void ratio(e) and clay content (C) and from Eq.1.7:

$$f = \frac{1-C}{1+e} \tag{6.3}$$

The present chapter is mainly concerned with normally consolidated clay/sand mixtures and from the initial granular specific volume of the mixtures compressed to 400 kPa f can be calculated using Eq.6.1. Table 6.1 presents the

relation between clay content(C) and granular volume fraction (f) employed in the present study.

In this chapter section 6.1 presents finite element analyses and section 6.2 discuses theoretical analyses of a particle reinforced composite. The results of these analyses are discussed in section 6.3 in which they are compared with the experimentally observed patterns.

6.1 FINITE ELEMENT ANALYSES

In order to predict the undrained and drained stress:strain response of clay/sand mixtures, a unit cell model has been used in finite element analysis. The idea behind unit cell modelling is the assumption that the overall response of clay/sand composite can be predicted by investigating a small repeating unit cell. The unit cell models are quite successful in finite element predictions of behaviour of composites such as shear behaviour of unidirectional composites (Nedele and Wisnom 1994a) and elastic response of particulate composites (Shen et al. 1994).

Evaluation of overall properties of the unit cell must be performed for a specific clay/sand model that approximates the microstructural geometry of the actual mixture. Although any periodic distribution of sand particles in a clay matrix can be considered, in this study a cubical array is assumed as shown in Fig.6.1. The cubical array has a unit cell with a sand particle in the middle of a square with sides of length 2units. Because of the symmetry of the unit cell, only one quarter of the unit cell has to be analysed. A typical finite element mesh is shown in Fig.6.2. The mesh consists of 116 cubic strain triangle elements. Each element has 16 integration points at which stresses and strains are calculated. Meshes based on Fig.6.2 corresponding to different granular volume fractions (Table 6.1) were used for the present study to represents clay contents from 0 to 70%. The finite element analysis of unit cell model was carried out in axisymmetric mode using the finite element program CRISP - double precision version (Britto and Gunn 1987).

6.1.1 Constitutive properties of constituents

In the analyses the sand particle is assumed to be very stiff linear elastic, isotropic material whilst the clay matrix is modelled as a non-linear elasto-plastic material. The interface between clay and sand was assumed to be perfectly rough therefore all the stress components are transferred from one material to the other. The following properties were assigned to sand and clay:

Sand particle: Young's modulus of 94 GPa (Lambe and Whitman 1979 - value for quartz mineral) and Poisson's ratio of $\nu = 0.495$.

The clay matrix was modelled as modified Cam clay: the slope of critical state line in v-ln p' space $\lambda = 0.21$ (Fig.5.28), the slope of the one-dimensional swelling line in v-lnσ'_v space $\kappa = 0.047$ (from Fig.3.20), the void ratio on the critical state line at p' = 1 kPa, $\Gamma = 2.45$ (from Fig.5.28), the slope of the critical state line in (q - p') space M = 0.8 (Fig.5.27), Poisson's ratio $\nu = 0.3$ (Al Tabbaa 1987).

To apply the modified Cam clay model it is also necessary to specify the initial stress state and the previous maximum isotropic consolidation pressure, p'_c. In the present analysis the initial stress state is assumed isotropic with mean effective stress p' and p'_c both equal to 400 kPa.

6.1.2 Boundary conditions

The analyses presented in this study attempt to match the boundary conditions of undrained and drained triaxial compression tests. Since a typical sample of clay sand mixture is assumed to be much larger than a unit cell the dimensions of neither the unit cell nor the finite element mesh used are of any consequence in the analysis. A strain controlled analysis is considered with 75 increments leading to a total axial strain of 5%. In Fig.6.2 AB is restricted to move horizontally and AC is restricted to move vertically. CD is displaced vertically downwards to simulate a strain controlled test. DB is laterally loaded to 400 kPa to simulate the stress controlled lateral boundary of the triaxial sample.

6.2 ANALYSIS OF PARTICLE REINFORCED ELASTIC-PLASTIC MATERIAL

Tandon and Weng (1988) considered a particle reinforced composite consisting of a volume fraction f of spherical inclusions with shear modulus G_i in a matrix with elastic-plastic properties. The elastic shear modulus of the matrix is G_m. They proposed a method for derivation of the stress:strain curve of the composite based on the secant stiffness of the matrix. The procedure seems to be as follows.

The stress:strain behaviour of the matrix is a function of (σ'_m, ε_{qm}), where σ'_m is equivalent stress for the matrix and ε_{qm} is shear strain of the matrix.

For a given value of ε_{qm} in the matrix, a composite stress (σ'_c) is calculated according to Eq.6.4

$$\sigma'_c = \frac{1}{b_m} f(\sigma'_m, \varepsilon_{qm}) \tag{6.4}$$

where

$$b_m = \frac{\beta_m (G_i - G_m) + G_m}{[f + (1-f)\beta_m](G_i - G_m) + G_m} \tag{6.5}$$

$$\beta_m = \frac{2(4 - 5\nu_m)}{15(1 - \nu_m)} \tag{6.6}$$

where ν_m is secant matrix Poisson's ratio.
$1/b_m$ and β_m are stress factor and matrix material factor respectively.
The composite modulus is modified as

$$\frac{G_c}{G_m} = 1 + \frac{f(G_i - G_m)}{(1-f)\beta_m (G_i - G_m) + G_m} \tag{6.7}$$

where G_c / G_m is stiffness factor.
The composite shear strain (ε_{qc}) is modified from the matrix strain from the ratio of the stress and stiffness ratio as

$$\varepsilon_{qc} = (1-f)\varepsilon_{qm} + \left[1 - \frac{G_m}{G_c} - \frac{f(G_i - G_m)}{[f + (1-f)\beta_m](G_i - G_m) + G_m}\right] \frac{\sigma'_c}{2G_m} \tag{6.8}$$

For infinitely stiff inclusions $G_i/G_m = \infty$ and for undrained incompressible deformation $\nu_m = 0.5$, then $\beta_m = 0.4$. The values of stress factor and stiffness factor as a function of granular volume fractions employed in this study (Table 6.1) are shown in Table 6.2. The composite shear strain (ε_{qc}) for $G_i/G_m = \infty$ from Eq.6.8 will simple be

$$\varepsilon_{qc} = (1-f)\varepsilon_{qm} \tag{6.9}$$

These results appear to be completely independent of the stress:strain response of the matrix -though that will control the current secant stiffness of the matrix and the composite.

6.2.1 Stress:strain relation for clay matrix

In the present study a hyperbolic relation (Konder 1963) was used for simulation of the stress:strain curve for clay matrix. Fig.6.3 illustrates such a relation, which can be expressed as:

$$q = \frac{\varepsilon_q}{a + b\varepsilon_q} \tag{6.10}$$

where q and ε_q represent deviator stress and shear strain respectively. If the stress:strain relation is plotted in terms of ε_q/q and ε_q then the hyperbolic expression leads to a straight line (Fig.6.4) and conversely, a plot with the axes ε_q / q and ε_q can be used to check whether the data from a test do fit a hyperbolic relationship or to find the parameters a and b from the test data.

Fig.6.5 shows the transformed plot for the normally consolidated undrained clay test results illustrated in Fig.5.10a up to the peak value of q. Regression analysis on these data give the value of intercept a = 1.845E-03, slope b = 5.177E-03. These values are assigned for clay matrix in the theoretical analysis of undrained shear response of clay/sand the composite.

6.3 RESULTS AND DISCUSSION

In this section comparisons will be made between certain features of the experimental results described in Chapter 5 and predictions made by:

- finite element predictions (results indicated by abbreviation FE, number following FE indicates clay content, U = undrained case; D = drained case); and
- theoretical predictions (results indicated by abbreviation TH, number following TH indicates clay content, only undrained case).

6.3.1 Finite element predictions

The finite element data are interpreted in terms of equivalent average states of stress and strain in the unit cell. The average stress:strain behaviour can be determined from the externally observed loads and externally applied specimen deformations in Fig.6.2. The overall stress:strain behaviour of unit cell was reduced using the following assumptions:

$$\text{Axial strain} = \varepsilon_a = \frac{\text{Applied displacement at the top boundary}}{\text{Initial height of the unit cell}}$$

$$\text{Axial stress} = \sigma_a = \frac{\text{Total nodal force at the top boundary}}{\text{Initial area of the unit cell}}$$

$$\text{Radial stress} = \sigma_r = \text{Applied stress}$$

Pore pressure and volumetric strains have no meaning in solid sand and average values were reduced at the top boundary. The unit cell that is analysed in the finite element calculation is of course not deforming homogeneously and the average values were calculated only during post processing of undrained and drained results.

6.3.1.1 Undrained case

The predicted undrained stress:strain responses of the unit cell clay/sand model are summarised in Fig.6.6 where the average deviator stress q, is plotted against the shear strain. Corresponding pore pressure and strain relations are shown in Fig.6.7. The effective stress paths of the unit cell model are shown in Fig.6.8. The values of secant shear stiffness for the data in Fig.6.6 deduced from Eq.5.21 are shown in Fig.6.9 plotted against the logarithm of shear strain.

6.3.1.2 Drained case

The stress:strain predictions for the drained unit cell model are shown in Fig.6.10 and corresponding volumetric strain relations are presented in Fig.6.11. The values of secant shear stiffness calculated from Fig.6.10 are shown in Fig.6.12.

6.3.2 Theoretical predictions of undrained shear response

Theoretical stress:strain predictions for undrained case are given in Fig.6.13 for different clay contents (i.e. granular volume fractions) presented in Table6.2. The values of secant shear stiffness for the above data deduced from Eq.5.21 are summarised in Fig.6.14 plotted against the logarithm of shear strain.

6.3.3 Comparison with experimental data

To facilitate a comparison between numerical results and experimental results, the results presented in this section were normalised with respect to the corresponding clay values.

6.3.3.1 Undrained response

Comparison between the finite element and theoretical predictions (Fig.6.6 & 6.13) with the experimental results presented in Fig.5.10a shows that the deviator stress is increasing with decrease in clay content (i e with increase in f). A more direct comparison among the three is depicted in Fig.6.15 for normalised deviator stress at the shear strain of 5%. With decrease in clay content both finite element and theoretical predictions are showing increasing deviator

stress at fixed clay content while the experimental data are clearly showing the dominant influence of the clay phase down to 40% clay content. This can be explained by the greater influence of the sand on the behaviour of the numerical clay/sand model. It has to be noted that finite element results shows less drastic influence of sand than the theoretical analysis. Similar trends can be seen in normalised shear stiffness (G) data in Fig.6.16. The information in Fig.6.16 is derived from Figs.6.9, 6.14 & 5.16a showing shear stiffness responses of finite element, theoretical and experimental data respectively.

Comparison between finite element predictions of pore pressure response (Fig.6.7) and the experimental result in Fig.5.11a shows that the unit cell model predicts steady increase in pore pressure with decrease in clay content throughout the shearing. These high values of pore pressure are mainly due to the high values of deviator stress observed in Fig.6.6.

6.3.3.2 Drained response

The general stress:strain patterns (Fig.6.10) predicted by the drained unit cell model are not in agreement with experimentally observed patterns in Fig.5.18a. The finite element analysis predicts increase in deviator stress with decrease in clay content whereas experiment (Fig.5.18a) shows almost constant deviator stress up to clay content 40% in the mixture. This pattern is clearly evident in Fig.6.17 that compares predicted and experimentally observed normalised deviator stress at a shear strain = 2.5%.

The predicted shear stiffness in Fig.6.12 shows that the shear stiffness of the unit cell model is increasing throughout shearing with decrease in clay content in the model. One of the striking features of the experimental data in Fig.5.23a is that shear stiffness is almost constant down to clay content 40% in the mixture at a given shear strain. For comparison, predicted and experimental normalised G values at shear strain of 2.5% are plotted against clay content in the Fig.6.18. Normalised G values predicted from theoretical and FE undrained analyses are also shown in Fig.6.18.

The predicted volumetric strain response shown in Fig.6.11 is different from the experimentally observed behaviour shown in Fig.5.19a. The model predicts an increase in volumetric strain with decrease in clay content in the unit cell model and experimental observations shown in Fig.5.19a suggest decreases in volumetric strain with decrease in clay content up to 40% in the mixture. This is mainly because deviator stress is increasing in Fig.6.10 with decreasing clay content.

6.3.4 Discussion

The finite element predictions of drained and undrained tests and theoretical predictions of the undrained case have shown poor agreement with experimental results and show a steadily growing influence of sand fraction (even at high clay content) on the behaviour of the clay/sand composite. The widening gap between the finite element and the experimental behaviour can be explained as follows. The axial shear deformation and deviator stress (values reported by CRISP) in r direction (i.e. CD in Fig.6.2) change rapidly with radius because of the influence of the sand particle in the unit cell. For example actual axial strains and deviator stresses experienced by the element nodes along CD are plotted in Fig.6.19a & b respectively for undrained case at a given applied uniform axial strain of 5%. The thickness of the soft and therefore deformable clay matrix in the z direction (i.e. AC in Fig.6.2) is the controlling parameter for the unit cell shear stiffness. With increase of sand volume fraction the thickness of clay matrix in the deformation region is small and hence appears to show a high average stiffness for the mixture. The result is that the model shows high pore pressures in undrained tests and high volumetric strains in drained tests throughout shearing.

The lack of agreement between undrained theoretical and experimental response can probably be attributed to the fundamental development of the mixture theory on which the theoretical treatment is based. The theory was mainly developed for metallic or polymeric composites where the hard particles are important load-carrying members and contribute significant strength increase in the overall behaviour of composite even at low concentrations of hard particles. In simplest terms theoretical method is an estimate of the solution form guided only by the requirement of the dilute solution at one end of concentration scale and at the opposite end of the scale by the requirement that at $f = 1$, the effective properties should be identical with those of the inclusion phase. The theory introduces dependence on the concentration of the inclusion phase through the factor which is a function of $1/(1-f)$. In Chapter 5 experimental results on shear behaviour have clearly shown that the influence of sand particles is almost nothing for sand contents below about 70% and furthermore critical state theory suggests that shear behaviour of soil is dependent on both the void ratio and the mean effective stress (Muir Wood 1990) and it is very difficult to predict the response based on granular volume fraction f alone.

Table 6.1 Relations between clay content and granular volume fraction

Clay content C	Initial specific volume v	Initial granular specific volume v_g	Separation/diameter in close packed hexagonal model (from Eq.1.11)	f
1.00	2.31	∞	∞	0.00
0.90	2.17	21.75	2.52	0.05
0.80	2.05	10.25	1.96	0.10
0.70	1.91	6.37	1.68	0.16
0.60	1.79	4.47	1.49	0.22
0.50	1.66	3.31	1.35	0.30
0.40	1.53	2.54	1.23	0.39
0.30	1.48	2.12	1.16	0.47

Table 6.2 Values of stress and strain factors as a function of granular volume fraction

Clay content C	f	Stress factor 1/bm	Stiffness factor	Strain factor = 1-f
1.00	0.00	1.00	1.00	1.00
0.90	0.05	1.07	1.12	0.95
0.80	0.10	1.15	1.27	0.90
0.70	0.16	1.24	1.47	0.84
0.60	0.22	1.34	1.72	0.78
0.50	0.30	1.45	2.08	0.70
0.40	0.39	1.59	2.62	0.61
0.30	0.47	1.71	3.23	0.53

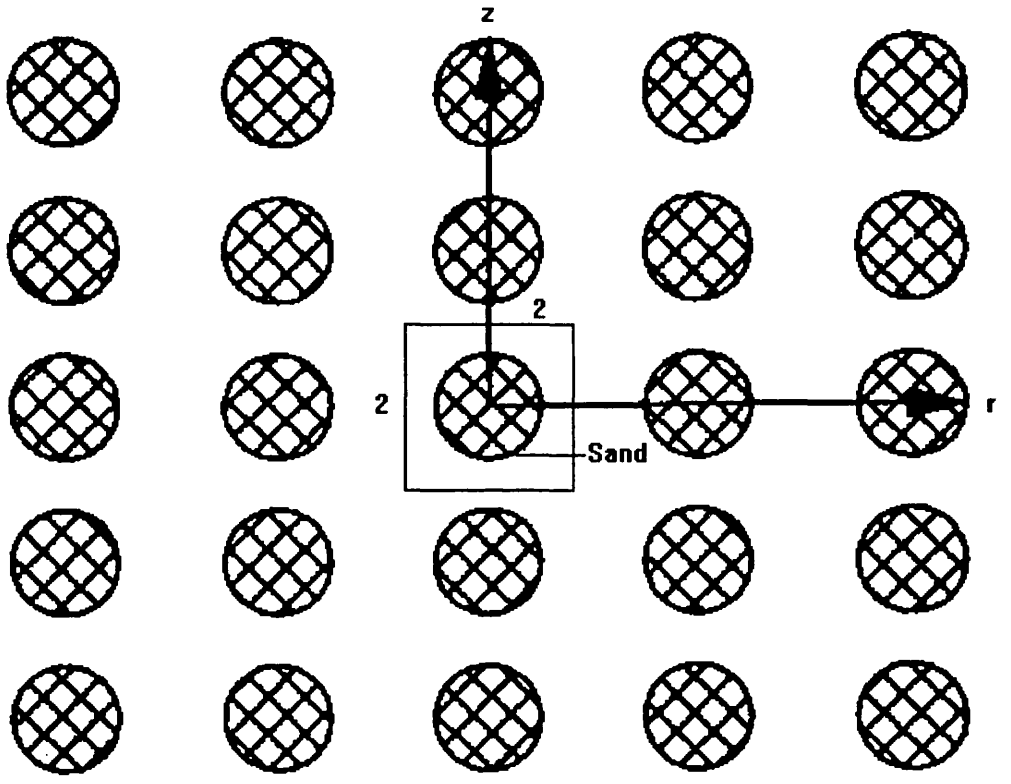

Fig.6.1 Unit cell with cubical array of sand

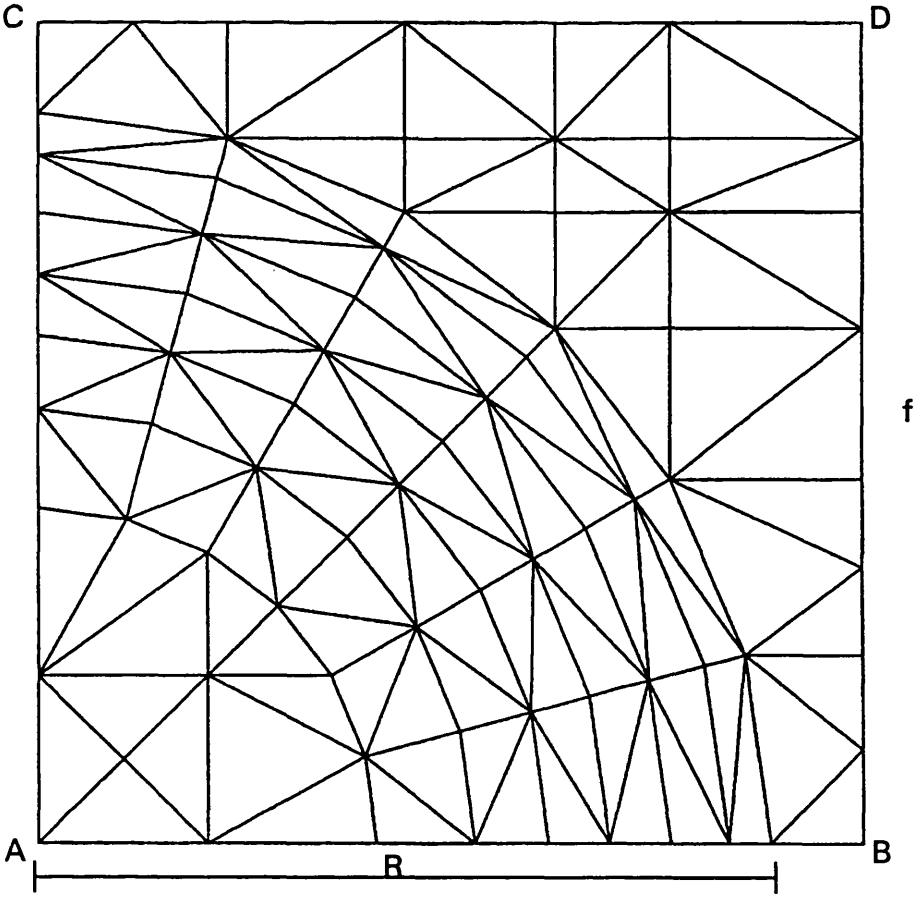

$$f = \frac{2R^3}{3}$$

Fig.6.2 Details of finite element mesh

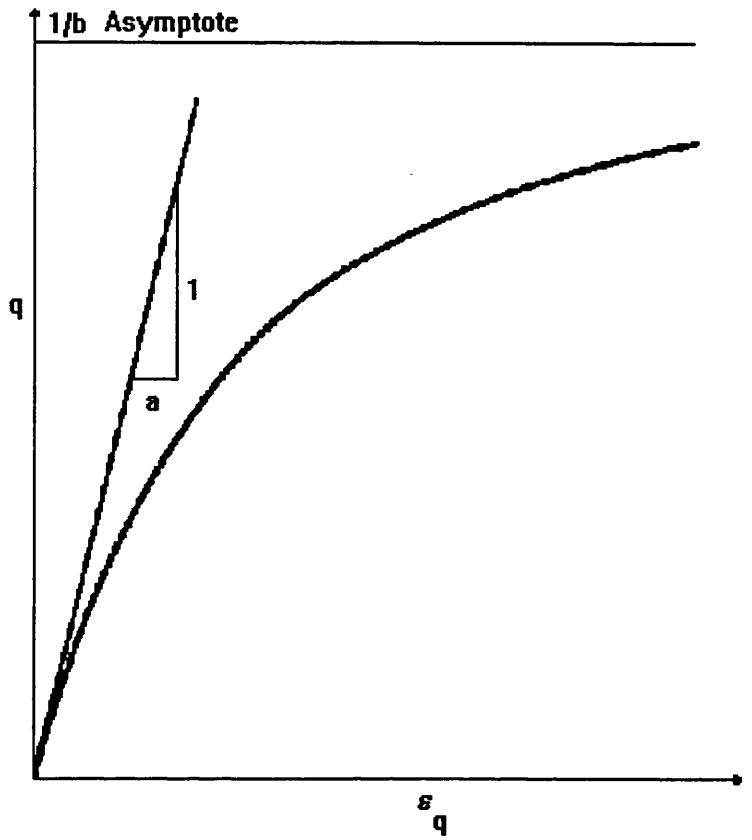

Fig.6.3 Hyperbolic model for non-linear soil

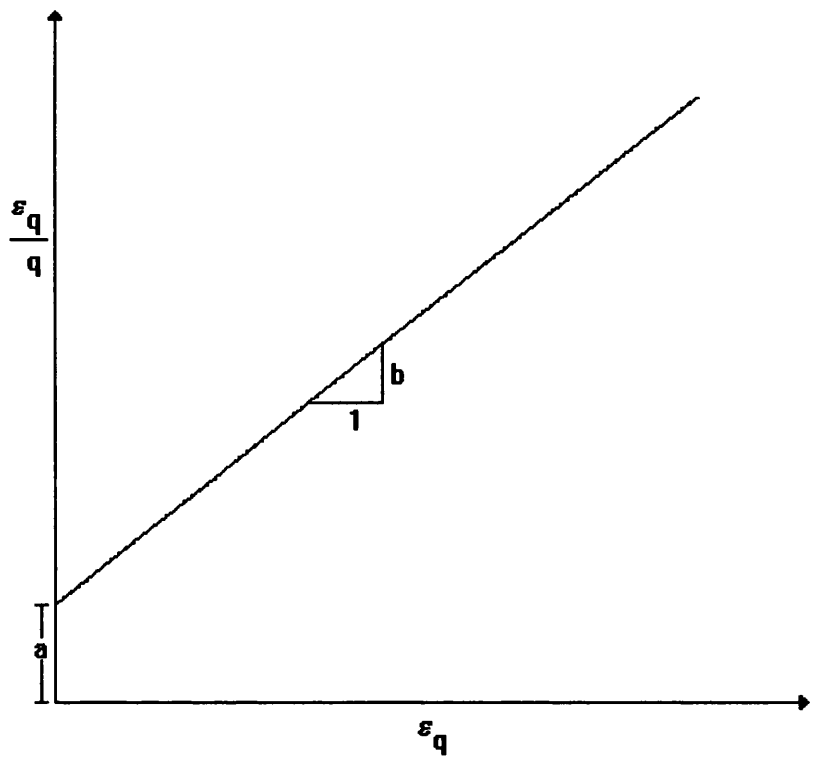

Fig.6.4 Hyperbolic model with transformed axes

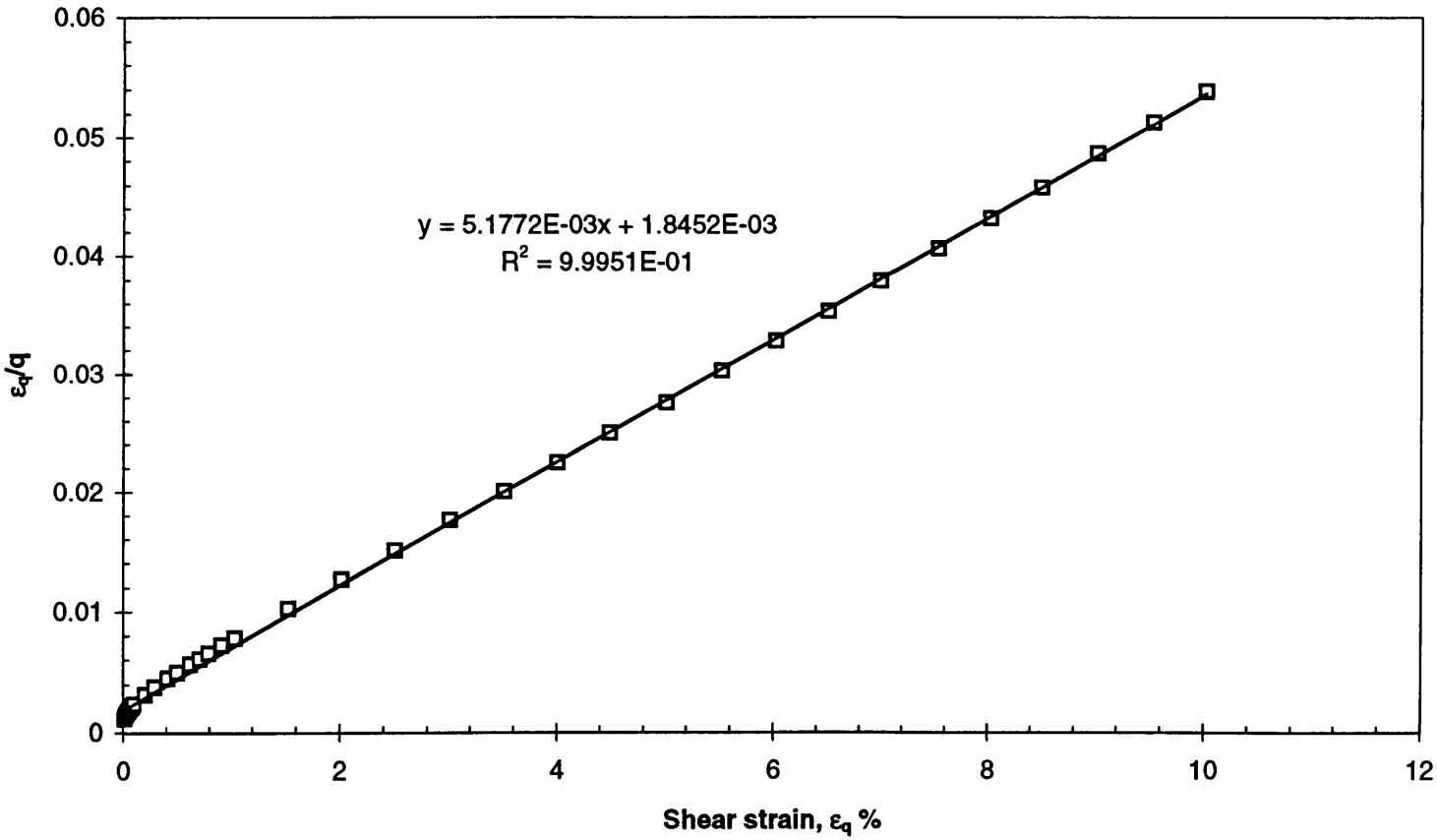

Fig.6.5 Transformed hyperbolic fit undrained normally consolidated clay

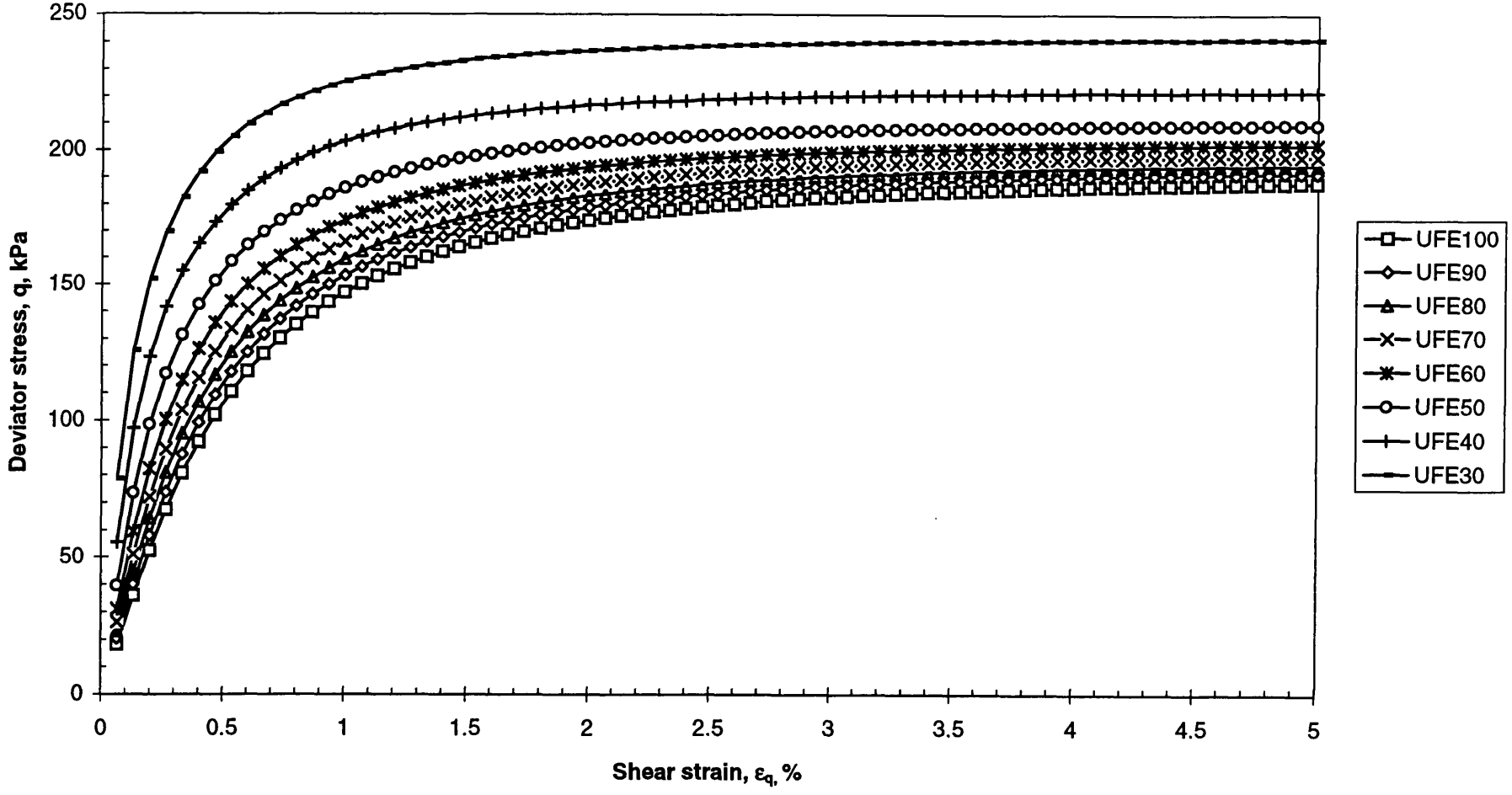

Fig.6.6 FE stress:strain predictions for undrained case

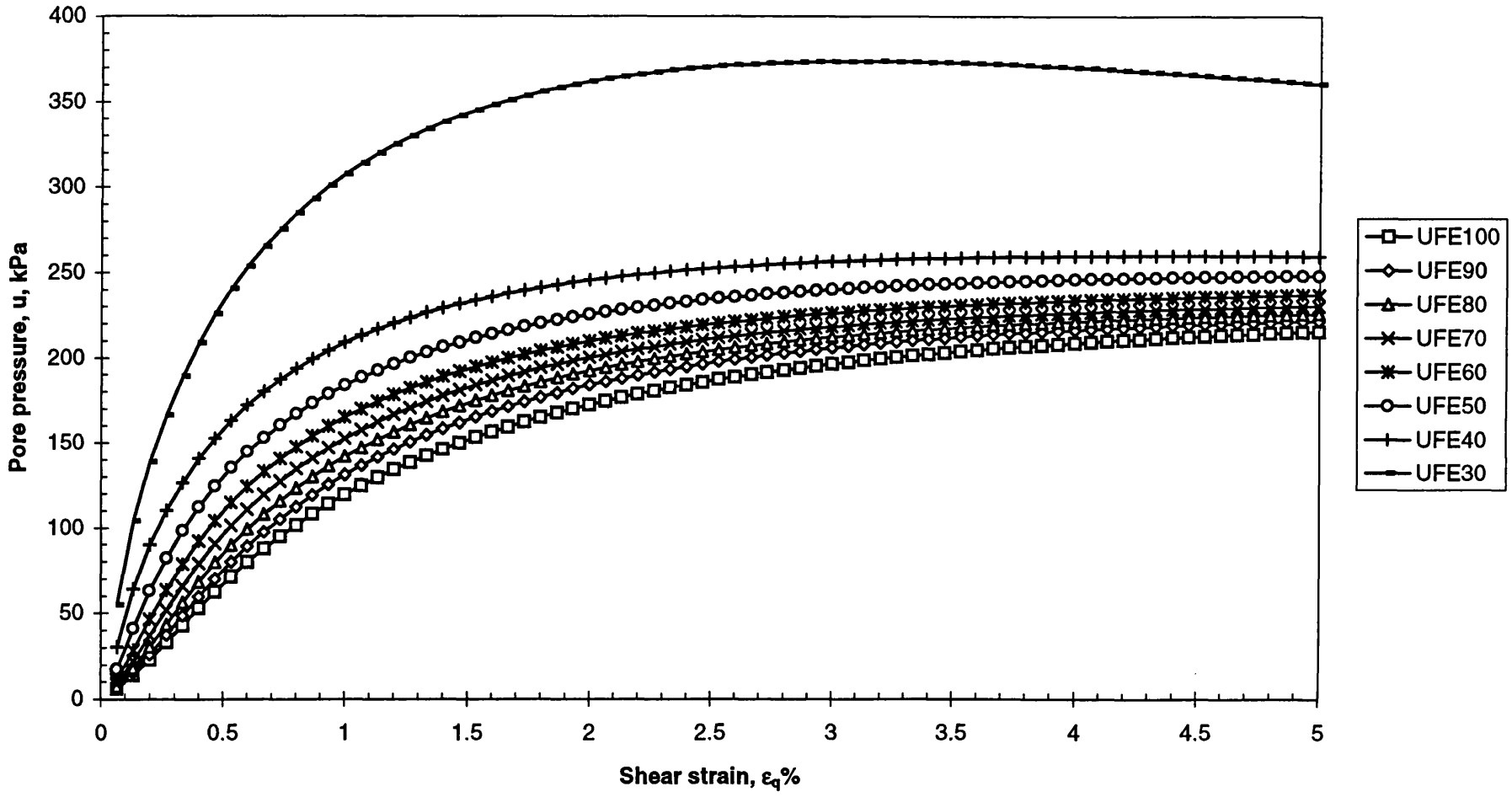

Fig.6.7 FE pore pressure and strain predictions for undrained case

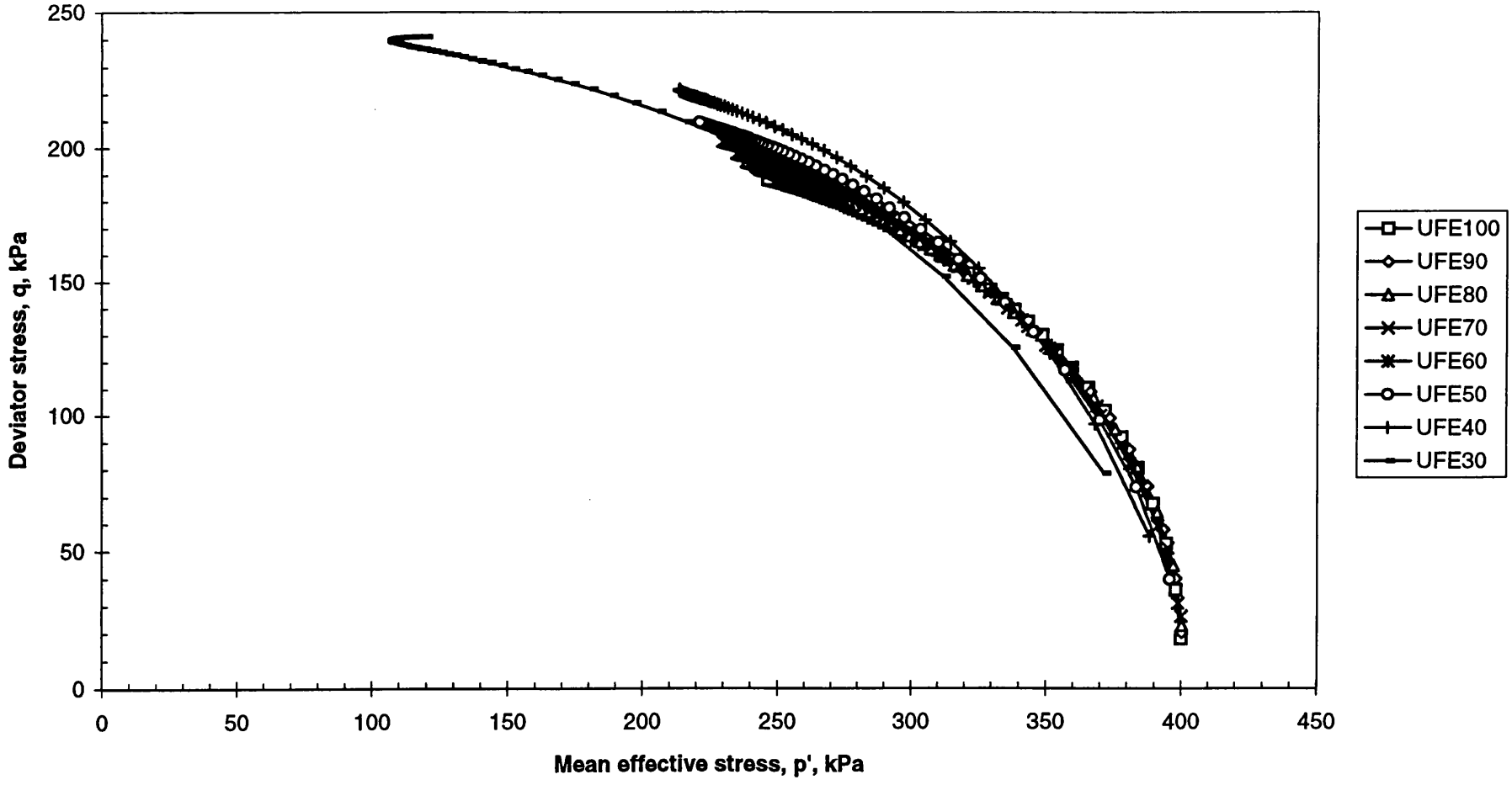

Fig.6.8 FE undrained effective stress path predictions

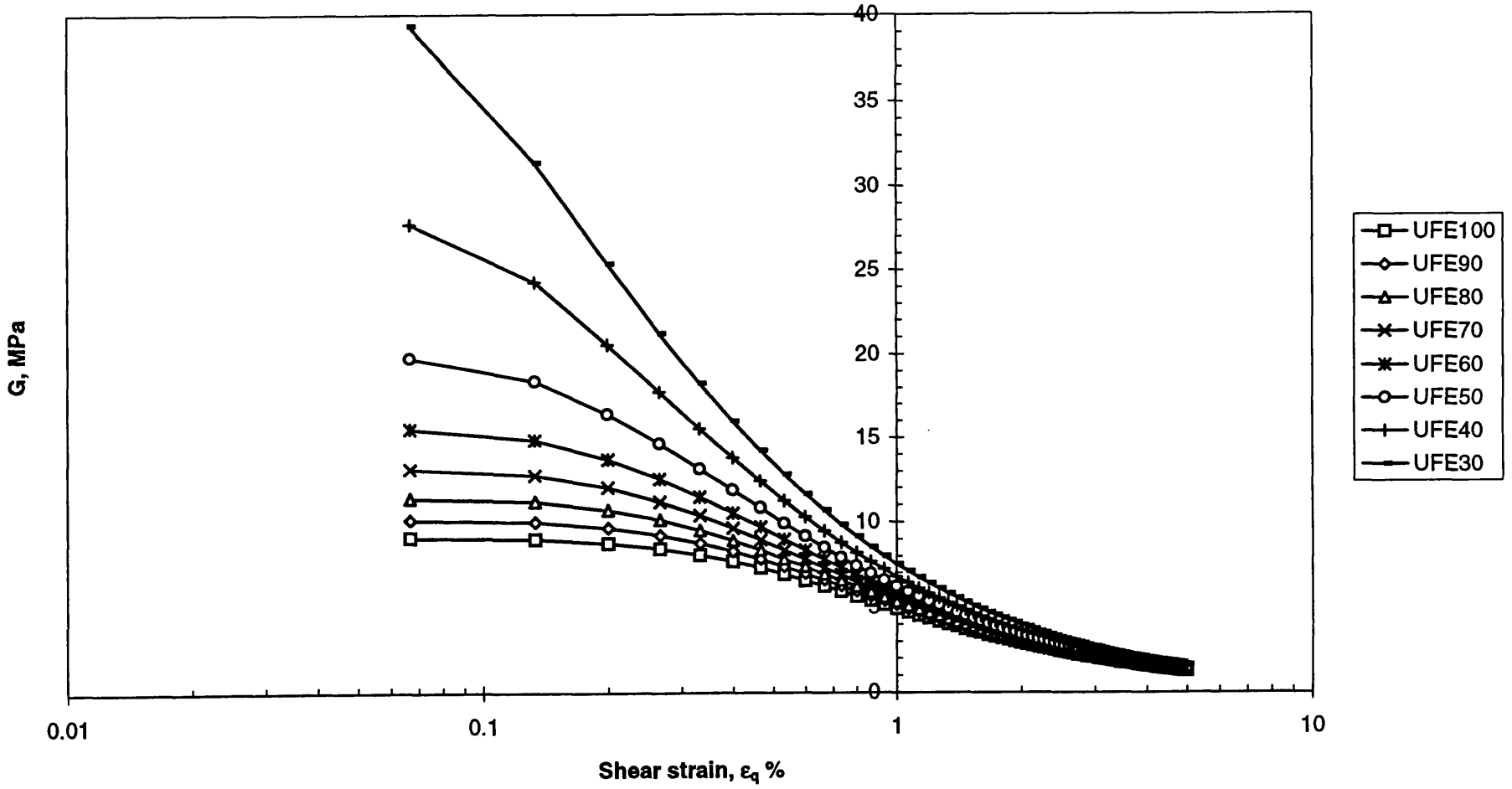

Fig.6.9 FE undrained shear stiffness response

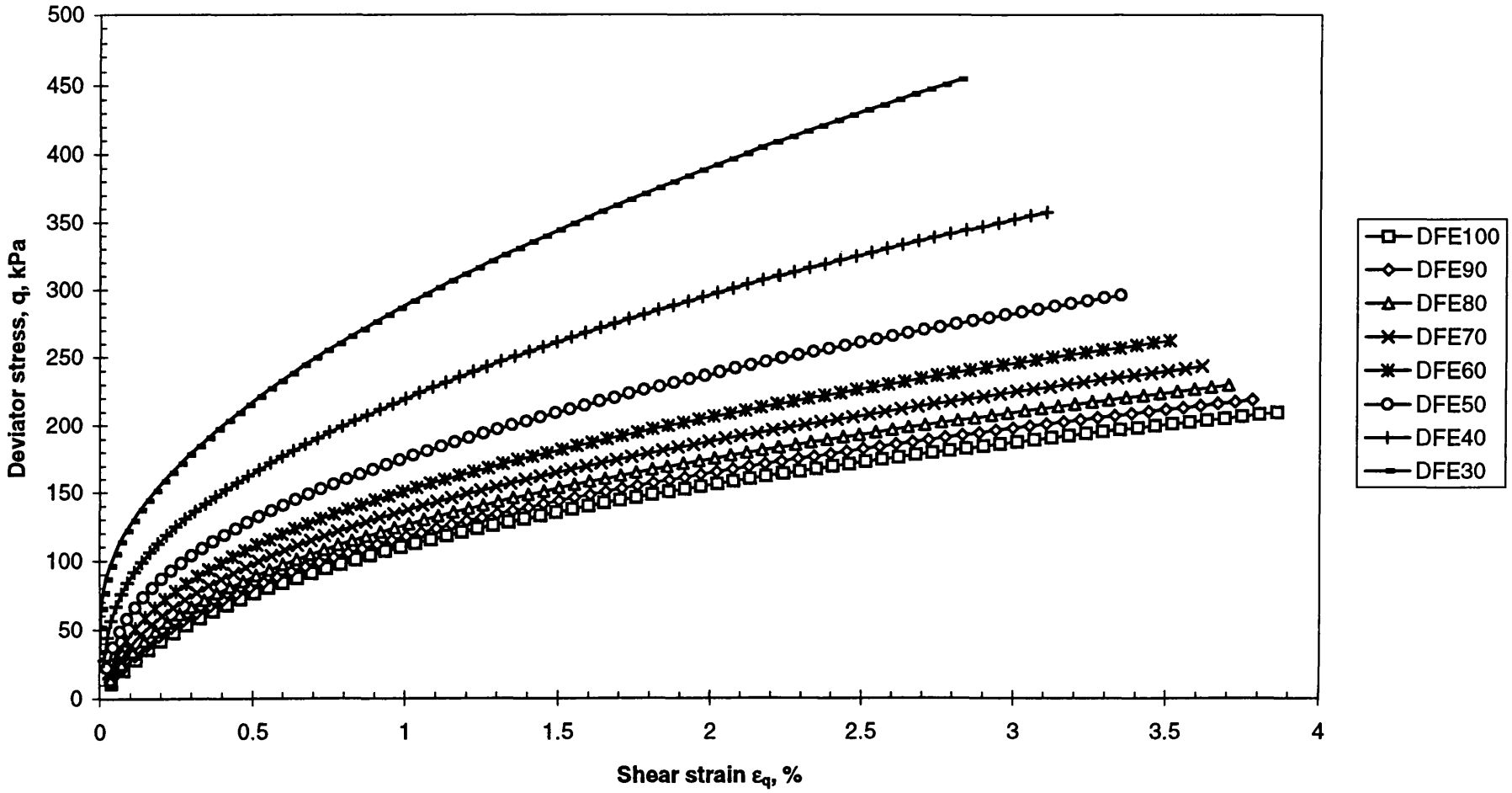

Fig.6.10 FE drained stress:strain response

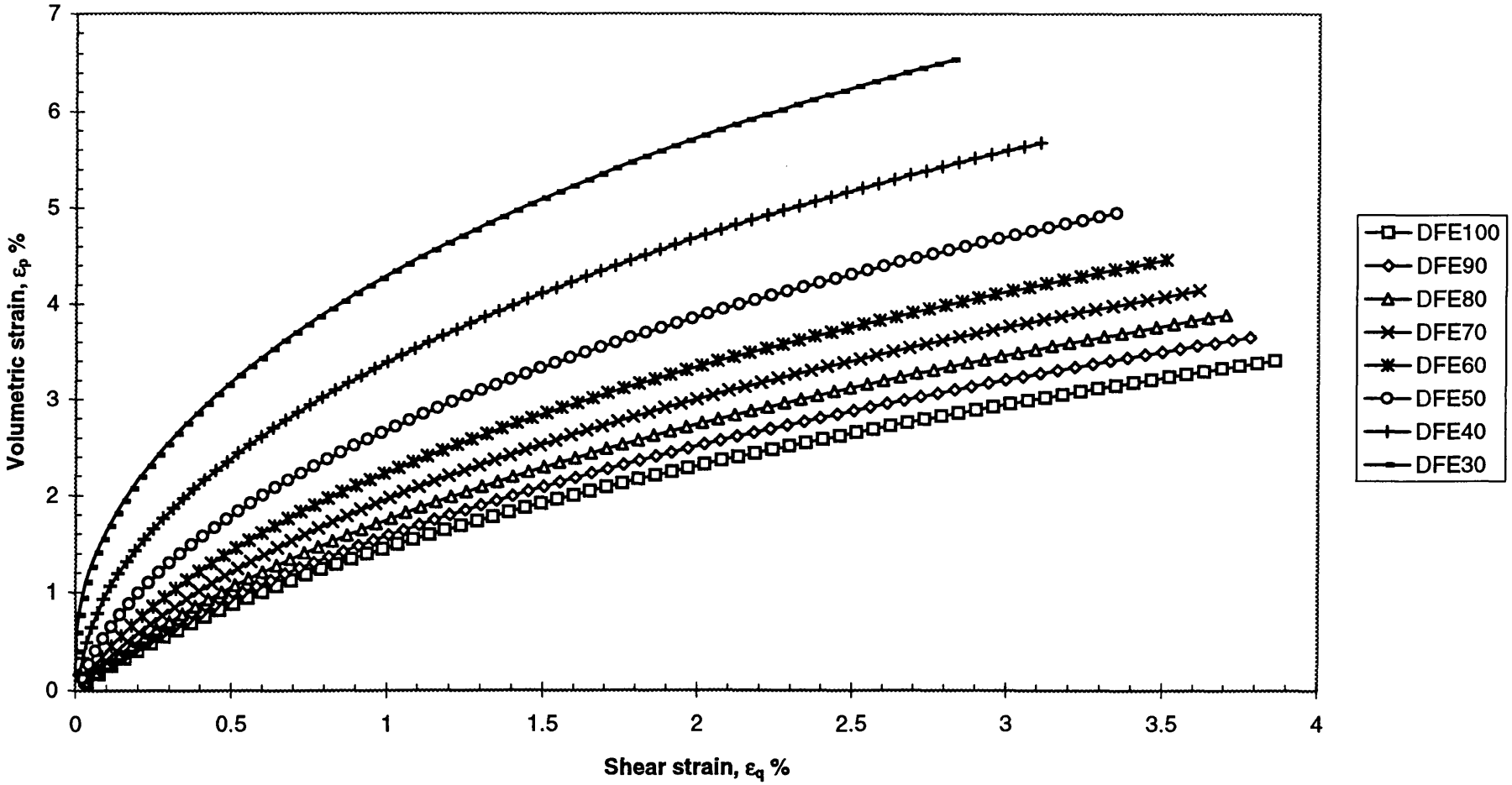

Fig.6.11 FE volumetric strain:shear strain response

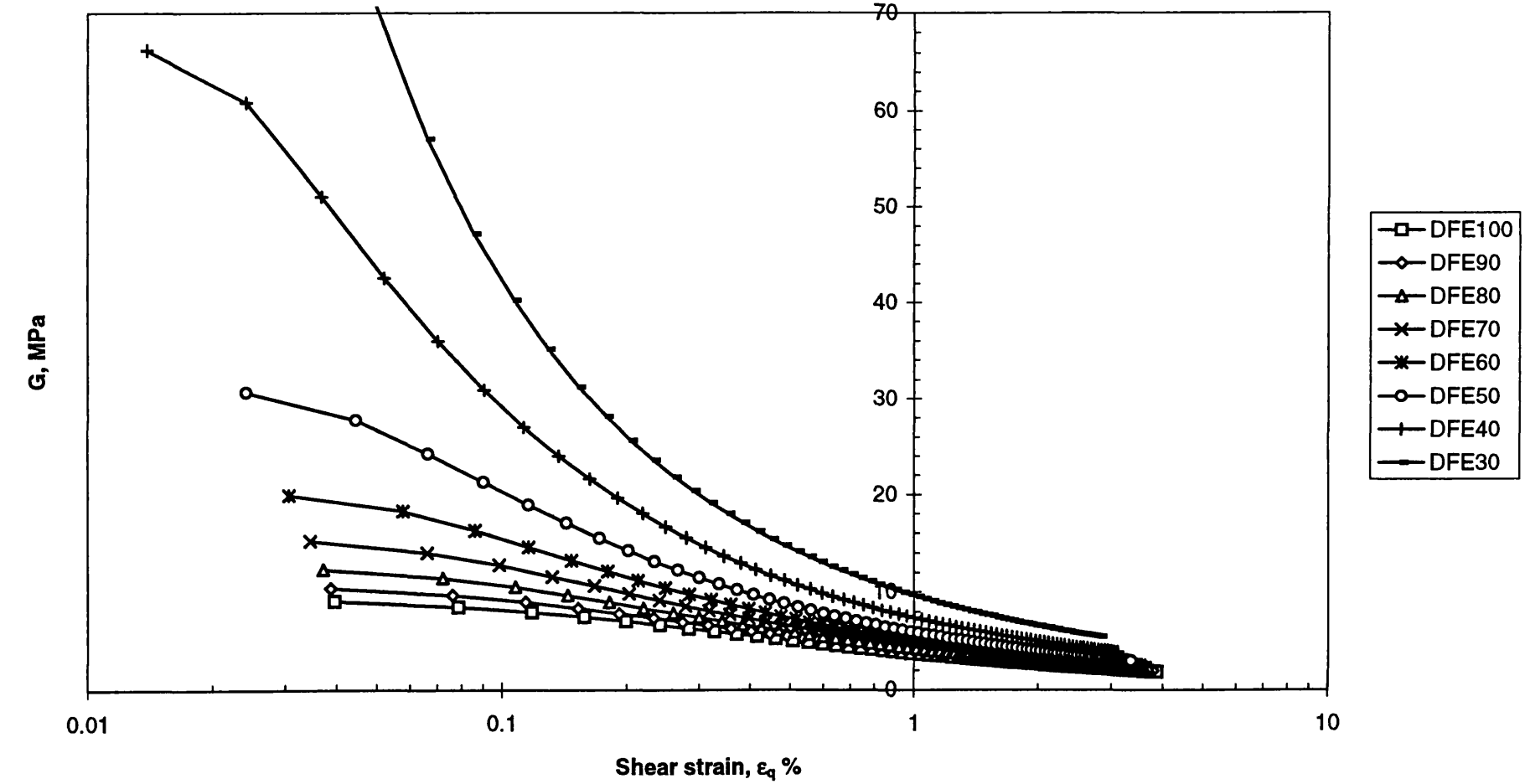

Fig.6.12 FE drained shear stiffness response

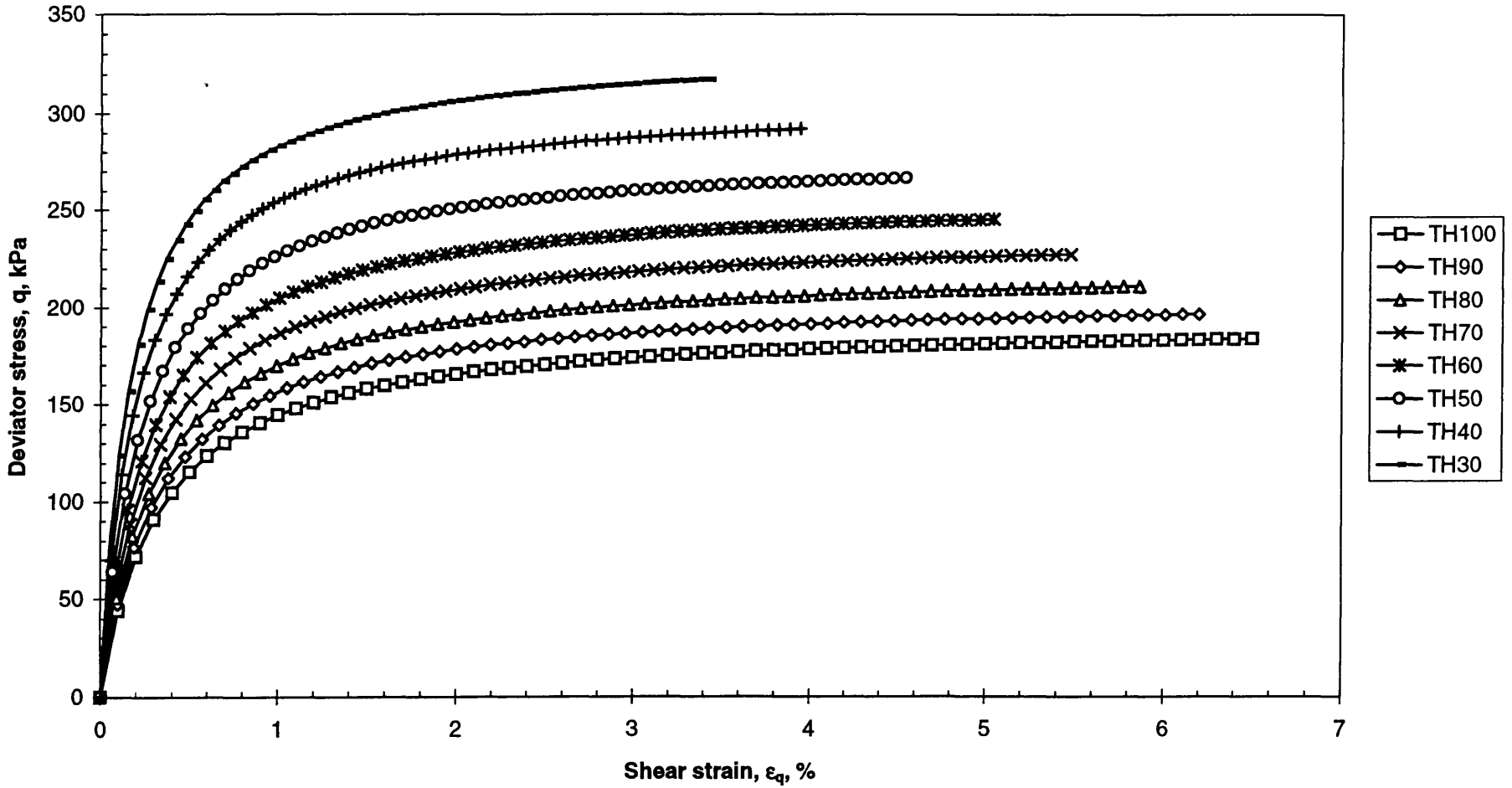

Fig.6.13 TH undrained stress:strain predictions

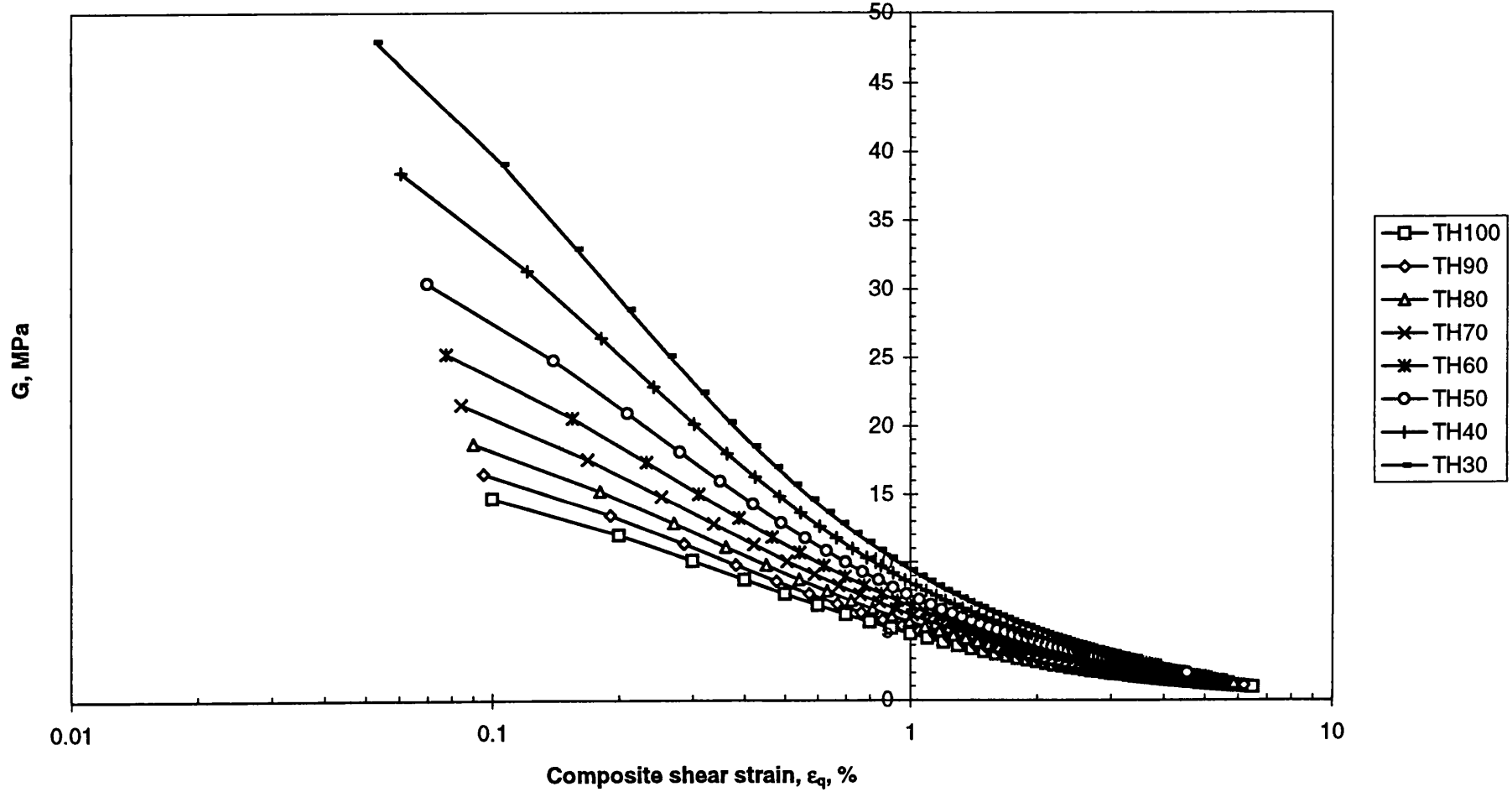

Fig.6.14 TH undrained shear stiffness response

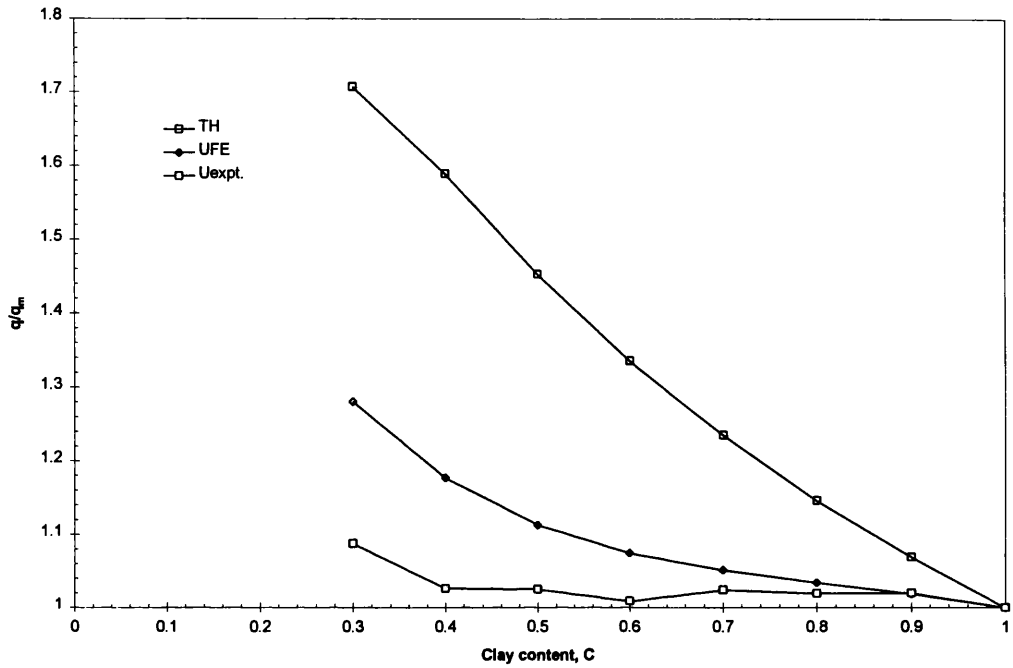

Fig.6.15 Comparison of undrained deviator stress from triaxial tests with numerical at 5% shear strain

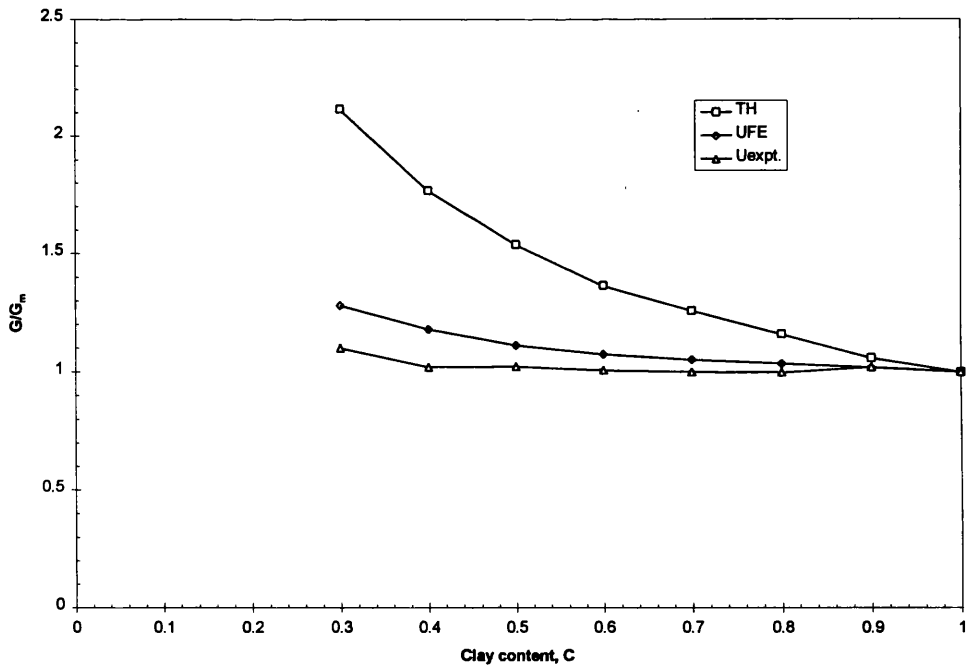

Fig.6.16 Comparison of undrained shear moduli from triaxial tests with numerical at 5% shear strain

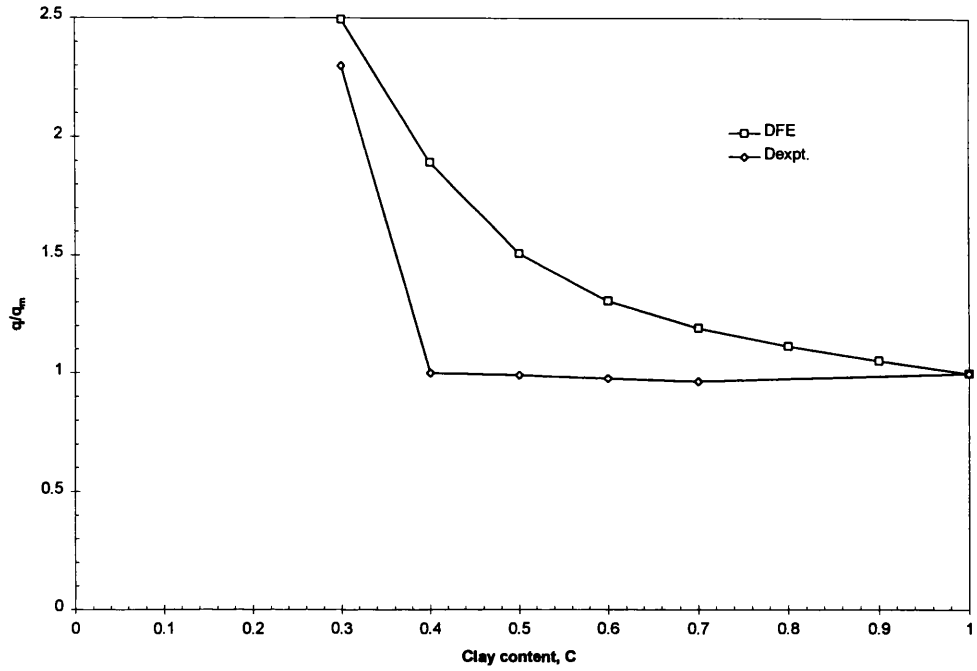

Fig.6.17 Comparison between predicted drained deviator stress with experimental results at 2.5% shear strain

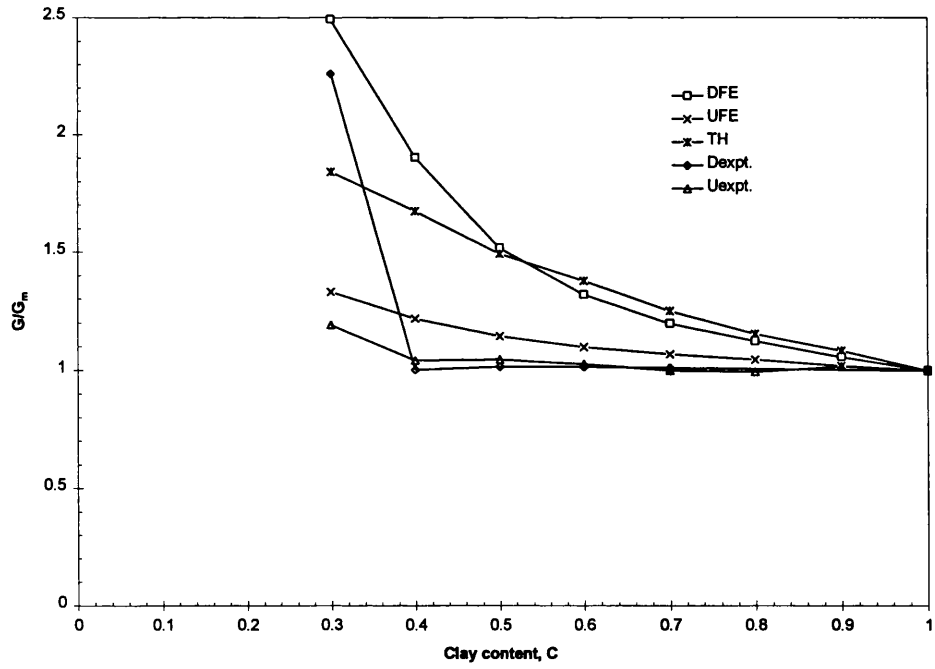

Fig.6.18 Comparison between experimental and numerical shear moduli at 2.5% shear strain

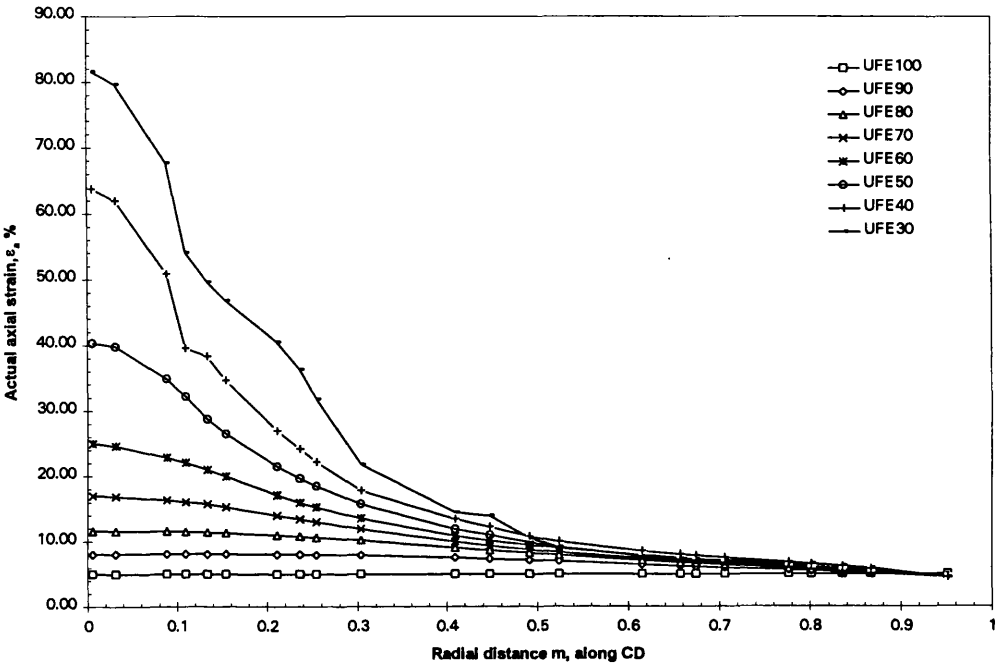

Fig.6.19a Variation of ε_a experienced by nodes near the top surface (CD) for a uniform axial strain of 5%

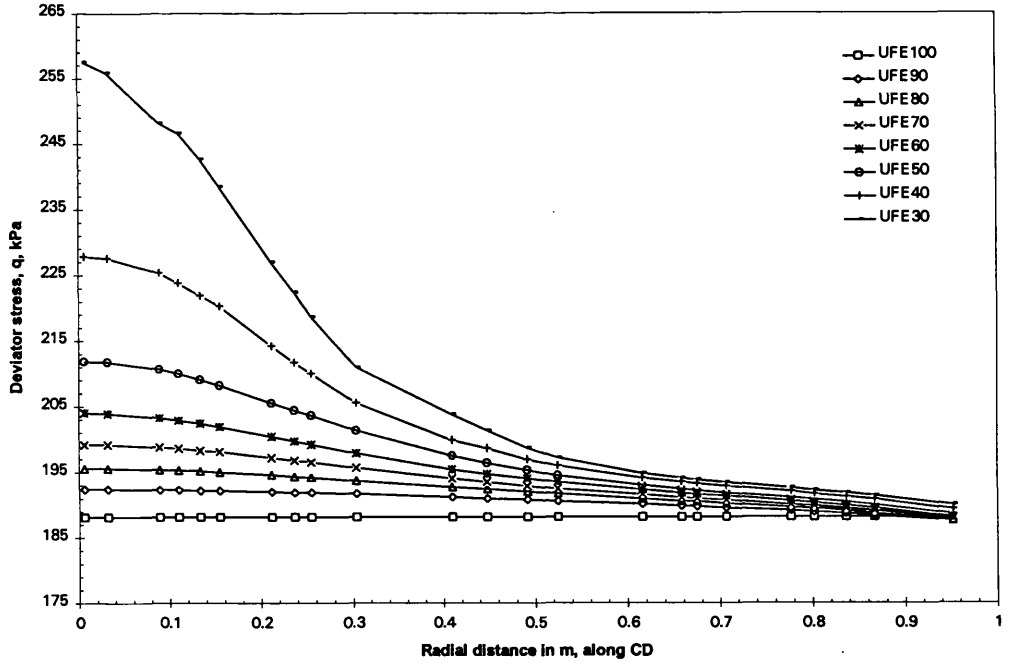

Fig.6.19b Variation of deviator stress along CD at a uniform axial strain of 5%

CHAPTER 7

CONCLUSIONS AND RECOMMENDATIONS

This chapter covers the main conclusions of the research described in this thesis. The conclusions presented in section 7.1-7.4 are concerned with studies on liquid limit characteristics, consolidation, permeability and shear behaviour of clay-sand mixtures and section 7.5 presents overall conclusions on the mechanical behaviour of clay-sand mixtures. Items covered in this chapter are intended to reflect this investigation and are limited to the clay and sand used, the methods of sample preparation used and test procedures employed. However the present study on kaolin-coarse sand mixtures provides a database of highly controlled tests over a full range of clay contents. These results are expected to initiate further research especially in the area of numerical modelling. Practising engineers can judge, on the basis of the clay content, whether the clay phase is likely to control the soil behaviour, and can use the findings in feasibility studies for selection of a site and in design of geotechnical structures.

7.1 LIQUID LIMIT TESTS

The liquid limit of the mixtures studied shows a linear variation with clay content above about 40% clay content (Fig.2.4). This implies that the presence of the coarse sand is not affecting the penetration resistance of the clay at the low strengths that it is has for water contents around the liquid limit (where the undrained strength of the clay is of the order of 2 kPa) until 60-70% of the volume of solid material is made up of sand particles (section 2.3.1, Chapter 2).

The liquid limit of soils which contain particles of 2mm size can be determined using fall cone tests. However, the limiting maximum size of coarse particles that could be present in the fall cone test has not been determined.

7.2 CONSOLIDATION CHARACTERISTICS

One-dimensional consolidation characteristics of clay/sand mixtures show that the relationship between logarithm of specific volume and logarithm of vertical effective stress is dependent on the both clay content and stress level (Fig.3.11 & 3.12). At low stress levels, the mixture with high clay content experiences large decrease in specific volume with small increase in vertical effective stress. More order can be obtained from the above data if they are plotted in terms of clay specific volume v_c instead of specific volume (Fig.3.14

& 3.15). It is then found that for the clay contents down to about 40% the relationship is more or less unique and it only for low clay contents-sand content above 60%- that the sand particles interact sufficiently to affect the one-dimensional compression relationships (Fig.3.16 & 3.17).

The slope of normal compression (λ_C^*) and swelling lines (κ_C^*) in $\ln v_c - \ln\sigma'_v$ space are almost constant up to clay content 40% in the mixture (Fig.3.19). The one-dimensional normal compression of clay phase can be described by a relationship of the form (section 3.2.2, Chapter 3):

$$\ln v_c = \ln A_c^* + \lambda_c^* \ln\sigma'_v \qquad (7.1)$$

where A_C^* is a reference value of clay specific volume for vertical effective stress $\sigma'_v = 1$ kPa.

A link is established between clay content C and the vertical effective stress σ'_V required to reach a specific granular specific volume v_g (section 3.3.3, Chapter 3):

$$\sigma'_v = \left[\left(\frac{1-C}{C}\right)\left(\frac{v_g - 1}{A_c^*}\right)\right]^{-\frac{1}{\lambda_c^*}} \qquad (7.2)$$

The use of a fall cone to determine the slope of normal compression lines as discussed by Muir Wood (1990) appears to be a confirmed (Fig.3.23).

7.3 PERMEABILITY CHARACTERISTICS

The present study of permeability characteristics (Fig.4.7) shows that the relationship between logarithm of permeability and logarithm of void ratio is approximately linear of form

$$k = X\, e^Y \qquad (7.3)$$

with the values of X increasing monotonically as the clay content falls, but the values of the slope Y being essentially independent of clay content for clay content above about 30%. This is clearly evident when the same data are presented in terms of clay void ratio e_C and it is found that the relationship is essentially unique for clay contents down to about 30% -sand content below 70% (Fig.4.8). It is for higher sand contents that the unique relationship breaks down - and for high sand contents, 80% and 90%, the permeability will tend to be

sufficiently high that the techniques of permeability determination devised for clays will not be appropriate.

The unique relationship established in the present study in terms of clay void ratio (e_c) is given by

$$k = 4.66\ e_c^{3.18} \times 10^{-10} \quad m/s \qquad (7.4)$$

for clay content greater than 30-40%. This expression is found to apply to clay/sand mixtures in the normally consolidated as well as in the overconsolidated states (Fig.4.8 & 4.10).

The permeability values deduced from consolidation analysis(Fig.4.15) and from transient phases of a flow pump test (Fig.4.18) are lower than those directly measured by about 0-50%.

7.4 SHEAR BEHAVIOUR

7.4.1 Experimental investigations

The results presented in Chapter 5 show that undrained and drained behaviour of clay/sand mixtures with clay contents from 40 to 100% at different OCRs is almost the same at each OCR within reasonable experimental errors if allowance is made in the volumetric response for the behaviour of the clay phase on its own (section 5.3, Chapter 5). Critical state data for undrained and drained tests on mixtures with clay content from 40 to 100% are similar with an angle of friction, $\phi' = 20.67°$ (Fig.5.27). This shows that the strength of the mixtures up to clay content 40% arises almost entirely from clay-water system and that the sand acts essentially only as a filler and does not contribute to the shear strength of the mixtures.

The presence of the sand particles does modify the volumetric behaviour of the mixtures again by acting as a filler of rigid material. The clay volumetric strain:shear strain relationships provide convincing evidence that the clay controls the volumetric behaviour down to 40% clay content in the mixture (Fig.5.21).

The parameter used to describe the packing of the clay phase, namely the clay specific volume v_c is required to produce a unique critical state line in v_c:lnp' space for different mixtures with clay content from 40 to 100% (Fig.5.28). The clay specific volume, v_c once again plays a major role in identifying an unique state boundary surface for undrained and drained tests on mixtures with clay contents from 40 to 100% at different OCRs (Fig.5.30 & 5.31).

On the other hand, the mixture with 30% clay content shows distinctly different response from other mixtures at each value of OCR used in this study. The mixture shows a high angle of internal friction $\phi' = 30°$ (Fig.5.27) which is an indication of response not controlled by clay minerals. At clay content 30%, interaction between sand particles is initiated leading to the high value of ϕ' and abrupt changes in other aspects of mechanical and volumetric response. At critical state the value of the angle of shearing resistance of the mixture is equal to that of pure sand (Fig5.26a & b). The implication of this is that the clay phase is sufficient to maintain a stable sand skeleton structure in an extremely loose state. Any further increase in clay content would tend to create a dispersed sand skeleton which could not exist independently.

In the present study undrained and drained test results show convincing evidence that the clay controls the shear behaviour of the mixtures with clay content from 100 to 40% at different OCRs and granular phase is only seriously involved at 30% clay content i.e. at 70% sand content.

7.4.2 Numerical studies

The theoretical and finite element analyses are not able to satisfactorily describe the experimentally observed patterns of shear behaviour of normally consolidated materials (section 6.33, Chapter 6).

7.5 OVERALL CONCLUSIONS

It is understood that presence of coarse fraction will modify the mechanical behaviour of mixtures. Nevertheless, it is possible to examine the engineering behaviour of clay/sand mixtures within a scientific framework. The clay specific volume is a key parameter, which appears to be sufficient to interpret the mechanical behaviour of mixtures satisfactorily as along as clay controls the behaviour.

Granular specific volume is a key parameter that reflects changes in packing due to compression and shear. The boundary at which granular interaction begins in one-dimensional compression (Fig.3.21 & 3.22) and in shear behaviour (Fig.5.33) is around 2.2-2.5. The clay phase controls the mechanical behaviour of clay/sand mixtures above a granular void ratio of 2.5.

These studies of some mechanical properties of mixtures of kaolin and coarse sand have indicated that for clay contents above about 40% the behaviour is controlled by the properties of the clay phase alone.

7.6 SUGGESTIONS FOR FUTURE RESEARCH

The experimental and numerical studies reported in this thesis have shown a better understanding of the behaviour of clay-sand mixtures and the extent of the clay phase. However many questions are still unanswered and further research can be carried out in this area. The future research opportunities include experimental and numerical investigations.

7.6.1 Experimental investigations

The experimental results presented in thesis have mainly concentrated on gap-graded clay-sand mixtures. It is obviously important to confirm that the general pattern of behaviour observed in these tests also applied to soil containing well-graded sand.

The present study of shear behaviour of clay-sand mixtures was limited to compression shear tests on isotropically consolidated samples. The shear behaviour of the soils would be different under different conditions of test. In order to obtain more comprehensive information on the extent of clay phase on the shear behaviour of the clay-sand mixtures, additional testing is desirable under various loading conditions which are possible to occur in the field such as : loading and unloading conditions; samples consolidated under anisotropic conditions. It is also worthwhile to study the influence of clay phase on shear behaviour during extension tests.

7.6.2 Numerical investigations

Finite element predictions on unit cell model were unable to capture the extent of clay phase in shear. The unit cell models do not accurately account for the effects of shape and spatial distribution of sand particles in clay matrix. Ideal model to analyse the stress:strain behaviour of clay-sand composite is a numerical model which contains several sand particles in the clay matrix. The best numerical approach would be a three-dimensional finite element model. If such a model is difficult to set-up because of expensive computational capability, then a two-dimensional analysis of the plane strain behaviour of unidirectional sand particles, distributed within a clay matrix might at least give some indication of the likely behaviour. Setting up a finite element model to examine the effects of sand particle shape and spatial distribution on the shear response of clay-sand composite might be simple in plane strain analysis.

In the quest of developing a computational model for describing shear response of unidirectional composites, Nedele and Wisnom (1994b) used newly developed concentric cylinder model. This model stands between the simple axisymmetric model and a fully three-dimensional model. It would be interesting

to study the shear response of clay-sand composites by using concentric cylinder model and assuming that a sand particle is surrounded by six neighbouring sand particles in hexagonal array.

8. REFERENCES

Aiban, S.A., and Znidarcic, D. (1989), 'Evaluation of the flow pump and constant head techniques for permeability measurements', Geotechnique 39(4), 655-666.

Al-Dhahir, Z.A., and Tan, S.B. (1968), 'A note on one-dimensional constant head permeability tests', Geotechnique 18(4), 499-505.

Al Tabbaa, A. (1987), 'Permeability and stress-strain response of speswhite kaolin,' Ph.D. thesis, Cambridge University.

Al Tabbaa, A., and Wood, D.M. (1987), 'Some measurements of the permeability of kaolin', Geotechnique 37(4), 499-503.

Al Tabbaa, A., and Wood, D.M. (1989), 'An experimentally based bubble model for clay', in S. Pietruszczak and G.N. Pande (eds.), Numerical Models in Geomechanics NUMOG III (London: Elsevier), 91-109.

Allman, M.A., and Atkinson, J.H. (1992), 'Mechanical properties of reconstituted Bothkennar soil', Geotechnique 42 (2), 289-301.

Amer A.M., and Awad, A.A. (1974), 'Permeability of cohesionless soils', Journal of the Geotechnical Engineering Division, ASCE, 100(GT12), 1309-1316.

Amerasinghe, S.F., and Parry, R.H.G. (1975), 'Anisotropy in heavily overconsolidated kaolin', Journal of the Geotechnical Engineering Division, ASCE, 101(GT12), 1277-1293.

Atkinson, J.H. (1993), ' Introduction to the mechanics of soils and foundations', McGraw-Hill, London.

Atkinson, J.H., and Richardson, D. (1987), 'The effect of local drainage in rupture zones on the undrained strength of overconsolidated clay', Geotechnique 37, 394-403.

Atterberg, A. (1911), 'Lerorans forhallande till vatten, deras plasticitetsgranser och plasticitetsgrader', Kungl. Lantbruks akademiens Handlingar och Tidskrift, 50(2) 132-158.

Barden, L., and McDermott, J.W. (1965), 'Use of free ends in triaxial testing of clays', Journal of the Soil Mechanics and Foundation Division, ASCE 91(SM6), 1-23.

Been, K., and Jefferies, M.G. (1985), 'A state parameter for sands', Geotechnique, 35(2), 99-112.

Been, K., Jefferies, M.G., and Hachey, J. (1991), 'The critical state of sands', Geotechnique, 41(3), 365-381.

Bijerrum, L., and Simons, N.E. (1960), 'Comparison of shear strength characteristics of normally consolidated clays', Proc. ASCE conf. on Shear Strength of cohesive soils, Boulder, Colorado, 711-726.

Bishop, A.W., and Henkel, D.J. (1962), 'The measurement of soil properties in the triaxial test', 2nd Edition, Edward Arnold, London.

Bishop, A.W., and Green, G.E. (1965), 'The influence of end restraint on compression strength of a cohesionless soil', Geotechnique 15(3), 243-266.

Black, D.K., and Lee, K.L. (1973), 'Saturating laboratory samples by back pressure', Journal of the Soil Mechanics and Foundation Division, ASCE 90(SM1), 75-93.

Blight, G.E. (1963), 'The effect of non-uniform pore pressure on laboratory measurements of the shear strength of soils', Symposium on Laboratory Shear Testing of Soils, ASTM STP.361, 173-184.

British Standards Institution, 1991, 'Methods of test for soils for civil engineering purposes', -BS1377, London.

Britto, A.M., and Gunn, M.J. (1987), 'Critical state soil mechanics via finite elements', Ellis Horwood Ltd., Chichester.

Butterfield, R. (1979), 'A natural compression law for soils', Geotechnique 29, 469-480.

Carman, P.C. (1956), 'Flow of gases through porous media', Butterworths, London

Carslaw, H.S., and Jaeger, J.C. (1959), 'Conduction of heat in solids', Oxford University press, New York.

Casagrande, A.C. (1932), 'Research on the Atterberg limits of soil', Public Roads 13(8), 121-130.

Casagrande, A.C. (1958), 'Note on the design of the liquid limit device', Geotechnique 8(2), 84-91.

Chapuis, R.P. (1990), 'Sand-bentonite liners: predicting permeability from laboratory tests', Canadian Geotechnical Journal 27, 47-57.

Collins, K., and McGown, A. (1974), 'The form and function of microfabric features in a variety of natural soils', Geotechnique 24(2), 223-254.

Daniel, D.E (1993), 'Clay liners', in D.E. Daniel (ed.), Geotechnical practice for waste disposal, Chapman and Hall, London.

Darcy, A. (1856), 'Les Fontaines Publiques de la Ville de Dijon', Dalmont, Paris.

Dumbleton, M.J., and West, G. (1966), 'The influence of the coarse fraction on the plastic properties of clay soils', Ministry of Transport, RRL Report No.36.

Dunn, R.J and Mitchell, J.K.(1984), 'Fluid conductivity testing of fine-grained soils', Journal of the Soil Mechanics and Foundation Division, ASCE, 110, 1648-1665.

Fukue, M., Okusa, S., and Nakamura, T.(1986), 'Consolidation of sand-clay mixtures', Consolidation of soils: Testing and Evaluation Eds. R.N.Yong and F.C. Townsend, ASTM STP 892, 627-641.

Gens, A. (1985), 'The state boundary surface for soils not obeying Rendulic's principle', Proc. 11th Int. Conf. Soil Mechanics and Foundation Eng., San Francisco 2, 473-476.

Georgiannou, V.N., Burland, J.B., and Hight, D.W. (1990), 'The undrained behaviour of clayey sands in triaxial compression and extension', Geotechnique 40(3), 431-449.

Georgiannou, V.N., Hight, D.W., and Burland, J.B.(1991), 'Undrained behaviour of natural and model clayey sands', Soils and Foundations, 31(3), 17-29.

Graham, J., Saadat, F., Gray, M.N., Dixon, D.A., and Zhang, Q.-Y. (1989), 'Strength and volume change behaviour of a sand-bentonite mixture', Canadian Geotechnical Journal 26, 292-305.

Graton, L.C., and Fraser, H.J. (1935), 'Systematic packing of spheres-with particular relation to porosity and permeability', Journal of Geology 43(8), 785-909.

Gribble, C.D. (1995), Personal communication.

Hamidon, A.B. (1994), 'Some laboratory studies of anisotropy of permeability of kaolin', Ph.D. thesis, University of Glasgow.

Hansbo, S. (1957), 'A new approach to the determination of the shear strength of clay by the fall-cone test', Swedish Geotechnical Institute, Stockholm, Proceedings 14.

Hansbo, S. (1960), 'Consolidation of clays with special reference to the influence of vertical sand drains', Swedish Geotechnical Institute, Stockholm, Proceedings 18.

Hardcastle, J.H., and Mitchell, J.K. (1974) 'Electrolyte concentration-permeability relationships in sodium, illite-silt mixtures', Clays and Clay Minerals 22, 143-154.

Head, K.H. (1982), 'Manual of soil laboratory testing', Vol.2, Pentech Press Ltd., London.

Head, K.H. (1985), 'Manual of soil laboratory testing', Vol.3, Pentech Press Ltd., London.

Henkel, D.J. (1956), 'The effect of overconsolidation on the behaviour of clays during shear', Geotechnique 6(4), 139-150.

Jardine, R.J., Symes, M.J., and Burland, J.B. (1984), 'The measurement of soil stiffness in the triaxial apparatus', Geotechnique 34(3), 323-340.

Jardine, R.J., Potts, D.M., Fourie, A.B., and Burland, J.B. (1986), 'Studies of the influence of non-linear stress-strain characteristics in soil-structure interaction', Geotechnique 36(3), 377-396.

Kamei, T., and Nakase, A. (1989), 'Undrained shear strength anisotropy of K_O-overconsolidated cohesive soils', Soils and Foundations 29(3), 145-151.

Kenney, T.C., Lau, D., and Ofoegbu, G.I. (1984), 'Permeability of compacted granular materials', Canadian Geotechnical Journal 21, 726-729.

Kenney, T.C., van Veen, W.A., Swallow, M.A., and Sungaila, M.A. (1992), 'Hydraulic conductivity of compacted bentonite-sand mixtures', Canadian Geotechnical Journal 29, 364-374.

Kimura, T., Takemura, J., Hiro-oka, A., and Okamura, M. (1994), 'Mechanical behaviour of intermediate soils', Centrifuge 94, Eds. by Leung, Lee and Tan, Balkema, Rotterdam, 13-24.

Konder, R.L. (1963), 'Hyperbolic stress-strain response: cohesive soils', Journal of the Soil Mechanics and Foundations Division, ASCE 89(SM1), 115-143.

Kozeny, J.S. (1927), 'Uber Kapillare Leitung des Wassers im Boden', Sitzungsberichte der Akadamie der Wissenschaften in Wien, Abteilung IIa. page 136.

Lambe, T.W., and Whitman, R.V. (1979), 'Soil Mechanics', SI version, John Wiley and Sons, New York.

Law , K.T., and Lee, C.F. (1981), 'Initial gradient in a dense glacial till', Proc. 10th Int. Conf. on Soil Mechanics and Foundation Eng., Stockholm, 441-446.

Leroueil, S., Magnan, J-P., and Tavenas, F. (1990), 'Embankments on soft clays', Eillis Horwood Ltd., Chichester.

Little, J.A., Wood, D.M., Paul, M.A. and Bouazza, A. (1992), 'Some laboratory measurements of permeability of Bothkennar clay in relation to soil fabric', Geotechnique 42(2), 355-361.

Loudon, A.G. (1952), 'The computation of permeability from simple soil tests', Geotechnique 3, 165-183.

Lupini, J.F., Skinner, A.E., and Vaughan, P.R. (1981), 'The drained residual strength of cohesive soils', Geotechnique 31(2), 181-213.

Menzies, B.K. (1988), 'A computer controlled hydraulic triaxial testing system', in R.T. Donaghe, R.C. Chaney and M.L. Silver (eds.), Advanced triaxial testing of soil and rock, ASTM STP 977, 82-94.

Mesri, G., and Olson, R.E. (1971), 'Mechanisms controlling the permeability of clays', Clays and Clay Minerals 19, 151-158.

Mitchell, J.K. (1976), 'Fundamentals of soil behaviour', John Wiley, New York.

Morin, R.H., and Olsen, H.W. (1987), 'Theoretical analysis of the transient pressure response from a constant flow rate hydraulic conductivity test', Water Resources Research 23(8), 1461-1470.

Morin, R.H., Olsen, H.W., Nelson, K.R., Gill, J.D. (1989), 'Graphical method for determining the coefficient of consolidation c_v from a flow pump permeability test', Geotechnical Testing Journal 12(4), 302-307.

Muir Wood, D. (1990), 'Soil behaviour and critical state soil mechanics', Cambridge University Press, Cambridge.

Nagaraj, T.S, Murthy, B.R.S., and Bindumadhava (1987), 'Liquid limit determination-further simplified', Geotechnical Testing Journal, Vol.10, No.3, 142-145.

Nagaraj, T.S., Pandian, N.S., and Raju, P.S.R.N. (1994), 'Stress-state-permeability relations for overconsolidated clays', Geotechnique 44(2), 349-352.

Nakase, A., and Kamei, T. (1983), 'Undrained shear strength anisotropy of normally consolidated cohesive soils', Soils and Foundations, 25(1), 91-101.

Nakase, A., Kamei, T., and Kusakabe, O. (1988), 'Constitute parameters estimated by plasticity index', Journal of Geotechnical Engineering 114(GT7), 844-858.

Nedele, M.R., and Wisnom, M.R. (1994a), 'Finite element micromechanical modelling of a unidirectional composite subjected to axial shear loading', Composites 25(4), 263-272.

Nedele, M.R., and Wisnom, M.R. (1994b), 'Stress concentration factors around a broken fibre in a unidirectional carbon fibre-reinforced epoxy', Composites 25(7), 547-557.

Norman, L.E.J. (1958), 'A comparison of values of liquid limit determined with apparatus having bases of different hardness', Geotechnique 8(2), 79-84.

Olsen, H.W. (1966), 'Darcy's law in saturated kaolinite', Water Resources Research 2(2), 287-295.

Olsen, H.E. (1985), 'Osmosis: a cause of apparent deviations from Darcy's law', Canadian Geotechnical Journal 22, 238-241.

Olsen, H.E., Nichols, R.W., and Rice, T.L. (1985), 'Low-gradient permeability measurements in a triaxial system', Geotechnique 32(2), 145-157.

Olson, R.E. (1986), 'State-of-the-art: consolidation testing', in R.N. Yong and F.C.Townsend (eds.), Consolidation of soils: Testing and Evaluation, ASTM:STP 892, 18-64.

Pane, V., Croce, P., Znidarcis, D., Ko, H.Y., Olsen, H.W., and Schiffman, R.L. (1983), 'Effects of consolidation on permeability measurements for soft clays', Geotechnique 33(1), 67-72.

Parry, R.H.G., and Nadarajah, V. (1974), 'Observations on laboratory prepared, lightly overconsolidated specimens of kaolin', Geotechnique 24(3), 345-358.

Rao, R.R. (1978), 'A study of swelling clay', Ph.D. thesis, University of Glasgow.

Remy, J.P. (1973), 'The measurement of small permeabilities in the laboratory', Geotechnique 23(3), 454-458.

Roberts, K. (1995), Personal communication.

Roscoe, K.H., Schofield, A.N., and Wroth, C.P. (1958), 'On the yielding of soils', Geotechnique 8(1), 22-52.

Rossato, G., Ninis, N.L., and Jardine, R.J. (1992), ' Properties of some kaolin-based model clay soils', Geotechnical Testing Journal, 15(2), 166-179.

Rowe, P.W., and Barden, L. (1964), 'Importance of free ends in the triaxial testing', Journal of the Soil Mechanics and Foundation Division, ASCE, 90(SM1), 1-27.

Rowe, P.W., and Barden, L. (1966), 'A new consolidation cell', Geotechnique, 16(2), 162-170.

Samarasinghe, A.M., Huang, Y.H., and Drnevich, V.P. (1982), 'Permeability and consolidation of normally consolidated soils', Journal of the Geotechnical Engineering Division, ASCE, 108(GT6), 835-850.

Seed, H.B., Woodward, R.J., and Lundgren, R. (1964), 'Fundamental aspects of the Atterberg limits', Journal of the Soil Mechanics and Foundation Division, ASCE, 90(SM6), 75-105.

Shen. Y.-L., Finot, M., Needleman, A., and Suresh, S. (1994), 'Effective elastic response of two-phase composites', Acta metall. mater 42(1), 77-97.

Sherwood, P.T., and Ryley, M.D. (1970), 'An investigation of a cone-penetrometer method for the determination of the liquid limits', Geotechnique, 20(2), 203-208.

Sivapullaiah, P.V, and Sridharan, A. (1985), 'Liquid limit of soil mixtures', Geotechnical testing Journal 8(3), 111-116.

Skempton, A.W. (1953), 'The colloidal activity of clays', Proc. 3rd Int. Conf. on Soil Mechanics and Foundation Eng., Zurich, Vol.1, 57-61.

Skempton, A.W., and Northey, R.D. (1953), 'The sensitivity of clays', Geotechnique 3(1), 30-53.

Skempton, A.W. (1954), 'The pore pressure coefficients A and B', Geotechnique 4(4), 143-147.

Tan, T.-S., Goh, T-C., Karunaratne, G.P., Lee, S.-L.(1994), 'Shear strength of very soft clay-sand mixtures', Geotechnical testing Journal 17(1), 27-34.

Tandon, G.P., and Weng, .G.J. (1988), 'A theory of particle-reinforced plasticity', ASME, Journal of Applied Mechanics 55, 126-135.

Tavenas, F., Leblond, P., Jean, P., and Leroueil, S. (1983-a), 'The permeability of natural clays. Part I: Methods of laboratory measurements', Canadian Geotechnical Journal 20(4), 629-644.

Tavenas, F., Jean, P., Leblond, P., and Leroueil, S. (1983-b), ' The permeability of natural soft clays. Part II: Permeability characteristics', Canadian Geotechnical Journal 20(4), 645-660.

Taylor, D.W. (1948), 'Fundamentals of Soil Mechanics', John Wiley, New York.

Terzaghi, K (1926), 'Simplified soil tests for subgrades and their physical significance', Public Roads, Vol.7, No.8, 153-162.

Terzaghi, K. (1943), 'Theoretical soil mechanics', John Wiley, New York.

Todd, D.K. (1980), 'Groundwater Hydrology', 2nd edition, John Wiley and Sons, New York.

Vaughan, P.R. (1994), 'Assumption, prediction and reliability in geotechnical engineering', Geotechnique 44(4), 573-609.

Vaughan, P.R., Hight, D.W., Sodha, V.G., and Walbancke, H.J. (1979), 'Factors controlling the stability of clay fills in Britain', In Clay Fills, Institute of Civil Engineers, London, 205-218.

Wroth, C.P., and Loudon, P.A. (1967), 'The correlation of strains within a family of triaxial tests on overconsolidated samples of kaolin', Proceedings of the Geotechnical Conference, Oslo, 159-163.

Wroth, C.P. and Wood, D.M.(1978), 'The correlation of index properties with some basic engineering properties of soils', Canadian Geotechnical Journal 15(2), 137-145.